UNIVERSITÄT ZU LÜBECK
KLINIK FÜR RHEUMATOLOGIE
UND KLINISCHE IMMUNOLOGIE

From the Department of Rheumatology and Clinical Immunology
of the University of Lübeck
Director: Prof. Dr. med. Gabriela Riemekasten

Combining in-depth immune profiling and multi-omics approaches identifies distinct signatures in the early stage of Systemic Sclerosis

Dissertation
for Fulfillment of
Requirements
for the Doctoral Degree
of the University of Lübeck

from the Department of Natural Sciences

Submitted by

Justus Maximilian Ohmes
from Bückeburg

Lübeck 2025

First referee: PD. Dr. Jens Humrich
Second referee: Prof. Dr. Rudolf Manz
Date of oral examination: 18.07.2025
Approved for printing. Lübeck, 13.08.2025

Acknowledgment

My first heartfelt thanks go to Prof. Dr. Gabriela Riemekasten and PD. Dr. Jens Humrich, who gave me the opportunity to work on my doctoral thesis in their group in the Department of Rheumatology and Clinical Immunology and supported and accompanied the research for this thesis both financially and through active supervision. Gabi and Jens were always interested in the progress of my research and were always willing to meet with me and discuss progress - even if it had to be spontaneous by phone in the evening. The great trust in my independent way of working and the constructive error culture never made me lose focus and motivation, even when a situation seemed unsolvable. In addition, both of you have strongly advocated for me and supported me by giving me the opportunity to present my research results at international congresses, for which I am deeply grateful.

Next, I would like to say a huge Thank You to my two mentors - Prof. Dr. Jennifer Hundt and PD. Dr. Reza Akbarzadeh. Jenny always maintained an independent perspective on my progress and well-being beyond the research group, offering valuable advice and tips from a different point of view. I took you straight to my heart with your warm and very personal manner and your close bond with dogs. Reza was always on site in the lab and always enriched me scientifically with his theoretical and practical knowledge and was always available if anything was unclear. I was also able to talk to you about everything else outside of the usual lab topics, so you ended up being a really good lab buddy, which I am thankful for.

As a member of the RTG2633 - Defining and Targeting Autoimmune Pre-Disease, I am of course also grateful to the spokesperson Prof. Dr. Ralf Ludwig and the Co-spokesperson Jenny for giving me the opportunity to being part of this graduate school and supporting my research project financially. The RTG has sharpened and significantly improved my ability to think, argue and present scientifically. In addition, the flawless organization by Dr. Skadi Lange, Dr. Laura Kirchhoff and Sina Jäschke has greatly simplified all bureaucratic hurdles and left no question unanswered, which has made it possible for me to focus exclusively on my scientific progress.

Next, I would like to thank the laboratory management PD. Dr. Antje Müller and Dr. Anja Stähle for allowing me to carry out and evaluate all my experiments in the lab. Antje and Anja have always done everything to make the laboratory the best place to work in the world and have always been on hand with help and advice when problems arose. Their understanding, trust and, of course, scientific expertise have brought the work to a very high level, both interpersonally and in terms of content. I can say that I have always enjoyed coming to the lab, and you were one of the main

reasons for that.
A massive thank you goes out to Dr. Hanna Graßhoff and Sara Comdühr. You both played an essential role in the design of my doctoral project. Thank you Hanna for your tireless efforts to ensure that all ideas and implementations on the clinical side were realized as quickly and effectively as possible. Recruiting suitable patients was just one part of your outstanding achievements for my work. Thank you Sara for fully introducing me to the secrets of flow cytometry and sharing your extraordinary methodological and mathematical expertise with me. You both never let me down in any situation and I am infinitely grateful to you for that!
And while we are on the subject of Sara: Many thanks to you too, Sarah from the AG Hundt. As a person who has always been in the same boat, the regular exchange with you was very valuable and I could always count on you when things were unclear. I would also like to thank you for the voluntary practical introduction to handling mice, even if the underlying project was not part of this thesis.
Next, I would like to thank the Master's students Silja and Maike, as well as Bachelor's student Chiara, for their extensive support with my practical lab work and for contributing not only to the success of the experiments but also to my daily motivation and mental well-being throughout the process. I would also like to thank the technical assistants Silke and Gabi for always having an overview of everything in the lab and sometimes calmly answering the same question three times. Thanks of course also to all the other members of the laboratory at the Department for Rheumatology and Clinical Immunology who contributed to a very pleasant working atmosphere!
I would also like to thank Prof. Dr. Timo Gemoll and Katja Klempt-Gießing from the section for Translational Surgical Oncology and Biomaterial Banks for their support in performing the Olink analysis, PD. Dr. David Juhl from the institute of Transfusion Medicine for providing the healthy blood samples and Dr. Harald Heidecke from the company CellTrend for measuring the autoantibody levels.
Last but not least, I would like to thank my wonderful parents, sisters and my best friend Julian. You were always interested in my progress and always distracted and cheered me up when needed. Lastly, a very special thanks goes to my girlfriend Aleksandra (together with our dog Maila), as you always stood by me during this - sometimes stressful - time and supported me as much as you could. You were always understanding of unusual working hours and mood swings, which I really appreciated.

I am very happy to have you all in my life!

THANK YOU!

Abstract

Systemic sclerosis (SSc) is a severe systemic autoimmune disease characterized by progressive immune dysregulation, inflammation, and fibrosis with an unknown etiology. Understanding the immunopathogenesis of SSc, particularly during its early preclinical stage, is critical for identifying novel therapeutic strategies. This dissertation provides an in-depth immunophenotypic analysis of disease progression from early to established disease, focusing on disturbances within the Treg-IL-2 and Th17-IL-17 axes as key drivers of immune dysregulation.

Part I of this dissertation presents a detailed immunophenotyping, revealing that an IL-2-deprived Treg phenotype emerges early in disease progression, even before the clinical diagnosis of an established SSc. The observed stepwise reduction in CD25hi Treg and the increased presence of CD25- and CD25lo Treg subsets along with a reduction of CD39+ cells among CD25+ Treg highlights the critical role of low availability of IL-2 in dysregulation of immune homeostasis. Furthermore, a machine-learning-based Random Forest analysis demonstrated that Th17 cells, along with CD25lo Treg and proliferating Ki67+ cells among CD25- Treg, are among the most significant immunological features distinguishing Very Early Diagnosis Of Systemic Sclerosis (VEDOSS) from established SSc. These results suggest that the interplay between the Treg-IL-2 and Th17-IL-17 axes contributes to the transition from early-stage immune dysregulation to established autoimmune pathology. Notably, increased serum IL-17A levels in established SSc, despite equal Th17 frequencies compared to VEDOSS patients, suggest additional regulatory mechanisms influencing IL-17 secretion. The chemokine CXCL10, induced by IL-17A signaling and known for promoting vascular pathology, showed a stepwise increase from VEDOSS to SSc and correlated with disease activity, suggesting its involvement in early immune dysregulation and fibrotic progression. In established SSc, CXCL10 levels also correlated with anti-GPCR autoantibodies, linking it to humoral autoimmunity. Alongside CXCL10, the inflammation-promoting proteins CCL20 and MCP1, as well as the tissue-remodeling factor MMP1, were significantly elevated in SSc compared to VEDOSS, further supporting a shift toward pathogenic inflammation and tissue damage. Beyond the immunological findings, this study highlights the potential of machine-learning algorithms for early disease classification. The integration of immunophenotypic, autoantibody and cytokine profiles in a multi-omics analysis achieved high classification accuracy between VEDOSS and SSc patients. This underscores the feasibility of AI-driven diagnostics for early disease detection and patient stratification. **Part II** of this dissertation explores a potential therapeutic approach aimed at restoring immune balance through *in vitro* Treg re-

covery by stimulation with low-dose recombinant IL-2. This stimulation successfully recovered CD25hi Treg frequencies, reinforcing prior findings from other autoimmune diseases, such as systemic lupus erythematosus. These results provide a strong rationale for conducting clinical trials investigating the efficacy of low-dose IL-2 therapy in SSc patients to restore Treg homeostasis and functional activity. Remarkably, this approach did not simply increase the total population of Treg expressing CD25 at low levels, which is indicative for an IL-2 deprived and unfit state, but rather shifted the existing Treg towards a CD25hi Treg phenotype, as evidenced by the lack of frequency changes in Ki67+ cells among CD25+ Treg subsets. These findings indicate that IL-2 selectively boosts the function of immunoregulatory cells rather than indiscriminately expanding Treg, thus preserving immune homeostasis. Given the early emergence of a Treg-IL-2 axis disturbance in VEDOSS patients, this study suggests that low-dose IL-2 therapy should be considered as a preventive strategy in VEDOSS patients. By intervening at this early disease stage, IL-2 supplementation may help to correct the proven Treg/Tcon imbalance, potentially preventing disease progression and organ damage. These findings highlight the need for future clinical trials to evaluate the efficacy of low-dose IL-2 therapy in VEDOSS patients and explore its potential role in delaying the transition to an established stage.

In summary, this dissertation sheds new light on the immunological mechanisms underlying early and established SSc, uncovering critical pathways that drive disease progression and presenting new potential therapeutic and diagnostic checkpoints.

Zusammenfassung

Systemische Sklerose (SSc) ist eine schwere systemische Autoimmunerkrankung, die durch progressive Immunregulationsstörungen, Entzündungen und Fibrose gekennzeichnet ist, wobei die Ätiologie unbekannt ist. Das Verständnis der Immunopathogenese der SSc, insbesondere in ihrer frühen präklinischen Phase, ist entscheidend, um neue therapeutische Strategien zu identifizieren. Diese Dissertation bietet eine detaillierte immunphänotypische Analyse des Krankheitsverlaufs von der frühen bis zur etablierten Krankheit und konzentriert sich auf Fehlregulationen innerhalb der Treg-IL-2- und Th17-IL-17-Achsen als wesentliche Treiber der Immunregulationsstörung. **Teil I** dieser Dissertation präsentiert eine detaillierte Immunphänotypisierung und zeigt, dass ein IL-2-deprivierter Treg Phänotyp früh im Krankheitsverlauf auftritt, noch bevor die klinische Diagnose einer etablierten SSc gestellt wird. Die beobachtete schrittweise Reduktion der CD25hi Treg und die erhöhte Präsenz von CD25- und CD25lo Treg Subsets sowie die Reduktion der CD39+ Zellen bezogen auf CD25+ Treg, heben die entscheidende Rolle der geringen Verfügbarkeit von IL-2 bei der Dysregulation der Immunhomöostase hervor. Darüber hinaus zeigte eine auf maschinellem Lernen basierende Random Forest-Analyse, dass Th17-Zellen zusammen mit CD25lo Treg und proliferierenden Ki67+ Zellen bezogen auf CD25- Treg, zu den signifikantesten immunologischen Merkmalen gehören, die VEDOSS von etablierter SSc unterscheiden. Diese Ergebnisse deuten darauf hin, dass das Zusammenspiel zwischen der Treg-IL-2 und der Th17-IL-17 Achse zur Progression von präklinischen Immunregulationsstörungen zu fulminanten Autoimmunpathologien beiträgt. Bemerkenswerterweise deuten erhöhte IL-17A Spiegel im Serum bei etablierter SSc, trotz gleicher Th17 Frequenzen im Vergleich zu VEDOSS Patienten, auf zusätzliche regulatorische Mechanismen hin, die die IL-17 Sekretion beeinflussen. Das Chemokin CXCL10, das durch die IL-17A Signalkaskade induziert wird und für die Förderung vaskulärer Pathologien bekannt ist, zeigte eine schrittweise Zunahme in der Frequenz von VEDOSS zu SSc und korrelierte mit der Krankheitsaktivität, was auf die Beteiligung an frühen Immunregulationsstörungen und fibrotischen Veränderungen hinweist. Bei etablierter SSc korrelierten die CXCL10 Spiegel auch mit Anti-GPCR Autoantikörperlevels, was es mit humoraler Autoimmunität verbindet. Neben CXCL10 waren auch die entzündungsfördernden Proteine CCL20 und MCP1 sowie der Matrixremodellierungs-Faktor MMP1 in ihren Leveln signifikant erhöht in SSc im Vergleich zu VEDOSS Patienten, was eine Verschiebung hin zu pathogenen Entzündungen und Gewebeschäden weiter unterstützt. Über die immunologischen Ergebnisse hinaus hebt diese Studie das Potenzial von maschinellen Lernalgorithmen für die frühe Krankheitsklas-

sifikation hervor. Die Integration von immunphänotypischen, Autoantikörper- und Zytokinprofilen in einer Multi-Omics-Analyse ermöglichte eine hohe Klassifikationsgenauigkeit zwischen VEDOSS- und SSc-Patienten. Dies unterstreicht die Umsetzbarkeit von KI-gesteuerten Diagnosen für die frühzeitige Krankheitsdetektion und Patientenstratifizierung. **Teil II** dieser Dissertation untersucht einen möglichen therapeutischen Ansatz zur Wiederherstellung des Immungleichgewichts durch *in vitro* Treg-Wiederherstellung mittels Stimulation mit niedrig dosiertem rekombinantem IL-2. Diese Stimulation führte erfolgreich zur Wiederherstellung der CD25hi Treg-Frequenzen, was sich mit früheren Studien aus anderen Autoimmunerkrankungen wie dem systemischen Lupus erythematodes deckt. Diese Ergebnisse liefern eine starke Grundlage für klinische Studien, die die Wirksamkeit der niedrig dosierten IL-2-Therapie bei SSc-Patienten zur Wiederherstellung der Treg-Homöostase und funktionellen Aktivität untersuchen. Bemerkenswerterweise erhöhte dieser Ansatz nicht einfach die Gesamtpopulation der Treg, die CD25 unzureichend als Merkmal des IL-2 Mangels exprimieren, sondern verschob die bestehenden Treg zu einem CD25hi Treg-Phänotyp, was durch das Fehlen von Frequenzänderungen in Ki67+ Zellen bezogen auf CD25+ Treg Subsets belegt wurde. Diese Ergebnisse zeigen, dass IL-2 selektiv die Funktion immunregulatorischer Zellen anregt, anstatt ungezielt Treg Proliferation zu induzieren und so die Immunhomöostase bewahrt. Angesichts des frühen Auftretens einer Störung der Treg-IL-2 Achse bei VEDOSS Patienten legt diese Studie nahe, dass eine niedrig dosierte IL-2 Therapie als präventive Strategie bei VEDOSS Patienten in Betracht gezogen werden sollte. Durch das Eingreifen in dieser frühen Krankheitsphase kann die IL-2 Supplementierung helfen, das nachgewiesene Treg/Tcon Ungleichgewicht wiederherzustellen und möglicherweise das Fortschreiten der Krankheit sowie Organschäden zu verhindern. Diese Ergebnisse unterstreichen die Notwendigkeit zukünftiger klinischer Studien, die die Wirksamkeit der niedrig dosierten IL-2-Therapie bei VEDOSS-Patienten evaluieren und ihre potenzielle Rolle bei der Verzögerung des Übergangs in eine etablierte Krankheitsphase untersuchen. Diese Dissertation beleuchtet die immunologischen Mechanismen, die der frühen und etablierten SSc zugrunde liegen und offenbart zentrale Wege, die den Krankheitsverlauf vorantreiben. Zudem werden potenzielle neue therapeutische und diagnostische Ansatzpunkte aufgezeigt.

Contents

CHAPTER 1

Introduction

The first chapter introduces the characterization, pathophysiology and molecular mechanisms of established Systemic Sclerosis, while also providing a comprehensive overview of current knowledge on the early stages of the disease.

1.1 Systemic Sclerosis

Systemic sclerosis (SSc), also known as scleroderma, is a rare autoimmune connective tissue disease that is essentially characterized by endothelial dysfunction leading to small vessel vasculopathy, fibroblast dysfunction resulting in excessive collagen production and fibrosis and immunological dysregulations resulting in organ inflammation [1 –3]. Since SSc has the highest morbidity and mortality rate among all rheumatic diseases and is considered as incurable, a targeted and individualized therapy is indispensable to achieve a sustained remission status in order to improve mortality and prognosis [4, 5].

1.1.1 Epidemiology and clinical characterization

The overall global prevalence of SSc is 17.6 per 100,000 with an incidence rate of 1.4 per 100,000 persons per year [6]. It is most common in North America, southern Europe and Australia and affects more women than men, with a ratio of between 3:1 and 14:1. The average age at diagnosis or disease onset is around 50 years [7 –9]. While it is more common in women, it has a more severe course in men, with complications in the affected organs, such as the heart and lungs and a higher mortality rate [10].

Based on the LeRoy criteria, SSc can be divided into a limited cutaneous (lcSSc) and diffuse cutaneous (dcSSc) form, with dcSSc occurring less frequently with a ratio of 2:3, while both are associated with particular organ manifestations [11, 12]. The main diagnostic criterion for dcSSc is skin involvement proximal to the elbow or knee joints, whereas lcSSc only affects the skin distal to these joints [12, 13]. For the general diagnosis of established SSc, in 2013, a joint committee of the American College of Rheumatology (ACR) and the European Alliance of Associations for Rheumatology (EULAR) developed new classification criteria for SSc, since the 1980 ACR classification criteria lack sensitivity for early SSc and lcSSc [14]. The specific categories including the criteria are listed in the table 1.1 below. Patients with a total score of $\geq$9 are classified as having definite systemic sclerosis.

Table 1.1 : ACR/EULAR2013 criteria for the classification of systemic sclerosis.

Item	**Sub-item(s)**	**Score**
Skin thickening of the fingers of both hands (*sufficient criterion*)	–	9
Skin thickening of the fingers	Puffy fingers	2
	Sclerodactyly of the fingers	4
Fingertip lesions	Digital tip ulcers	2
	Fingertip pitting scars	3
Telangiectasia	–	2
Abnormal nailfold capillaries	–	2
Pulmonary arterial hypertension and/or interstitial lung disease (*maximum score is 2*)	Pulmonary arterial hypertension	2
	Interstitial lung disease	2
Raynaud's phenomenon	–	3
SSc-related autoantibodies (*maximum score is 3*)	Anti-Centromer	3
	Anti–Topoisomerase I	3
	Anti–RNA polymerase III	3

As shown in the table of diagnostic criteria, autoantibody (aAb) profiles play a decisive role in clinical characterization and prognosis of SSc. The most important ones include anti-centromere, anti-topoisomerase I (Scl-70) and anti-RNA polymerase III antibodies, each of which is associated with different disease phenotypes and progression. For instance, anti-centromere antibodies are strongly associated with lcSSc and correlate with a higher risk of pulmonary arterial hypertension (PAH), but a lower risk of severe skin and lung fibrosis. In contrast, anti-topoisomerase I antibodies are predominantly associated with dcSSc and indicate a higher likelihood of lung involvement and progressive skin thickening [15 –17]. The presence of these aAbs serves as a predictor of disease course and potential complications, thereby guiding individualized therapeutic strategies. In addition to the necessity of clear and standardized diagnostic criteria, accurately assessing disease severity is crucial for setting up individualized therapeutic options for SSc patients. Given that SSc is predominantly characterized by pathological skin fibrosis and vasculopathic manifestations, particularly Raynaud's phenomenon (RP), a standardized skin scoring system has been developed to evaluate and monitor disease progression [18]. The modified Rodnan

Skin Score (mRSS) provides an objective assessment of skin thickness, grading it on a scale from 0 (normal) to 3 (severe) across 17 defined anatomical regions, thereby enabling a systematic evaluation of cutaneous involvement in SSc [19, 20]. Although the mRSS serves as a surrogate marker of disease severity and has been correlated with internal organ involvement, it is not sufficient to reflect true disease activity due to the heterogeneity of systemic manifestations [19]. To solve this and incorporate various clinical and laboratory parameters in addition to the mRSS, the EUSTAR (European Scleroderma Trials and Research) group has developed the EUSTAR Activity Index (EUSTAR-AI) to assess and implement a more complex and comprehensive disease activity score for SSc patients. In addition to the mRSS, the EUSTAR-AI includes active digital ulceration, tendon friction rubs (TFR) and C-reactive protein (CRP) levels as well as the diffusing lung capacity for carbon monoxide (DLCO). This index has proven to be more powerful compared to previous indices and more accurately reflects overall disease activity in SSc patients [21].

1.1.2 Organ involvement

Since SSc is a heterogeneous and systemic autoimmune disease affecting multiple organ systems, the extent and severity of organ involvement significantly influence patient prognosis and therapeutic strategies. Although virtually any organ system can be involved in the disease process, the fibrotic and vascular pulmonary manifestations of SSc, including interstitial lung disease (ILD), PAH and cardiac involvement, are the leading cause of morbidity and mortality. [3, 22]. The overall pulmonary involvement among patients with established SSc is about 50–56% [23, 24]. ILD, characterized by progressive fibrosis of lung tissue, leads to impaired gas exchange and respiratory failure and PAH results from vascular remodeling and increased pulmonary vascular resistance, culminating in right heart failure if untreated [25, 26]. Cardiac involvement is clinically present in approximately 10 to 30% of patients with SSc and includes myocardial fibrosis, conduction system abnormalities and pericardial disease [22]. Myocardial fibrosis can lead to diastolic dysfunction, arrhythmias and, in severe cases, heart failure and ambulatory monitoring as well as cardiac imaging are essential for early identification and intervention [27 –29]. Renal complications, particularly scleroderma renal crisis (SRC), is a severe complication of SSc and the prevalence varies among SSc patients with an estimated average around 5%. SRC is characterized by the sudden onset of hypertension and rapidly progressive renal failure. While SRC was once a common and often fatal complication, its incidence has decreased with improved management strategies [30, 31]. The use of angiotensin-converting enzyme (ACE) inhibitors has significantly improved outcomes

for patients with SRC. Regular monitoring of blood pressure and renal function is crucial for early detection and management of renal involvement [30, 32]. The gastrointestinal (GI) tract is frequently affected already in early SSc and present in up to 90% of patients, while the manifestations are ranging from dysmotility of the esophagus to malabsorption syndromes [33, 34]. Esophageal involvement can lead to gastroesophageal reflux disease (GERD) and dysphagia due to reduced peristalsis and lower esophageal sphincter incompetence. Involvement of the small intestine may result in bacterial overgrowth and malabsorption, while colonic involvement can cause pseudo-obstruction and severe constipation. Management includes dietary modifications, prokinetic agents and, in some cases, antibiotics for bacterial overgrowth [35, 36]. Involvement of the musculoskeletal system is a rather frequent complaint of SSc patients (between 40-80%) and associated with a severe course of the disease. The manifestations include joint contractures, tendon friction rubs and myopathy [37, 38]. Skin thickening over joints can lead to reduced mobility and significant functional impairment. Generally, muscular weakness is the main symptom, optionally accompanied by muscle inflammation reflected by an increase in creatine kinase (CK) levels. Physical therapy and occupational interventions are vital to maintain joint function and quality of life [37, 39].
The systemic and complex organ involvement in SSc requires a comprehensive and multidisciplinary approach to patient care. Early detection and targeted management of organ-specific manifestations are crucial in improving outcomes and reducing disease-related morbidity and mortality.

1.1.3 Molecular pathogenesis

The pathogenesis of SSc involves a complex interplay between vasculopathy, autoimmunity, including the production of aAbs targeting G protein-coupled receptors (GPCRs) and fibrosis (fig. 1.1). On the one hand, an underlying genetic predisposition is assumed which, in combination with endogenous and exogenous triggers, can lead to phenotypic changes promoting the onset of the disease. On the other hand, however, negative environmental influences such as air pollution, toxic oils or nutrition are also thought to play a significant role [40 –42]. Microvascular injury and vasculopathy are considered as early and pivotal events in SSc. Endothelial cell damage leads to apoptosis and increased vascular permeability, which are, together with perivascular inflammation and platelet aggregation, often found in patients with SSc prior to the onset of disease [43, 44]. This endothelial dysfunction is associated with impaired angiogenesis and vasculogenesis, despite elevated levels of pro-angiogenic factors such as platelet-derived growth factor (PDGF) and vascular endothelial growth

factor (VEGF) [45]. Due to increased levels of endothelin-1 (ET-1) and von Willebrand factor (vWF), along with reduced levels of nitric oxide (NO) and endothelial nitric oxide synthase, an imbalance between vasodilation and vasoconstriction favors vasoconstriction, contributing to tissue ischemia and the generation of reactive oxygen species [46, 47]. These vascular abnormalities are further exacerbated by the presence of anti-endothelial cell antibodies, particularly those targeting the endothelin-1 type A receptor (ETAR) and the angiotensin II type 1 receptor (AT1R), which target endothelial cells and may contribute to disease progression. [48, 49]. The excessive production of aAbs against endogenous GPCRs by differentiated plasma cells is triggered by a dysregulated regulatory mechanism of innate and adaptive immunity and contributes to the autoimmune component of the disease. These autoimmune mechanisms are central to SSc pathogenesis, since the damaged endothelial cells overexpress adhesion molecules, chemokines and cytokines, attracting leukocytes, mainly T helper (Th) 2 and Th17 cells which infiltrate the tissue and further promote inflammation [50]. Additionally, the altered expression of cell adhesion molecules and chemokines attracts monocytes which differentiate to macrophages and accelerate fibro-proliferative vascular remodeling and tissue fibrosis [51, 52]. At this stage, the main endogenous regulator and inhibitor of uncontrolled adaptive immune responses, namely regulatory T cells, may have lost their suppressive capacity and ongoing tissue infiltration cannot be controlled [53]. Due to this process of excessive triggering of the adaptive immune system, over time there is a loss of tolerance to various antigens, such as topoisomerase I, RNA polymerase III and Centromer. Together with aAbs targeting GPCR signaling pathways, vascular tone, fibroblast activity and immune responses become severely dysregulated, further contributing to the vasculopathy and especially fibrosis that characterize SSc [54 –56].

One of the pathophysiological hallmarks of SSc is tissue fibrosis, which results from excessive deposition of extracellular matrix (ECM) components, particularly collagen, leading to defective tissue repair and organ dysfunction. [57]. The serum of SSc patients is enriched with a great variety of pro-fibrotic cytokines secreted by different immune cells, including interleukin (IL)-1, IL-6, IL-17 and transforming growth factor beta (TGFβ) and correlate positively with the production of these ECM components [58]. Fibroblasts are subsequently recruited and differentiate upon stimulation by the pro-fibrotic molecules into myofibroblasts. These cells are characterized by the expression of α-smooth muscle actin (α-SMA) and have an enhanced capacity for collagen synthesis, contributing to tissue fibrosis [59, 60]. In this context, an altered Th1/Th2 balance, with a dominance of Th2, promotes immune dysregulation and fibrosis in established SSc. T follicular helper (Tfh) cells are also enriched in SSc, contributing

to B cell activation and aAb production, while CD8+ T cells participate by secreting IL-13 and infiltrating fibrotic tissues [61 –63]. B cells further exacerbate fibrosis through antigen presentation, aAb production and cytokine secretion, notably IL-6, which promotes fibroblast activation [61, 64]. In summary, fibrosis in SSc is driven by a complex interaction network of pro-fibrotic cytokines, epigenetic modifications and dysregulated signaling pathways that promote fibroblast activation and excessive ECM deposition. Understanding these mechanisms is crucial for developing targeted and individualized therapies to mitigate tissue fibrosis and improve clinical outcomes in SSc patients [65].

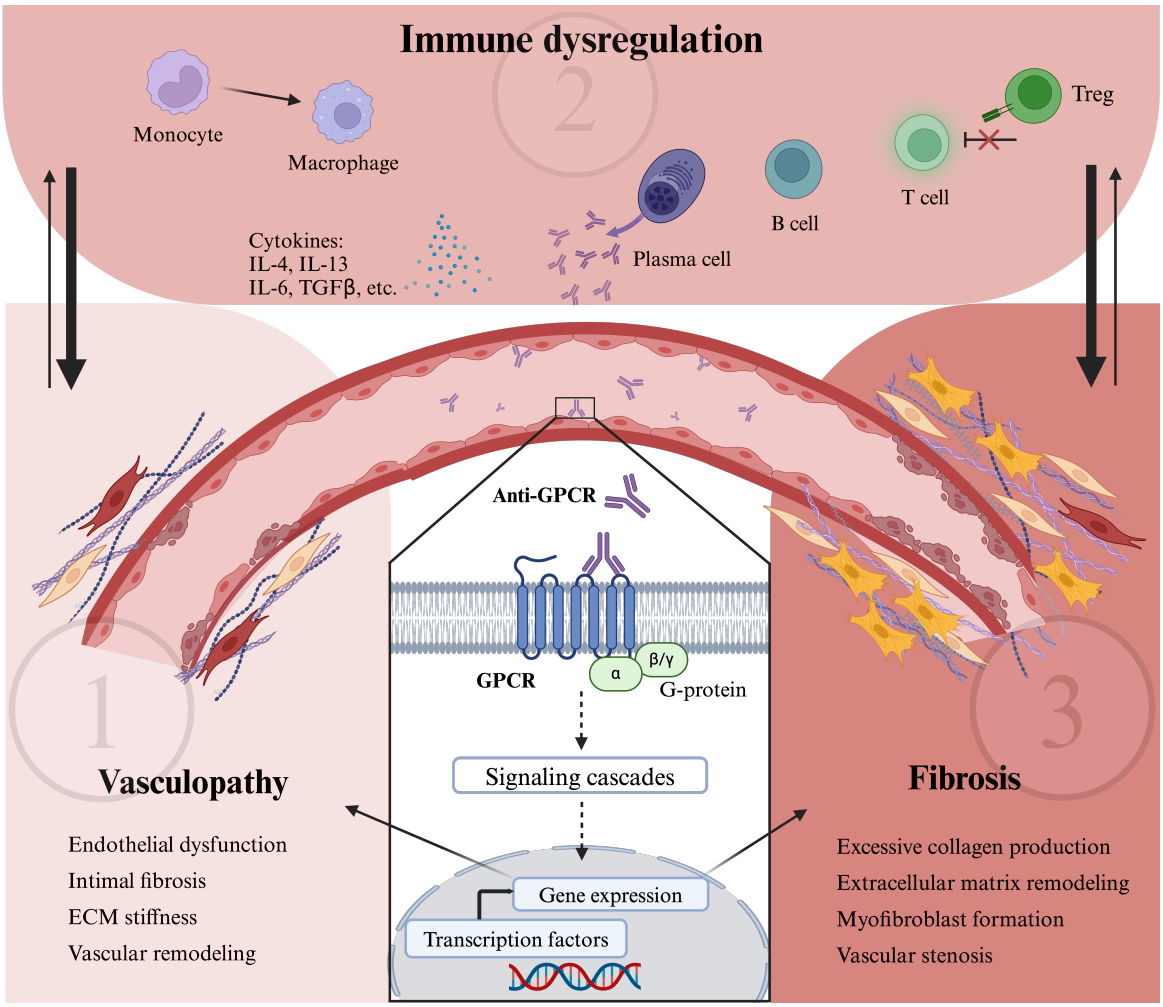

Figure 1.1 : Pathogenesis of SSc involves a complex interplay of vasculopathy, immune responses and fibrosis. Endothelial dysfunction and vascular remodeling initiate the disease (1), followed by immune dysregulation with cytokine release and aAb production (2). Anti-GPCR antibodies contribute to abnormal signaling, promoting excessive collagen deposition and extracellular matrix remodeling, leading to fibrosis and vascular stenosis (3). Illustration modified according to Akbarzadeh et al. [66]

1.1.4 Anti-GPCR and anti-GF autoantibodies

GPCRs contain seven membrane-spanning helices and constitute one of the largest families of integral membrane receptors in the human body. They are expressed in several different tissues by various immune cells and mediate physiological responses by converting extracellular signals into intracellular actions. Most disease-associated anti-GPCR aAbs develop through B cell activation and subsequent antibody maturation and emerging evidence suggests these aAbs play a significant role in the pathogenesis of SSc, particularly due to their agonistic nature [67, 68]. Among the most studied anti-GPCR aAbs in SSc are those targeting the AT1R and endothelin receptor type A (ETAR), both of which are implicated in vascular dysfunction and fibrosis [69]. Additionally, aAbs against C-X-C motif chemokine receptor 3 (CXCR3) have been linked to increased cardiovascular risk [70]. These aAbs may contribute to SSc pathology by promoting endothelial cell activation, vascular remodeling and fibroblast dysregulation. Furthermore, their presence has been associated with disease severity and vasculopathic complications such as PAH [66, 71, 72]. The generation of these high-affinity aAbs can be driven by various mechanisms, including molecular mimicry (cross-reactivity between foreign and self-antigens), post-translational modifications altering self-antigens, increased exposure of normally sequestered antigens due to tissue damage, elevated inflammatory signaling, or impairments in self-tolerance mechanisms [67, 73, 74]. In addition to anti-GPCR aAbs, aAbs against certain growth factors (GF) also play an essential role in the pathogenesis of SSc, as they interfere with the proliferation and differentiation of various cell types and disturb proper regulation [75, 76]. Notably, aAbs against the fibroblast growth factor (FGF) have been implicated in fibroblast activation and excessive extracellular matrix deposition, contributing to fibrosis [77, 78]. Given their role in disease mechanisms, both anti-GPCR and anti-GF aAbs are being explored as potential biomarkers for SSc progression and therapeutic targets. The following table 1.2 provides an overview of the key GPCRs and GFs that have been shown to be targeted by aAbs in SSc and other related diseases and are important for this study.

Table 1.2 : Relevant GPCRs and GFs in SSc.

Full Name (abbreviation)	**Physiological function**	**Source**
Angiotensin II Type 1 Receptor (AT1R)	Mediates the effects of angiotensin II, regulating blood pressure and fluid balance.	[79]
Endothelin Receptor Type A (ETAR)	Binds endothelin-1, leading to vasoconstriction and cell proliferation.	[80]
Beta-1 Adrenergic Receptor (β1)	Responds to epinephrine and norepinephrine, increasing cardiac output.	[81]
Beta-2 Adrenergic Receptor (β2)	Mediates smooth muscle relaxation and bronchodilation in response to catecholamines.	[82]
Muscarinic Acetylcholine Receptor M4 (M4)	Involved in modulating neurotransmission in the central nervous system.	[83]
Muscarinic Acetylcholine Receptor M3 (M3)	Regulates smooth muscle contraction and glandular secretion.	[84]
C-X-C Chemokine Receptor Type 3 (CXCR3)	Directs migration of immune cells to inflammation sites.	[70]
Protease-Activated Receptor 1 (PAR1)	Activated by thrombin, playing a role in coagulation and inflammation.	[85]
Protease-Activated Receptor 2 (PAR2)	Responds to trypsin and other proteases, involved in inflammatory responses.	[86]
Placenta Growth Factor (PlGF)	Promotes angiogenesis and is involved in pathological conditions.	[87]
Fibroblast Growth Factor 2 (FGF2)	Stimulates cell growth, has an antifibrotic effect and promotes tissue repair.	[88]

1.1.5 Regulatory CD4+ T cells

Regulatory CD4+ T cells (Treg) that express the lineage-specific transcription factor forkhead box P3 (FoxP3), play a crucial role in the maintenance of peripheral self-tolerance and are essential for the prevention and control of excessive inflammation and autoimmune reactions through various molecular and cellular interactions (fig. 1.2) [89, 90]. The majority of endogenous Treg originate from the thymus as functionally unique and mature T cell subpopulation and only a small fraction differentiate *de novo* from naive T cells after antigen exposure upon activation of innate immune response [91]. CD4+FoxP3+ Treg recognize auto-antigens through their T cell receptor and are vital for regulating the activation and proliferation of auto-reactive T cells and other potentially harmful immune cells in peripheral lymphoid organs [92]. As early as 1995, Sakaguchi et al. found that certain subgroups of CD4+ T cells constitutively express the high-affinity IL-2 receptor alpha chain (CD25) and were proved to be highly immunosuppressive. These CD4+FoxP3+CD25+ Treg population has been consistently shown to display suppressive properties across species and in multiple disease models [89, 93]. The interaction between the ligand IL-2 and its corresponding trimeric receptor, consisting of the three receptor chains CD25, CD122 and CD132, is critical for the development, proliferation and survival of Treg and maintains immune homeostasis. Expression of this receptor enables Treg to effectively compete for IL-2 and limit its availability to conventional T cells (Tcon), which also requires IL-2 as a growth factor, thus modulating and inhibiting immune responses. This mechanism highlights the dual role of IL-2 in supporting Treg-mediated suppression and controlling the expansion of effector T cells, including CD4+ T cells, CD8+ T cells, B cells and NK cells [94, 95]. Mechanisms of Treg-mediated immunosuppression include the production of inhibitory cytokines and growth factors such as IL-10 and transforming growth factor beta (TGFβ) that inhibit the production of pro-inflammatory cytokines and dampen the activation and proliferation of Tcon [96, 97]. Further, Treg express additional inhibitory molecules critical for their suppressive function, including cytotoxic T-lymphocyte-associated protein 4 (CTLA4), which downregulates immune responses by competing with CD28 for costimulatory signals and the ectonucleotidase CD39, which hydrolyzes ATP to generate immunosuppressive adenosine. [97 –99].

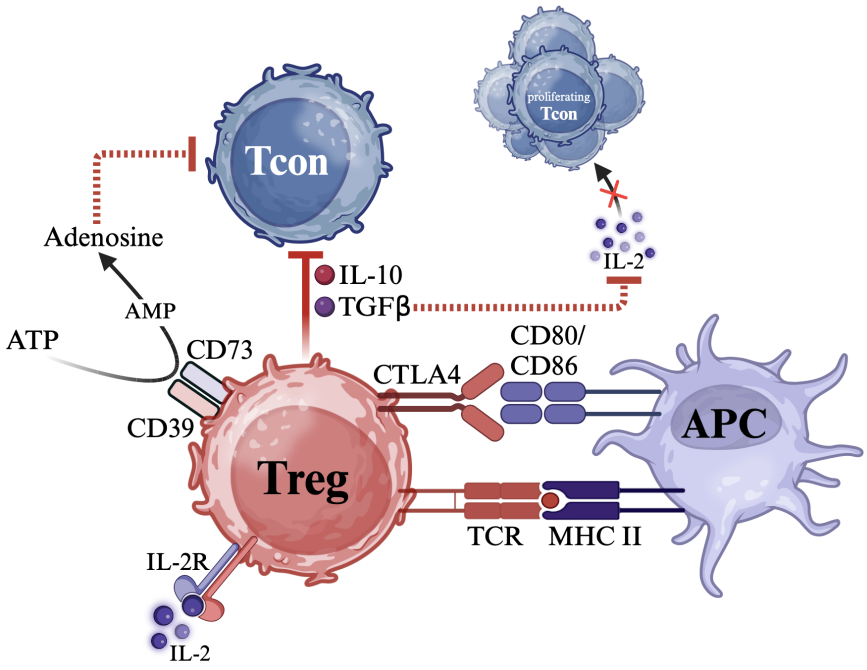

Figure 1.2 : Treg-mediated immunosuppressive mechanisms. Treg inhibit Tcon activity by the release of IL-10 and TGFβ and interfere with Tcon proliferation via consumption and depletion of the growth factor IL-2. Interaction of CD39 and CD72 generates extracellular adenosine from adenosine triphosphate (ATP) leading to an inhibition of T-cell activation. APC = antigen presenting cell. Illustration modified according to Goldmann et al. [97].

Based on the physiological function of Treg in the maintenance of immune homeostasis and tolerance, Treg dysregulations are known to play essential roles in the preclinical progression of autoimmune diseases. In systemic lupus erythematosus (SLE), a systemic autoimmune disease, Humrich and colleagues demonstrated in an *in vivo* lupus-prone mouse model that an acquired deficiency of IL-2 levels occur already early in disease progression and promotes Treg defects and Tcon hyperactivity, leading to an imbalance between Treg and Tcon [100, 101]. This finding underscored the critical role of IL-2 in maintaining Treg function and immune equilibrium. Consecutively, Spee-Mayer et al. stimulated PBMC of SLE patients with low-dose IL-2 and successfully restored levels of highly active CD25hi Treg [102]. Building on these *in vivo* and *in vitro* insights, again Humrich et al. demonstrated in proof of concept trials the suitability of applying low-dose IL-2 therapy to restore and expand functionally active Treg directly in SLE patients. Initially, a single-centre phase 1 and 2a clinical trial in SLE patients demonstrated good tolerability of low-dose IL-2 therapy, along with the selective expansion of Treg which was accompanied by a reduction in disease activity in the majority of treated patients. A subsequent randomized, placebo-controlled

phase II trial confirmed that selective expansion of Treg by low-dose IL-2 therapy is safe and clinically effective in patient with active SLE. [103, 104].
Transitioning to SSc, the role of Treg remains less well-defined. Despite some similarities between SLE and SSc, particularly regarding autoimmune characteristics, the general understanding of Treg phenotype and function in SSc is limited. The majority of the studies reported decreased frequencies and impaired function of peripheral Treg which may contribute to SSc pathogenesis [105, 106]. Further, it has been pointed out that a decreased production of TGFβ and IL-10 marks the diminished inhibitory ability of Treg [105, 107]. However, there is neither evidence nor a detailed characterization of functional Treg subsets as well as the availability of IL-2 in SSc, so further research is needed to clarify their exact role in disease progression and identify potential therapeutic targets.

1.1.6 Conventional CD4+ T cell subsets

CD4+ Tcon cells are an important subset of T lymphocytes which coordinate adaptive immune responses by assisting other immune cells in recognizing and eliminating pathogens. They accomplish this through cell-cell interactions and by secreting cytokines that regulate the activity of B cells, cytotoxic T cells (Tc), macrophages and other immune components. Under physiological conditions, CD4+ Tcons provide a balance between pro-inflammatory and anti-inflammatory signals, ensuring an effective defense against infection while preventing excessive immune activation that could lead to tissue damage or autoimmunity [108, 109]. This balance is maintained by distinct Th subsets, each with specialized functions, including, among others, Th1, Th2, Th9, Th17 [110, 111]. Dysregulation of certain subsets is a key feature of autoimmune diseases, including SSc, which may occur already early during disease development.
Th1 cells, traditionally associated with pro-inflammatory responses and interferon-gamma (IFN-γ) production, activate macrophages and promote cellular immunity. Their differentiation from naive T cells and function are largely driven by the lineage-specific transcription factor called T-box expressed in T cells (T-bet), which regulates the expression of key Th1-associated cytokines and receptors [112]. In SSc, the role of Th1 cells is complex and somehow contradictory. For instance, a study by Bălănescu et al. found higher serum IFN-γ levels in SSc patients compared to healthy controls, with elevated levels associated with pulmonary hypertension (PH) [113]. Conversely, a longitudinal analysis observed that serum levels of IL-12, a Th1-inducing cytokine, were initially lower in SSc patients compared to controls but increased significantly over time during disease progression [114].

In addition to the pro-inflammatory Th1 subset, Th2 cell-associated cytokines trigger a variety of immune responses essential for defending against parasitic infections and promoting tissue repair [115–117]. However, these same cytokines also contribute to the dysregulated immune reactions seen in several allergies. The differentiation and function of Th2 cells are primarily regulated by the lineage-specific transcription factor GATA Binding Protein 3 (GATA-3), which controls the expression of key Th2 cytokines [118]. These cytokines, including IL-4, IL-5, IL-6, IL-9 and IL-13, work together to drive B cell proliferation and immunoglobulin class switching [117, 119]. In SSc, Th2 cells make up the majority of all T cell subgroups in the peripheral blood and are also detectable in the affected tissues [119, 120]. It is implicated that an altered balance between Th1 and Th2 cytokines promotes organ manifestations and that polarized Th2 cells abundantly secrete IL-4, IL-5 and IL-13 that enhance collagen deposition [120–122].

Another Tcon subset are Th9 cells, which express IL-9 but not the key signature cytokines of other Th cell subsets and is not as well investigated as the others mentioned before. However, Th9 cells have been implicated in autoimmune conditions but their specific role in SSc remains unclear, but emerging evidence suggests they may contribute to inflammation and fibrosis [123–125].

Th17 cells, characterized by the production of IL-17, play an important role in promoting inflammation by recruiting neutrophils and enhancing inflammatory responses. Their differentiation and function are primarily regulated by the lineage-specific transcription factor RAR-related orphan receptor-γ-t (RORγt), which drives the expression of IL-17 and other pro-inflammatory cytokines, contributing to both protective immunity and autoimmune pathology [126, 127]. Additionally, the maintenance and proliferation of Th17 cells is regulated by the pro-inflammatory cytokine IL-6, which supports their survival and expansion [128]. In SSc, elevated levels of Th17 cells and increased secretion IL-17A compared to healthy controls have been reported in several studies [129, 130]. Further, these elevation of Th17 cells correlate with increased skin and lung fibrosis. Studies have shown that IL-17 can stimulate fibroblast proliferation and collagen production, contributing to severe deposition promoting the fibrotic processes in SSc [131, 132].

T follicular helper (Tfh) cells are essential for memory B cell differentiation, antibody maturation and germinal center formation. Their development is driven by the transcription factor B-cell lymphoma 6 (Bcl-6), which regulates genes critical for Tfh cell identity, migration and interaction with B cells [133]. A key effector function of Tfh cells is the production of IL-21, a cytokine that enhances B cell proliferation, supports antibody class switching and sustains germinal center responses [134–136]. In

SSc, Sahinoglu et al. found that elevated levels of Tfh cells are associated with lung involvement and stated a correlation between Tfh cell levels and the severity of the lung manifestation [137]. Correspondingly, T peripheral helper (Tph) cells, a subset distinct from Tfh cells, play a similar role in physiological and pathological context. Tph cells recruit B cells in inflamed peripheral tissue by the secretion of high levels of C-X-C motif chemokine 13 (CXCL13), a chemokine that binds to CXCR5 [138, 139]. In SSc, it had been shown that the patients exhibited elevated frequencies of Tph cells in the peripheral blood and proved the connection towards PAH progression [140].
Memory T cells are essential for immune responses upon re-exposure to foreign antigens. Effector memory T cells (EM T) rapidly infiltrate inflamed peripheral tissues and exert immediate effector functions, providing immune protection. In contrast, central memory T cells (CM T) primarily reside in lymphoid organs and circulate in the blood. While they exhibit little to no immediate effector function, they possess a high proliferative capacity and can differentiate into effector cells upon antigenic stimulation. [141 –143]. In SSc, alterations in the distribution and function of these memory T cell subsets have been hardly observed, but thought to potentially influence disease chronicity and progression. Almanzar et al. showed that memory T cells and effectors are producers of intracellular tumor necrosis factor alpha (TNFα), IL-13 and IL-4, particularly in dcSSc and contribute therefore to disease progression [144, 145].

1.1.7 Natural killer cells

Natural killer (NK) cells are critical components of the innate immune system, unique for their ability to identify and eliminate virally infected and malignant cells without prior sensitization and without expressing antigen-specific receptors [146]. Beyond their cytotoxic functions, NK cells secrete various cytokines that modulate the activity of other immune cells, thereby bridging innate and adaptive immunity. Therefore, NK cells are primarily categorized in two main subsets based on the relative expression of the adhesion molecule CD56: CD56hi and CD56lo NK cells [147]. Jacobs et al. showed that the cytotoxic activity of CD56lo NK cells is significantly higher than that of CD56hi NK cells and that they contain larger amounts of granzymes, perforin and cytolytic granules [148]. The opposite is observed for cytokine production, with CD56hi NK cells being the most efficient producers. The key cytokines they release include IFN-γ, TNFα, IL-10 and IL-13 [149, 150]. Similar to Treg, the cytokine and growth factor IL-2 has been found to be critical for the development of NK cells, particularly for CD56hi NK cells [150]. A recent study proved that this subset

increases in patients who are treated daily with a low dose of IL-2, pronouncing its importance for maintaining physiological conditions [151].
In the context of SSc, several alterations in NK cell subsets have been described in the past years. Notably, patients with SSc exhibit a reduction in total NK cells [152]. More precisely, NK cells in SSc patients display deficient cytotoxic activity and granzyme B secretion, potentially contributing to immunological abnormalities by insufficient elimination of autoreactive immune cells [153]. Additionally, natural killer T (NK T) cells, a unique subset expressing both NK cell markers and T cell receptors, have been implicated in the pathogenesis of SSc. Their persistent downregulation, seen in SSc patients, may contribute to the abnormal immune responses, in particular in early disease stages [154].

1.1.8 B cells and plasma cells

B cells represent an indispensable component of the adaptive immune system and are primarily responsible for the production of antibodies that contribute to systemic inflammatory responses, thus neutralizing pathogens. In addition to antibody secretion, B cells also serve as antigen-presenting cells (APCs) and secrete cytokines, thereby controlling immune responses and influencing the local environment at sites of infection and inflammation [155, 156]. This versatile role ensures a robust immune response against infections while maintaining immune homeostasis. In addition, B cells undergo a complex developmental process that gives rise to different phenotypes that divide these subgroups into different functional units [157]. Besides naive B cells, which have not yet encountered their specific antigen, transitional B cells represent an intermediate stage between immature and mature and migrate from the bone marrow to peripheral lymphoid tissues [157]. This stage is crucial for central tolerance, ensuring that self-reactive B cells are eliminated to prevent autoimmunity [158]. Already several years ago, human studies indicate that various autoimmune diseases may exhibit a weakened regulation of transitional B cells, resulting in heightened autoreactivity within the mature naive B cell compartment leading to a progressive imbalance, promoting uncontrolled inflammation [159, 160]. B lymphocytes that have previously been exposed to antigens and have undergone activation and differentiation into memory B cells are able to trigger a rapid and robust secondary immune response upon re-exposure to the same antigen [161]. Following antigen stimulation, B cells can further differentiate into plasma cells, which serve as primary producers of large quantities of antibodies and are considered as terminal differentiation step of mature B cells with an extended lifespan. They mediate long-term humoral immunity and contribute to immune memory [162, 163]. Further, they do not longer express

the typical B cell surface marker CD19. Instead, plasma cells express a range of certain surface markers and proteins associated with their antibody secretion function [164].

In SSc, the frequency of the relative count of B cells in peripheral blood mononuclear cells (PBMC) is increased compared to healthy controls and is therefore increasingly recognized for its significant role in disease pathogenesis and promotion of organ manifestations [165]. For instance, a study by De Santis et al. demonstrated increased levels of CD19+ B cells in bronchoalveolar lavage fluid (BAL) in the lung of SSc patients which could also be correlated with worsening of pulmonary function [166]. Correspondingly, these CD19+ B cells induce SSc-specific aAb production targeting self-antigens. As already described earlier, the presence of these aAbs is a hallmark of SSc and is associated with specific clinical features. For instance, the prevalence of anti-nuclear antibodies (ANA) in SSc patients is greater than 90% [167]. Besides the uncontrolled aAb secretion, dysregulated B cells secrete various pro-inflammatory and pro-fibrotic cytokines. Research done by Dumoitier et al. showed that activated B cells in SSc patients secrete high levels of IL-6 and TGFβ and the IL-6 concentrations were correlated positively with the mRSS score, suggesting a crucial involvement of B cells in fibrosis progression [64]. These few findings already pronounce the essential role of B cells in SSc pathogenesis, highlighting the need for further investigations to better understand their contribution to disease progression.

1.1.9 Monocyte subsets

Monocytes are a subset of circulating innate immune cells that play a crucial role in host defense, tissue repair and immune regulation. They develop from hematopoietic stem cells in the bone marrow and enter the bloodstream as precursor cells before differentiating into macrophages or dendritic cells during migration into the tissue. [168]. These cells have a high plasticity and can take on different functional phenotypes, which are divided into classical, intermediate and non-classical monocytes, based on their expression of the cell surface proteins CD14 and CD16. [169]. Classical monocytes are the largest subset. They migrate to sites of infection, guided by monocyte-specific chemokines such as CCL2 (MCP-1) and CCL7 (MCP-3), where they differentiate into inflammatory macrophages, while non-classical monocytes patrol blood vessels and contribute to vascular homeostasis and debris removal [170 –172]. Intermediate monocytes possess inflammatory characteristics and are thought to not actively patrol the vasculature. Generally, monocytes participate in immune responses by producing cytokines such as TNFα, IL-12, IL-6 and IL-1β, which con-

tribute to general functionality, inflammation and immune cell recruitment [171, 173, 174]. Additionally, monocytes play an essential role in fibrosis and wound healing by secreting TGF-β and other pro-fibrotic mediators that regulate extracellular matrix (ECM) remodeling [175].
In SSc, these profibrotic properties are implicated in the pathogenesis and associated with the development of ILD. Mathai et al. proved the existence of this profibrotic phenotype in SSc-ILD patients, which is characterized by the expression of CD163 and by enhanced secretion of CCL18 and IL-10 [176]. In addition, these monocytes differentiate into myofibroblast-like cells characterized by their collagen and α-SMA expression and contribute to excessive collagen deposition in the affected organs [177]. In addition, ECM remodeling and increased fibroblast activation in SSc patients is accompanied by excessive secretion of IL-6 and TGF-β, leading to skin and organ fibrosis [178, 179].

1.1.10 Current therapeutic options

The pathophysiology of SSc remains incompletely understood due to the heterogeneous interactions between the endothelium, the innate immune system and the adaptive immune system. Consequently, no curative or long-term effective treatment is currently available. [180]. The central therapeutic approach for treating the inflammatory manifestations is immunosuppression and the choice of appropriate medication depends on the severity and activity of the disease as well as the comorbidities [181]. The most important medications are listed in Table 1.3 below.

Table 1.3 : Most important medications for SSc treatment. IMPDH, Inosine 5'-monophosphate dehydrogenase. Sources: [181 –183]

Treatment type	**Medications**	**Function**
Immunosuppression	Mycophenolate mofetil	IMPDH inhibitor
	Azathioprine	Purine nucleotide inhibitors
	Cyclophosphamide	DNA alkylating agent
	Rituximab	anti-CD20 antibody
	Tocilizumab	IL-6 receptor antagonist
	Methotrexate	Folate pathway inhibitor
Anti-fibrotic	Nintedanib	Tyrosine kinase inhibitor
Vasoactive	Bosentan	Endothelin receptor antagonist
	Iloprost	Prostacyclin analog
	Nifedipin	Calcium channel blocker

1.2 Very early diagnosis of systemic sclerosis

The introduction of the early disease stage classification named Very Early Diagnosis Of Systemic Sclerosis (VEDOSS) aims to identify SSc patients at its earliest stage, long before clinically relevant organ manifestations and damage occur. Early detection is crucial for improving patient outcomes, as SSc is often progressive and associated with high morbidity and mortality. However, the lack of reliable biomarkers to predict disease progression poses a challenge, making the decision to start treatment in the earliest stages of the disease a constant dilemma [184]. VEDOSS focuses on recognizing potential predictive factors of disease progression in asymptomatic or mildly symptomatic individuals at risk of developing established SSc, thereby enabling timely interventions that can modify disease progression and prevent irreversible damage [185, 186]. Advances in biomarker identification, imaging techniques and risk stratification models are instrumental in identifying those at high risk, leading to a more personalized and effective therapeutic approach.

1.2.1 Clinical characterization

The concept VEDOSS was introduced already in 2009 by the EUSTAR society to identify individuals at high risk of developing SSc before irreversible organ damage occurs [187]. Since the traditional ACR/EULAR classification criteria for SSc are designed to diagnose established disease, therefore lacking sensitivity for detecting early stages of disease, particularly those without significant skin or organ involvement. To address this gap, the VEDOSS approach emphasizes early identification through targeted clinical assessments and biomarker discovery approaches [188]. The VEDOSS criteria take into account RP, puffy fingers (PF) and the presence of specific ANAs, which are associated with the development of early-stage SSc [189, 190]. By facilitating earlier recognition and closer monitoring of at-risk individuals, the VEDOSS framework provides an opportunity for timely intervention, potentially altering disease progression and improving long-term outcomes [191].

1.2.2 Pathophysiological alterations

Little is known about pathological changes in components involved in the regulation of the innate and adaptive immune response in VEDOSS patients. However, emerging evidence suggests that early immune dysregulation, for instance promoting excessive fibroblast activation, are already present in VEDOSS, potentially driving disease progression toward established SSc. A study by Ross et al. investigated skin biopsies

from VEDOSS patients and revealed increased collagen deposition, thickened skin and an infiltration of CD45+ immune cells. Furthermore, dermal fibroblasts from these patients exhibit increased expression of profibrotic genes and heightened contractility, similar to fibroblasts in established SSc [192].

Regarding early organ involvement, first evidence suggests that cardiac manifestations can occur already at the very early stages of SSc. Case reports highlight three distinct clinical manifestations of cardiac dysfunction in VEDOSS patients, mirroring the three key pathogenic mechanisms of SSc: vascular abnormalities, inflammation and fibrosis. Summarized, these cases illustrate cardiac inflammation and fibrosis as comorbidities associated with VEDOSS [193]. Similarly, involvement of the gastrointestinal tract (GIT) is also observed in VEDOSS patients, with early signs of dysmotility and other GIT disturbances reflecting the systemic nature of the disease even at its initial stages [194].

Despite not fulfilling the classification criteria for SSc, VEDOSS patients exhibit significant immune dysregulation and early fibrosis, both in tissues and serum markers. Further research is needed to identify key biomarkers that are responsible for disease progression to effectively develop preventive strategies.

1.3 Aims of this study

This thesis primarily aims to explore immune dysregulation at a cellular and molecular level observed in patients with VEDOSS and their contribution to the progression towards an established SSc. The central hypothesis of this study is that immunological changes and imbalances occur already in the very early stages of the disease. These early alterations, reflected in key biomarkers, are believed to drive inflammation and tissue remodeling processes, thereby promoting disease progression. To investigate this, five task units were established:

I

Performing a detailed immunophenotyping of blood from VEDOSS and SSc patients, as well as healthy controls, to identify disease-specific immune alterations, investigate their correlation with clinical markers and disease activity indices and to implement a machine-learning prediction algorithm to distinguish between healthy individuals, VEDOSS and SSc patients based on immune cell composition.

II

Employing an Olink® proteomics approach, combined with multivariate and pathway analyses, using sera from VEDOSS and SSc patients, measuring >90 inflammatory proteins to identify distinct inflammatory signatures that could serve as novel biomarkers for disease stratification and progression.

III

Measuring the levels of several known SSc-associated aAbs targeting GPCRs and GFs and correlating them with clinical parameters, immune cell frequencies and proteomic profile to identify potential links between aAb profiles, immune dysregulation and disease severity.

IV

Applying a multi-omics approach by integrating all data layers - immunophenotypic, aAb and proteomic data - to improve disease classification, to identify key markers driving disease progression and refine predictive models for distinguishing VEDOSS from SSc patients at multiple levels.

V

Conducting functional stimulation experiments on PBMC from SSc patients to investigate the potential of low-dose IL-2 on restoring Treg activity by assessing gene and protein expression changes and evaluating whether targeted interventions can reestablish Treg homeostasis in SSc.

Overall, this study aims to provide new insights into early immunological changes in VEDOSS patients, offering potential strategies for early diagnosis, risk stratification and future therapeutic interventions to prevent disease progression.

CHAPTER 2

Materials and devices

The second chapter presents all the materials and electronic devices used for this thesis.

2.1 Chemicals and buffers

Table 2.1 : Chemicals and buffers used.

Denotation	**Supplier**
Acetic acid 100%	Merck, Darmstadt, DE
Agarose Wide Range	SERVA, Heidelberg, DE
Ampuwa® H_2O	Fresenius Kabi, Bad Homburg, DE
BioColl® separating solution	Bio&SELL, Feucht, DE
Bovine serum albumin	Sigma, Taufkirchen, DE
CytoFLEX Sheath Fluid	Beckman Coulter, Brea, US
Dimethyl sulfoxide	Sigma-Aldrich, St. Louis, US
Ethanol absolut	Th.Geyer, Warschau, PL
Ethylenediaminetetraacetic acid	Sigma-Aldrich, St. Louis, US
FlowClean Cleaning Agent	Beckman Coulter, Brea, US
Phosphate Buffered Saline	Biowest, Bradenton, US
Tris(hydroxymethyl)-aminomethane	SERVA, Heidelberg, DE
β-Mercaptoethanol	Sigma, St. Louis, US
70% Ethanol	Roth, Karlsruhe, DE

2.2 Cell culture media and additives

Table 2.2 : Cell culture media and additives used.

Denotation	**Supplier**
FCS Ultra Low Endotoxin	Bio&SELL, Feucht, DE
L-Glutamine 200 mM	PAN-Biotech, Aidenbach, DE
Penicillin-Streptomycin Solution	Biowest, Bradenton, US
VLE RPMI 1640	Bio&SELL, Feucht, DE

2.3 Recombinant proteins

Table 2.3 : Recombinant proteins used.

Denotation	**Source**	**Supplier**
Recombinant Human IL-2	*E. coli*	R&D Systems, Minneapolis, US

2.4 Antibodies

Table 2.4 : Antibodies used for multicolor flow cytometry.

Antigen	**Conjugate**	**Clone**	**Supplier**
CD3	AF700	UCHT1	Biolegend, San Diego, US
CD3	APC-Cy7	UCHT1	Biolegend, San Diego, US
CD4	PerCP/Cy5.5	RPA-T4	Biolegend, San Diego, US
CD4	PerCP	RPA-T4	Biolegend, San Diego, US
CD39	PE/Cy7	A1	Biolegend, San Diego, US
CD25	PE	BC96	Biolegend, San Diego, US
CD25	PE	M-A251	BD, New Jersey, US
CD127	BV510	A019D5	Biolegend, San Diego, US
CD137	BV650	4B4-1	Biolegend, San Diego, US
FoxP3	AF647	206D	Biolegend, San Diego, US
Helios	AF488	22F6	Biolegend, San Diego, US
CTLA4	PE/Dazzle594	BNI3	Biolegend, San Diego, US
Ki-67	BV421	Ki-67	Biolegend, San Diego, US
LAG3	BV605	11C3C65	Biolegend, San Diego, US
PD-1	PE/Dazzle594	EH12.2H7	Biolegend, San Diego, US
CCR7	PE	G043H7	Biolegend, San Diego, US
CCR4	PE/Cy7	L291H4	Biolegend, San Diego, US
CD28	APC/Cy7	CD28.2	Biolegend, San Diego, US
CD45RO	BV510	UCHL1	Biolegend, San Diego, US
CXCR5	BV605	J252D4	Biolegend, San Diego, US
CCR6	BV650	G034E3	Biolegend, San Diego, US
CXCR3	FITC	G025H7	Biolegend, San Diego, US
CD19	FITC	HIB19	Biolegend, San Diego, US
CD268	PE	11C1	Biolegend, San Diego, US
CD27	APC	O323	Biolegend, San Diego, US
CD20	BV510	2H7	Biolegend, San Diego, US
CD24	PE/Dazzle594	ML5	Biolegend, San Diego, US
CD38	BV605	HB-7	Biolegend, San Diego, US
HLA-DR	BV650	L243	Biolegend, San Diego, US
IgM	PerCP/Cy5.5	MHM-88	Biolegend, San Diego, US
IgD	PE/Cy7	IA6-2	Biolegend, San Diego, US
CD8a	BV510	RPA-T8	Biolegend, San Diego, US
CD11c	PE/Dazzle594	Bu15	Biolegend, San Diego, US

CD56	PE/Cy7	Qa17A16	Biolegend, San Diego, US
CD16	APC/Cy7	3G8	Biolegend, San Diego, US
CD14	FITC	63D3	Biolegend, San Diego, US
Mouse IgG1 Isotype	PE	MOPC-21	Biolegend, San Diego, US
TruStain FcX™	-	-	Biolegend, San Diego, US
Zombie NIR™	APC-Cy7	-	Biolegend, San Diego, US

2.5 Oligonucleotides

Table 2.5 : Primer systems for qPCR analysis.

Target gene	**Sequence (sense/antisense)**	**Amplificate size [bp]**
IL2RA	GAGATCCCACACGCCACATT TGTTCCGAGTGGCAGAGCTT	181
IL2RB	CCTGTGTCTGGAGCCAAGAT GGGTGACGATGTCAACTGTG	183
IL2RG	GGATGGGCAGAAACGCTACA ATTCGGGGCATCGTCCGTT	231
IL10	GTTCTTTGGGGAGCCAACAG GCTCCCTGGTTTCTCTTCCT	155
CTLA4	AGGCAACGGAACCCAGATTT GCTCTGTTGGGGGCATTTTC	197
ENTPD1	ACTATCGAGTCCCCAGATAATGC CCTGATCCTTCCCATAGCACAA	97
18sRNA	GTAACCCGTTGAACCCCATT CCATCCAATCGGTAGTAGCG	151

2.6 Commercial reaction systems

Table 2.6 : Commercial reaction systems used.

Denotation	**Supplier**
CytoFLEX Daily QC Fluorospheres	Beckman Coulter, Brea, US
FOXP3 Fix/Perm Buffer Set	Biolegend, San Diego, US
GelRed® Nucleic Acid Stain	Biotium, Fremont, US
iScript™ cDNA Synthesis Kit	Bio-Rad, Hercules, US
LEGEND MAX™ IL-10 ELISA Kit	Biolegend, San Diego, US

LEGEND MAX™ Total TGF-β1 ELISA Kit	Biolegend, San Diego, US
NucleoSpin RNA II Kit	Macherey-Nagel, Düren, DE
Olink® Target 96 Inflammation Kit	Olink, Uppsala, SE
QuantiBRITE™ PE* Kit	BD, New Jersey, US
SsoAdvanced Universal SYBR Green Supermix	Bio-Rad, Hercules, US
VersaComp Antibody Capture Bead Kit	Beckman Coulter, Brea, US

2.7 Consumable material

Table 2.7 : Consumable materials used.

Denotation	**Supplier**
Acella 50 sample carrier	Anvajo, Dresden, DE
Combitips Advanced® (5 ml)	Eppendorf, Hamburg, DE
Centrifuge Tube 15 ml	Th.Geyer, Warschau, PL
CryoPure Tube (1.6 ml)	Sarstedt, Nürnbrecht, DE
Disposal bag	Sarstedt, Nürnbrecht, DE
Filter tip (2.5, 20, 100, 1000 µl)	Sarstedt, Nürnbrecht, DE
Hard-Shell® 96 microplate	Bio-Rad, Hercules, US
Leucosep tube 50 ml	Greiner bio-one, Frickenhausen, DE
Microseal®	Bio-Rad, Hercules, US
Microtest plate 96 well	Sarstedt, Nürnbrecht, DE
Microtube (0.2, 1.5, 2, 5 ml)	Sarstedt, Nürnbrecht, DE
Multi-Task Cleaning Cloths	WypAll, Dallas, US
Polystyrene Round-Bottom Tube (5 ml)	Falcon, New York, US
S-Monovette® (1.6 mg EDTA/ml)	Sarstedt, Nürnbrecht, DE
S-Monovette® (clot activator)	Sarstedt, Nürnbrecht, DE
Serological pipette (5, 10, 25 ml)	Sarstedt, Nürnbrecht, DE
Tube (15, 50 ml)	Sarstedt, Nürnbrecht, DE
48 well plate (suspension cells)	Sarstedt, Nürnbrecht, DE

2.8 Devices

Table 2.8 : Electronic devices used.

Denotation	**Supplier**
BioMark	Fluidigm, San Francisco, US
BioPhotometer	Eppendorf SE, Hamburg, DE
Biosafety cabinet class II type a/b3	NuAire, Plymouth, US
Biosafety cabinet Safe 2020	Thermo Fisher Scientific, San Diego, US
Centrifuge Allegra™ X-12R	Beckman Coulter, Brea, US
CO_2 Incubator	Binder, Tuttlingen, DE
Centrifuge Micro Star 30 R	VWR, Radnor, US
Centrifuge Universal 320 R	Hettich, Kirchlengern, DE
CytoFLEX S	Beckman Coulter, Brea, US
FACSCanto II	BD, New Jersey, US
Fluidlab R-300	Anvajo, Dresden, DE
Gel Doc® EZ Imager	Bio-Rad, Hercules, US
Ice machine	Manitowoc Ice, Manitowoc, US
Innova U360 Ultra Low Freezer	Eppendorf, Hamburg, DE
Juno™	Fluidigm, San Francisco, US
Laboratory Balance L2200	Sartorius, Goettingen, DE
Laboratory heating bath	GFL, Burgwedel, DE
LaminAir HV PCR	Holten, Allerød, DK
Microwave	Sharp, Sakai, JP
Mini-centrifuge Plus	Biozym, Hessisch Oldendorf, DE
Multipette® Xstream	Eppendorf, Hamburg, DE
Olympus B061 microscope	Olympus, Tokio, JP
Pipetus®	Hirschmann, Rankweil, AT
Power Pack P25	Biometra, Goettingen, DE
qTOWER^3 G	Analytik Jena, Jena, DE
Roller mixer RM10	CAT, Ballrechten-Dottingen, DE
SpectraMax® iD5	Molecular Devices, San José, US
T3 Thermocycler	Biometra, Göttingen, DE
Vacusafe	Integra Biosciences, Zizers, CH
Vortex Genius 3	IKA-Werke, Staufen, DE
Vortex REAX 2000	Heidolph, Schwabach, DE

2.9 Software

Table 2.9 : Software used.

Denotation	**Supplier**
BioRender	Science Suite, Toronto, CA
CytExpert	Beckman Coulter, Brea, US
FACSDiva™	BD, New Jersey, US
FlowJo™ 10.9	BD, New Jersey, US
GraphPad Prism 9.0	GraphPad Software, San Diego, US
Image Lab 4.1	Bio-Rad, Hercules, US
Jamovi 2.3	jamovi, AUS
Kaluza 2.1	Beckman Coulter, Brea, US
LaTeX Overleaf	Digital Science UK Ltd, London, UK
Microsoft Office	Microsoft Corp, Redmond, US
NPX Signature	Olink, Uppsala, SE
qPCRsoft 4.1	Analytik Jena, Jena, DE
RStudio	Posit PBC, Boston, US
Zotero 7.0.7	Corporation for Digital Scholarship, Fairfax, US

CHAPTER 3

Methods

The third chapter outlines the methods used in this thesis. That includes multicolor flow cytometry from isolated human PBMC and the analysis of the pro-inflammatory proteome. Functionally, rIL-2 stimulation of PBMC with subsequent protein and gene expression analysis is described, followed by advanced statistical methods to analyze multi-omics datasets.

3.1 Cell biological methods

3.1.1 Ethical approval

Isolation of primary cells from human blood was performed after written consent according to local and international guidelines (Declaration of Helsinki). The isolation and further experimental procedures were ethically approved by the ethics commission of the University of Lübeck (approval reference number 2023-113).

3.1.2 Isolation of PBMC and serum from peripheral blood

PBMC isolation from EDTA blood is a crucial step in immunological studies, as these cells play a key role in various immune responses [195]. A careful isolation process is essential to ensure the viability and purity of PBMC for downstream applications such as flow cytometry, functional assays and RNA analysis.
Initially, 15 ml of BioColl® was pipetted into the filter within a Leucosep tube. The tube was then centrifuged at 1000 × g for 30 seconds at room temperature (RT) to allow the BioColl® to settle below the filter. Blood samples, collected in EDTA-coated tubes (which contain ethylenediaminetetraacetic acid as an anticoagulant to prevent clotting and preserve blood cells), were then carefully added onto the filter without disturbing the BioColl® layer and phosphate-buffered saline (PBS) was used to fill the tube to a final volume of 50 ml. Following this, the sample was centrifuged at 800 × g for 15 minutes at RT, with the brake switched off after centrifugation. The yellowish/white cloudy PBMC layer was then carefully transferred into a new 50 ml tube using a 1000 µl pipette. After topping up with PBS to a 50 ml volume, the sample was centrifuged again at 650 × g for 10 minutes at RT, this time with the brake on. The supernatant was discarded and the pellet was resuspended by scratching the tube against the stand. PBS was added to bring the volume back to 50 ml and the sample was centrifuged once more at 650 × g for 6 minutes at RT. The supernatant was discarded again and the remaining pellet was resuspended in either 1000 µl warm RPMI medium or phosphate-buffered saline (PBS) + 0.5% bovine serum albumin (BSA), depending on the further applications.

In contrast, serum tubes, which are coated with a clot activator to promote blood coagulation, were used to facilitate the separation of serum from the cellular components during centrifugation. Following collection, the blood was centrifuged at 2350 × g for 10 minutes at RT. The resulting serum was carefully aliquoted into 2 ml tubes for further analysis or storage at -80°C.

3.1.3 Multicolor flow cytometry

Flow cytometry is a technology for rapidly analysing individual cells or particles that are directed into the centre of a narrow, fast-flowing stream of buffered salt-based solution and arranged in such a way that there is a large distance between the cells in relation to their diameter. Each cell is analysed for visible light scattering and one or more fluorescence parameters. The scattering of visible light is measured in two different directions: in the forward direction (forward scatter or FSC), which can indicate the relative size of the cell and in the 90° direction (side scatter or SSC), which indicates the internal complexity or granularity of the cell. Light scattering is independent of fluorescence. Samples are prepared for fluorescence measurement by staining with fluorescent conjugated antibodies. Flow cytometers use lasers with different excitation wavelengths as light sources to generate both scattered and fluorescent light signals, which are read by detectors such as photodiodes or photomultipliers. These signals are converted into electronic signals that are analysed by a computer. Cell populations can be analysed based on their fluorescence or light scattering characteristics [196, 197].

Following the successful isolation of PBMC, the cell pellet was resuspended in 1000 µl of PBS supplemented with 0.5% BSA. To block nonspecific binding to Fc receptors (FcRs), 40 µl of *Human TruStain FcX™* was added. FcRs are commonly expressed on various immune cells, including monocytes, granulocytes, B cells and dendritic cells and can lead to false-positive or false-negative results due to Fc-mediated antibody binding [198]. By blocking FcRs, this step ensures that only specific antibody-antigen interactions are measured. The single-cell suspension (SCS) was vortexed and incubated for 10 minutes in the dark at RT. For samples not requiring a live/dead dye, a 50 µl aliquot of the SCS was separated for further panel staining. For the remaining SCS, 1.5 µl of Zombie NIR, a viability dye, was added. The suspension was vortexed and incubated for 10 minutes in the dark at RT to allow live/dead discrimination. Next, antibodies specific to surface proteins, according to the panel setup (see fig. 3.1 and 3.6), were added to the 50 µl SCS in 2 µl volumes per antibody. The reaction tubes were vortexed and incubated for 15 minutes in the dark at RT to ensure proper binding of the antibodies to their respective surface antigens. Following this, 1 ml of PBS was added to each sample and the suspension was centrifuged at 650 × g for 6 minutes at 4°C. After discarding the supernatant, the two panels containing only cell surface markers were resuspended in 300 µl of PBS/0.5% BSA and transferred to a transparent 96-well plate for measurement.

For panels requiring intracellular staining, fixation and permeabilization were performed using the *True-Nuclear™ Transcription Factor Buffer* set from Biolegend.

First, 200 µl of 1× Fix Buffer was added to each sample, followed by vortexing and incubation for 45 minutes in the dark at RT. After fixation, the samples were centrifuged at 650 × g for 6 minutes at 4°C and the supernatant was discarded. For permeabilization, 200 µl of 1× Perm Buffer was added and the samples were centrifuged at 650 × g for 6 minutes at 4°C. This permeabilization step was repeated two additional times for a total of three washes. After the final wash, 100 µl of Perm Buffer was added, along with 2 µl of antibodies targeting intracellular proteins, specific to the respective panel. The samples were vortexed and incubated for 30 minutes in the dark at RT to allow for intracellular staining. The samples were then centrifuged at 650 × g for 6 minutes at 4°C, the supernatant was discarded and the cells were resuspended in 300 µl of PBS/0.5% BSA. The prepared samples were either transferred to a 96-well plate or round-bottom tubes for flow cytometric analysis. Flow cytometry was conducted using either the Beckman Coulter *CytoFLEX S* or the BD *FACSCanto™ II*, selected based on the experimental setup and utilizing the specific acquisition settings described in figures 3.1 and 3.6. In some approaches, an additional measurement with *QuantiBRITE™ PE** beads was performed following the initial acquisition for quantifying PE-coupled molecules per cell. After the measurement, panel-specific gating strategies were developed to clearly identify the frequencies of immune cell types and visualised in the following figures (fig. 3.2 - 3.7). As an internal control for the identification and discrimination of low expressed markers on cells, either Fluoresence Minus One (FMO) samples or isotype control antibodies were used.

A

Intracellular				Surface			
Treg Panel		Tcon Panel		B cell Panel		Myeloid Panel	
CD3	AF700	**CD3**	AF700	**CD3**	AF700	**CD3**	AF700
CD4	PerCP/Cy5.5	**CD4**	PerCP/Cy5.5	**CD19**	FITC	**CD4**	PerCP/Cy5.5
CD39	PE/Cy7	**PD-1**	PE-Dazzle	**CD268**	PE	**CD8**	BV510
CD25	PE	**CCR7**	PE	**CD27**	APC	**CD11c**	PE-Dazzle
CD127	BV510	**CCR4**	PE/Cy7	**CD20**	BV510	**CD56**	PE/Cy7
CD137	BV650	**FoxP3**	AF647	**CD24**	PE-Dazzle	**CD16**	APC-Cy7
FoxP3	AF647	**CD28**	APC/Cy7	**CD38**	BV605	**CD25**	PE
Helios	AF488	**CD45RO**	BV510	**HLA-DR**	BV650	**HLA-DR**	BV650
CTLA4	PE-Dazzle	**Ki-67**	BV421	**IgM**	PerCP/Cy5.5	**CD38**	BV605
Ki-67	BV421	**CXCR5**	BV605	**IgD**	PE-Cy7	**CD14**	FITC
Zombie	APC-Cy7	**CCR6**	BV650				
LAG3	BV605	**CXCR3**	FITC				

B

Events to record	Time to record [s]	Volume to record [µl]	Sample flow rate [µl/min]
400,000 events	330	250	30

Figure 3.1 : Flow cytometry panels and acquisition conditions for immunophenotyping. **A**) The Treg and Tcon panel had to be prepared according to the intranuclear staining protocol, whereas the B cell and Myeloid panel only contained markers that are expressed on the cell surface. **B**) The acquisition conditions were applied to each sample, with the main objective of each measurement being to capture the 400,000 events.

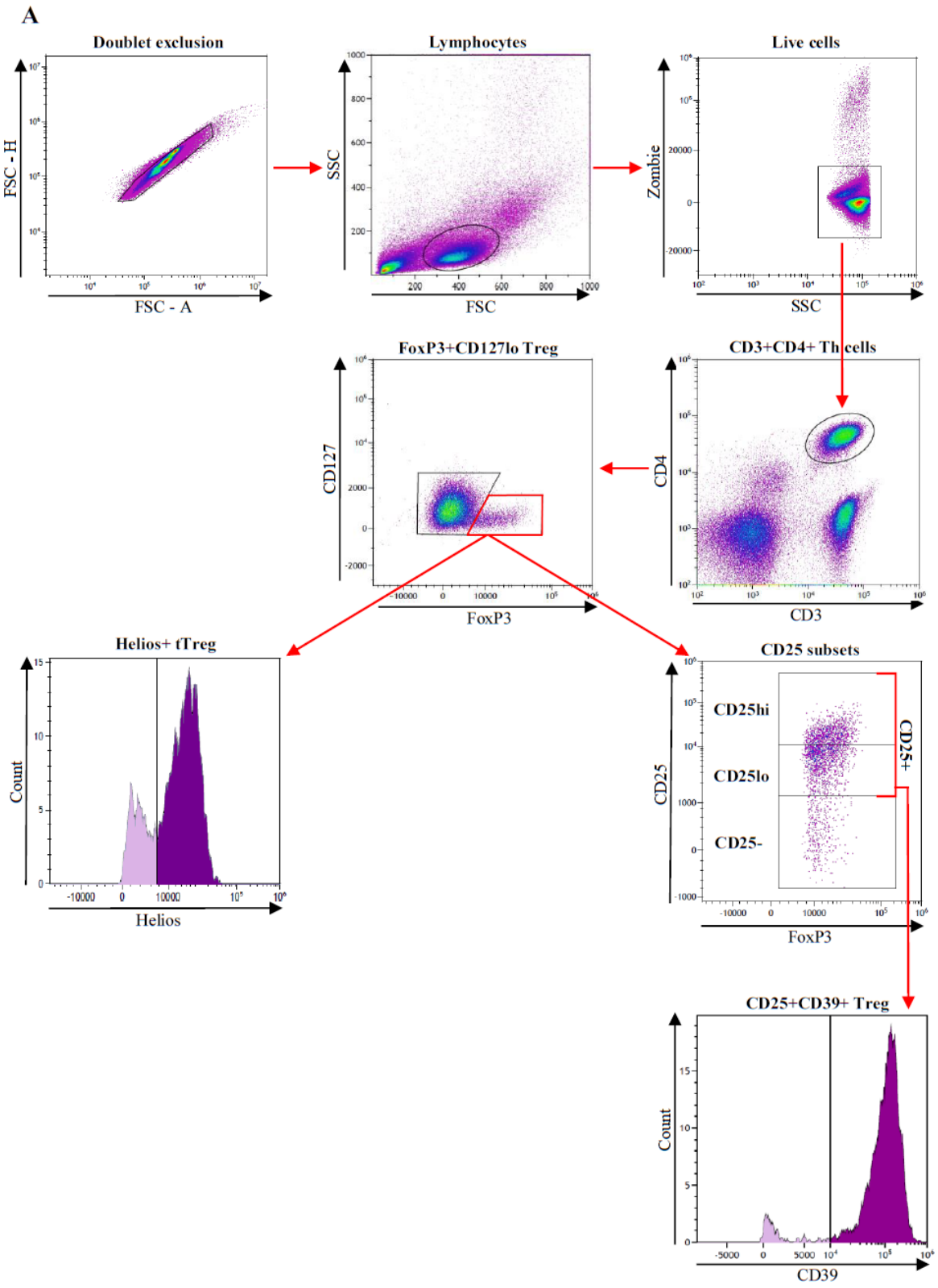
A
Doublet exclusion
FSC - H
FSC - A
Lymphocytes
SSC
FSC
Live cells
Zombie
SSC
FoxP3+CD127lo Treg
CD127
FoxP3
CD3+CD4+ Th cells
CD4
CD3
Helios+ tTreg
Count
Helios
CD25 subsets
CD25hi
CD25lo
CD25-
CD25+
CD25
FoxP3
CD25+CD39+ Treg
Count
CD39

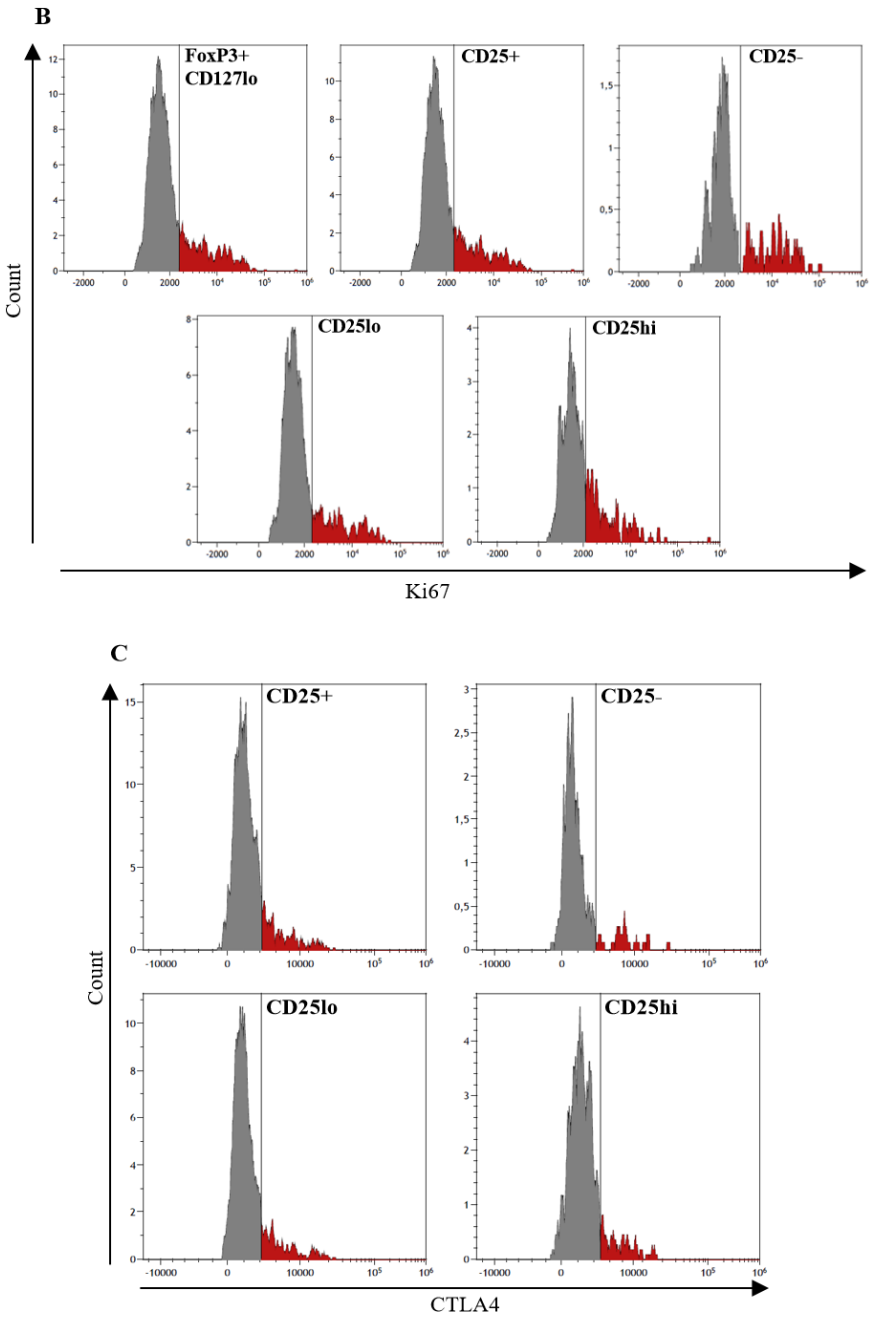

Figure 3.2 : Treg gating strategy. **A**) Before Treg-specific gatings, duplicates and dead cells were excluded, as well as FoxP3- cells. **B**) Gating of the Ki67+ cells among Treg and CD25 subsets. Threshold value for positivity was determined on the basis of a Ki67 FMO control sample. **C**) Gating of the CTLA4+ cells among CD25 subsets. Threshold value for positivity was determined on the basis of a CTLA4+ FMO control sample.

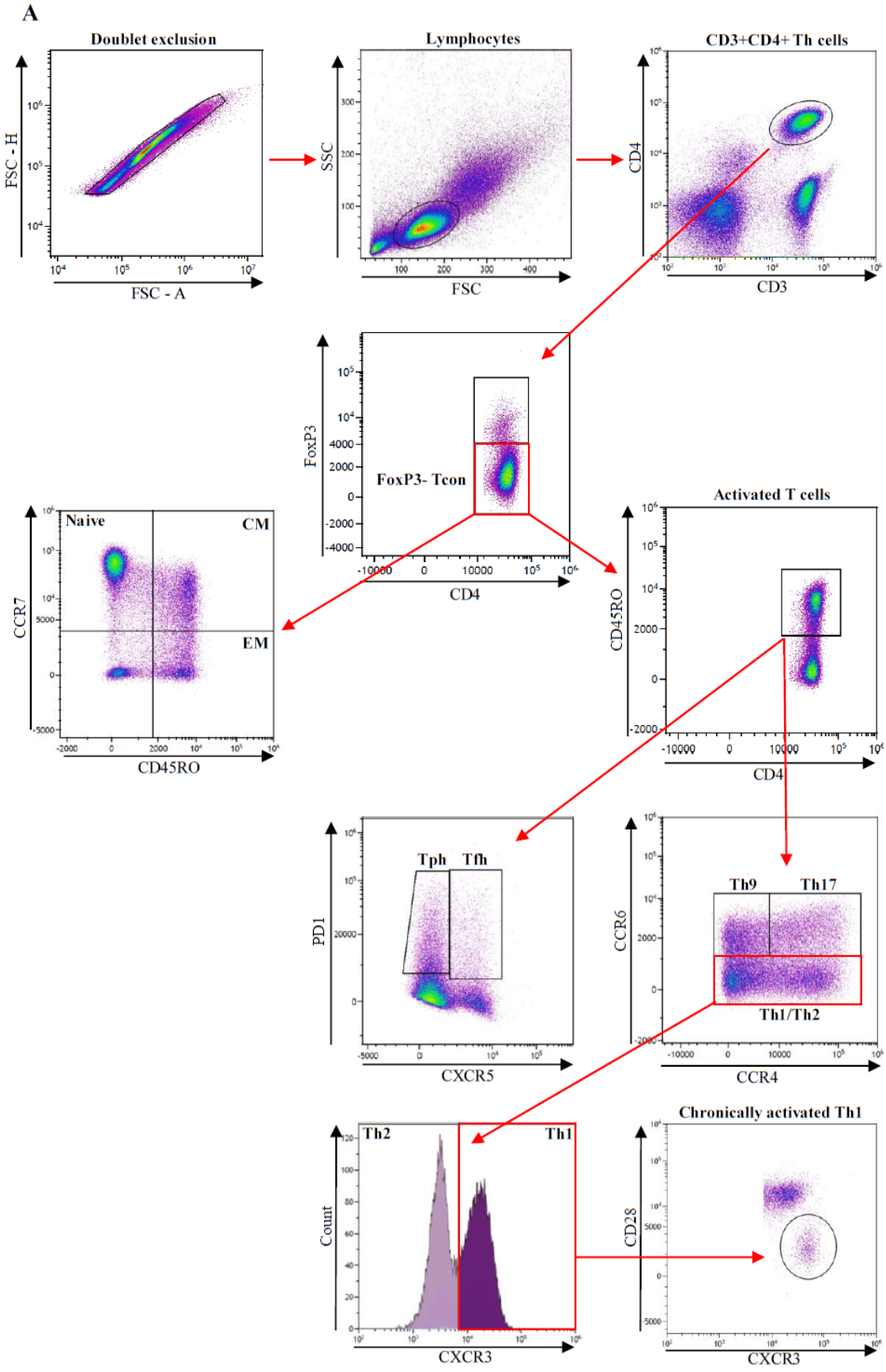
A
Doublet exclusion
FSC - H
FSC - A
Lymphocytes
SSC
FSC
CD3+CD4+ Th cells
CD4
CD3
FoxP3
FoxP3- Tcon
CD4
Naive
CM
EM
CCR7
CD45RO
Activated T cells
CD45RO
CD4
Tph
Tfh
PD1
CXCR5
Th9
Th17
Th1/Th2
CCR6
CCR4
Th2
Th1
Count
CXCR3
Chronically activated Th1
CD28
CXCR3

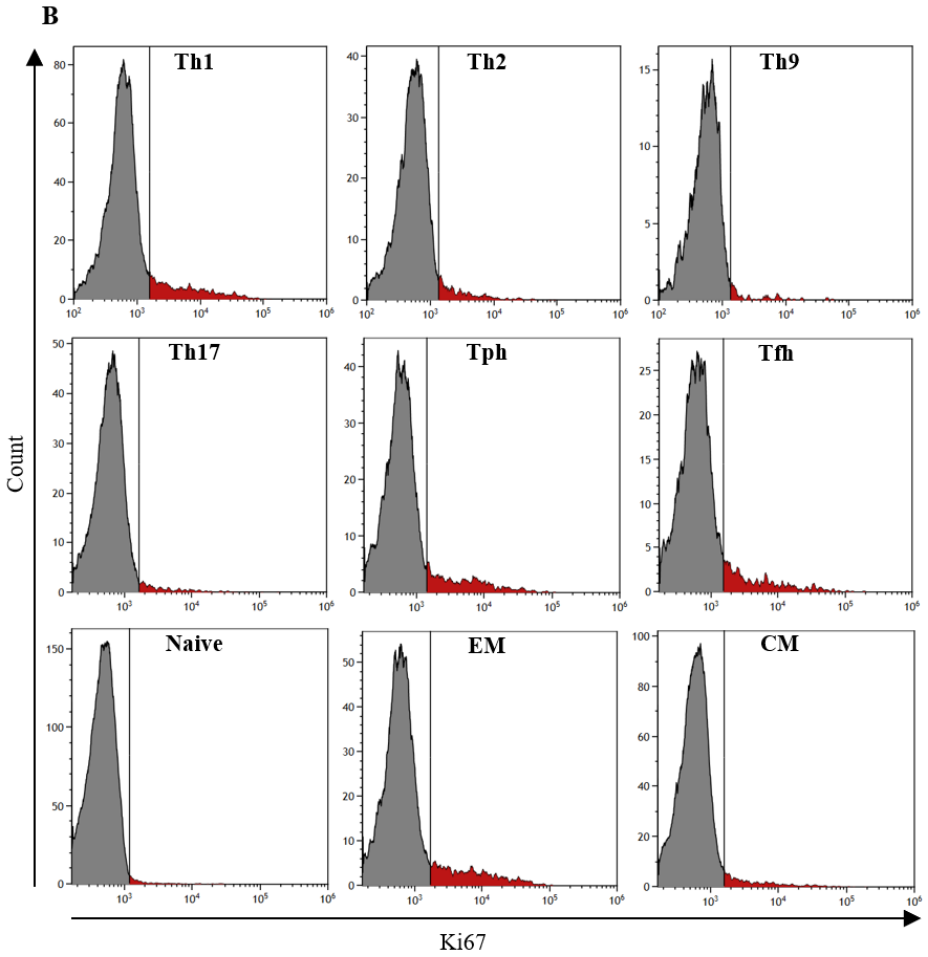

Figure 3.3 : Tcon gating strategy. **A**) Before Tcon-specific gatings, duplicates were excluded as well as FoxP3+ cells. **B**) Gating of the Ki67+ among Tcon subsets. Threshold value for positivity was determined on the basis of a Ki67 FMO control sample.

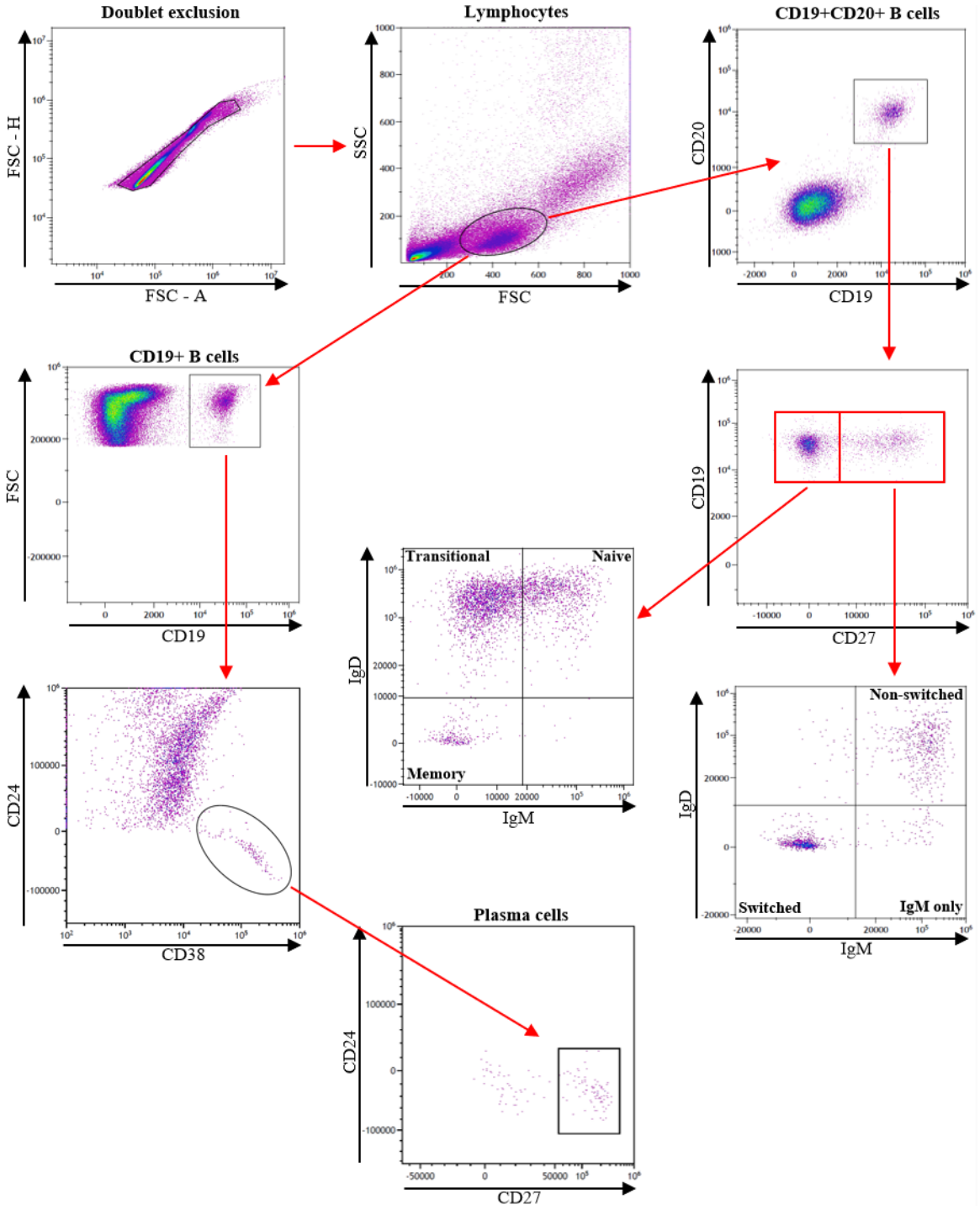

Figure 3.4 : B cell gating strategy. Before B cell-specific gatings, duplicates were excluded.

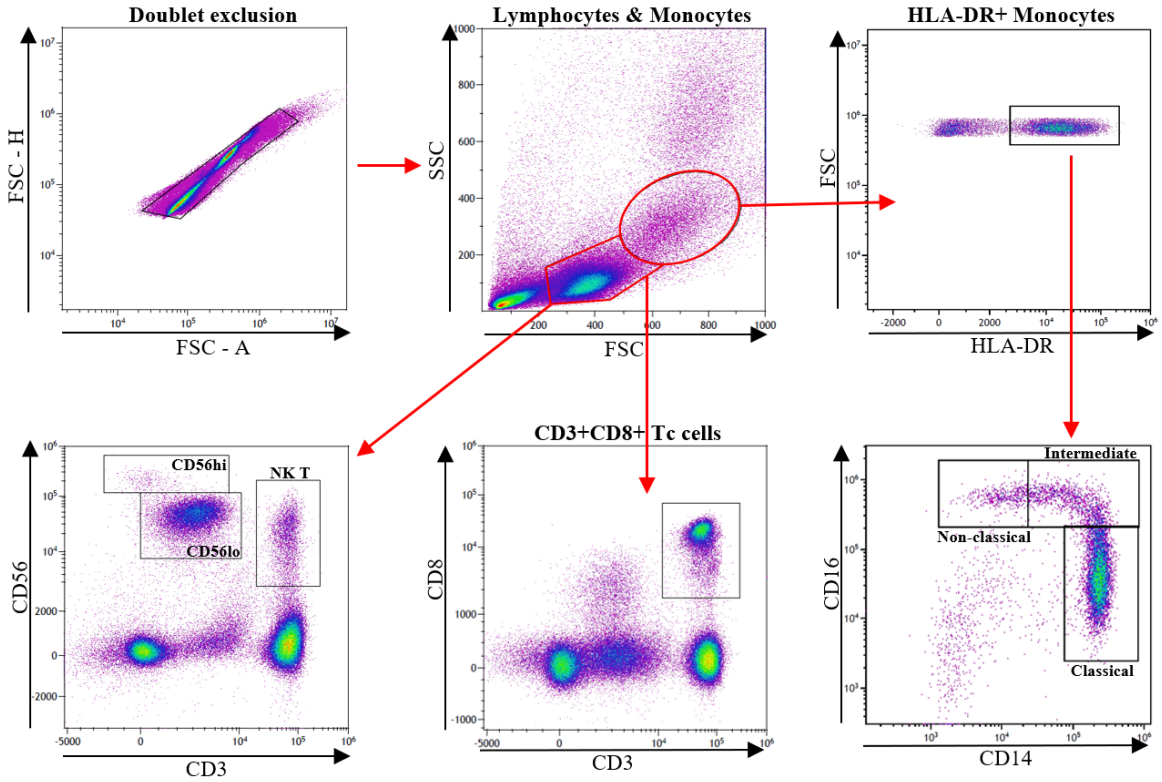

Figure 3.5 : Myeloid cell gating strategy. Before myeloid cell-specific gatings, duplicates were excluded.

For the measurements performed with the *FACSCanto™ II* from BD, following panel, acquisition conditions and gating strategy was used. Every flow cytometric measurement described in "Chapter 5 Results II" was executed using these procedures.

A

Treg Panel	
CD3	APC/Cy7
CD4	PerCP
CD39	PE/Cy7
CD25	PE
CD127	BV510
FoxP3	AF647
Helios	AF488
Ki-67	BV421

B

Events to record	Time to record [s]	Volume to record [µl]	Sample flow rate [µl/min]
100,000 events in Lymphocytes	-	250	60

Figure 3.6 : Flow cytometry panel and acquisition conditions for the rIL–2 stimulation approach. **A**) The Treg panel had to be prepared according to the intranuclear staining protocol. **B**) The acquisition conditions were applied to each sample, with the main objective of each measurement being to capture the 100,000 events in the lymphocyte gate.

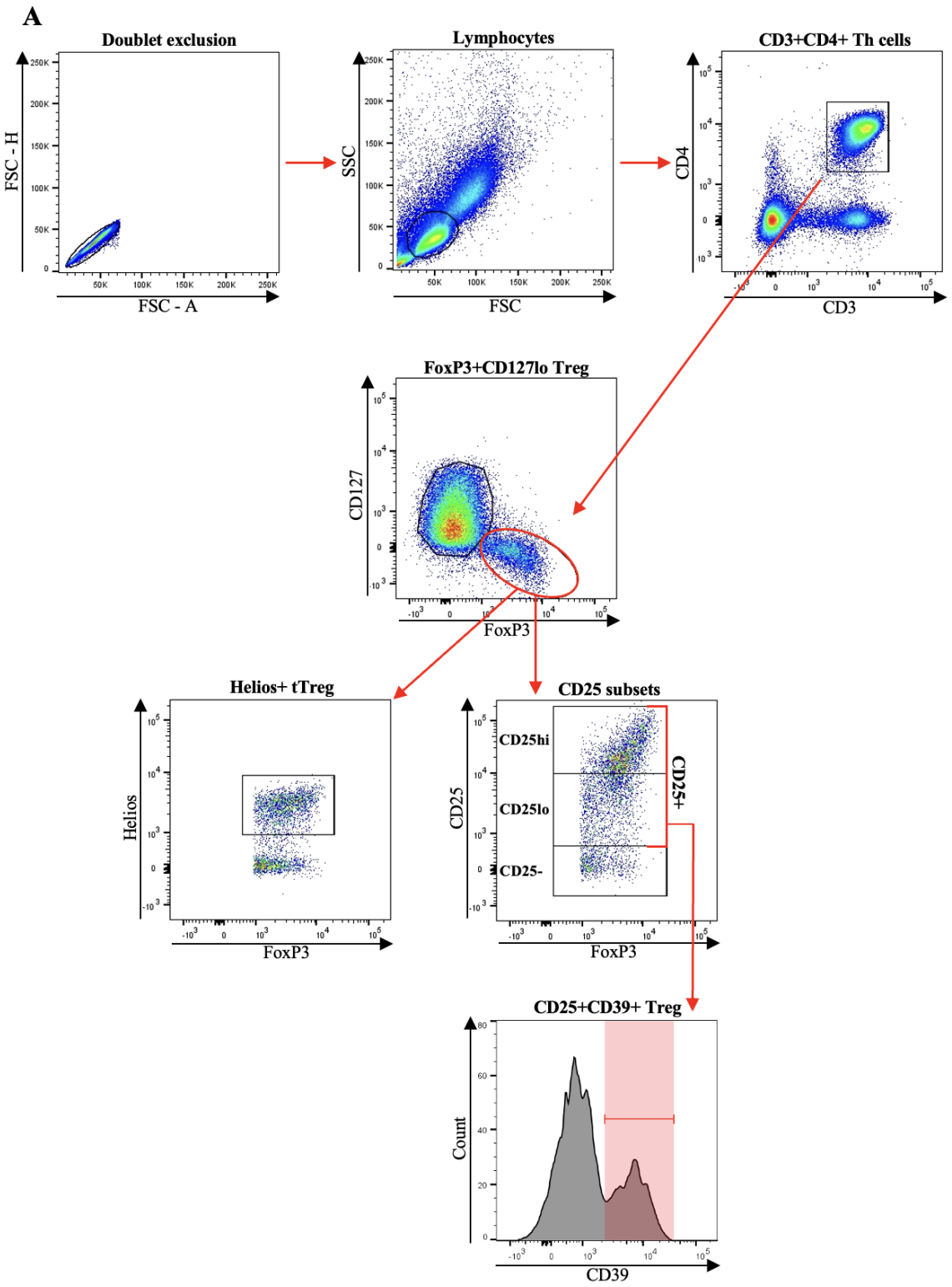
A
Doublet exclusion
FSC - H
FSC - A
Lymphocytes
SSC
FSC
CD3+CD4+ Th cells
CD4
CD3
FoxP3+CD127lo Treg
CD127
FoxP3
Helios+ tTreg
Helios
FoxP3
CD25 subsets
CD25hi
CD25lo
CD25-
CD25+
CD25
FoxP3
CD25+CD39+ Treg
Count
CD39

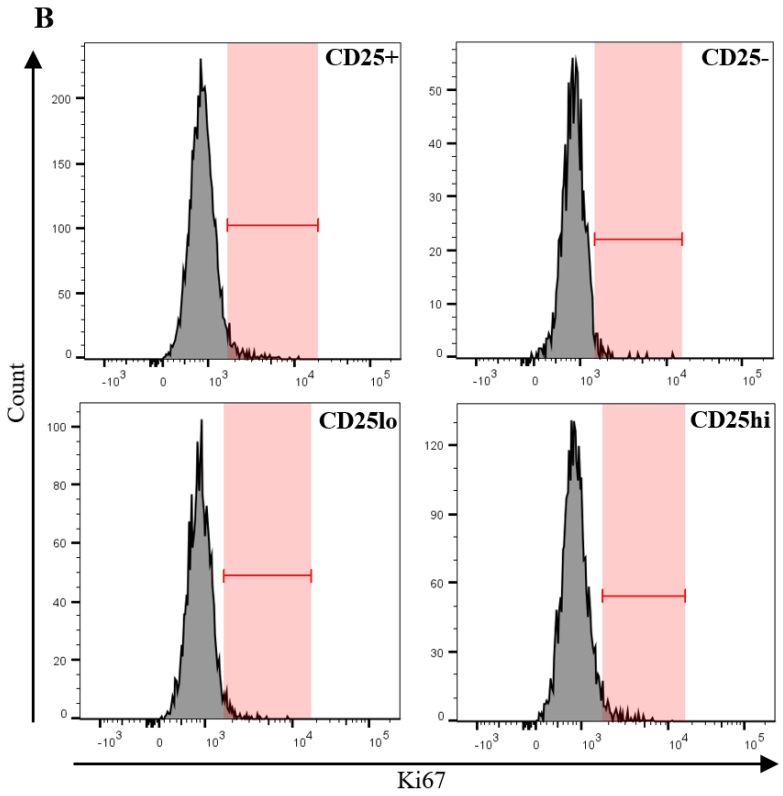

Figure 3.7 : **A**) Treg Gating Strategy after rIL-2 stimulation. Before Treg-specific gatings, duplicates were excluded, as well as FoxP3- cells. **B**) Gating of the Ki67+ cells among CD25 subsets of Treg.

For a simplified assignment of the different immune cell subtypes to the respective individual marker profiles, a legend was created in table 3.1 in addition to the gating strategies shown above. If a specific cell type is referenced during this study, the corresponding marker profile should be taken from this table, unless stated otherwise.

Table 3.1 : Cell type assignments to specific marker profiles.

Cell type	**Marker profile**
Th	CD3+CD4+
Tc	CD3+CD8+
Th1	CD3+CD4+FoxP3-CD45RO+CCR6-CXCR3+
Th2	CD3+CD4+FoxP3-CD45RO+CCR6-CXCR3-
Th9	CD3+CD4+FoxP3-CD45RO+CCR4-CCR6+
Th17	CD3+CD4+FoxP3-CD45RO+CCR4+CCR6+
Tph	CD3+CD4+FoxP3-CD45RO+CXCR5-PD1+
Tfh	CD3+CD4+FoxP3-CD45RO+CXCR5+PD1+
Tcon	CD3+CD4+FoxP3-
(Total) Treg	CD3+CD4+FoxP3+CD127lo
Naive T	CD3+CD4+FoxP3-CD45RO-CCR7+
CM T	CD3+CD4+FoxP3-CD45RO+CCR7+
EM T	CD3+CD4+FoxP3-CD45RO+CCR7-
B cell	CD19+CD20+
Naive B	CD19+CD20+CD27-IgM+IgD+
Memory B	CD19+CD20+CD27-IgM-IgD-
Transitional B	CD19+CD20+CD27-IgM-IgD+
IgM memory only B	CD19+CD20+CD27+IgM+IgD-
Non-switched memory B	CD19+CD20+CD27+IgM+IgD+
Switched memory B	CD19+CD20+CD27+IgM-IgD-
Plasma B	CD19+CD20-CD38hiCD24-CD27+
NK T	CD3+CD56+
NKbright	CD3-CD56hi
NKdim	CD3-CD56lo
Classical Monocytes	HLA-DR+CD16-CD14+
Intermediate Monocytes	HLA-DR+CD16+CD14+
Non-classical Monocytes	HLA-DR+CD16+CD14-

3.1.4 PBMC cultivation and rIL-2 stimulation

Following the isolation of PBMC from blood samples of SSc patients (as outlined in subsection 3.1.2), cell counts were measured using the *Anvajo Fluidlab R-300* device. The SCS was diluted 1:100 in warm RPMI medium and 10 µl of this diluted suspension was transferred into the 50 µm chamber of the *Acella 50* slide. The SCS was then adjusted to a concentration of 4 x 10^6 cells/ml using RPMI medium. Aliquots of 500 µl of the adjusted SCS were dispensed into each well of a 48-well plate, resulting in a final cell count of 2 x 10^6 cells per well. Recombinant IL-2 (rIL-2) stock solution, initially at a concentration of 100 µg/ml, was diluted with RPMI medium to achieve final concentrations of 1, 5, or 10 ng/ml in each well. The PBMC were then stimulated with rIL-2 for 24 hours at 37°C in a humidified incubator and harvested depending on the further purpose.

3.2 Molecular biological methods

3.2.1 RNA isolation from cell lysates

The *RNA Spin Blood* Kit from Macherey Nagel was used, according to manufacturer instructions, to isolate and purify the RNA from the cell lysates. First, cell lysates were generated by adding 350 µl of RA1 lysis buffer with 3.5 µl of β-mercaptoethanol to the cell pellet. After vortexing the lysates, they were applied to an extraction column and then centrifuged for 1 min at 11,000 x g. Afterwards the flow-through got mixed with 350 µl of 70% ethanol, dripped onto a NucleoSpin RNA column to bind the RNA on the silica membrane and centrifuged again for 1 min at 11,000 x g. The flow-through was discarded and the column was set on a new collection tube. To desalt the silica membrane and to make the following rDNase digest more effective, the addition of 350 µl of membrane desalting buffer (MDB) was indispensable. Another centrifugation step at 11,000 x g for 1 min followed immediately. For the enzymatic breakdown of contaminating DNA, a 1:10 DNase reaction mix (10 µl rDNase + 90 µl rDNase reaction buffer) was prepared and 95 µl added to the middle of the silica membrane. A 15 min incubation step at RT followed. After getting rid of DNA, the membrane was washed within three steps. The first step included the addition of 200 µl RAW2 buffer and a centrifugation for 1 min at 11,000 x g. The flow-through was again discarded and the column was placed on a new collection tube. The second and third wash steps ensued by firstly pipetting 600 µl RA3 buffer right on the column, followed by the same centrifugation step and repeating the process with 250 µl RA3 and centrifugation for 2 min. Afterwards, the RNA got eluted in 40 µl RNase free

H_2O, followed by a short incubation step for 1 min and was centrifuged for 1 min at 11,000 x g. The purified RNA was stored at -80 °C.

3.2.2 Photometric determination of RNA concentration

To determine the concentration and purity of extracted RNA, the *BioPhotometer* from Eppendorf was used. While contaminants like proteins absorb most of the light in the wavelength of 280 nm, nucleic acids have an absorption maximum at 260 nm. The *BioPhotometer* calculates the quotient from the absorption at 260 nm and 280 nm. The value of the quotient A260/A280 for pure RNA samples is 2.0 and for pure DNA 1.8. Lower values indicate contaminations with proteins. The second quotient A260/A230 provides information about possible contamination with, for example, thiocyanates, which have an absorption maximum at 230 nm. Before measuring the RNA samples with the *BioPhotometer*, a blank value with nuclease-free H_2O must be set. For every measurement, an amount of 1.5 µl per sample was used.

3.2.3 RNA gel electrophoresis

RNA electrophoresis is performed after RNA isolation to assess the integrity and quality of the isolated RNA. This step is crucial as RNA is highly sensitive to degradation by RNases and compromised RNA can lead to unreliable results in downstream applications such as quantitative real-time PCR (qPCR) [199].
First, a 1.5% agarose gel had to be prepared by dissolving 0.75 g agarose in 50 ml TAE buffer in the microwave. After a clear solution was obtained, 2 µl of the nucleic acid stain *GelRed®* was added to visualize the RNA bands under UV light. Next, the comb was attached, the solution was transferred to the gel chamber and the prepared RNA samples, consisting of 3 µl RNase-free H_2O, 2 µl pure RNA and 1 µl 6x loading buffer, were carefully applied to the gel. The electrophoresis was carried out at a voltage of 80 V for 30 min and visualized under UV light using the *Gel Doc™ EZ Imager* from Bio-Rad. The typical result for eukaryotic total RNA should include two clear ribosomal RNA (rRNA) bands (fig. 3.8).

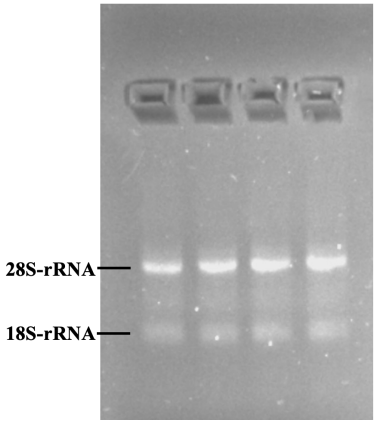

Figure 3.8 : RNA integrity analysis using gel electrophoresis. Exemplary visualization of four RNA samples isolated from human PBMC.

3.2.4 cDNA synthesis

For the synthesis of cDNA from pure RNA, the *iScript™ cDNA Synthesis* Kit from Bio-Rad was used. The first step was performed by mixing a volume of 100 ng purified RNA with 4 µl 5x iScript Reaction Mix, 1 µl iScript Reverse Transcriptase (25 mM) and nuclease-free H_2O water to get a total volume of 20 µl (table 3.2). To carry out the cDNA synthesis, an initial priming time of 5 min at 25 °C was required, followed by the reverse transcription at 46 °C for 20 min. Finally, the enzyme was inactivated by heating at 95 °C for 1 minute and the resulting cDNA was stored at -20 °C.

Table 3.2 : List of components used for transcribing one RNA sample into cDNA.

Components	**Volume [µl]**
5x iScript Reaction Mix	4
iScript Reverse Transcriptase	1
Nuclease-free H_2O	Variable
Purified RNA [100 ng]	Variable
Σ	**20**

3.2.5 Quantitative real-time PCR

For quantifying the relative gene expression in real time, a qPCR is carried out. The basic principle corresponds to that of a conventional PCR. The chemical reaction includes a fluorescent dye called SYBR-Green, which absorbs blue (λmax = 497 nm)

and emits green (λmax = 520 nm) light. This specific dye has the property to intercalate with double-stranded DNA and therefore measures the fluorescence signals emitted after each cycle. [200].
The qPCR approach was performed using the *SsoAdvanced™ Universal SYBR®* Kit from Bio-Rad, which contains, besides the fluorophore itself, an Sso7d fusion polymerase, dNTPs, $MgCl_2$ and ROX Normalization Dyes necessery for DNA amplification. The mixture (table 3.3) was pipetted into a white 96-well plate and then centrifuged for 3 min at 1000 x g. For the real-time amplification, the *qTOWER³ G* device with a specific temperature profile (table 3.4) was used.

Table 3.3 : List of components used for one qPCR approach.

Components	**Volume [µl]**
SYBR Green Mix I	10
Nuclease-free H_2O	7
Primer antisense	1
Primer sense	1
cDNA	1
Σ	**20**

Table 3.4 : Temperature profile for one qPCR approach.

Reaction	**Time [s]**	**Temperature [°C]**	**Cycles**
Preliminary denaturation	300	95	1
Denaturation	10	95	
Annealing	15	primer-specific	40
Elongation	20	72	
Melting curve	540	60-95	

After the first few qPCR cycles, an increase in fluorescence will hardly be noticeable, since the initial cDNA concentration is at a very low level. After exceeding the cycle threshold value (CT), the concentration increases exponentially per cycle. The expression level of the gene of interest influences the CT value. A low CT value correlates with a strong gene expression and vice versa. Following the amplification, a melting curve analysis is carried out in order to control the specificity of the product.

The relative gene expressions of the samples are determined using the Livak ΔΔCT method. The CT values of the reference genes are first subtracted from the CT values of the target genes (ΔCT). Afterwards, the ΔCT values of stimulated cells are normalized to the unstimulated ones (ΔΔCT).

3.3 Protein biochemical methods

3.3.1 Enzyme-linked immunosorbent assay (ELISA)

TGF-β1 and IL-10 are key cytokines secreted by Treg cells, playing crucial roles in suppressing immune responses and maintaining immune homeostasis [201, 202]. Detecting the levels of these cytokines provides insights into Treg activity and immune regulation. To measure these cytokines, a sandwich ELISA was performed. ELISA is a sensitive immunoassay that uses specific antibody-antigen interactions to quantify target proteins in a sample by generating a color change proportional to the protein concentration.
For TGF-β1 detection, 40 µl of cell culture supernatant was added to a polypropylene microfuge tube, followed by the addition of 10 µl of Acidification Solution. The mixture was vortexed and incubated for 10 minutes at RT, after which 10 µl of Neutralization Solution was added and mixed thoroughly. This acidification and neutralization step was required only for TGF-β1 and not for IL-10. For standard preparation:

- TGF-β1: A 500 pg/ml top standard was prepared by diluting 12.5 µl of the stock solution in 487.5 µl of Assay Buffer C. Six two-fold serial dilutions of the 500 pg/ml top standard were performed in separate tubes using Assay Buffer C as the diluent.

- IL-10: A 250 pg/ml top standard was prepared by diluting 6.25 µl of the stock solution in 493.75 µl of Assay Buffer A. Six two-fold serial dilutions of the 250 pg/ml top standard were performed in separate tubes using Assay Buffer A as the diluent.

The plate was washed four times with 300 µl of 1X Wash Buffer per well and any remaining buffer was removed by firmly tapping the plate upside down on absorbent paper. After washing, 50 µl of Assay Buffer C was added to the wells designated for TGF-β1 and 50 µl of Assay Buffer A was added to those for IL-10. Subsequently, 50 µl of the prepared standard dilutions or samples were added to the appropriate wells. The plate was sealed and incubated at RT for 2 hours with shaking at 200 rpm. After incubation, the plate was washed again four times with 1X Wash Buffer

and 100 µl of the TGF-β1/IL-10 detection antibody solution was added to each well. The plate was sealed and incubated for 1 hour at RT with shaking. Following the incubation, the plate was washed again and 100 µl of Avidin-HRP D for TGF-β1 and Avidin-HRP A for IL-10 solution was added to each well. The plate was sealed and incubated for 30 minutes at RT with shaking. After this step, the plate was washed five times with 1X Wash Buffer, allowing a 30-second to 1-minute soak in each wash to minimize background. Next, 100 µl of Substrate Solution F was added to each well and the plate was incubated in the dark for 10 minutes for TGF-β1 and 20 minutes for IL-10. Positive wells turned blue, indicating the presence of the target proteins. The reaction was stopped by adding 100 µl of Stop Solution, which changed the color from blue to yellow. Absorbance was measured at 450 nm, with a reference reading at 570 nm. The absorbance at 570 nm was subtracted from the absorbance at 450 nm to ensure accurate quantification.

3.3.2 Detection of autoantibodies against GPCRs and GFs in sera

The role of antibodies targeting GPCRs and GFs in the pathogenesis of SSc has been confirmed through both *in vitro* and *in vivo* studies, demonstrating their involvement in key aspects of SSc pathogenesis, including immune dysregulation, vasculopathy and fibrosis [56, 66].

In cooperation with the company CellTrend (Luckenwalde, DE), anti-GPCR and anti-GF antibody enzyme immunoassays (EIA) were performed to screen for antibodies against GPCRs and GFs in serum samples of VEDOSS and SSc patients. In this assay, the target GPCR or GF was pre-coated onto a microtiter plate. During the first incubation, anti-GPCR and anti-GF antibodies in the serum samples bound to the respective immobilized GPCR or GF. These antibodies were then detected using a peroxidase-conjugated anti-human IgG antibody. Finally, an enzymatic substrate reaction was carried out and the resulting color intensity was proportional to the concentration of the anti-GPCR or anti-GF antibody of interest. The general assay procedure is shown in table 3.5 and refers to the datasheet of the anti-GPCR and anti-GF antibody EIA from CellTrend.

Table 3.5 : EIA assay procedure.

Step	**Volume [µl]**	**Incubation [min, °C]**
Incubation of samples/standards/controls	100	120, 4 °C
Wash		
Incubation of detection antibody	100	60, RT
Wash		
Substrate incubation	100/well	20, RT
Add Stopp solution	100/well	
Read at 450 nm		

3.3.3 Proximity extension assay

The Olink® Proximity Extension Assay (PEA) was performed to quantify specific protein targets with high sensitivity and specificity. This assay utilizes dual antibody binding to each target protein, followed by proximity-dependent DNA polymerization and qPCR for signal detection (fig 3.9).

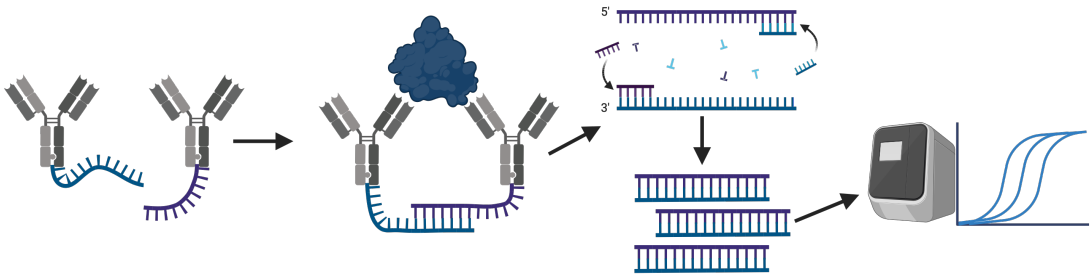

Figure 3.9 : Functionality of a PEA. Two target-specific antibodies with unique DNA oligonucleotides bind to different epitopes of the protein of interest. Upon proximity, DNA strands hybridize and are extended by DNA polymerase, creating a unique DNA barcode. This product is then quantified via microfluidic qPCR, allowing for sensitive and specific protein detection.

An incubation mix was prepared by combining the Olink® Target 96 Incubation Solution, Stabilizer and A- and B-probes in specified volumes to ensure optimal probe binding (see table 3.6). Each well of a 96-well plate (called Incubation Plate) received

3 µl of the mastermix, followed by the addition of 1 µl of sample. Negative controls, interplate controls and pooled plasma as sample controls were also included as per plate layout recommendations. The plate was sealed, centrifuged briefly and incubated overnight at 4°C to allow optimal binding of the proximity probes to the target proteins.

Table 3.6 : List of components used for one incubation mastermix.

Components	**Volume [µl]**
Olink® Incubation Solution	280
Olink® Incubation Stabilizer	40
Olink® A-probes	40
Olink® B-probes	40
Σ	**400**

The next step involved preparing an extension mix containing high-purity H_2O, Olink® Target 96 PEA solution, PEA enzyme and PCR polymerase (see table 3.7). For each well, 96 µl of this mastermix was added to the wells of the Incubation plate, followed by vortexing at 2000 rpm for 30 sec and a brief spin-down to ensure thorough mixing. The plate was then placed in a thermal cycler, where the proximity extension reactions were carried out under controlled cycling conditions (see table 3.8), facilitating DNA polymerization for detection.

Table 3.7 : List of components used for one extension mastermix.

Components	**Volume [µl]**
High purity H_2O	9385
Olink® PEA Solution	1100
Olink® PEA Enzyme	50
Olink® PCR Polymerase	22
Σ	**10562**

Table 3.8 : Extension and pre-amplification program.

Reaction	**Time [s]**	**Temperature [°C]**	**Cycles**
Extension	1200	95	1
Hot start	300	95	1
PCR	30	95	17
	60	54	
	60	60	
Hold	∞	10	

The detection phase began with priming an Olink® 96.96 IFC plate on the *Juno* device from Fluidigm. After thawing and vortexing the Primer plate, the Detection mastermix (see table 3.9) was prepared and 7.2 µl was carefully pipetted to each well of a new 96-well plate (designated as the Sample Plate). Next, 2.8 µl of the reaction mix from each well of the Incubation Plate was transferred to the corresponding well on the Sample Plate. The plate was vortexed and centrifuged for 1 minute at RT to ensure thorough mixing. To prepare for loading, 5 µl from each well of both the Primer Plate and the Sample Plate was transferred to the left and right inlets of the pre-primed 96.96 IFC chip, respectively. Finally, the chip was loaded into the *Biomark* device from Fluidigm and the plate was run according to the instrument's specifications, ensuring that the correct interface plate was in use for accurate measurement.

Table 3.9 : List of components used for one detection mastermix.

Components	**Volume [µl]**
Olink® Detection Solution	550
High purity H_2O	230
Olink® Detection Enzyme	7.8
Olink® PCR Polymerase	3.1
Σ	**790.9**

Olink® reports protein expression levels using an arbitrary unit termed Normalized Protein eXpression (NPX). NPX provides a relative quantification on a log2 scale, enabling the comparison of protein levels across samples and facilitating the identification of specific protein expression patterns within a dataset. NPX is derived from

the Ct values obtained from the qPCR using the following equations:

Extension Control

$$\mathrm{Ct}_{\mathrm{Analyte}} - \mathrm{Ct}_{\mathrm{Extension\ Control}} = \mathrm{dCt}_{\mathrm{Analyte}}$$

Inter-plate Control

$$\mathrm{dCt}_{\mathrm{Analyte}} - \mathrm{dCt}_{\mathrm{Inter\text{-}plate\ Control}} = \mathrm{ddCt}_{\mathrm{Analyte}}$$

Adjustment against a correction factor

$$\mathrm{Correction\ factor} - \mathrm{ddCt}_{\mathrm{Analyte}} = \mathrm{NPX}_{\mathrm{Analyte}}$$

3.4 Bioinformatics and statistics

Statistical significance was assessed using a threshold of $p<0.05$, with significance levels represented by asterisks: * for $p<0.05$, ** for $p<0.01$, *** for $p<0.001$ and **** for $p<0.0001$. The creation and development of the code in R was supported by generative artificial intelligence (AI). The generated code was reviewed, adapted and integrated into the specific requirements of the individual analyses.

3.4.1 Data transformation

Data transformation was performed in R to normalize and optimize the distribution of variables in the dataset, important for data analysis which requires normally distributed data. The *bestNormalize* package was employed to identify and apply the most appropriate transformation for each variable, ensuring improved normality and comparability [203]. A loop was implemented to systematically process each column of the dataset. Using the *bestNormalize()* function, transformations were identified and applied and the resulting transformed values were stored in a new dataset. The applied transformations were saved in a list for documentation and reproducibility. The distributions of the data before and after transformation were visualized using *ggplot2*, creating histograms for each variable to highlight the improvements in distribution [204]. Finally, the transformed dataset was saved to an Excel file using the *writexl* package, ensuring accessibility for subsequent analyses [205].

3.4.2 Multivariate dimensionality-reduction analyses

Principal Component Analysis (PCA) was performed in R to reduce dimensionality and explore clustering patterns within the normally distributed dataset in an unsupervised way. The dataset, which included the diagnostic categories and associated predictor variables, was imported and missing values were imputed using the *missMDA* package, applying the *imputePCA* function with two principal components specified for the imputation process [206]. The PCA itself was conducted with the *prcomp* function, scaling the predictor variables to standardize the data. The *dplyr* package was used to preprocess the dataset by separating the diagnostic groups (response variable) from the predictor variables, which were analyzed through PCA [207]. This produced a matrix of principal components (scores) and loadings, which were used to assess the explained variance. The first two components, accounting for a substantial proportion of the variance, were selected for visualization. To illustrate the PCA results, the *ggplot2* package was employed to create a scatter plot of the first two principal components (PC1 and PC2), with points colored and filled according to diagnostic groups [204]. Ellipses representing a 95% confidence level were created to perform clustering for each group. Additionally, the importance of variables contributing to PC1 and PC2 was calculated by summing their absolute loadings.

Partial Least Squares-Discriminant Analysis (PLS-DA) was conducted to assess clustering patterns within the not-normally distributed dataset across predefined diagnostic groups. To provide robust tools for carrying out a PLS-DA, the *mixOmics* package in R was used [208]. The dataset comprised diagnostic categories as labels alongside associated predictor variables and was imported with the response variable "Diagnosis" specified as the outcome variable Y and predictor variables for multivariate analysis stored as X. The PLS-DA was executed with the *plsda* function, extracting two principal components to visualize primary sources of variance among the groups. This dimensionality reduction facilitates comparison of class separation among different groups. To illustrate the results, a scatter plot was generated using the *plotIndiv* function. Ellipses representing a 95% confidence level were superimposed to visualize the grouping tendencies for each category and colors were assigned to each group to distinguish clusters. This analysis highlighted potential group separation in the multivariate space, providing insights into the relationships among diagnostic groups within the context of the dataset.

3.4.3 Confounder analyses

Analysis of covariance (ANCOVA) was performed using R, to examine the influence of diagnosis, age and sex on various immune cell types. Categorical variables, such as diagnosis and sex, were converted into factors. A linear model was constructed for each immune cell type, incorporating diagnosis, age and sex as independent variables. This was executed through a loop that applied the *lm()* function, with results compiled for further analysis. To visualize the findings, *ggplot2* was utilized to create boxplots and scatterplots, illustrating the effects of diagnosis on immune cell levels and the relationship between age and these levels [204]. This approach enabled the assessment of potential confounders and clarified the relationships between clinical factors and immune cell populations.

3.4.4 Univariate group comparisons

For univariate group comparisons, analyses were performed using GraphPad Prism. Depending on the number of groups and data distribution, t-tests or Mann-Whitney U tests were conducted for two-group comparisons, while ANOVAs or Kruskal-Wallis tests were used to compare more than two groups. Data distribution was analysed by using the Kolmogorov-Smirnow and Shapiro-Wilk test. For more complex visualizations, such as a Volcano Plot, basic R together with the package *dplyr* was used to identify and highlight significant differences in features between the groups [207]. For that purpose, a target variable was converted into a factor to facilitate grouping. A loop iterated through each feature, applying either a t-test or Mann-Whitney U test depending on the distribution and characteristics of the dataset. Fold changes were calculated for each feature and p-values were obtained to assess statistical significance. The resulting data, including log2 fold change and p-values, was compiled in a new data frame for visualization. For the visualization itself, the packages *ggplot2* and *ggrepel* were used, either to create plots and to avoid overlapping text labels, respectively [204, 209].

3.4.5 Correlation analyses

For correlation analyses, both GraphPad Prism and R were employed depending on the scope and complexity of the analysis. Simple pairwise correlations were performed in GraphPad Prism using Spearman's r test to assess relationships between variables. A detailed correlation matrix was computed in R and visualized as a heatmap. Spearman's rank correlation coefficients were calculated for all pairwise comparisons using

the *cor* function, with handling of missing values via pairwise complete observations. A corresponding matrix of p-values was generated using the *corr.test()* function from the *psych* package to assess statistical significance [210]. The visualization of the correlation matrix was performed with the *corrplot* package, leveraging advanced customization options such as color gradients, significance annotations and type-specific visualizations [211]. This approach highlights meaningful correlations by combining statistical significance thresholds with visually intuitive heatmap representations.
To explore relationships between variables, a correlation network analysis was conducted in R. Based on the same Spearman's r test, associated p-values were computed using the *rcorr()* function from the *Hmisc* package [212]. Correlations with an absolute value above 0.2 ($r > 0.2$) and p-values below 0.05 were retained for further analysis. The *igraph* package was used to construct an undirected graph, with nodes representing variables and edges representing significant correlations [213]. To avoid redundancies, duplicate edges and self-loops were excluded. Isolated nodes (variables without any significant connections) were removed to simplify the network. The resulting network was visualized using the *ggraph* package, an extension of *ggplot2* designed for graph drawing [214]. Edge widths and colors were mapped to correlation strength, with thicker and darker edges indicating stronger correlations. Node size was scaled by degree (the number of connections) and node labels were displayed for clarity. This approach highlights the structural relationships among variables, with visually intuitive cues for correlation magnitude and significance.

3.4.6 Predictive analyses based on machine learning

A Random Forest prediction algorithm was developed and employed in R to classify data, evaluate the significance of variables and assess prediction accuracy using a separate test data set. First, the data underwent preprocessing to ensure robustness which was performed by missing data imputation using k-nearest neighbors via the *VIM* package [215]. The target variable was converted to a factor and the dataset was split into training and test sets to ensure unbiased evaluation of model performance. To address class imbalance within the training data, Synthetic Minority Over-sampling Technique (SMOTE) was applied using *DMwR* [216]. This balanced dataset was further checked for any variables with fewer than two levels, removing them as needed to maintain analysis integrity. Model training involved a grid search with cross-validation for hyperparameter tuning. Using *caret*, a combination of parameters - mtry, ntree and nodesize - were optimized through five-fold cross-validation to maximize classification accuracy [217]. Parallelization was implemented via *doParallel* to reduce computation time [218]. Following grid search, the

best-performing parameter set was used to train the final Random Forest model using *randomForest* [219]. To assess model performance, predictions were made on the test dataset, calculating accuracy, sensitivity and specificity. An additional evaluation of classification quality was conducted by plotting a receiver operating characteristic (ROC) curve and calculating the Area Under the Curve (AUC), both enabled by the *pROC* package [220]. Feature importance was assessed through MeanDecreaseGini values, visualized as an Elbow Plot and a Variable Importance Plot with *ggplot2* to determine the features contributing most to model accuracy [204].

3.4.7 Functional enrichment analyses

Enrichment analysis was performed in R to identify significantly enriched pathways, molecular functions and processes based on previously computed p-values. The analysis began with converting UniProt IDs to Entrez IDs using *biomaRt*, which enabled compatibility with Kyoto Encyclopedia of Genes and Genomes (KEGG) pathway analysis and Gene Ontology (GO) enrichment analysis [221]. After conversion, significant genes or proteins were identified and the *clusterProfiler* and *org.Hs.eg.db* packages were used to conduct KEGG enrichment analysis, revealing pathways associated with differential expression patterns [222, 223]. The analysis pipeline involved transforming gene-to-pathway data using the *tidyr* package to split linked gene identifiers into different rows for each pathway-gene association [224]. This transformation enabled clear mapping of individual proteins to their respective pathways, providing data in a format suitable for visualization. For GO enrichment analysis on molecular functions (MF), proteins with significant differential expression were mapped to GO terms. Visualizations for both were created using *ggplot2* for dot plots and *circlize* as well as *RColorBrewer* for chord plots [204, 225, 226]. Dot plots illustrated the enriched pathways as well as MF, while chord diagrams were generated to map protein-pathway associations, with pathways color-coded and key proteins highlighted. To further investigate specific pathways, the *pathview* package was employed to visualize selected KEGG pathways, applying color scales to represent significance thresholds for protein expression [227]. This pipeline facilitated the identification and visualization of key pathways and functions enriched among significantly differentially expressed proteins, providing insights into the molecular mechanisms of interest.

CHAPTER 4

Results I

In-depth immunophenotyping and multi-omics approaches

The first results chapter focuses on differences in the immunophenotype of diverse immune cell subsets between HC, VEDOSS and SSc patients to identify distinct immune signatures at a global and cell-type specific level. Correlation analyses explored interactions between cell frequencies, clinical parameters and autoantibody levels. In addition, a random forest prediction algorithm was developed to distinguish disease states and an inflammatory proteome analysis was performed in patients with VEDOSS and SSc. Finally, a multi-omics approach, combining all data layers, was conducted for a clear separation of VEDOSS and SSc patients.

4.1 Clinical characterization of patients

Given the heterogeneity of clinical manifestations in SSc and VEDOSS patients, personalized treatment strategies are essential for comprehending pathological issues and improving prognosis [228, 229].
Consequently, the initial step involved a comprehensive clinical assessment and precise characterization of each recruited patient by an experienced physician prior to obtaining blood samples. This characterization included not only the assessment of core disease manifestations but also an in-depth evaluation of associated comorbidities, laboratory parameters and relevant organ involvement to better understand the systemic and immunological impact of the disease. The characteristics of patients from the SSc and VEDOSS cohorts who have been declared suitable for this study are listed in tables 4.1 and 4.2. The inclusion criteria for an established SSc primarily required either fulfillment of the ACR/EULAR criteria or, in a few exceptional cases, patients who were on the verge of meeting them but were already classified as SSc based on clinical presentation (see table 1.1). The specifically defined criteria for a VEDOSS diagnosis can be taken from section 1.2.1. These criteria ensure that the patient population accurately reflects the clinical spectrum and stage of these diseases. Additional demographic and clinical factors such as age, sex and medication were also recorded to allow for a detailed stratification of disease subsets. To provide a comparative reference to healthy individuals during the analyses, 23 donors were recruited in cooperation with the *Institute for Transfusion Medicine* at the *University Medical Centre Schleswig-Holstein*. These individuals were free from acute or chronic inflammatory or infectious diseases. To ensure comparability, the healthy donor cohort was matched to the patient groups by age and sex, with a median age of 56 years and 70% female representation.

Table 4.1 : Characteristics of patients with established SSc.

Demographics	**Total (n=54)**
Female, *n (%)*	41 (76)
Age [years], *median (range)*	55 (24 - 84)
Body weight [kg], *median (range)*	68.5 (45 - 105)
Clinical characteristics	
ACR/EULAR criteria fulfilled, *n (%)*	44 (81)
EUSTAR AI, *median (range)*	1.168 (0 - 6.25)
Diffuse cutaneous SSc, *n (%)*	22 (41)
Limited cutaneous SSc, *n (%)*	32 (59)
Raynaud's phenomenon, *n (%)*	52 (96)
Teleangiectasia, *n (%)*	41 (76)
Digital ulcers (active), *n (%)*	7 (13)
mRSS, *median (range)*	4 (0 - 23.5)
Calcinosis cutis, *n (%)*	15 (28)
Laboratory characteristics	
ANA positive, *n (%)*	52 (96)
Anti-Topo I (Scl-70) positive, *n (%)*	15 (28)
Anti-RNA-Pol-III positive, *n (%)*	7 (13)
Anti-Centromer positive, *n (%)*	21 (39)
CK [U/l], *median (range)*	101.5 (30 - 374)
CRP [mg/l], *median (range)*	1.19 (<0.6 - 20.7)
NTproBNP [ng/l], *median (range)*	146.5 (<50 - 20051)
Creatinine [µmol/l], *median (range)*	74 (42 - 316)
Organ involvement	
Pulmonary involvement (ILD), *n (%)*	20 (37)
Pulmonary arterial hypertension, *n (%)*	6 (11)
Renal involvement (renal crisis), *n (%)*	2 (4)
Cardiac involvement, *n (%)*	11 (20)
Gastrointestinal tract involvement, *n (%)*	33 (61)
Comorbidities	
Rheumatoid arthritis, *n (%)*	20 (37)
Inflammatory Myopathies (IMP), *n (%)*	3 (6)
Hypothyerosis, *n (%)*	9 (17)
Sicca syndrome, *n (%)*	34 (63)
Iron deficiency anaemia, *n (%)*	7 (13)
Concomitant medication *no (%)*: 44 (81)	
Immunosuppressive medications	
Azathioprine, *n (%)*	1 (2)
Ciclosporin, *n (%)*	8 (15)
Hydroxychloroquine, *n (%)*	7 (13)
Methotrexate, *n (%)*	7 (13)
Mycophenolate, *n (%)*	19 (35)
Prednisolon, *n (%)*	8 (15)
Rituximab, *n (%)*	11 (20)
Antifibrotic medications	
Nintedanib, *n (%)*	10 (19)
Vasoactive medications	
Bosentan, *n (%)*	9 (17)
Iloprost, *n (%)*	8 (15)
Nifedipin, *n (%)*	6 (11)

Table 4.2 : Characteristics of patients with VEDOSS.

Demographics	**Total (n=23)**
Female, *n (%)*	15 (65)
Age [years], *median (range)*	51 (19 - 82)
Body weight [kg], *median (range)*	68 (46 - 125)
Clinical characteristics	
EUSTAR AI, *median (range)*	0.042 (0 - 1.84)
Raynaud's phenomenon, *n (%)*	22 (96)
Teleangiectasia, *n (%)*	4 (17)
Digital ulcers (active), *n (%)*	1 (4)
mRSS, *median (range)*	0 (0 - 10)
Calcinosis cutis, *n (%)*	1 (4)
Laboratory characteristics	
ANA positive, *n (%)*	23 (100)
Anti-Topo I (Scl-70) positive, *n (%)*	5 (22)
Anti-RNA-Pol-III positive, *n (%)*	4 (17)
Anti-Centromer positive, *n (%)*	8 (35)
CK [U/l], *median (range)*	92 (25 - 190)
CRP [mg/l], *median (range)*	1.20 (<0.6 - 8.44)
NTproBNP [ng/l], *median (range)*	89 (<50 - 626)
Creatinine [µmol/l], *median (range)*	75 (7.6 - 93)
Organ involvement	
Pulmonary involvement (ILD), *n (%)*	0 (0)
Pulmonary arterial hypertension, *n (%)*	0 (0)
Renal involvement (renal crisis), *n (%)*	0 (0)
Cardiac involvement, *n (%)*	2 (9)
Gastrointestinal tract involvement, *n (%)*	12 (52)
Comorbidities	
Rheumatoid arthritis, *n (%)*	1 (4)
Inflammatory Myopathies (IMP), *n (%)*	0 (0)
Hypothyerosis, *n (%)*	0 (0)
Sicca syndrome, *n (%)*	9 (39)
Iron deficiency anaemia, *n (%)*	0 (0)
Concomitant medication *no (%)*: 8 (35)	
Immunosuppressive medications	
Azathioprine, *n (%)*	0 (0)
Ciclosporin, *no (%)*	0 (0)
Hydroxychloroquine, *n (%)*	4 (17)
Methotrexate, *n (%)*	4 (17)
Mycophenolate, *n (%)*	1 (4)
Prednisolon, *n (%)*	2 (9)
Rituximab, *n (%)*	0 (0)
Antifibrotic medications	
Nintedanib, *n (%)*	1 (4)
Vasoactive medications	
Bosentan, *n (%)*	0 (0)
Iloprost, *n (%)*	1 (4)
Nifedipin, *n (%)*	1 (4)

By comparing the cohort of SSc and VEDOSS, several prominent clinical differences were observed. Regarding demographic characteristics, the majority of patients in both cohorts were female, 76% in the SSc cohort and 65% in the VEDOSS cohort. The median age was 55 years (range: 24–84 years) in the SSc cohort and 51 years (range: 19–82 years) in the VEDOSS cohort. In terms of disease characteristics, calcinosis cutis was observed in 28% of SSc patients, whereas only 4% of VEDOSS patients exhibited this condition. Additionally, telangiectasia was more frequent in the SSc cohort (76%) compared to the VEDOSS cohort (17%). The SSc cohort achieved a median mRSS score of 4, while the VEDOSS patients had a score of 0. In line with that, SSc patients reached a score of 1.168 in the EUSTAR AI, compared 0.042 in the VEDOSS chohort. In almost all patients of both groups (96%), however, Raynaud's phenomenon was observed and ANA positivity was also present in both groups almost without exception (SSc 96%; VEDOSS 100%). Only negligible differences were found in other autoantibody-titers and inflammation markers. Differences in organ involvement were also evident between the cohorts. Lung fibrosis was reported in 37% of SSc patients but was entirely absent in VEDOSS patients. Similarly, pulmonary arterial hypertension affected 11% of SSc patients, with no cases in the VEDOSS cohort. In contrast, the prevalence of gastrointestinal tract involvement was similar, with 61% in SSc patients and 52% in the VEDOSS group. Finally, use of immunosuppressive or vasoactive medications was significantly higher in the SSc cohort, with 81% of patients receiving such treatments compared to 35% in the VEDOSS group. These findings illustrate distinct differences in clinical characteristics and disease severity between patients with established SSc and those in the pre-clinical VEDOSS state within this study's cohorts.

4.2 Global differences in immune signatures across the cohorts

PLS-DA was performed on immunophenotyping data from HC, VEDOSS and SSc patient cohorts. The PLS-DA provides an advantage due to its ability to handle high-dimensional and collinear data, as is commonly used for the analysis of complex immunophenotyping datasets [230]. By maximizing the separation between predefined cohorts (HC, VEDOSS and SSc) based on immune cell frequency profiles, PLS-DA enhances the identification of patterns and provides initial indications of group-specific differences between the cohorts. The analysis included the frequencies of 55 distinct immune cell types to assess clustering and separation among the three cohorts. To obtain this data, multicolor flow cytometric measurements, using the

panels shown in figure 3.1, were performed with PBMC isolated from EDTA blood from 23 HC, 23 VEDOSS and 54 SSc patients (see section 4.1). The acquisition conditions and gating strategies that were essential for the unambiguous identification of the individual immune cell types are listed in the section 3.1.3.

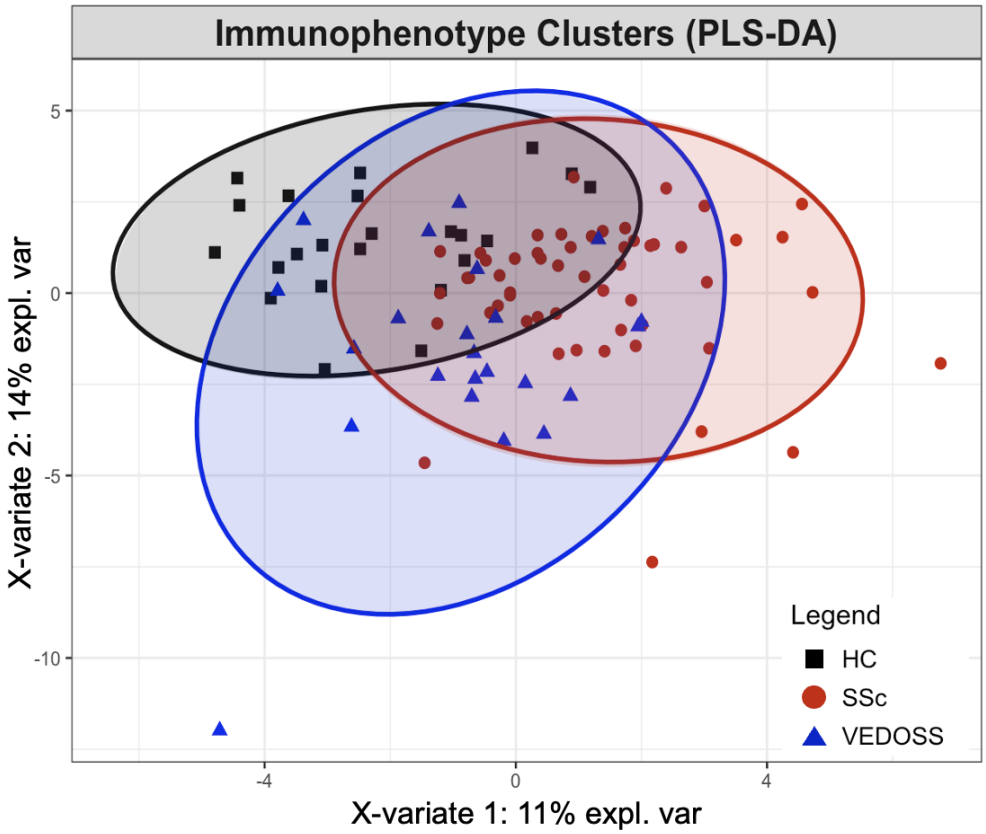

Figure 4.1 : Two-dimensional distribution of HC, VEDOSS and SSc immunophenotype. Clustering was performed based on the frequencies of 55 different immune cell subsets, measured via flow cytometry. Each ellipse represents the 95% confidence interval, while each dot represents one patient (colorcode: HC=black; VEDOSS=blue; SSc=red). The axes correspond to the first two components of the PLS-DA: the x-axis (X-variate 1) explains 11% of the variance and the y-axis (X-variate 2) explains 14% of the variance in the dataset (HC: n=23; VEDOSS: n=23; SSc: n=54).

In the PLS-DA score plot (fig. 4.1), each cohort is represented by a unique color and corresponding ellipse, indicating the 95% confidence interval for each group, with each dot representing one individual. The X-variate 1 (11% explained variance) and X-variate 2 (14% explained variance) axes together capture 25% of the variance among groups. The HC and SSc groups showed a distinct separation, while the VEDOSS group partially overlaped with both the HC and SSc clusters, which suggests that VE-

DOSS patients exhibit an intermediate immune profile, sharing characteristics with both healthy individuals and SSc patients.

Following the PLS-DA and to further examine the differential frequencies of immune cells, a Mann-Whitney U test was applied to specific cohort pairs to assess statistical differences in immune cell subset distributions between the cohorts and the results are visualized in two separate volcano plots (fig. 4.2A and B).

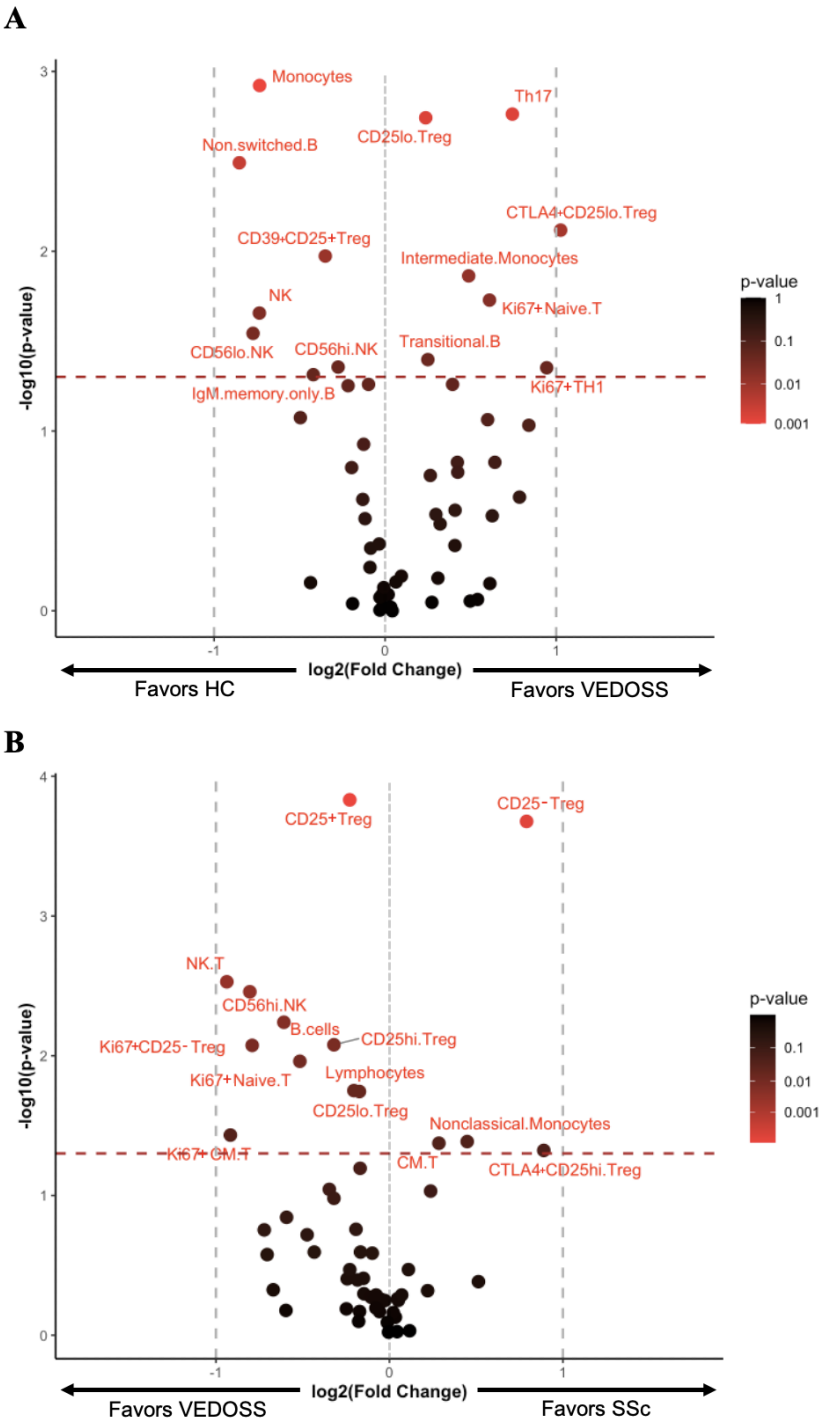

Figure 4.2 : Changes in immune cell subset frequencies between cohort pairs (HC vs. VEDOSS and SSc vs. VEDOSS), visualized as volcano plot. Each point represents an immune cell subset, with the x-axis displaying the log2 fold change between groups and the y-axis showing the -log10 transformed p-value based on a Mann-Whitney U test. Red color intensity reflects p-value significance, with brighter red color indicating higher statistical significance. The dashed red line marks the significance threshold of $p < 0.05$. The cell types to the left of the zero point of the x-axis favor (**A**) HC or (**B**) VEDOSS, while those to the right of the zero point favor (**A**) VEDOSS or (**B**) SSc, respectively (HC: n=23; VEDOSS: n=23; SSc: n=54).

The frequencies of immune cells between healthy individuals and VEDOSS patients were compared (fig. 4.2A). Each point on the plot represents an immune cell subset, with the x-axis indicating the log2 fold change between the groups and the y-axis showing the -log10 transformed p-value. Immune cell subsets such as CD25lo Treg, non-switched memory B cells and Th17 cells displayed prominent fold changes, with several subsets showing statistically significant p-values (specific p-values and log2FC values are listed in A.1). In figure 4.2B, the comparison between SSc and VEDOSS is illustrated. Notably, cell subsets with significant differences in cell frequency included CD25- Treg, CD25+ Treg, NK T and CD56hi NK cells (specific p-values and log2FC values are listed in A.2).
These volcano plots complement the PLS-DA findings by quantifying and visualizing specific subsets of immune cells that differ significantly between cohorts, providing a more detailed view at cell type-specific differences between disease stages from healthy to established SSc and highlighting cell types that should be examined in more depth in following individual analyses to confirm the findings above.

4.2.1 Differences in frequencies of Treg subsets based on CD25 expression

After conducting a confounder analysis, which showed no significant influence of age or sex on the distribution of Treg subsets allocated by CD25 expression (CD25hi, CD25lo and CD25-) across the cohorts (appendix fig. A.1), the focus shifted to a direct comparison of CD25 Treg subset frequencies among HC, VEDOSS and SSc groups. Using the cell frequencies, acquired by flow cytometry (for gating strategy see fig. 3.2), these comparisons provided deeper insights into cohort-specific differences in Treg phenotypes with regard to CD25 expression.

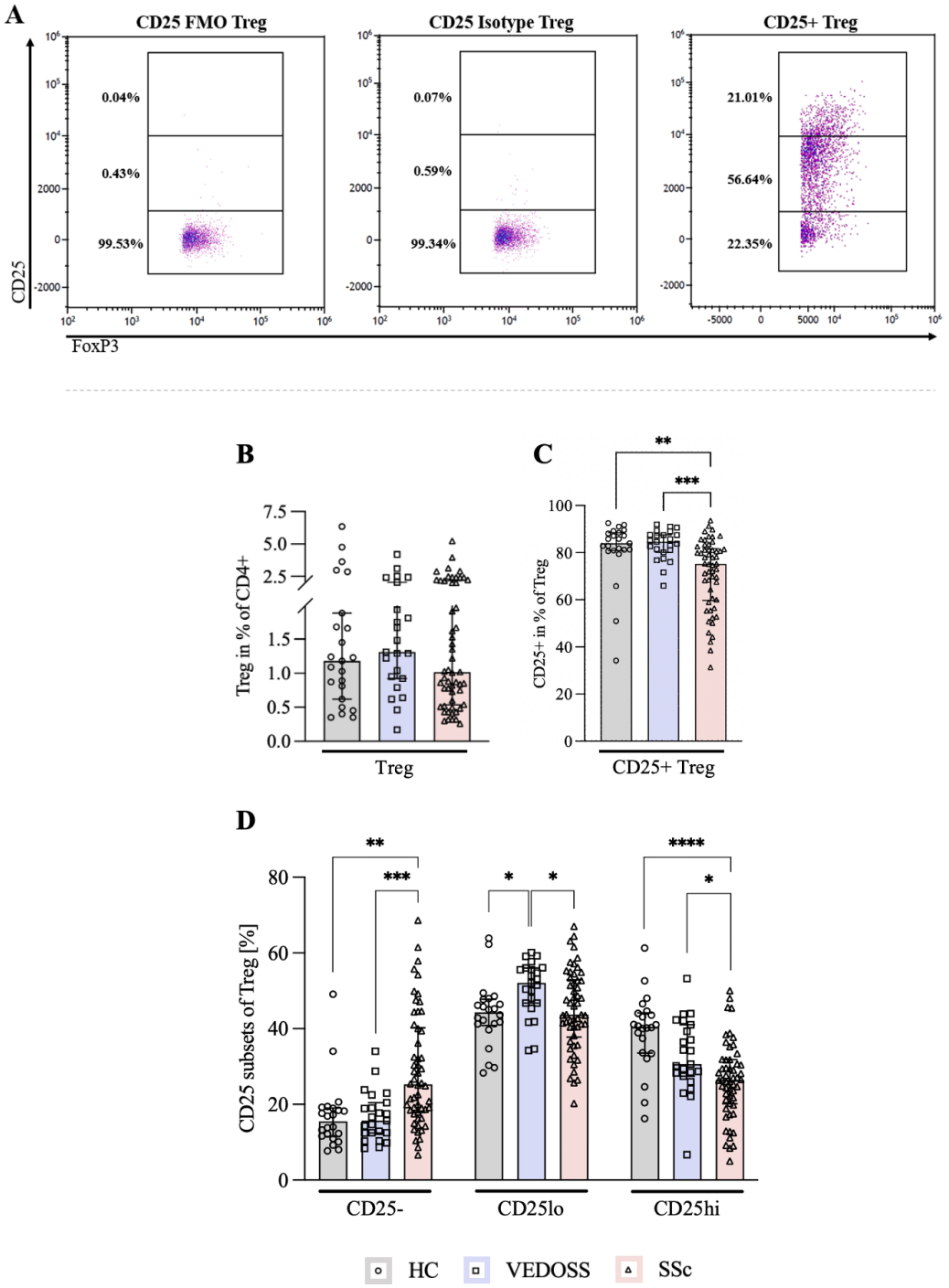

Figure 4.3 : Changes in Treg subsets according to expression of CD25 in VEDOSS and SSc compared to HC. **A**) Representative dot plots of frequencies of CD25-, CD25lo and CD25hi subsets among FoxP3+CD127lo Treg from isolated PBMC, determined via flow cytometry and confirmed by an FMO and isotype control sample. The frequencies of (**B**) FoxP3+CD127lo Treg among CD3+CD4+ T cells, (**C**) CD25+ among CD3+CD4+FoxP3+CD127lo Treg and (**D**) CD25-, CD25lo and CD25hi subsets among CD3+CD4+FoxP3+CD127lo Treg were determined and statistically compared using a Kruskal-Wallis test with Dunn's correction. Median values with error bars, indicating the IQR, are shown (HC: n=23; VEDOSS: n=23; SSc: n=54).

For the correct identification of CD25-expressing Treg subsets, an incorporation of a CD25 FMO and isotype control from one exemplary VEDOSS patient is illustrated (fig. 4.3A). The FMO and isotype control showed low background fluorescence, but set a clear threshold for detection of the Treg subset expressing CD25 at low and high levels. The frequencies of total FoxP3+CD127lo Treg within the CD3+CD4+ T cell population were compared among the groups (fig. 4.3B). No significant differences were found, however, a tendency toward a slightly lower median frequency of Treg was observed in the SSc cohort compared to HC and VEDOSS. The SSc group also exhibited greater variability in frequencies of Treg than the other cohorts. With regard to frequencies of CD25+ cells among FoxP3+CD127lo Treg (fig. 4.3C), significant differences were observed, with SSc showing lower frequencies compared to HC ($p < 0.01$) and to VEDOSS ($p < 0.001$). In addition, frequencies of the CD25 subsets (CD25-, CD25lo and CD25hi among FoxP3+CD127lo Treg) were compared across HC, VEDOSS and SSc cohorts (fig. 4.3D). The frequencies of the CD25- Treg subset was significantly higher in SSc patients compared to both HC and VEDOSS cohorts ($p < 0.01$ and $p < 0.001$, respectively). Correspondingly, the VEDOSS group exhibited a significantly elevated frequency of CD25lo Treg compared to HC ($p < 0.05$; fig. 4.3D). For the CD25hi Treg subset, a stepwise decline in frequencies was visually evident across the cohorts, aligning with disease progression. Notably, the median frequency of CD25hi Treg was nearly halved in SSc patients compared to HC (40.5% vs. 26.5%; $p < 0.0001$). In addition, the SSc cohort showed a significant reduction in frequencies of CD25hi Treg compared to the VEDOSS patients ($p < 0.05$), while the VEDOSS cohort showed a trend towards lower frequencies of CD25hi Treg in comparison to HC, but this was not statistically significant ($p = 0.37$; fig. 4.3D).
Taken together, the analyses revealed significant differences in Treg subsets based on CD25 expression, highlighting a disturbance in Treg biology across the cohorts. Notably, there were marked changes in the distribution of CD25 subsets among Treg at different disease stages, with the most pronounced reduction in CD25hi expression observed in patients with established SSc.

4.2.2 Phenotype and activation state of Treg subsets

Building on the general comparison of frequencies of CD25 subsets among FoxP3+CD127lo Treg across the three cohorts, the analysis was further extended to explore additional phenotypic markers of Treg to gain deeper insights into their immunoregulatory capacities. The frequencies of the thymic-derived Helios+ subset among FoxP3+CD127lo Treg (4.4A) and the potentially higher suppressive CD39+ subset among FoxP3+CD127loCD25+ Treg (4.4B) across HC, VEDOSS and SSc cohorts

were determined by flow cytometry and subsequently analysed.

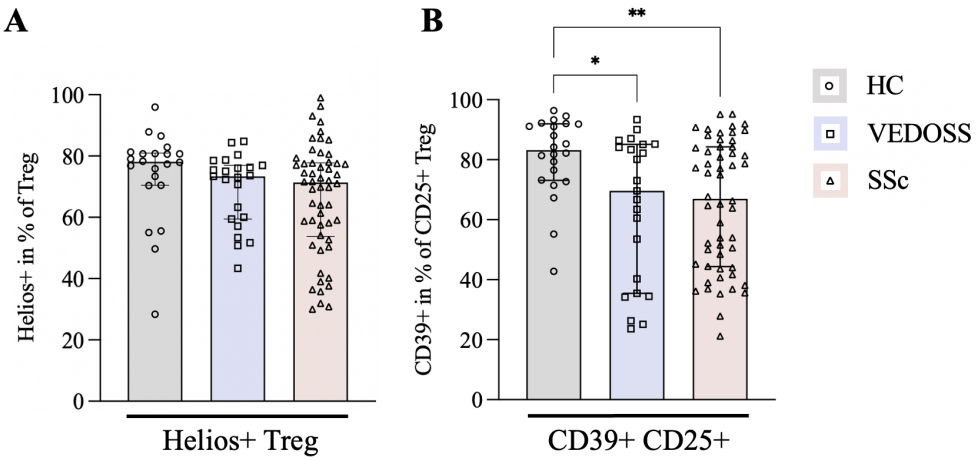

Figure 4.4 : Changes in origin and suppressive state of Treg in VEDOSS and SSc compared to HC. Isolated PBMC were used to identify frequencies of (**A**) Helios+ cells among CD3+CD4+FoxP3+CD127lo Treg and (**B**) CD39+ cells among CD3+CD4+FoxP3+CD127loCD25+ Treg via flow cytometry across the cohorts. Statistical comparisons were done using a Kruskal-Wallis test with Dunn's correction for multiple comparisons. Median values with error bars, indicating the IQR, are shown (HC: n=23; VEDOSS: n=23; SSc: n=54).

The frequencies of the Helios+ Treg subset among total FoxP3+CD127lo Treg showed no differences across the cohorts (fig. 4.4A). Only SSc patients showed a trend towards lower frequencies compared to HC, without being statistically significant ($p < 0.086$). The frequencies of CD39+ cells among CD25+ Treg (fig. 4.4B) was significantly lower in VEDOSS and SSc patients compared to HC ($p < 0.05$ and $p < 0.01$, respectively). No significant differences were noted between VEDOSS and SSc cohorts. In summary, while no significant differences were observed in the Helios+ Treg subset across the cohorts, the trend towards lower frequencies in SSc patients suggests a potential alteration in Treg composition. In contrast, the significantly lower frequencies of the CD39+ Treg subset in both VEDOSS and SSc patients compared to HC indicates a possible dysfunction in the suppressive capacity of Treg.

Following the analysis of the original and potentially more suppressive Treg subsets, the focus shifted towards assessing markers associated with proliferation and activation. Specifically, the expression of Ki67 and CTLA4 within distinct CD25 subsets was investigated to further characterize the functional diversity of Treg across the groups.

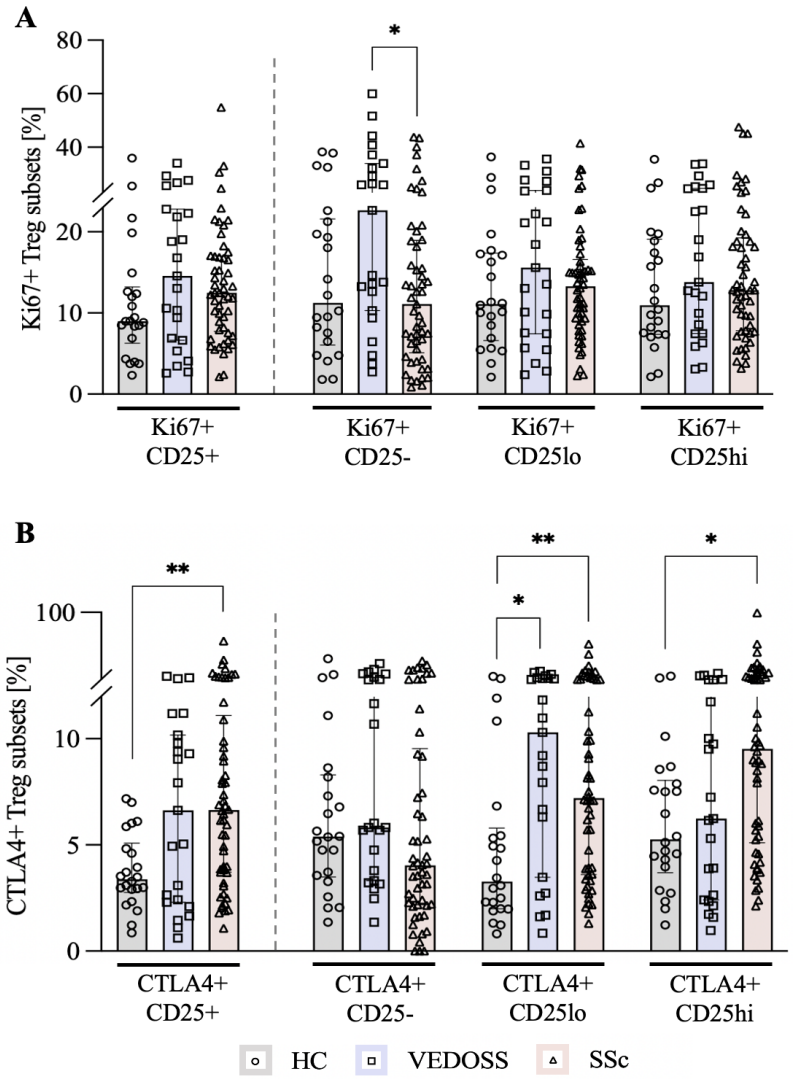

Figure 4.5 : Changes in proliferative and activation state of CD25 Treg subsets in VEDOSS and SSc compared to HC. Isolated PBMC were used to identify frequencies of (**A**) Ki67+ cells and (**B**) CTLA4+ cells among CD25 subsets in CD3+CD4+FoxP3+CD127lo Treg via flow cytometry. Statistical comparisons were done using a Kruskal-Wallis test with Dunn's correction. Median values with error bars, indicating the IQR, are shown (HC: n=23; VEDOSS: n=23; SSc: n=54).

The frequencies of Ki67+ cells were analyzed across CD25-expressing FoxP3+CD127lo Treg subsets in HC, VEDOSS and SSc patients (fig. 4.5A). The frequencies of Ki67+ cells among CD25+ Treg showed no statistically significant differences between the three groups. In contrast, Ki67+ cells among CD25- Treg were significantly more frequent in VEDOSS patients compared to SSc and have doubled in the median (22.67% vs 11.11%; $p < 0.05$). The frequencies of Ki67+ cells among CD25lo Treg and Ki67+ cells among CD25hi Treg revealed no significant differences between the

groups (fig. 4.5A).
In figure 4.6B, the analysis of CTLA4+ cells across CD25-expressing FoxP3+CD127lo Treg subsets was similarly stratified. The frequencies of CTLA4+ cells among CD25+ Treg was significantly increased in SSc compared to HC ($p < 0.01$). No significant differences were observed in the frequencies of CTLA4+ cells among CD25- Treg between the groups. In the CTLA4+ among the CD25lo Treg subset of the VEDOSS cohort, the median frequency was dramatically elevated with a threefold increase from 3.28% to 10.32% compared to HC ($p < 0.05$). Additionally, the SSc group also showed significantly increased frequencies of CTLA4+ cells among CD25lo Treg in comparison to HC ($p < 0.01$). Finally, only the SSc cohort displayed higher frequencies of CTLA4+ cells among CD25hi Treg in comparison to HC ($p < 0.05$; fig. 4.5B).
The analysis of Ki67+ cells revealed increased proliferation of the CD25- Treg subset in VEDOSS compared to SSc and HC, suggesting early immune changes in this cohort. In contrast, CTLA4+ expression was elevated in both SSc and VEDOSS patients across various CD25-expressing Treg subsets, indicating an altered immune regulation and a potential compensatory mechanism.

4.2.3 Correlation analysis between clinical parameters and frequencies of Treg subsets

In the previous sections, the immunophenotype of various FoxP3+CD127lo Treg subsets was analyzed, comparing their frequency distribution among HC, VEDOSS and SSc cohorts. To further explore the potential clinical relevance of these findings, the following section investigated correlations between these FoxP3+CD127lo Treg subsets and clinical parameters, including CRP, CK, creatinine, Nt-proBNP and the composite index for assessing global disease activity (EUSTAR AI). This analysis was essential as it allows for the identification of distinct relationships between FoxP3+CD127lo Treg subsets and markers of inflammation or organ dysfunction during the preclinical phase of the disease compared to the established stage. For this purpose, the dataset of the Treg immunophenotype, acquired by flow cytometry using PBMC from 23 VEDOSS and 54 SSc patients, was used and a correlation network and matrix were developed.

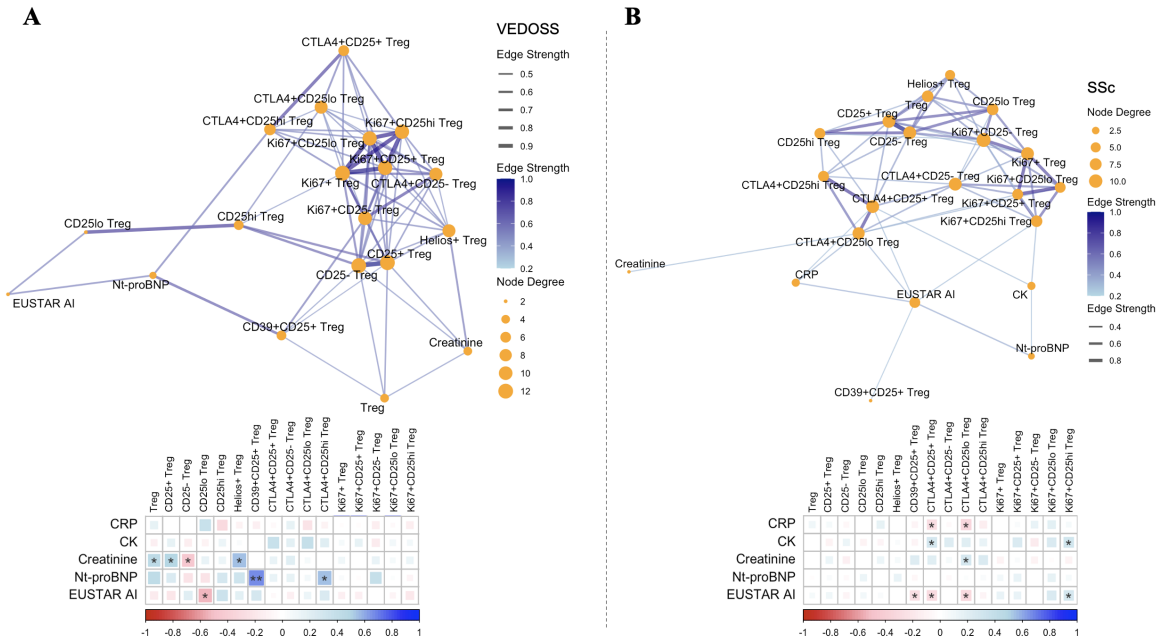

Figure 4.6 : Correlations between Treg subsets and clinical parameters. Immunophenotyping of PBMC from VEDOSS and SSc patients was performed via flow cytometry and a correlation network and matrix were developed in R with the CD3+CD4+FoxP3+CD127lo Treg immunophenotype of (**A**) VEDOSS and of (**B**) SSc patients. Statistical correlation analyses were performed using a Spearman's r test (matrix colorcode: red=negative correlation, blue=positive correlation). For correlation networks, specific threshold values were set: $p < 0.05$, $r > 0.2$ (node degree = degree of connectivity; edge strength color and thickness = correlation level; VEDOSS: n=23; SSc: n=54).

The network diagrams (fig. 4.6A and B, top) represent FoxP3+CD127lo Treg subsets and clinical parameters as nodes, with the node size indicating the degree of connectivity. Edges (=connection lines) between nodes denote correlations, with edge thickness and color intensity corresponding to the strength of the correlation. The correlation coefficient (r value), which ranges from 0.2 (weak correlation) to 1.0 (very strong correlation), was set as indicated in the legend.

In the correlation matrix, representing the VEDOSS cohort (fig. 4.6A, bottom), a statistically significant moderate negative correlation was observed between CD25- Treg and creatinine levels ($p < 0.05$; $r = -0.451$). In addition, creatinine levels showed a moderate positive correlation with the frequencies of total Treg, of CD25+ and of Helios+ Treg subsets (all $p < 0.05$; $r = 0.444$, $r = 0.482$ and $r = 0.556$, respectively). Nt-proBNP levels showed a significant positive correlation with frequencies of CD39+ cells among CD25+ Treg and CTLA4+ cells among CD25hi Treg ($p < 0.01$ and $p < 0.05$, respectively; $r = 0.669$ and $r = 0.552$). The EUSTAR AI presented a moderate

negative correlation with frequencies of CD25lo Treg ($p < 0.05$; r = -0.523). Other clinical parameters, such as CRP and CK, did not display significant correlations with the analyzed Treg subsets. In the correlation matrix, representing the SSc cohort (fig. 4.6B, bottom), two statistically significant weak negative correlations were observed between CRP levels and the CTLA4+ among CD25+ Treg and CTLA4+ among CD25lo Treg subsets (both $p < 0.05$; r = -0.280 and r = -0.325, respectively). In contrast to that, the CTLA4+ among CD25lo Treg subset correlated positively with creatinine levels ($p < 0.05$; r = 0.298) and the EUSTAR AI correlated negatively with the same subset ($p < 0.01$; r = -0.316). Additionally, the EUSTAR AI showed also significant negative correlations with the CD39+ among CD25+ Treg and CTLA4+ among CD25+ Treg subset (both $p < 0.05$; r = -0.275 and r = -0.296, respectively). Lastly, CK levels showed a significant weak positive correlation with CTLA4+ among CD25+ Treg and Ki67+ among CD25hi Treg (both $p < 0.05$; r = 0.297 and r = 0.307, respectively). Nt-proBNP levels did not display significant correlations with the analyzed Treg subsets in this cohort. Finally, the network visualization in both cohorts (4.6A and B, top) highlighted the centrality of specific functional Treg subsets, such as Ki67+ and CTLA4+ Treg subsets, in the overall interaction framework.
The correlation analysis revealed several significant correlations between Treg subsets and clinical parameters in both the VEDOSS and SSc cohorts. Notably, creatinine levels were correlated with various Treg subsets in VEDOSS, while CRP levels and the EUSTAR AI were more prominently associated with CTLA4+ and CD39+ Treg subsets in SSc. These findings suggest that specific Treg subsets may play central roles in disease progression and could be influenced by key clinical markers, highlighting their potential as indicators of disease activity.

4.2.4 Distribution of conventional CD4+ T cell subsets

Given the opposing roles of FoxP3+CD127lo Treg and FoxP3- Tcon cells in immune regulation, described in section 1.1.5, the analysis transitioned from examining various alterations in Treg subsets to investigating Tcon subsets to further explore this dynamic balance. The following figure demonstrates the distribution and frequencies of different CD3+CD4+FoxP3- Tcon subsets across HC, VEDOSS and SSc groups, acquired by flow cytometry (for gating strategy see fig. 3.3).

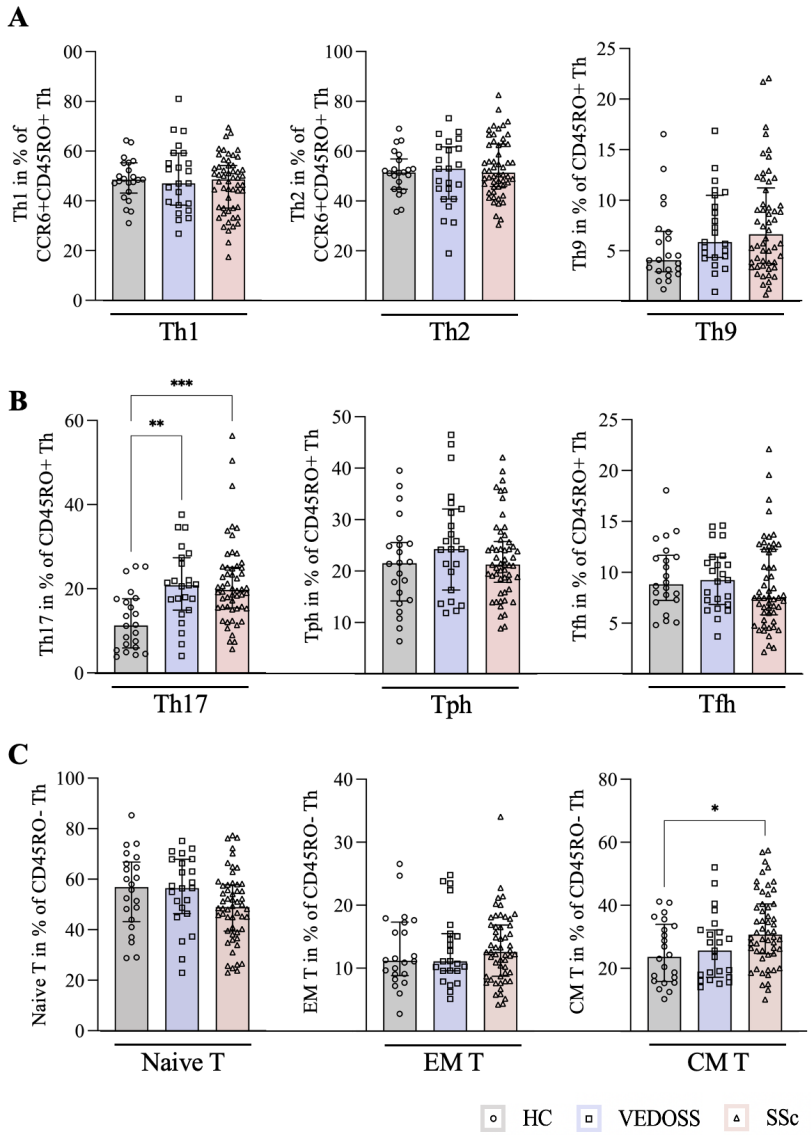

Figure 4.7 : Changes in Tcon subsets in VEDOSS and SSc compared to HC. Isolated PBMC were used to identify frequencies of (**A**) CCR6-CXCR3+ Th1 cells, CCR6-CXCR3- Th2 cells, CCR4-CCR6+ Th9 cells and (**B**) CCR4+CCR6+ Th17 cells, CXCR5-PD1+ Tph cells, CXCR5+PD1+ Tfh cells and (**C**) CCR7+ CM T cells and CCR7- EM T cells among CD3+CD4+FoxP3-CD45RO+ T cells, as well as CD3+CD4+FoxP3-CD45RO-CCR7+ naive T cells via flow cytometry. Statistical comparisons were performed using a Kruskal-Wallis test with Dunn's correction. Median values with error bars, indicating the IQR, are shown (HC: n=22; VEDOSS: n=23; SSc: n=54).

The frequencies of Th1 and Th2 cells did not display significant differences between the three groups (fig. 4.7A). Similarly, frequencies of Th9 cells remained comparable across HC, VEDOSS and SSc cohorts, even if a slight upward trend can be recog-

nized. Frequencies of Th17 cells were significantly higher to a similar extent in both VEDOSS and SSc patients compared to HC ($p < 0.01$ and $p < 0.001$, respectively; fig. 4.7B). In contrast, Tph and Tfh subsets did not show remarkable differences among the groups (fig. 4.7B). Lastly, the distribution of naive T cells and EM T cells were similar across all groups (fig. 4.7C), while frequencies of CM T cells were significantly higher in SSc patients compared to HC ($p < 0.05$; fig. 4.7C). With regard to proliferating Th subsets (Ki67+), only frequencies of Ki67+ naive T cells in the VEDOSS cohort showed a statistically significant increase in comparison to the SSc cohort ($p < 0.05$; data not shown). Compared to HC, VEDOSS patients showed tendencies towards an increase in frequencies of Ki67+ naive T cells without reaching statistical significance ($p = 0.056$; data not shown).
These results indicate a selective dysregulation of certain important CD4+ Tcon subsets across disease stages. While most CD4+ Tcon subsets remained unchanged in terms of frequencies, a significant increase in frequencies of Th17 cells in VEDOSS and SSc patients suggests a potential role in disease progression. Additionally, the elevated frequencies of CM T cells in SSc patients and the increased proliferation of naive T cells in VEDOSS patients may reflect early immune activation and uncontrolled immune responses.

4.2.5 Correlation between clinical parameters and the frequencies of CD4+ Tcon subsets

In addition to the comparative analyses of the different CD4+ Tcon subsets in the different cohorts, a correlation analysis with clinical parameters was performed for VEDOSS and SSc patients. The CD4+ Tcon immunophenotype dataset, obtained by flow cytometry using PBMC from 23 VEDOSS and 54 SSc patients, was used and a correlation matrix was developed.

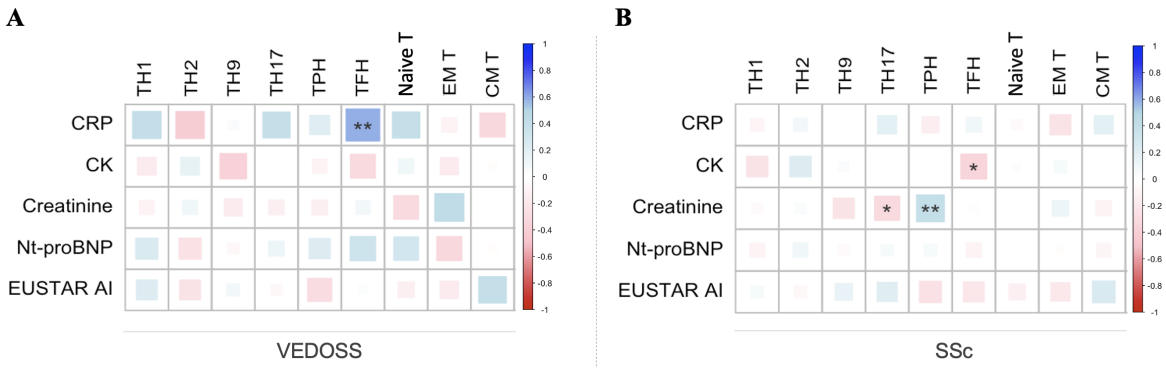

Figure 4.8 : Correlations between Tcon subsets and clinical parameters. Immunophenotyping of PBMC from VEDOSS and SSc patients was performed via flow cytometry and a correlation matrix was developed in R with the CD3+CD4+FoxP3- Tcon immunophenotype of (**A**) VEDOSS and of (**B**) SSc patients. Statistical correlation analyses were performed using a Spearman's r test (matrix color-code: red=negative correlation, blue=positive correlation; VEDOSS: n=23; SSc: n=54).

The correlation matrix of the VEDOSS cohort (fig. 4.8A) showed only one significant positive moderate correlation between frequencies of Tfh cells and CRP levels ($p < 0.01$; $r = 0.586$). For SSc patients (fig. 4.8B), frequencies of Tfh cells correlated negatively with CK levels ($p < 0.05$; $r = -0.343$) and, lastly, creatinine levels correlated on the one hand side positively with frequencies of Tph cells and on the other hand side negatively with frequencies Th17 cells ($p < 0.01$ and $p < 0.05$; $r = 0.397$ and $r = -0.319$, respectively). A correlation network analysis carried out did not reveal any interaction patterns and was therefore not shown here. These findings suggest that frequencies of Tfh and Tph cells show distinct associations with inflammatory and organ-related markers in VEDOSS and SSc, respectively, indicating potential links between specific Th subsets and disease-related immune or tissue alterations.

4.2.6 Shifts in Treg/Tcon ratios

After observing distinct differences in frequencies of Treg and Tcon cell subsets across cohorts, along with significant correlations to clinical parameters and disease severity, the next step was to analyze their ratios. Assessing the ratios of total Treg to Tcon subsets, as well as CD25hi Treg to Tcon subsets, provides deeper insight into immune homeostasis and helps reveal imbalances between regulatory and effector T cells across different disease stages.

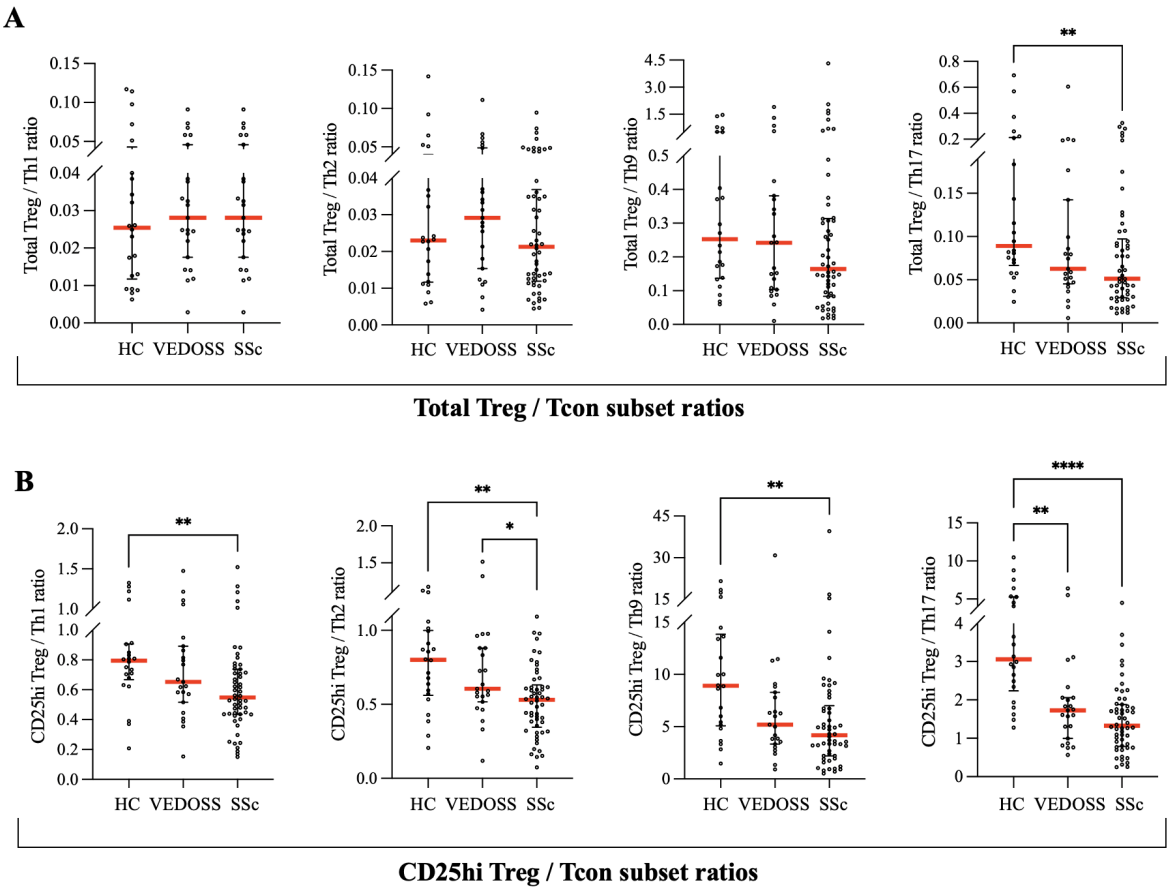

Figure 4.9 : Changes in Treg/Tcon subset ratios in VEDOSS and SSc compared to HC. Isolated PBMC were used to identify ratios between (**A**) FoxP3+CD127lo Treg per CCR6-CXCR3+ Th1 cells, CCR6-CXCR3- Th2 cells, CCR4-CCR6+ Th9 cells and CCR4+CCR6+ Th17 cells among CD3+CD4+FoxP3-CD45RO+ T cells, as well as (**B**) FoxP3+CD127loCD25hi Treg per the same Th subsets. Statistical comparisons were performed using a Kruskal-Wallis test with Dunn's correction. Median values with error bars, indicating the IQR, are shown (HC: n=22; VEDOSS: n=23; SSc: n=54).

The comparison of the overall ratio of total Treg/Tcon subsets (fig. 4.9A) showed only one significant result. The ratio of total Treg to Th17 cells was significantly lower in SSc patients compared to HC ($p < 0.01$), meaning that there were proportionally fewer Treg per Th17 cells in SSc in terms of frequencies. The more specific comparison of the CD25hi Treg/Tcon subset ratio (fig. 4.9B) showed an overall significant decrease in CD25hi Treg per each Tcon subset compared to HC. The CD25hi Treg/Th1 and CD25hi Treg/Th9 ratio was only in SSc patients significantly lower in comparison to HC ($p < 0.01$), but the CD25hi Treg/Th2 ratio showed, besides the reduction in SSc patients ($p < 0.01$) also a further decrease comparing VEDOSS and SSc patients ($p < 0.05$). The most pronounced difference compared to HC was in the CD25hi

Treg/Th17 ratio, which already decreased highly significantly in VEDOSS patients ($p < 0.01$) and worsened even further in SSc patients ($p < 0.0001$).
These results highlight a reduction in Treg/Tcon balance, particularly in the CD25hi Treg subset, across disease stages. While the total Treg/Th17 ratio was significantly lower in SSc patients, the CD25hi Treg ratios showed a broader decline across multiple Th subsets, with the most pronounced decrease observed in the CD25hi Treg/Th17 ratio.

4.2.7 Differences in frequencies of NK cell subsets

Building on the observed differences in Tcon subsets among the cohorts and considering a potential interplay between T cell and NK cell subsets, where T cells are modulating NK cell activity and vice versa, broader immune cell dynamics were further explored to uncover additional alterations in innate immune homeostasis [231, 232]. The volcano plots in figure 4.2 already showed significant changes in various immune cell subsets, particularly highlighting distinct patterns in NK cell subsets between HC, VEDOSS and SSc patients. This led to a more detailed examination of these subsets to assess their potential contributions to the immunological landscape of disease progression. The distribution and frequencies of CD3+CD56+ NK T cells and CD3-CD56+ NK cell subsets among total lymphocytes across HC, VEDOSS and SSc groups were acquired by flow cytometry (for gating strategy see fig. 3.5) and subsequently analysed.

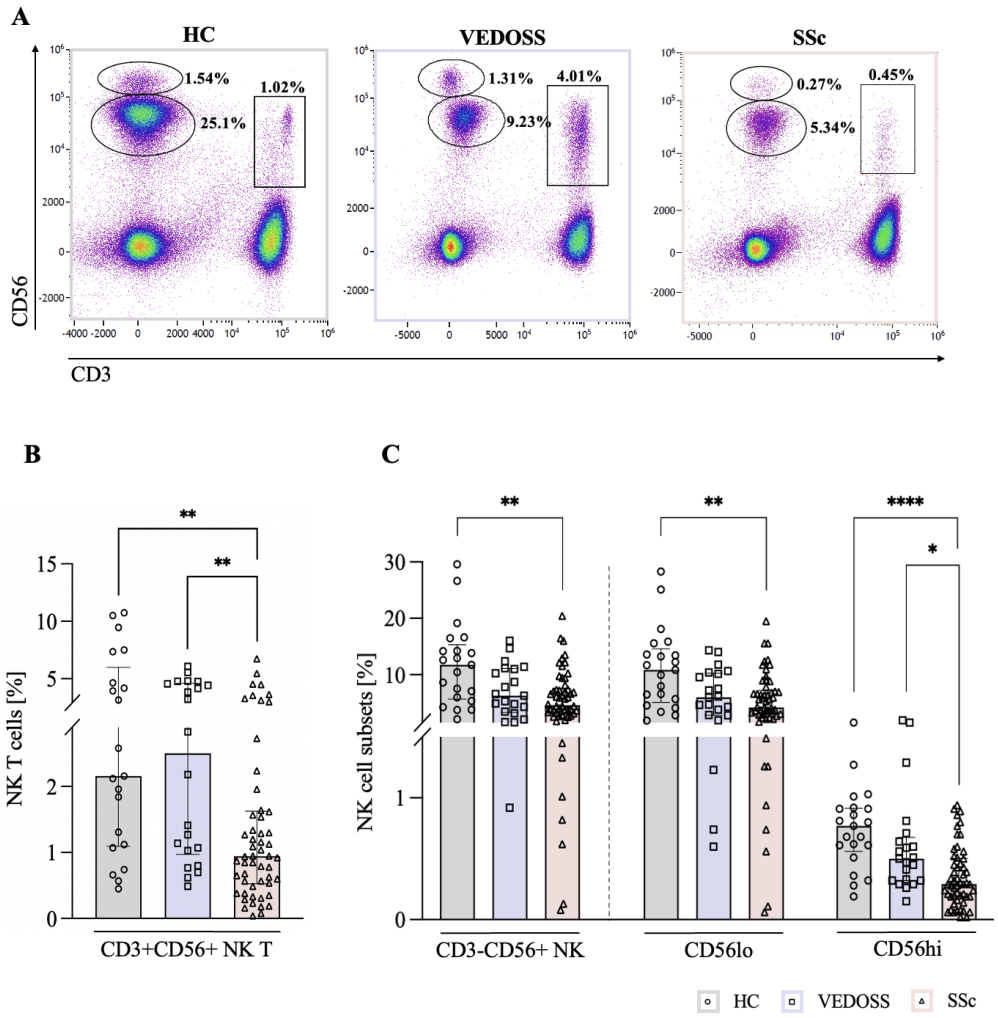

Figure 4.10 : Changes in NK cell subsets in VEDOSS and SSc compared to HC. **A**) Representative dot plots of frequencies of CD3-CD56lo NK, CD3-CD56hi NK and CD3+CD56+ NK T subsets among total lymphocytes from isolated PBMC. The frequencies of (**B**) CD3+CD56+ NK T cells and (**C**) CD3-CD56+, CD3-CD56lo and CD3-CD56hi NK cell subsets among total lymphocytes were determined and statistically compared using a Kruskal-Wallis test with Dunn's correction. Median values with error bars, indicating the IQR, are shown (HC: n=21; VEDOSS: n=23; SSc: n=54).

The dot plots (fig. 4.10A) show the gating and frequencies of CD56lo and CD56hi NK cells as wells as CD3+CD56+ NK T cells in a representative sample per group. After quantification, CD3+CD56+ NK T cells (fig. 4.10B) showed significantly decreased frequencies in the SSc cohort compared to HC and VEDOSS patients (both $p < 0.01$). The frequencies of the CD3-CD56+ NK cells (fig. 4.10C) were significantly reduced in SSc patients compared to HC ($p < 0.01$). This tendency towards a decline of CD3-CD56+ NK cell frequencies is also visible in comparison to the VEDOSS patients,

but without reaching the threshold of significance ($p < 0.08$). A comparable stepwise decline in cell frequencies was observed in both CD56lo and CD56hi NK cell subsets, with the most pronounced reduction in frequencies of CD56hi NK cells between HC and SSc patients, where the median frequency decreased from 0.77% in HC to 0.29% in the SSc group ($p < 0.0001$). A statistically significant decrease in frequencies of CD56hi NK cells was also observed when comparing the frequencies of SSc patients with those of the VEDOSS cohort ($p < 0.05$; fig. 4.10C). Regarding CD56lo NK cells, again, significantly lower frequencies were observed in SSc patients compared to HC ($p < 0.01$). The frequencies of CD56lo NK cells were also lowered in VEDOSS patients in comparison to HC but without being statistically significant ($p = 0.07$). The results indicated a progressive decline in NK cell frequencies across disease stages, with SSc patients showing the most pronounced reduction in multiple NK cell subsets. Notably, the marked loss of CD56hi NK cells, known for their immunoregulatory functions, may contribute to the dysregulation of immune homeostasis observed in SSc. The reduction of CD56+ NK cell subset frequencies seen in VEDOSS patients suggests a gradual shift toward a similar immunological profile, potentially reflecting early disease progression.

4.2.8 Correlation between clinical parameters and the frequencies of NK cell subsets

Similar to the analyses done with Treg subsets (see section 4.2.4), correlations between CD56+ NK cell subsets and the same clinical parameters were elucidated. The CD56+ NK cell immunophenotype dataset, obtained by flow cytometry using PBMC from 23 VEDOSS and 54 SSc patients, was used and a correlation matrix was developed.

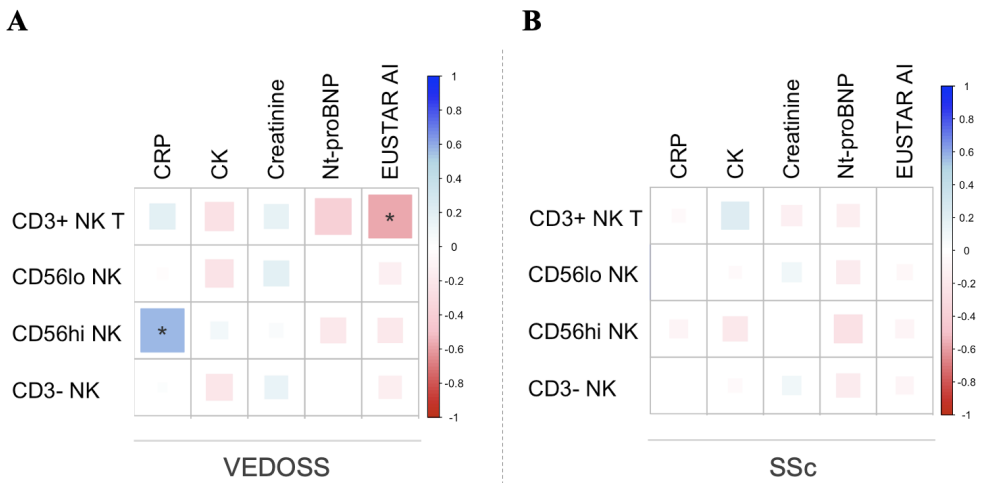

Figure 4.11 : Correlations between NK cell subsets and clinical parameters. Immunophenotyping of PBMC from VEDOSS and SSc patients was performed via flow cytometry and a correlation matrix was developed in R with the CD56+ NK immunophenotype of (**A**) VEDOSS and of (**B**) SSc patients. Statistical correlation analyses were performed using a Spearman's r test (matrix color-code: red=negative correlation, blue=positive correlation; VEDOSS: n=23; SSc: n=54).

In the correlation matrix, representing the VEDOSS cohort (fig. 4.11A), frequencies of CD56hi NK cells displayed a moderate positive correlation with CRP levels ($p < 0.05$; $r = 0.571$). In contrast, frequencies of CD3+CD56+ NK T cells correlated negatively with the EUSTAR AI ($p < 0.01$; $r = -0.562$). The correlation matrix, representing the SSc cohort (fig. 4.11B), showed no statistically significant correlation. Similar to the correlation analyses of the CD4+ T cell subsets, a correlation network analysis carried out did not reveal any interaction patterns and was therefore not shown here. However, the VEDOSS patients may exhibit an association between NK cell presence and inflammation, suggesting potential links between NK cell subsets and disease severity.

4.2.9 Distribution of B cell subsets and plasma cells

The analysis of NK cell subsets revealed notable differences among disease stages compared to HC, VEDOSS and SSc patients, particularly regarding the CD56hi NK and NK T subset. To further elucidate the immune profile of these groups, the immunophenotype of CD19+ B cell subsets was investigated, which play a complementary and crucial role in autoimmune processes and immune regulation. The distribution and frequencies of different CD19+ B cell subsets among total B cells across HC, VEDOSS

and SSc cohorts were acquired by flow cytometry (for gating strategy see fig. 3.4) and subsequently analysed. Due to current treatment with the B cell depleting agent rituximab (see table 4.1), only 44 SSc patients could be included in the analysis of the CD19+ B cell phenotype.

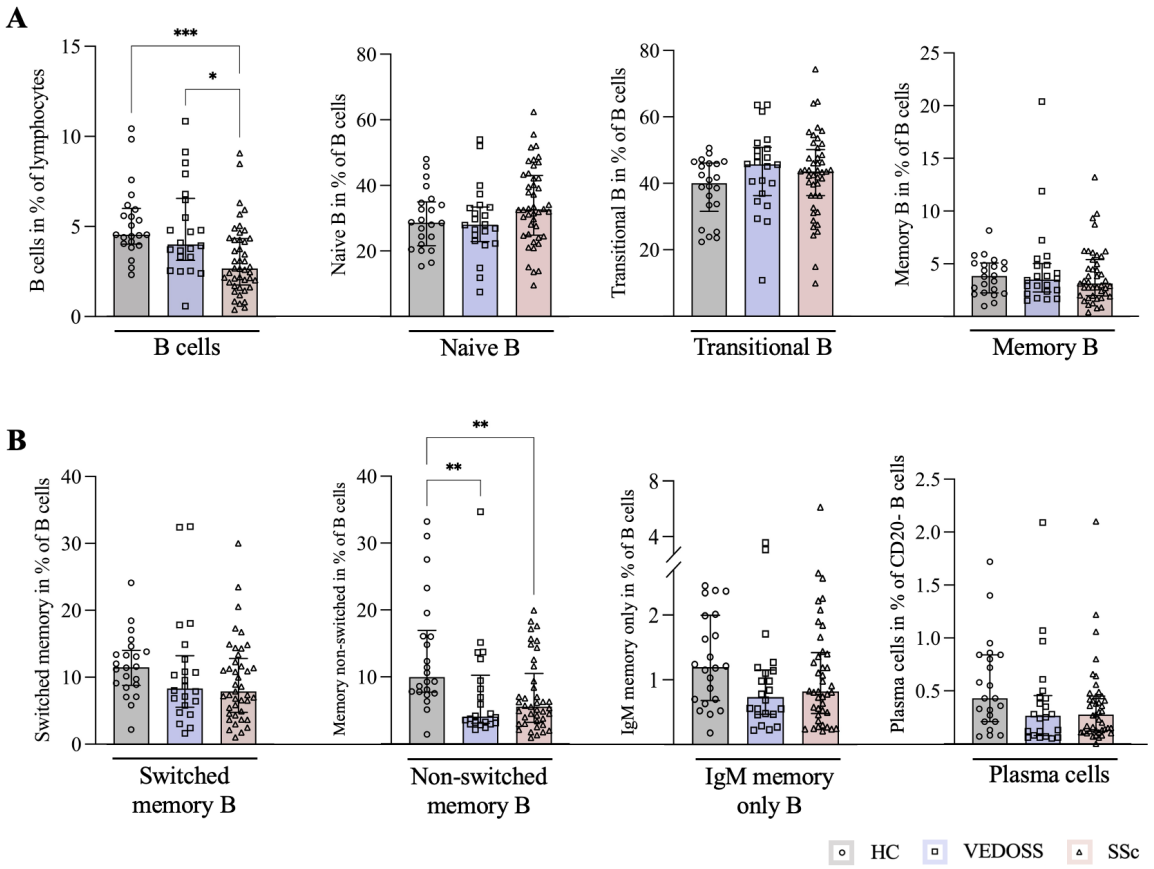

Figure 4.12 : Changes in B cell subsets and plasma cells in VEDOSS and SSc compared to HC. Isolated PBMC were used to identify frequencies of (**A**) CD19+CD20+ B cells among total lymphocytes and CD27-IgM+IgD+ naive B cells, CD27-IgM-IgD+ transitional B cells, CD27-IgM-IgD- memory B cells among CD19+CD20+ B cells and (**B**) CD27+IgM-IgD switched memory B cells, CD27+IgM+IgD+ non-switched memory B cells, CD27+IgM+IgD- IgM memory only B cells among CD19+CD20+ B cells, as well as CD20-CD38hiCD24-CD27+ plasma cells among CD19+ B cells via flow cytometry. Statistical comparisons were performed using a Kruskal-Wallis test with Dunn's correction. Median values with error bars, indicating the IQR, are shown (HC: n=22; VEDOSS: n=22; SSc: n=44).

Analysis of the total CD19+ B cell population (fig. 4.12A) revealed a significant decrease in frequencies of SSc patients, compared to HC and VEDOSS patients ($p < 0.001$ and $p < 0.05$, respectively). A similar result was found in the frequencies of non-switched memory B cells (fig. 4.12B), in which VEDOSS patients showed a

median reduction of 59.2% and SSc patients of 44.29% compared to HC (both $p < 0.01$). For all other B cell subsets, no significant differences were found between the three cohorts.
These findings indicate a notable decrease in total B cells in SSc patients and non-switched memory B cell frequencies in SSc and VEDOSS patients, with the latter suggesting an imbalance between the tolerogenic and activated memory B cell types, promoting early alterations in B cell populations, with VEDOSS patients approaching a similar trend to SSc patients.

4.2.10 Correlation between clinical parameters and the frequencies of B cell subsets

As the B cell subsets showed differences in frequency and distribution in the HC, VEDOSS and SSc cohorts, a possible influence of the clinical parameters mentioned in the previous sections was investigated. The dataset of the B cell immunophenotype, acquired by flow cytometry using PBMC from 22 VEDOSS and 44 SSc patients, was used to develop a correlation network and matrix.

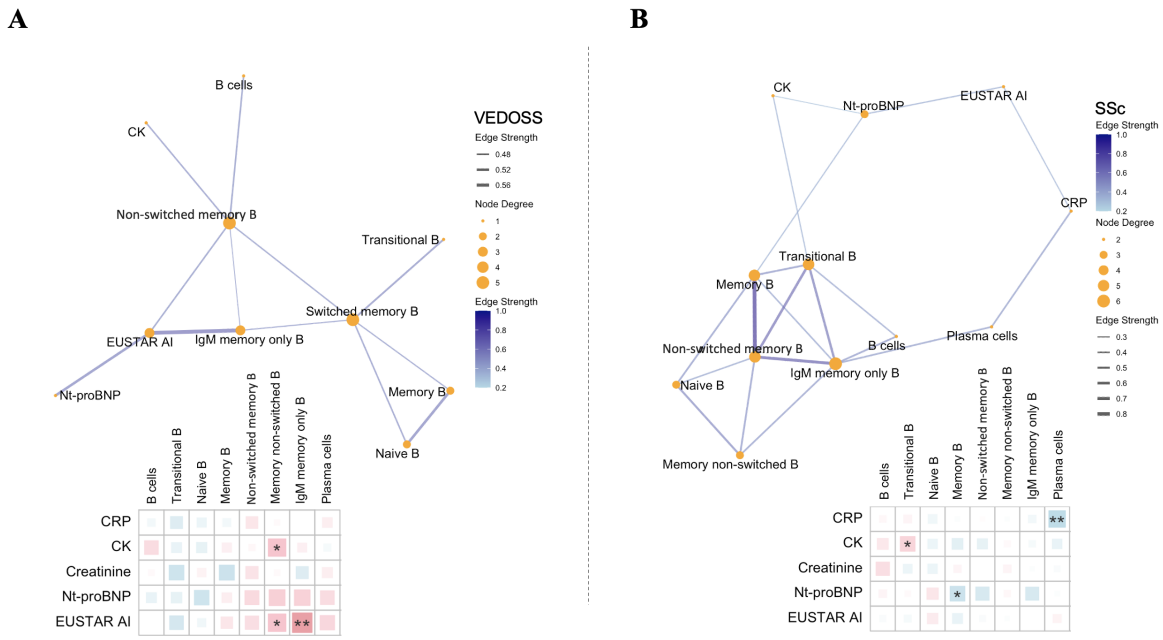

Figure 4.13 : Correlations between B cell subsets and clinical parameters. Immunophenotyping of PBMC from 22 VEDOSS and 44 SSc patients was performed via flow cytometry and a correlation network and matrix were developed in R with the CD19+ B cell immunophenotype of (**A**) VEDOSS and of (**B**) SSc patients. Statistical correlation analyses were performed using a Spearman's r test (matrix colorcode: red=negative correlation, blue=positive correlation). For correlation networks, specific threshold values were set: $p < 0.05$, $r > 0.2$ (node degree = degree of connectivity; edge strength color and thickness = correlation level; VEDOSS: n=22; SSc: n=44).

The correlation matrix (fig. 4.13A) revealed three negative correlations between CD19+ B cell subsets and clinical parameters. Frequencies of non-switched memory B cells correlated significantly either with CK levels and the EUSTAR AI (both $p < 0.05$; $r = -0.474$ and $r = -0.476$, respectively). Additionally, the EUSTAR AI also showed a moderate negative correlation with frequencies of IgM memory only B cells ($p < 0.01$; $r = -0.597$). In contrast to that, SSc patients presented various positive correlations (matrix in fig. 4.13B). Frequencies of plasma cells correlated significantly with CRP levels ($p < 0.01$; $r = 0.430$) and frequencies of memory B cells with Nt-proBNP levels ($p < 0.05$; $r = 0.341$). Only the frequencies of transitional B cells showed a significant negative correlation in SSc patients, which was related to CK levels and represented a weak interaction ($p < 0.05$; $r = -0.341$; fig. 4.13B). With regard to the correlation networks, clear interaction structures became visible, which showed that in SSc patients different B cell subsets influence each other, with inflammatory markers and disease activity scores being less important (fig. 4.13B).

In contrast, VEDOSS patients showed a less interactive network, although the clinical parameters had a greater influence here (fig. 4.13A). The correlation analysis highlights a shift in the relationship between B cell subsets and clinical parameters across disease stages. In VEDOSS patients, frequencies of non-switched memory and IgM memory only B cells were associated with markers of disease activity, suggesting a potential protective or regulatory role of these subsets. In contrast, SSc patients showed positive correlations between pro-inflammatory B cell subsets and markers of inflammation and organ involvement, indicating a possible contribution of activated B cells to disease progression.

4.2.11 Differences in frequencies of monocyte subsets

Building on the observed alterations in certain B cell subsets among the cohorts and considering the crucial crosstalk between B cells and monocytes in shaping immune responses, the analysis was extended to monocyte populations to further investigate potential dysregulations in innate immune homeostasis [233]. The distribution and frequencies of different HLA-DR+ monocyte cell subsets among total monocytes across HC, VEDOSS and SSc cohorts were acquired by flow cytometry (for gating strategy see fig. 3.5) and subsequently analysed.

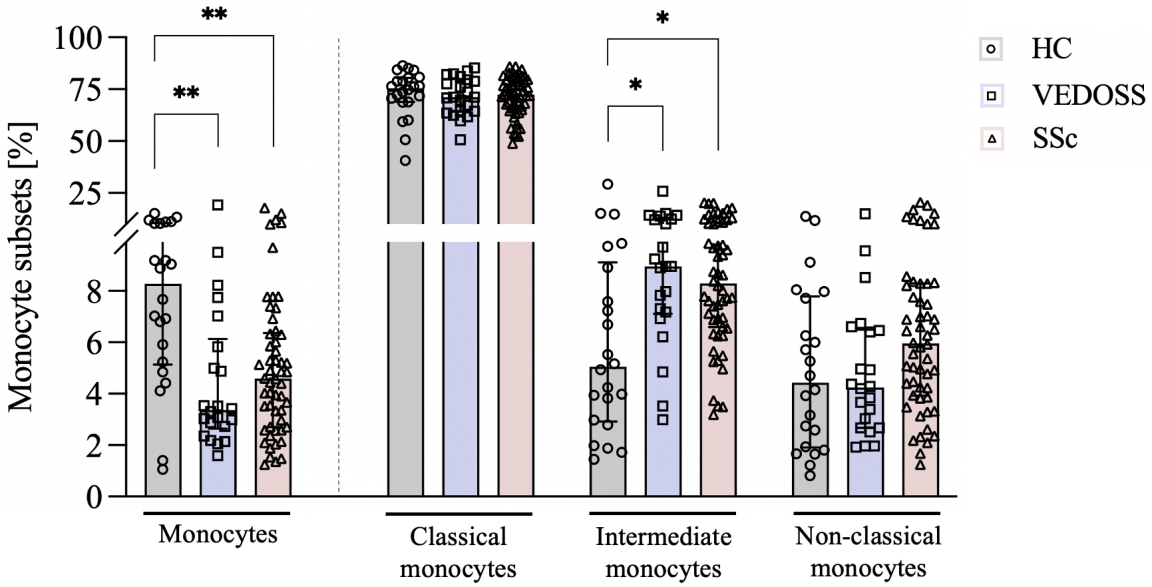

Figure 4.14 : Changes in monocyte subsets in VEDOSS and SSc compared to HC. Isolated PBMC were used to identify frequencies of total monocytes among whole PBMC, CD16-CD14+ classical monocytes, CD16+CD14+ intermediate monocytes and CD16+CD14- non-classical monocytes among HLA-DR+ monocytes via flow cytometry. Statistical comparisons were performed using a Kruskal-Wallis test with Dunn's correction for each subset. Median values with error bars, indicating the IQR, are shown (HC: n=22; VEDOSS: n=22; SSc: n=54).

The analysis of the frequencies of the entire monocyte population showed a significant decrease by about half in VEDOSS and SSc patients in comparison to HC (fig. 4.14, left graph). For VEDOSS patients, the median frequency dropped to 3.37% and for SSc patients to 4.59% compared to 8.29% in HC (both $p < 0.01$). In contrast, the frequencies of intermediate monocytes were significantly increased in both patient groups compared to the HC group (both $p < 0.05$). Frequencies of classical and non-classical monocytes did not display any significant differences among the cohorts.
The analyses demonstrated significant shifts in monocyte composition from health to disease, with a notable decrease in total monocyte frequencies in both VEDOSS and SSc patients, accompanied by an increase in pro-inflammatory intermediate monocytes compared to HC. These alterations may contribute to the immune dysregulation observed during disease development.

4.2.12 Correlation between clinical parameters and the frequencies of monocyte subsets

After the analysis and identification of aberrations in the immunophenotype of monocyte subsets in both disease states compared to HC (see section 4.2.11), a correlation approach with clinical parameters was carried out. For that purpose, the frequencies of the monocyte subsets, obtained by flow cytometry using PBMC from 22 VEDOSS and 54 SSc patients, was used and a correlation matrix and network was developed.

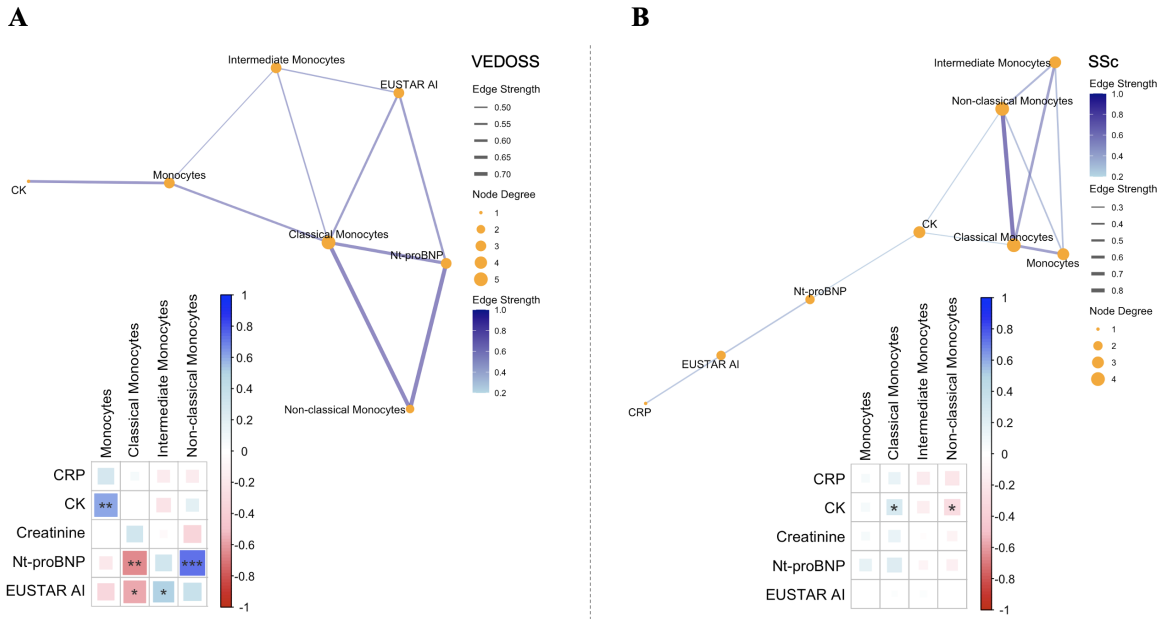

Figure 4.15 : Correlations between monocyte subsets and clinical parameters. Immunophenotyping of PBMC from VEDOSS and SSc patients was performed via flow cytometry and a correlation network and matrix were developed in R with the monocyte immunophenotype of (**A**) VEDOSS and of (**B**) SSc patients. Statistical correlation analyses were performed using a Spearman's r test (matrix colorcode: red=negative correlation, blue=positive correlation). For correlation networks, specific threshold values were set: $p < 0.05$, $r > 0.2$ (node degree = degree of connectivity; edge strength color and thickness = correlation level; VEDOSS: n=22; SSc: n=54).

In the correlation matrix of the VEDOSS cohort (fig. 4.15A, bottom), a significant positive correlation between the frequencies of total monocytes and CK levels was identified ($p < 0.01$; $r = 0.615$). More specifically and in contrast to that, frequencies of classical monocytes correlated negatively either with Nt-proBNP levels and the EUSTAR AI ($p < 0.01$ and $p < 0.05$; $r = -0.655$ and $r = -0.561$). The EUSTAR AI also correlated positively with frequencies of intermediate monocytes ($p < 0.05$; $r =$

0.522). Lastly, the only correlation seen in the non-classical monocytes was a strong positive correlation with Nt-proBNP levels ($p < 0.001$; $r = 0.733$; fig. 4.15A). In SSc patients, generally less significant correlations were found (fig. 4.15B). Only CK levels correlated either negatively with frequencies of non-classical monocytes and positively with frequencies of classical monocytes (both $p < 0.05$; $r = -0.282$ and $r = 0.270$). The network analyses in both cohorts (4.15A and B, top) showed distinct interactions between the monocyte subsets, partly influenced by the clinical parameters. It should be particularly emphasized that the monocyte subsets of VEDOSS patients were significantly influenced by the disease activity compared to the SSc group.
The correlation analysis suggests that in VEDOSS patients, distinct monocyte subsets are differentially associated with clinical markers of disease activity and organ involvement, highlighting their potential role in disease progression. In contrast, SSc patients showed fewer and weaker correlations, indicating a possible shift in immune regulation as the disease advances.

4.3 Prediction of disease trajectories

While univariate analyses provide valuable insights into individual immune cell subsets and their differences among HC, VEDOSS and SSc patients, they are not able to capture the complex interactional effects and interdependencies between these immune cell populations. Given the heterogeneous nature of autoimmune diseases, in which several immune pathways interact, a multivariate approach is crucial to fully understand these interactions. By integrating data from multiple immune cell subsets simultaneously, predictive analyses can reveal complex immune signatures that would remain hidden in the individual analyses. Such analyses are particularly powerful for precision medicine, enabling the identification of immune signatures that can guide the development of individualized therapies and improve clinical decision-making in autoimmune diseases.

4.3.1 Random Forest-based prediction of HC and VEDOSS classification

A random forest prediction algorithm was developed to classify the HC and VEDOSS cohorts based on immunophenotype frequencies (23 HC, 23 VEDOSS patients). The procedure outlined in subsection 3.4.6 was followed, with only cohort-specific adjustments applied. The dataset was split into a 70/30 ratio, allocating 70% for training the algorithm and 30% for evaluating prediction accuracy. To optimize the grid search, parameter ranges were predefined: mtry (the number of variables considered at each node split) ranged from 5 to 13, ntree (the number of decision trees) ranged from 30 to 500 and nodesize (the minimum size of terminal nodes) ranged from 3 to 10. The optimal parameter combination consisted of an mtry of 7, ntree of 60 and nodesize of 4 (fig. 4.16A, small table). Additionally, an error tree plot was employed to visualize how the error rates of the random forest model evolved as the number of trees in the forest increased (appendix section A.4, table A.2).

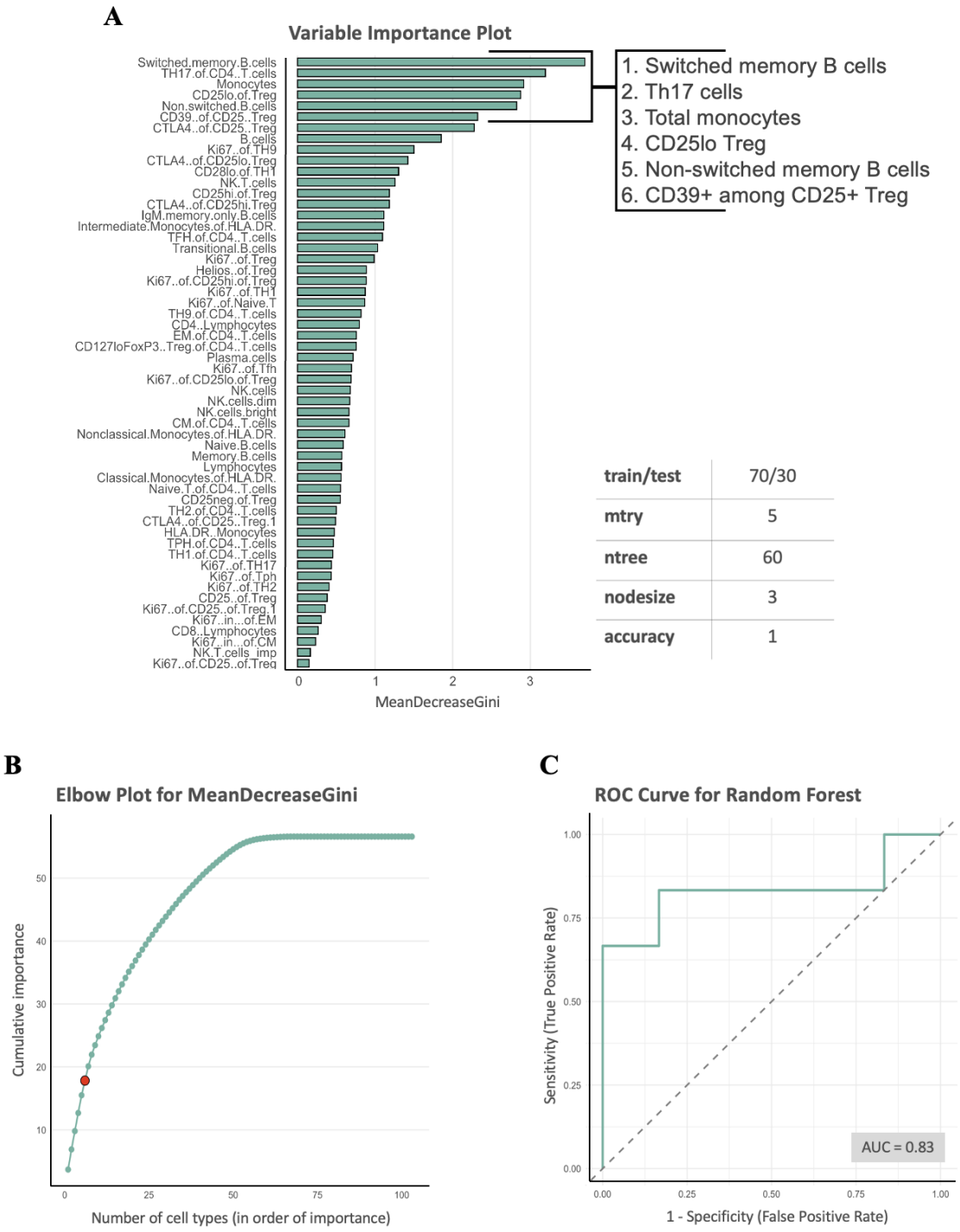

Figure 4.16 : Random forest prediction analysis discriminating HC and VEDOSS patients based on the immunophenotype frequencies. For the PBMC of 23 HC, 23 VEDOSS patients, immunophenotyping via flow cytometry was performed. **A**) Optimal hyperparameter combination as well as variable importance analysis based on MeanDecreaseGini values was conducted and visualized, followed by an (**B**) elbow plot presenting the cumulative importance and the number of variables for decision-making. **C**) A ROC curve analysis with an AUC value quantified the model's overall discriminatory power.

Once the algorithm had been successfully optimized using the training dataset, the test dataset was used to assess the actual prediction accuracy. First, a variable importance plot and the Gini index (fig. 4.16A) were used to break down which variables had a major influence on the model performance and thus the improved class separation. The relative measure MeanDecreaseGini was used to determine the importance of a variable with regard to the improvement of class purity in the decision trees of the random forest. Since the MeanDecreaseGini shows how much a variable contributes to the reduction of the Gini index across all trees and nodes, larger values mean that the variable has a greater impact on model performance as it better supports class separation. As an example, the highest MeanDecreaseGini value was reached by switched memory B cells, which meant that this B cell subset contributed the most to class segregation in the decision-making process. However, while the variable importance plot only created a rank of the variables, an elbow plot was added to visualize the cumulative importance of features and identify the point where adding more features yields diminishing returns (fig. 4.16B). This was crucial for feature selection, as it helps pinpoint the optimal number of features needed for model performance, balancing complexity and interpretability. Referring to the cumulative importance, the elbow plot presented the first six variables as most important for deciding whether an immunophenotype belongs to an HC or VEDOSS patient. Therefore, switched memory B cells, Th17 cells, total monocytes, CD25lo Treg, non-switched memory B cells and CD39+ cells among CD25+ Treg were highlighted. Lastly, a ROC curve was employed (fig. 4.16C) to evaluate the classification ability to differentiate between the cohorts across different threshold values and the AUC value quantified the model's overall discriminatory power. The analysis yielded an AUC of 0.83 (83% probability of correct decision), indicating a satisfactory ability to discriminate between an HC and a VEDOSS patient based only on the measured cell frequencies.

The predictive model demonstrated a strong performance and identified switched memory B cells as the most influential variable, underlining their potential role in early disease processes. The elbow plot further refined feature selection, identifying a core set of six variables, including Th17 cells and crucial Treg subsets, that optimized model performance while maintaining interpretability. The ROC analysis confirmed the model's reliability, indicating a high probability of correct classification.

4.3.2 Random Forest-based prediction of VEDOSS and SSc classification

After successfully applying a random forest prediction algorithm to discriminate between HC and VEDOSS patients, the entire procedure also had to be taken one step further and adapted to discriminate between VEDOSS and SSc patients. For this purpose, the immunophenotype frequencies of 23 VEDOSS and 54 SSc patients were used and again a 70/30 split into training and test data sets was made. After testing all combinations of hyperparameters, the following optimal parameters were identified: mtry = 7, ntree = 60, nodesize = 4 (fig. 4.17A, small table). The respective error tree plot can be found in section A.5, table A.3.

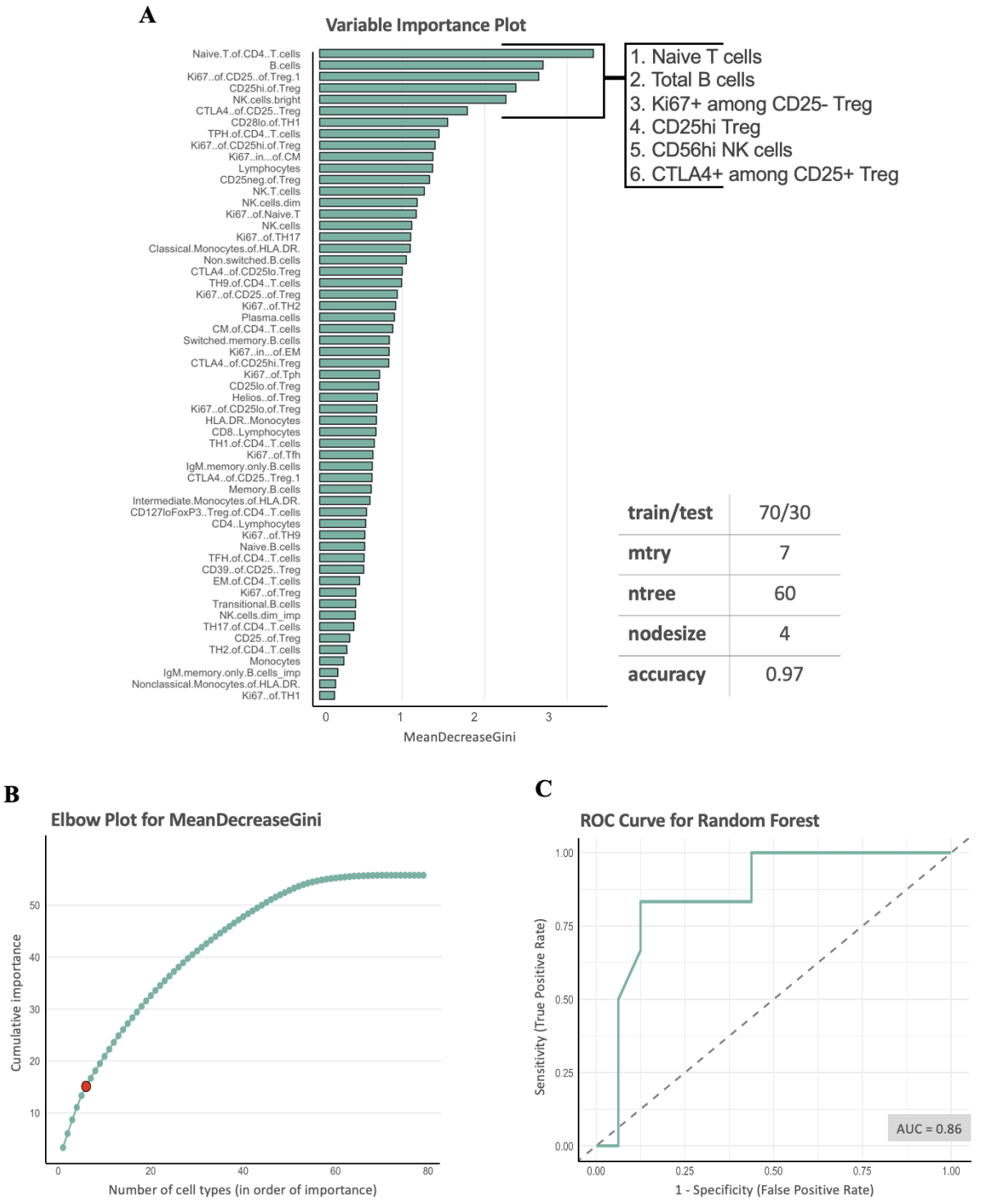

Figure 4.17 : Random forest prediction analysis discriminating VEDOSS and SSc patients based on the immunophenotype frequencies. For the PBMC of 23 VEDOSS, 54 SSc patients, immunophenotyping via flow cytometry was performed. **A**) Optimal hyperparameter combination as well as variable importance analysis based on MeanDecreaseGini values was conducted and visualized, followed by an (**B**) elbow plot presenting the cumulative importance and the number of variables for decision-making. **C**) A ROC curve analysis with an AUC value quantified the model's overall discriminatory power.

The variable importance plot (fig. 4.17A) revealed naive T cells as most important variable in decision-making whether a patient is diagnosed with a VEDOSS or SSc, based on its MeanDecreaseGini value. However, the elbow plot (fig. 4.17B) proved that, again, the first six cell types in combination were of decisive importance for model's performance. Therefore, besides naive T cells, also total B cells, Ki67+ cells among CD25- Treg, CD25hi Treg, CD56hi NK cells and CTLA4+ cells among CD25+ Treg. With that, a pattern consisting of different functional Treg subsets was pronounced, which played a major role in the decision-making process between VEDOSS and SSc patients. Lastly, the AUC value from the ROC curve analysis (fig. 4.17C) highlighted a robust probability of 86% correct decisions within the test dataset.
With 86% reliability, the prediction model proved to be even more powerful than the model that distinguishes between HC and VEDOSS patients. Naive T cells were identified as the most influential variable and, again, the elbow plot pointed out the importance of six cell types for optimal model performance. Notably, multiple functional Treg subsets played a decisive role in classification, highlighting their relevance in disease progression. Both random forest analyses emphasized the potential of machine learning approaches in identifying immunological predictors of disease progression.

4.4 Investigation of the inflammatory proteome in VEDOSS and SSc

While the detailed immunophenotyping of peripheral blood has provided valuable insights into the cellular landscape and its variations across HC, VEDOSS and established SSc, it is crucial to extend the investigation beyond cell frequencies. Secreted inflammatory proteins in the serum represent an essential component of the immune response, often reflecting signaling dynamics and the functional state of immune cells. Analyzing these proteins can reveal complementary and potentially unique insights into the pathophysiological differences between early and established SSc.
To this end, a targeted proteomic analysis was performed using the Olink® platform to quantify the expression levels of 92 inflammatory proteins in serum samples from 32 VEDOSS and 56 SSc patients (see subsection 3.3.3). Due to the fact that there was space for 88 test sera on an Olink® plate, additional VEDOSS and SSc patient sera from the serum bank was taken and added accordingly. The initial step in this analysis involved a PLS-DA based on the NPX values. This method was applied to visualize the separation and distribution between the two groups, offering a prelimi-

nary assessment of how their serum proteomic profiles differ and highlighting potential markers of disease progression.

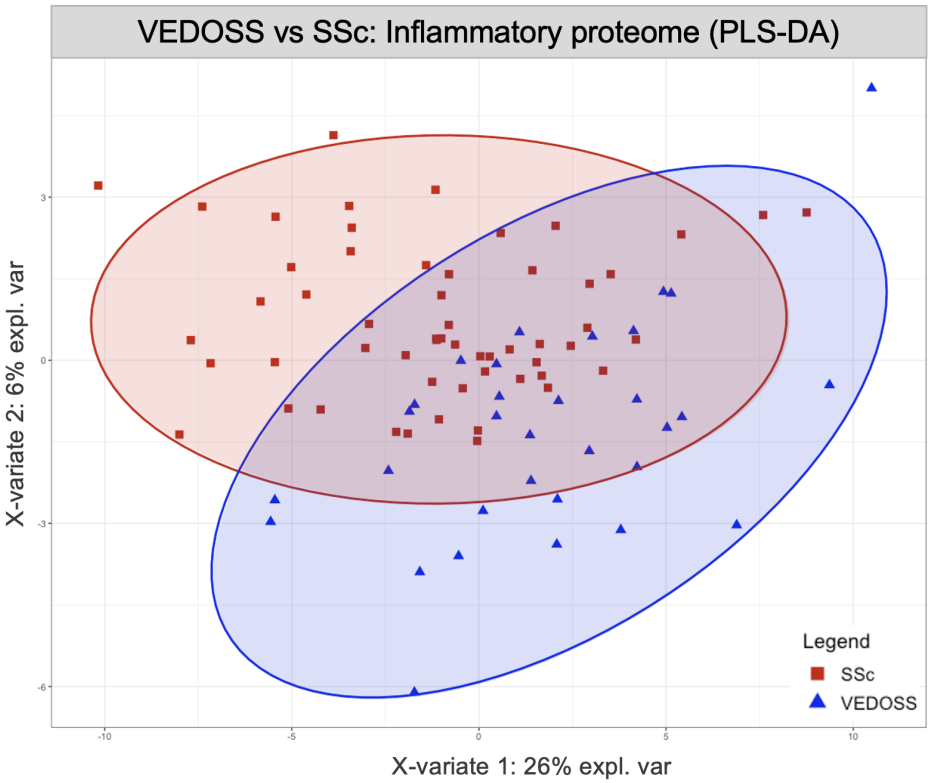

Figure 4.18 : Two-dimensional distribution of the inflammatory proteome using serum of VEDOSS and SSc patients. Clustering performed based on the NPX values of 92 different proteins, measured via PEA. Each ellipse represents the 95% confidence interval, while each dot represents one patient (colorcode: VEDOSS=blue; SSc=red). The axes correspond to the first two components of the PLS-DA: the x-axis (X-variate 1) explains 26% of the variance and the y-axis (X-variate 2) explains 6% of the variance in the dataset (VEDOSS: n=32; SSc: n=56).

In the PLS-DA score plot (fig. 4.18), both cohorts are represented by a unique color and corresponding ellipse, indicating the 95% confidence interval for each group, with each dot representing one individual. The X-variate 1 (26% explained variance) and X-variate 2 (6% explained variance) axes together capture 32% of the variance among groups. The ellipses of the VEDOSS and SSc groups showed large areas of overlap, although the VEDOSS cohort still showed some significant deviations, indicating that there are distinct differences in the proteome profile.

After PLS-DA revealed notable differences in the distribution of the measured inflammatory proteome between VEDOSS and SSc patients, a Welch's t-test was applied

to further investigate specific differences in individual proteins to assess statistically relevant differences, which were visualized in a volcano plot (fig. 4.19).

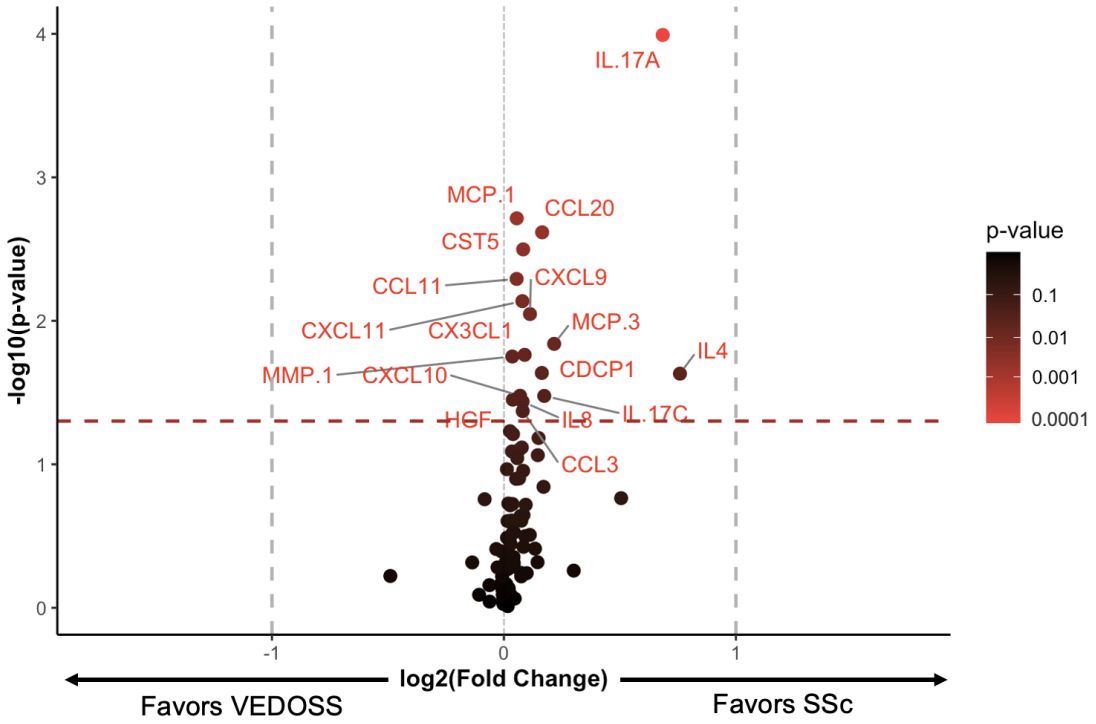

Figure 4.19 : Volcano plot of differential inflammatory protein expressions between VEDOSS and SSc patients. Each point represents a single protein, with the x-axis displaying the log2 fold change between groups and the y-axis showing the -log10 transformed p-value based on a Welch's t-test. Red color intensity reflects p-value significance, with brighter red color indicating higher statistical significance. The dashed red line marks the significance threshold of $p < 0.05$. The proteins to the left of the zero point of the x-axis favor VEDOSS patients, while those to the right of the zero point favor SSc patients (VEDOSS: n=32; SSc: n=56).

The expression of each protein between VEDOSS and SSc patients was compared (fig. 4.19). The most noticeable proteins in terms of expression differences between the cohorts was IL-17A, followed by MCP1 and CCL20. In total, 17 proteins showed statistically significant differences in expression patterns that exclusively favored SSc patients (specific p-values and log2FC values are listed in A.6).

These volcano plots complement the PLS-DA findings by quantifying and visualizing specific inflammatory proteins that differ significantly between VEDOSS and SSc cohorts. They provide a more detailed view of protein-level differences between early and established disease stages, highlighting key inflammatory mediators that warrant

further investigation in subsequent targeted analyses to better understand their roles in SSc progression.

4.4.1 Functional characterization of differentially expressed proteins

The group comparison identified 17 inflammatory proteins with significantly different expression levels between VEDOSS and SSc patients (see fig. 4.19). To systematically classify these proteins and understand their biological implications, Kyoto Encyclopedia of Genes and Genomes (KEGG) pathway enrichment analysis was performed to map them to relevant cellular and molecular pathways. Additionally, a Gene Ontology (GO) molecular function analysis was conducted to provide further insights into their specific roles in molecular processes (see subsection 3.4.6).

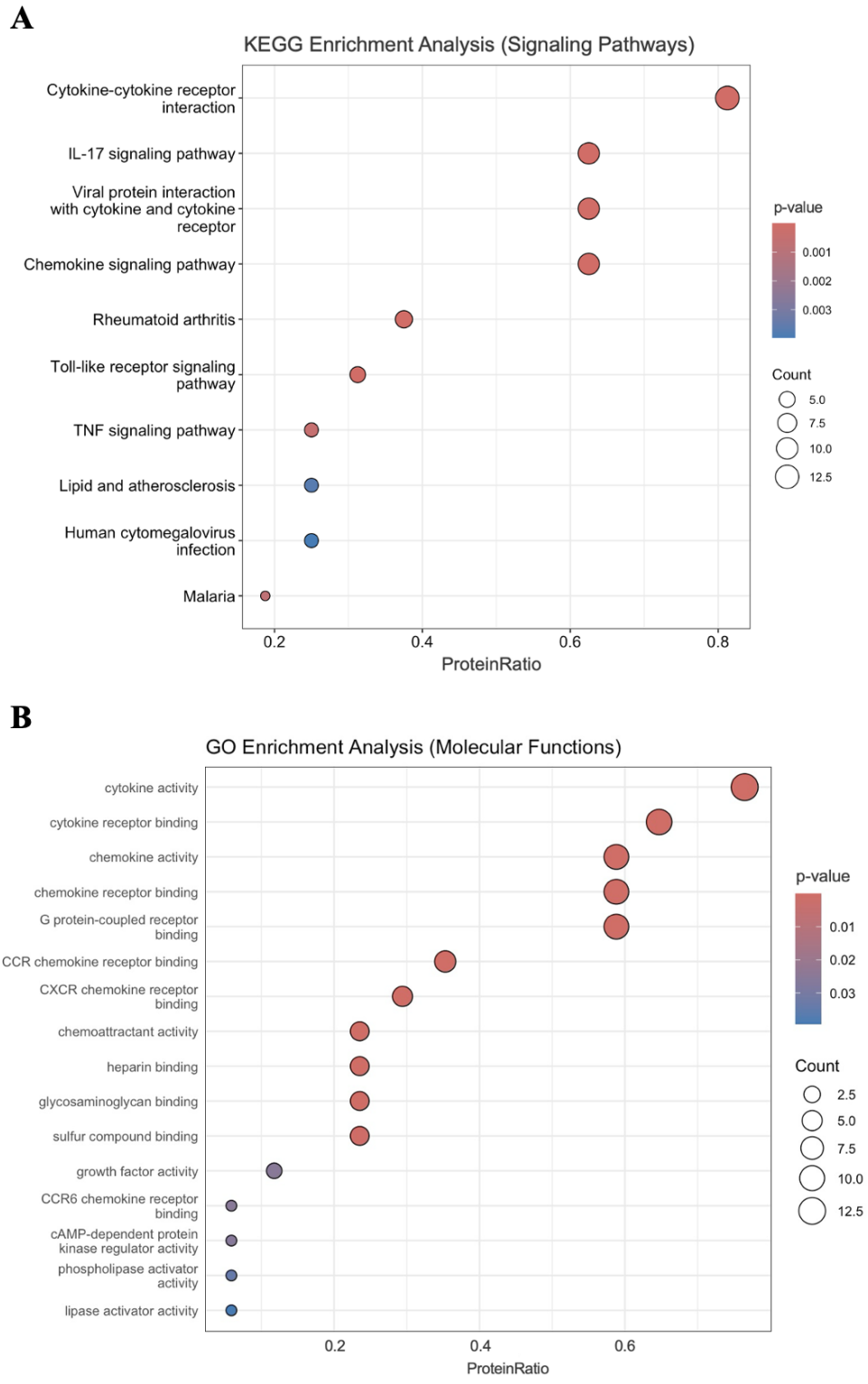

Figure 4.20 : **A**) KEGG and (**B**) GO enrichment analysis based on 17 significantly different expressed proteins in the serum of VEDOSS and SSc patients, acquired by PEA via the Olink® platform. The ProteinRatio on the x axis indicates the proportion of proteins mapped to the respective pathway, while the circle size represents the count of proteins associated with each pathway. The p-value gradient indicates the p-value of the enrichment (VEDOSS: n=32; SSc: n=56).

The KEGG enrichment analysis (fig. 4.20A) revealed several signaling pathways associated with the differentially expressed proteins of interest between VEDOSS and SSc. The most enriched pathways included cytokine-cytokine receptor interaction, IL-17 signaling, viral protein interaction with cytokine and cytokine receptors and the chemokine signaling pathway. Another metabolic pathway with remarkable enrichment was the signaling pathway of rheumatoid arthritis, which is very similar to that of SSc (the KEGG library does not contain an explicit SSc pathway). The other pathways shown had a lower protein ratio, meaning that fewer proteins were involved. The protein ratio for each pathway indicates the proportion of significant proteins mapped to the respective pathway, while the circle size represents the count of proteins associated with each pathway. The p-value gradient indicates the statistical significance of the enrichment. The GO enrichment analysis for molecular functions (fig. 4.20B) identified several enriched categories, including cytokine activity, cytokine receptor binding, chemokine activity, chemokine receptor binding and GPCR binding. Other enriched molecular functions were less abundant among the proteins. Similar to the KEGG analysis, protein ratios indicate the proportion of proteins contributing to each molecular function, while the circle size reflects the protein count and the p-value gradient denotes statistical significance.
The KEGG and GO enrichment analyses highlight a strong involvement of cytokine- and chemokine-related pathways and functions in the transition from VEDOSS to SSc. These findings suggest that dysregulated immune signaling, particularly through cytokine and chemokine interactions, plays a central role in disease progression and may reflect underlying mechanisms shared with other inflammatory conditions such as rheumatoid arthritis.

To assign the identified top 10 signaling pathways from the KEGG enrichment analysis (see fig. 4.20A) to the significantly differentially expressed proteins, visualized in the volcano plot (fig. 4.19), a KEGG chord plot was added. For this purpose, the results of the previous KEGG enrichment analysis were extracted and protein-to-pathway mapping has been implemented.

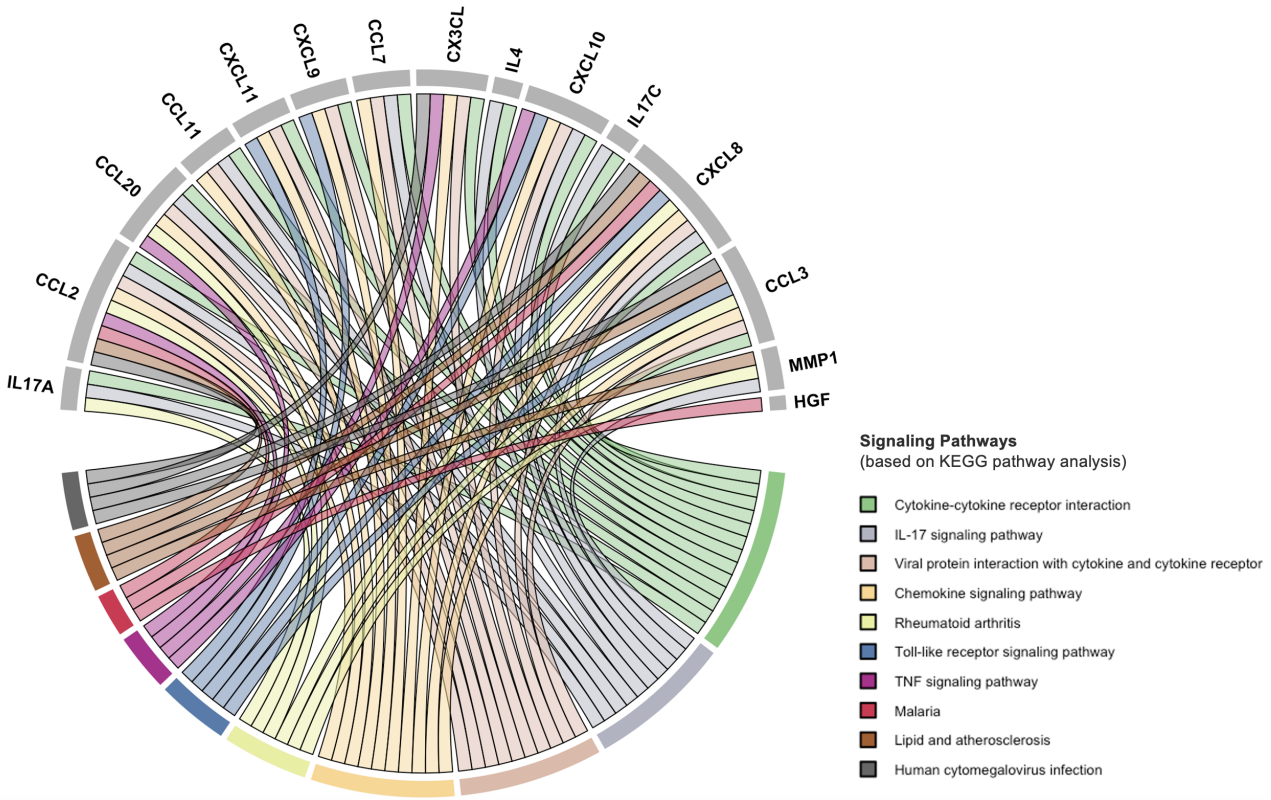

Figure 4.21 : KEGG Chord plot visualizing protein-to-pathway analysis. Chord plot basing on the KEGG enrichment results, which included 15 significantly different expressed proteins in the serum of VEDOSS and SSc patients, acquired by Olink® inflammatory proteome analysis. Different string colors represent the 10 signal pathways that emerged as the most important in the previous analysis (VEDOSS: n=32; SSc: n=56).

The chord plot (fig. 4.21) revealed the contribution of each protein to the top 10 most important pathways based on the KEGG enrichment analysis. In total, 15 of the original 17 significantly differentially expressed proteins between VEDOSS and SSc patients could be assigned to the top 10 enriched KEGG pathways. Some of the proteins showed involvement in a variety of signaling pathways. These include CCL2 and CXCL8 with presence within 9 of the 10 signaling pathways, followed by CCL3 with involvement in 7 signaling pathways and CXCL10 and CCL20 with involvement in 6 pathways. Particularly important was IL17A, which was in the IL-17 signaling pathway, cytokine-cytokine receptor interaction and the rheumatoid arthritis signaling pathway, highlighting its involvement in diverse immune and inflammatory processes. A similar contribution pattern was shown by MMP1 which also contributed to the rheumatoid arthritis and IL-17 signaling pathway. The cytokine-cytokine receptor interaction pathway represented the most broadly connected one, involving nearly

all the proteins displayed. Additionally, pathways like the chemokine pathway, viral protein interaction pathway and IL-17 signaling pathway demonstrated significant overlap in protein involvement. Overall, the plot underscored the multifunctionality of these proteins and the interconnected nature of the pathways they regulate.

To further explore the role of IL-17A and its associated proteins within the IL-17 pathway, for instance CXCL10 and MMP1, a detailed visualization of the entire KEGG IL-17 pathway (hsa04657) was performed, which provided a comprehensive overview of how the differentially expressed proteins favoring all SSc patients (volcano plot, fig. 4.19) are integrated into this pathway, highlighting their specific interactions and contributions to the signaling cascade. By mapping these proteins into the entire IL-17 pathway, it became possible to pinpoint their exact positions and roles, offering deeper insights into the molecular mechanisms driving disease-related inflammation and immune dysregulation.

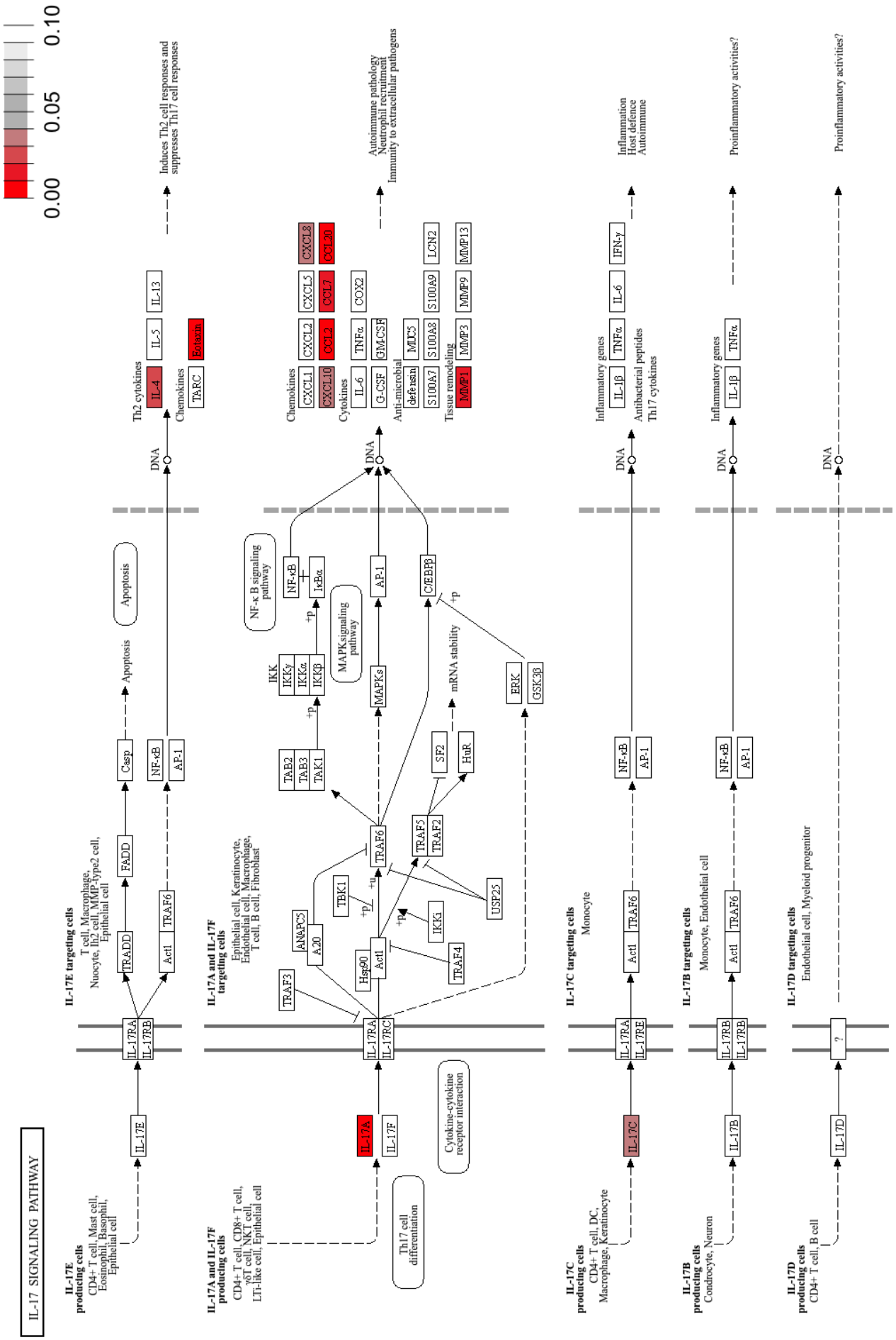

Figure 4.22 : KEGG IL-17 signaling pathway (hsa04657). Proteins that were significantly differentially expressed between VEDOSS and SSc patients within the pathway are highlighted in red, with the color brightness corresponding to the respective p-value. Proteins that remained white were either not significantly differentially expressed or not measured (VEDOSS: n=32; SSc: n=56).

The mapping of differentially expressed proteins, which were all higher in their expression in SSc patients, to the detailed IL-17 signaling pathway shown (fig. 4.22) proved the dependence and regulation of several other inflammatory and matrix remodeling proteins downstream of the signaling cascade by IL-17A expression. It was important to point out that a great variety of chemokines with C-C and C-X-C motif were elevated in their expression in SSc patients compared to VEDOSS patients, namely CCL2 ($p < 0.01$), CCL7 ($p < 0.05$), CCL20 ($p < 0.01$), CXCL8 ($p < 0.05$) and CXCL10 ($p < 0.05$). Lastly, MMP1 expression was also significantly higher ($p < 0.05$) in the the IL-17A-dependent pathway. Regarding the IL-17E pathway, (IL-17E was not part of the Olink® Inflammation Panel), IL-4 and eotaxin (=CCL11) showed significantly higher expression levels in SSc compared to VEDOSS patients ($p < 0.05$ and $p < 0.01$, respectively).
Finally, the whole pathway enrichment analyses revealed the upregulation and thus the importance of several IL-17A-dependent inflammatory and matrix remodeling proteins in SSc patients, underlining the role of this pathway in disease progression. Notably, several chemokines associated with immune cell recruitment, such as CXCL10, were significantly upregulated, accompanied by increased levels of tissue remodeling mediators like MMP1. These results further highlighted the role of IL-17 signaling and general cell migration in influencing the inflammatory environment in SSc.

4.4.2 Correlation between the IL-17 pathway-dependent proteins and clinical parameters

The previous subsection has shown significant correlations between IL-17 pathway-dependent proteins and aAb levels across VEDOSS and SSc patients. Building on these findings, the next subsection explored the relationship between IL-17 pathway-dependent proteins and key clinical parameters to investigate how IL-17 signaling may contribute to disease progression and clinical manifestations in VEDOSS and SSc patients.

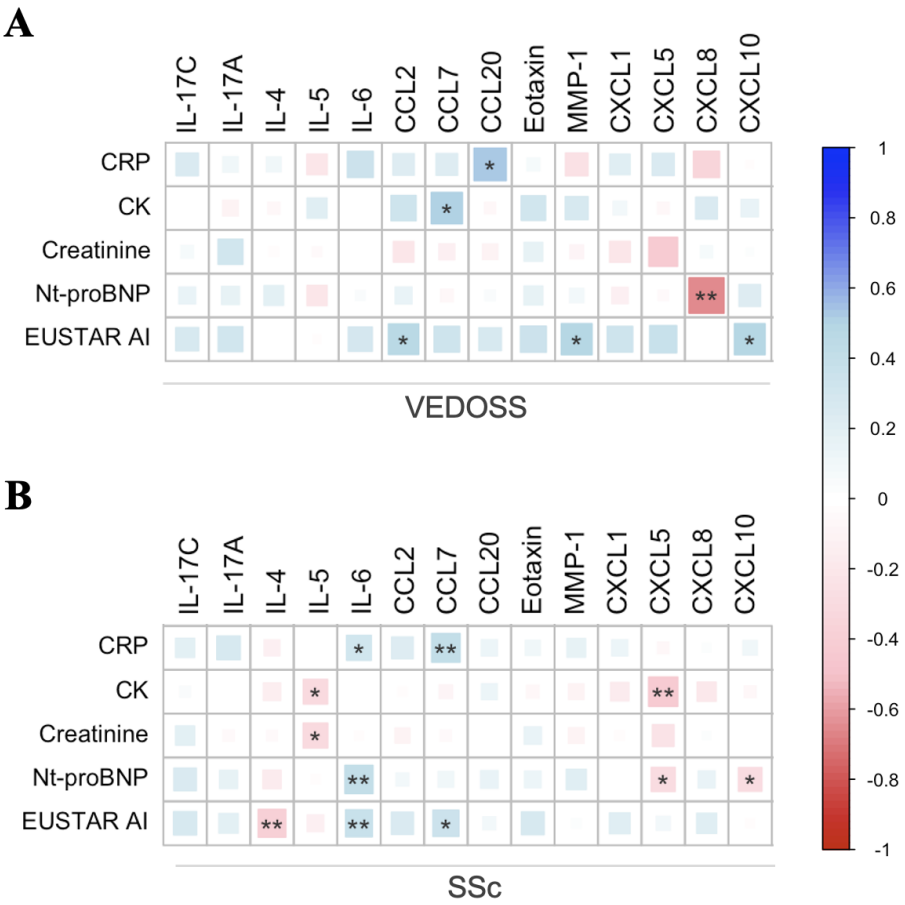

Figure 4.23 : Correlations between IL-17 pathway-dependent proteins and clinical parameters. Protein expression analysis via PEA with serum samples of (**A**) VEDOSS and (**B**) SSc patients was performed and NPX values were used to develop a correlation matrix in R. Statistical correlation analyses were performed using a Spearman's r test (matrix colorcode: red=negative correlation, blue=positive correlation; VEDOSS: n=20; SSc: n=51).

The correlation pattern of VEDOSS and SSc patients differed visually comparing the significant correlations. In VEDOSS patients (fig. 4.23A), CCL7 correlated positively with CK levels and CCL20 with CRP levels (both $p < 0.05$; $r = 0.501$ and $r = 0.539$, respectively). In addition, three significant positive correlations with the EUSTAR AI were found: CCL2 ($p < 0.05$; $r = 0.476$), MMP1 ($p < 0.05$; $r = 0.492$) and CXCL10 ($p < 0.05$; $r = 0.491$). The only significant negative correlation was found between CXCL8 and Nt-proBNP levels ($p < 0.01$; $r = -0.641$).

In contrast, in SSc patients several significant negative correlations were present (fig. 4.23B). IL-4 correlated negatively with the EUSTAR AI ($p < 0.01$; $r = -0.390$) and IL-5 correlated negatively either with CK levels ($p < 0.05$; $r = -0.302$) and with creatinine levels ($p < 0.05$; $r = -0.309$). Further, CXCL5 showed a significant negative correlation

with CK levels ($p < 0.01$; r = -0.436) and with Nt-proBNP levels ($p < 0.05$; r = -0.292). Nt-proBNP levels also correlated negatively with CXCL10 ($p < 0.05$; r = -0.281). Notably, IL-6 showed significant positive correlations with three parameters: CRP levels ($p < 0.05$; r = 0.312), NtproBNP levels ($p < 0.01$; r = 0.402) and the EUSTAR AI ($p < 0.01$; r = 0.367). Lastly, CCL7 correlated positively with CRP levels ($p < 0.01$; r = 0.414) and EUSTAR AI ($p < 0.05$; r = 0.345). Comparing the strength of the correlations, VEDOSS patients showed rather moderate correlations, while the correlations within the SSc group were weak on average.
The correlation analysis revealed distinct expression patterns between VEDOSS and SSc patients. In VEDOSS, several inflammatory proteins, particularly chemokines like CCL2, CCL7, CCL20 and CXCL10, were moderately associated with markers of disease activity and inflammation, indicating a potentially active immune involvement at this early disease stage. In contrast, the SSc cohort showed predominantly weak negative correlations, especially involving IL-4, IL-5 and CXCL5, suggesting a shift toward a different immunoregulatory profile in established disease. IL-6 remained a consistent marker positively associated with disease severity in established SSc.

4.5 Influence of anti-GPCR and anti-GF autoantibodies in VEDOSS and SSc

The previous subsections have shown a great variety of significant differences in the immunophenotype and inflammatory proteome across diesease stages, particularly during the progression from the pre-disease VEDOSS phase to an established SSc. Based on the fact that specific anti-GPCR and anti-GF aAbs have already been identified as key drivers in development of autoimmunity and subsequent disease progression (see subsection 1.1.4), the next step included the investigation of the influence of these aAbs on VEDOSS and SSc patients [66, 234]. Therefore, special attention was paid to the detection of differences in aAbs levels between VEDOSS and SSc patients and the identification of correlation patterns with clinical parameters, the immunophenotype and IL-17 pathway-dependent proteins to elucidate possible aberrations and to broaden the horizon with regard to complex interactions beyond the cellular immunophenotype.

4.5.1 Differences in anti-GPCR and anti-GF autoantibody levels

Comparison of aAb levels between VEDOSS and SSc patients may reveal differences that could contribute to disease modulation and provide insight into disease status. For this purpose, a Mann-Whitney U-based volcano plot was created, incorporating the levels of all measured aAb levels, which were assessed by the company CellTrend using patient sera and determined via the EIA described in subsection 3.3.2.
Accordingly, serum samples for the determination of the aAb levels (in units) of 51 SSc patients and 20 VEDOSS patients were used. The levels of the following anti-GPCR and anti-GF aAbs were determined: AT1R, ETAR, β1, β2, M3, M4, CXCR3, PAR1, PAR2, PlGF and FGF2.

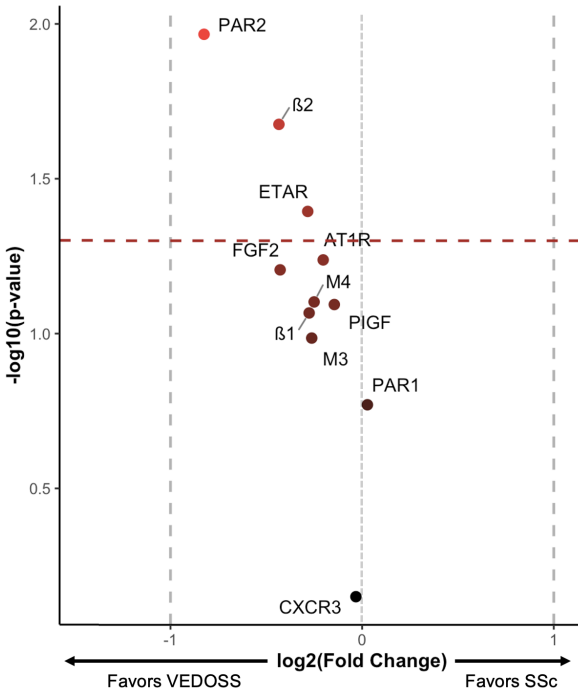

aAb	p value	log2FC
PAR2	0.01076739*	-0.82488760
ß2	0.02103886*	-0.43418334
ETAR	0.04020550*	-0.28385465
AT1R	0.05766469	-0.20321892
FGF2	0.06209361	-0.42779271
M4	0.07881081	-0.25048667
PIGF	0.08036224	-0.14514352
ß1	0.08556343	-0.27642950
M3	0.10314365	-0.26302061
PAR1	0.16939648	0.02754948
CXCR3	0.70610589	-0.03245572

Figure 4.24 : Changes in aAb levels between VEDOSS and SSc patients, visualized as volcano plot. Each point represents one aAb, with the x-axis displaying the log2 fold change between groups and the y-axis showing the -log10 transformed p-value based on a Mann-Whitney U test. Anti-GPCR aAbs included: AT1R, ETAR, β1, β2, M3, M4, CXCR3, PAR1, PAR2; anti-GF aAbs included: PlGF, FGF2. Red color intensity reflects p-value significance, with brighter red color indicating higher statistical significance. The dashed red line marks the significance threshold of $p < 0.05$. The aAb levels to the left of the zero point of the x-axis favor VEDOSS, while those to the right of the zero point favor SSc. The data table shows the exact p and log2FC values of every aAb (VEDOSS: n=20; SSc: n=51).

The aAb levels of PAR2, β2 and ETAR were significantly higher in VEDOSS patients compared to the SSc cohort (all $p < 0.05$; fig. 4.24). Interestingly, AT1R and FGF2 also tended towards a higher concentration in VEDOSS patients, but did not reach statistically significance ($p = 0.058$ and $p = 0.062$, respectively). The analysis revealed higher levels of specific anti-GPCR aAbs (PAR2, β2 and ETAR) in VEDOSS patients compared to those with established SSc, suggesting a potentially more pronounced or active aAb response at the early disease stage. Trends towards elevated AT1R and FGF2 aAbs levels further support this early immunological activity.

4.5.2 Correlation between autoantibody levels and clinical parameters

As already described earlier, clinical markers and the EUSTAR AI play a decisive role in assessing the current disease state, particularly in autoimmune conditions. As it has already been shown in the previous subsections that these markers correlate significantly with a great variety of different immune cell subsets and inflammatory proteins in VEDOSS and SSc patients, the next step included the investigation of correlations between the clinical parameters as well as the EUSTAR AI and aAbs levels. This analysis aimed to further elucidate the potential mechanistic pathways linking inflammatory and immunological profiles to disease-specific aAb production. The experimental procedure was similar to that described in the previous subsection and included therefore the aAb levels and clinical parameters of 51 SSc patients or 20 VEDOSS patients.

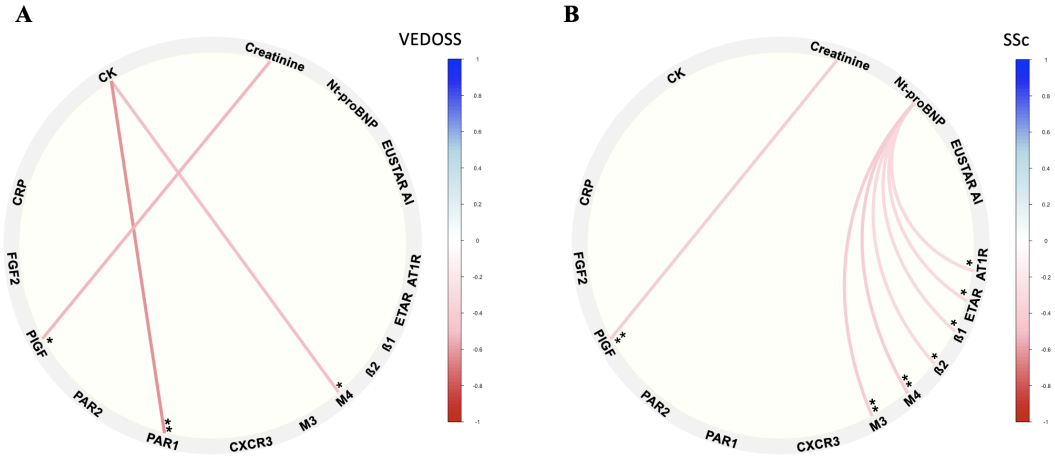

Figure 4.25 : Correlations between aAb levels and clinical parameters. The aAb level determination was performed by EIA with serum samples of (**A**) VEDOSS and (**B**) SSc patients and a correlation chord diagram was developed in R. Statistical correlation analyses were performed using a Spearman's r test (matrix color-code: red=negative correlation, blue=positive correlation; VEDOSS: n=20; SSc: n=51).

When comparing the string networks of the two patient cohorts, two almost completely different correlation patterns were revealed. The VEDOSS chohort (fig. 4.25A) presented three negative and statistically significant correlations. Thereby, CK levels correlated significantly with M4 and PAR1 ($p < 0.01$ and $p < 0.05$; r = -0.637 and r = -0.501, respectively) and creatinine levels with PlGF ($p < 0.05$; r = -0.532). The latter was also reflected in SSc patients (fig. 4.16B) with an r value of -0.404 and a p value <0.05. Interestingly, Nt-proBNP levels correlated significantly with various different aAbs in SSc patients. It correlated negatively with M3 ($p < 0.01$; r = -0.400), M3 ($p < 0.01$; r = -0.411), $\beta 2$ ($p < 0.05$; r = -0.299), $\beta 1$ ($p < 0.05$; r = -0.312), ETAR ($p < 0.05$; r = -0.312) and AT1R ($p < 0.05$; r = -0.288). In summary, the correlation analysis suggested differences in how aAbs interact with clinical parameters across disease stages. While VEDOSS patients exhibited a few moderate negative correlations, SSc patients displayed a broader yet weaker correlation network with a notable association of Nt-proBNP levels with several aAbs, hinting at potential links between cardiovascular markers and humoral immune alterations.

4.5.3 Correlation between autoantibody levels and immunophenotype

Based on the observed correlations between aAb levels and clinical parameters in VEDOSS and SSc patients, the focus shifted to investigating how the aAb levels correlate

with specific subset frequencies of cells of the innate and adaptive immune system. For this purpose, a correlation matrix was created, incorporating the frequencies of all measured cell types and the aAb levels (as units), which were assessed by the company CellTrend using patient sera and determined via the EIA described in subsection 3.3.2. Accordingly, either PBMC for flow cytometric measurements or serum samples for the determination of the aAb levels of 51 SSc patients or 20 VEDOSS patients were used.

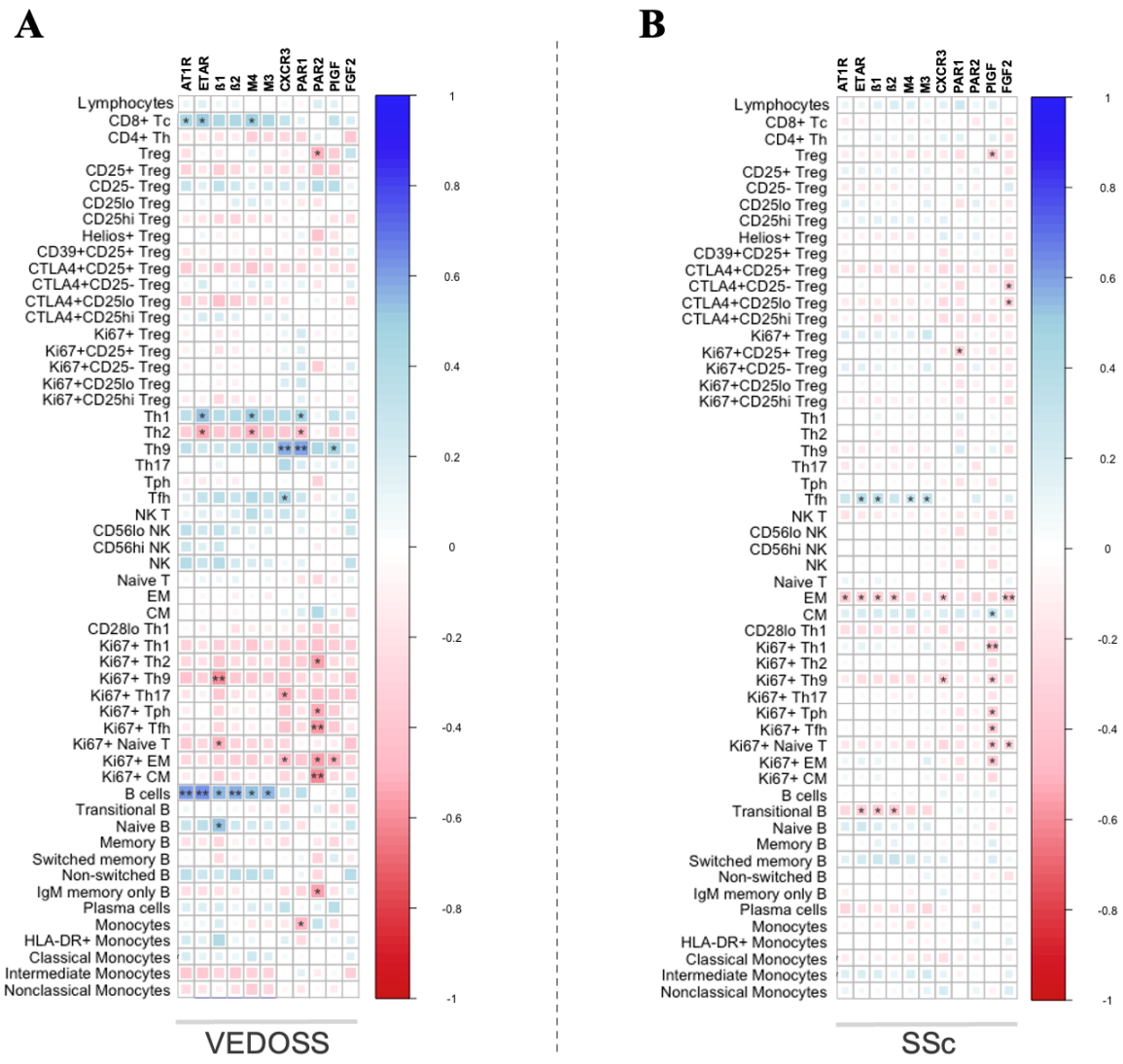

Figure 4.26 : Correlations between frequencies of immune cell subsets and aAb levels. Immunophenotyping via flow cytometry and aAb level determination by EIA with PBMC and serum samples of (**A**) VEDOSS and (**B**) SSc patients was performed and a correlation matrix was developed in R. Statistical correlation analyses were performed using a Spearman's r test (matrix colorcode: red=negative correlation, blue=positive correlation; VEDOSS: n=20; SSc: n=51).

Comparing the overall visual correlation patterns, VEDOSS patients showed a pronounced pattern of several negative correlations between frequencies of proliferating (Ki67+) Th and memory T cell subsets and certain aAb levels (fig. 4.26A). Noticeable, PAR2 levels played a predominant role with respect to the mentioned cell types by correlating significantly with frequencies of Ki67+ Th2, Ki67+ Tph, Ki67+ Tfh, Ki67+ EM and Ki67+ CM cells. In addition, frequencies of Th1 and Th2 cells each showed opposite correlations with the three aAbs ETAR, M4 and PAR1, with frequencies of Th1 cells always correlating significantly positively and frequencies of Th2 cells significantly negatively. The last conspicuous pattern in the VEDOSS patients was shown by frequencies of total B cells, which correlated significantly positively with the following 6 aAbs: AT1R, ETAR, β1, β2, M3 and M4 (the exact p- and r-values can be found in the appendix section A.3, table A.3).
In contrast in SSc patients (fig. 4.26B), no correlation between frequencies of Ki67+ T cell subsets and PAR2 levels could be detected but PlGF correlated significantly negatively with frequencies of Ki67+ Th1, Ki67+ Th9, Ki67+ Tph, Ki67+ Tfh, Ki67+ naive T and Ki67+ EM cells. Another difference to the VEDOSS patients was that frequencies of several Treg subsets correlated negatively with different aAbs. Overall, frequencies of total Treg, CTLA4+ among CD25-, CTLA4+ among CD25lo and Ki67+ among CD25+ Treg were affected. The last difference between the two cohorts was related to B cell correlations. Where VEDOSS patients presented certain significant positive correlations with frequencies of total B cells in general, frequencies of transitional B cells of SSc patients correlated negatively with ETAR, β1 and β2.
These findings highlight distinct correlation patterns between aAb levels and immune cell subsets in VEDOSS and SSc patients, suggesting potential shifts in immune regulation during disease progression. While VEDOSS patients showed a pattern with several negative correlations, including proliferating Th and memory T cells, this correlation was largely absent in SSc, where instead PlGF emerged as a key correlate of proliferating T cell subsets. Additionally, the shift from predominantly positive B cell correlations in VEDOSS to negative correlations with transitional B cells in SSc further underlines potential alterations in humoral immunity as the disease advances. All specific p- and r- values from the analyses of the SSc cohort can be found in the appendix section A.3, table A.4.

4.5.4 Correlation between the IL-17 pathway-dependent proteins and aAb levels in VEDOSS and SSc

Given the observed differences in the correlation patterns of immunophenotype and aAb levels, the study was further extended to investigate the role of aAbs in VEDOSS and SSc patients in their correlation with IL-17 pathway-dependent proteins. For this purpose, a correlation matrix was created, incorporating the NPX values of the proteins and the aAb levels (as units) measured both in the serum of 20 VEDOSS and 51 SSc patients.

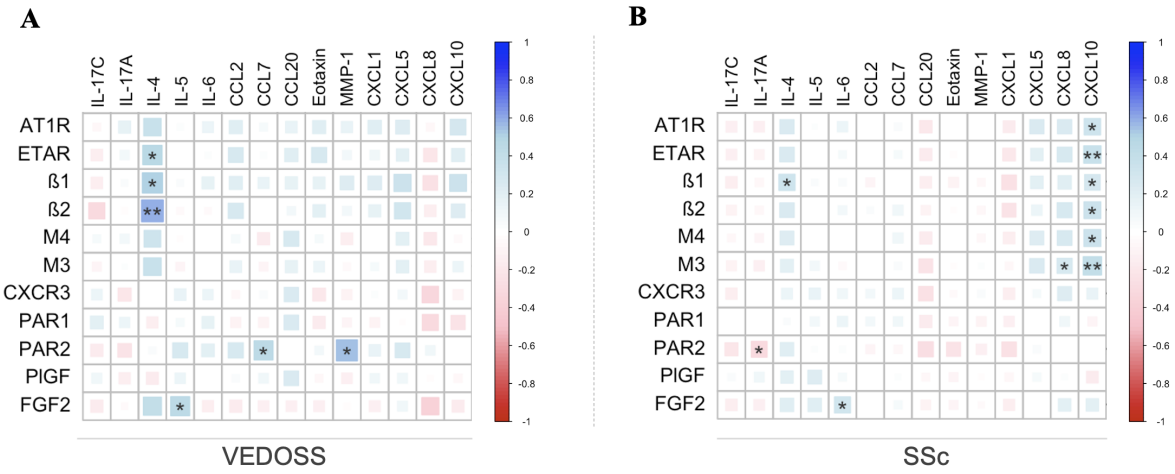

Figure 4.27 : Correlations between IL-17 pathway-dependent protein concentrations and aAb levels. Protein expression analysis via PEA and aAb level determination by EIA with serum samples of (**A**) VEDOSS and (**B**) SSc patients was performed and a correlation matrix was developed in R. Statistical correlation analyses were performed using a Spearman's r test (matrix colorcode: red=negative correlation, blue=positive correlation; VEDOSS: n=20; SSc: n=51).

Comparing the overall visual correlation patterns of VEDOSS and SSc patients, a clear trend towards positive correlations between protein concentrations and aAb levels was identified (fig. 4.27). VEDOSS patients (fig. 4.27A) showed three significant positive correlations with IL-4: ETAR ($p < 0.05$; $r = 0.460$), $\beta 1$ ($p < 0.05$; $r = 0.502$) and $\beta 2$ ($p < 0.01$; $r = 0.589$). Further, IL-5 correlated significantly positively with FGF2 ($p < 0.05$; $r = 0.444$) and PAR2 correlated either with CCL7 ($p < 0.05$; $r = 0.445$) and MMP-1 ($p < 0.05$; $r = 0.547$). In contrast, in SSc patients (fig. 4.27B) PAR2 correlated significantly negatively with IL-17A ($p < 0.05$; $r = -0.305$). Similar to the VEDOSS cohort, SSc patients showed a positive correlation of IL-4 and $\beta 1$ ($p < 0.05$; $r = 0.321$). IL-6 correlated significantly with FGF2 ($p < 0.05$; $r = 0.316$) and CXCL8 with M3 ($p < 0.05$; $r = 0.414$). Most pronounced were several significant

positive correlations between CXCL10 and six different aAbs: AT1R ($p < 0.05$; $r = 0.330$), ETAR ($p < 0.01$; $r = 0.370$), $\beta 1$ ($p < 0.05$; $r = 0.297$), $\beta 2$ ($p < 0.05$; $r = 0.347$), M4 ($p < 0.05$; $r = 0.352$) and M3 ($p < 0.01$; $r = 0.414$).
The correlation analysis suggests distinct interaction patterns between aAbs and inflammatory proteins in VEDOSS and SSc. In VEDOSS, exclusively positive correlations, particularly between IL-4 and several anti-GPCR aAbs, point to a coordinated early immune activation. In contrast, SSc patients showed a broader and more complex network, with both positive and negative correlations. Notably, CXCL10 emerged as a central hub in SSc, correlating with multiple aAbs, highlighting its potential role in the chronic inflammatory state and aAb-mediated pathology in later disease stages.

4.6 Multi-omics analysis for group separation

Building on the previous analyses of individual data layers in VEDOSS and SSc patients - including the detailed immunophenotyping, the assessment and correlation of aAb levels and the profiling of the inflammatory proteome - these datasets were integrated to perform a multi-omics analysis via PCA. To achieve this, the data were transformed to approximate a normal distribution, ensuring their suitability for a PCA. The optimal transformation method was selected for each individual parameter using the *bestNormalize* algorithm (see 3.4.1) and in the end it was decided to transform according to Yeo-Johnson. Building on the results of the PLS-DA analysis based on the immunophenotype of the HC, VEDOSS and SSc cohorts (fig. 4.1), an attempt was now made to achieve a clearer class separation between diesease stages within a shared multi-omics framework. A total of 23 VEDOSS and 54 SSc patients were included in the multi-omics analysis. Missing values, such as those in the aAb dataset, where measurements were available for only 20 VEDOSS and 51 SSc patients, were imputed using the *missMDA* package in R.

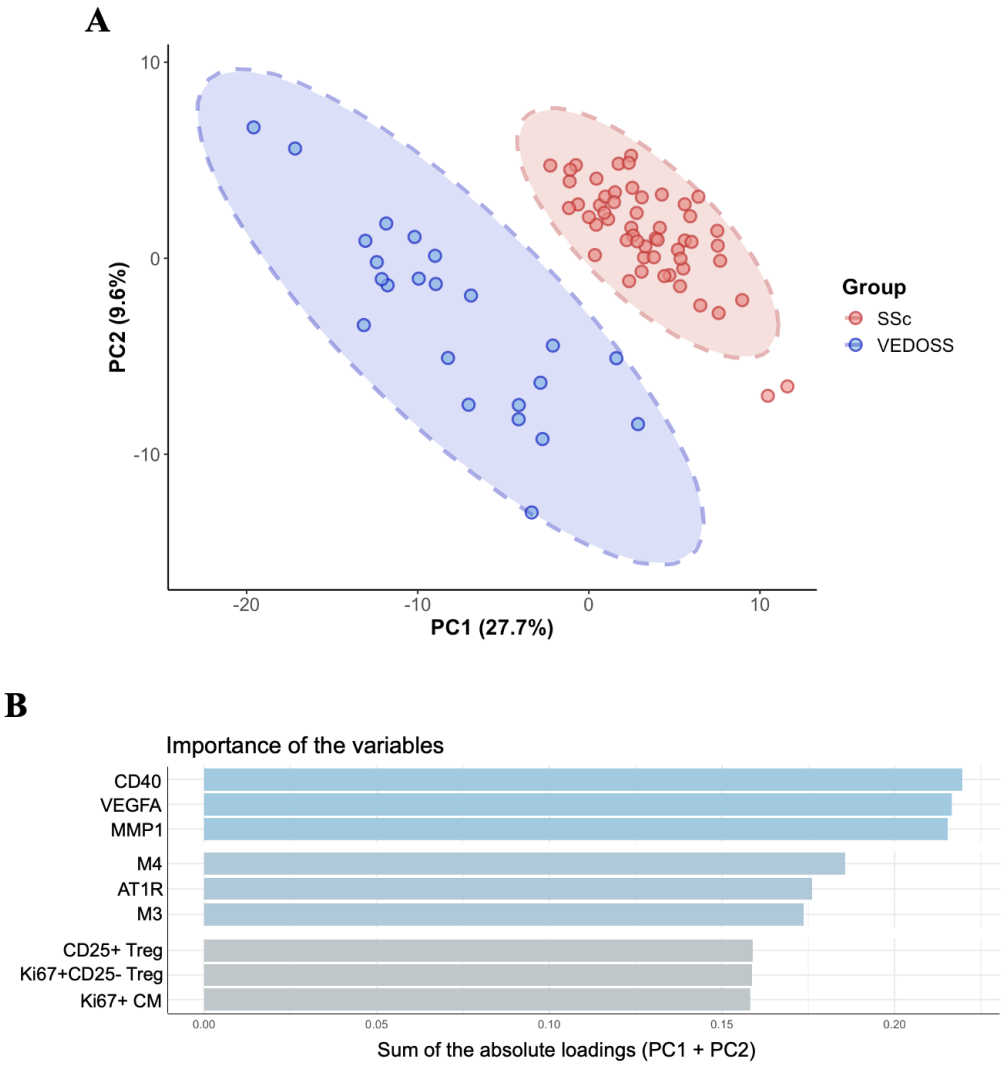

Figure 4.28 : Multi-omics approach via PCA and importance analysis in VEDOSS and SSc patients based on the immunophenotype, aAb measurement and inflammatory proteome data layers. **A**) Yeo-Johnson transformed data were used to conduct a PCA and ellipses (red: SSc; blue: VEDOSS) represent the 95% confidence interval, while each dot represents one patient. The axes correspond to the first two components of the PCA: the x-axis (PC1) explains 27.7% of the variance and the y-axis (PC2) explains 9.6% of the variance in the dataset. **B**) The importance plot shows the top 3 most important variables from each data layer in order of total importance, calculated by determining the sum of absolute loadings (VEDOSS: n=23; SSc: n=54).

The PCA results (fig. 4.28A) are showing the distribution of VEDOSS and SSc patients across the first two principal components (PC1 and PC2), explained 27.7% and 9.6% of the variance, respectively. The groups exhibited distinct clustering patterns, with no overlap between the VEDOSS and SSc clusters, which were marked by the

95% confidence interval. Figure 4.28B illustrated the top 3 parameters from each of the individual data levels - top: proteome analysis, middle: aAb levels, bottom: immunophenotype - that contributed most to the separation observed in the PCA, based on the sum of absolute loadings for PC1 and PC2. The most influential variables were CD40, VEGFA and MMP1 from the proteome analysis, followed by the aAbs M4, AT1R and M3 and finally, the immunophenotype-related variables CD25+ among total Treg, Ki67+ among CD25- Treg and Ki67+ among CM T cells.
The PCA results demonstrated a clear distinction between VEDOSS and SSc patients, with no overlap between groups, indicating a strong separation in their immune and molecular profiles. The top contributing parameters across all data layers highlight key proteins, aAb levels and immune cell frequencies driving this separation. These findings support the value of a multi-omics approach in capturing the progressive shift in immune regulation and inflammation from VEDOSS to SSc.

CHAPTER 5

Results II

Recovery of Treg by rIL-2 stimulation

This chapter builds on the differences in Treg biology observed in SSc patients in the previous chapter and addresses the attempt to achieve a recovery of functionally active Treg in SSc PBMC through in vitro rIL-2 stimulation.

5.1 Changes in Treg phenotype of SSc patients upon rIL-2 stimulation

The first set of results highlighted significant dysregulation in Treg subsets in SSc patients, characterized by a marked decrease in frequencies of CD25hi Treg and a concomitant increase in frequencies of CD25- Treg compared to HC (see fig. 4.3), as well as an imbalanced Treg/Tcon ratio (fig. 4.9), suggesting for a low availability of IL-2. Notably, VEDOSS patients exhibited a trend towards reduced frequencies of CD25hi Treg, suggesting that this perturbation may emerge early in disease progression. These findings underscore the relevance of Treg regulation in SSc pathogenesis and the potential for targeted therapeutic interventions. Building on these observations, the following chapter aims to investigate whether the CD25hi Treg population in SSc patients can be recovered *in vitro* through stimulation with low-doses of rIL-2, a key cytokine for Treg survival and expansion [235]. By employing varying doses of rIL-2, this study seeks to determine optimal conditions for reconstituting CD25hi Treg, which may provide insight into potential therapeutic strategies to counteract immune dysregulation in SSc. In addition, this chapter reviews the functional properties of IL-2-stimulated Treg, including markers describing origin and activation status, to assess their potential utility in mitigating disease-related inflammation. By elucidating the mechanisms underlying the restoration of CD25hi Treg, these findings may contribute to a broader understanding of dysregulated Treg biology in SSc and accelerate the development of an IL-2-based immunotherapy.

5.1.1 Changes in CD25 Treg subsets and expression levels of CD25 upon *in vitro* rIL-2 stimulation

To investigate the effect of different concentrations of rIL-2 on FoxP3+CD127lo Treg subset expansion in SSc, PBMC were isolated from 21 SSc patients and stimulated with 0 ng/ml (unstimulated, medium control), 1 ng/ml (low-dose), 5 ng/ml (mid-dose) and 10 ng/ml (high-dose) rIL-2 in a short-term cell culture for 24h, according to the protocol described in subsection 3.1.4. The frequencies of the CD25 subsets among Foxp3+CD127lo Treg were measured with the *FACSCanto™ II* device and analyzed according to the gating strategy in figure 3.7.

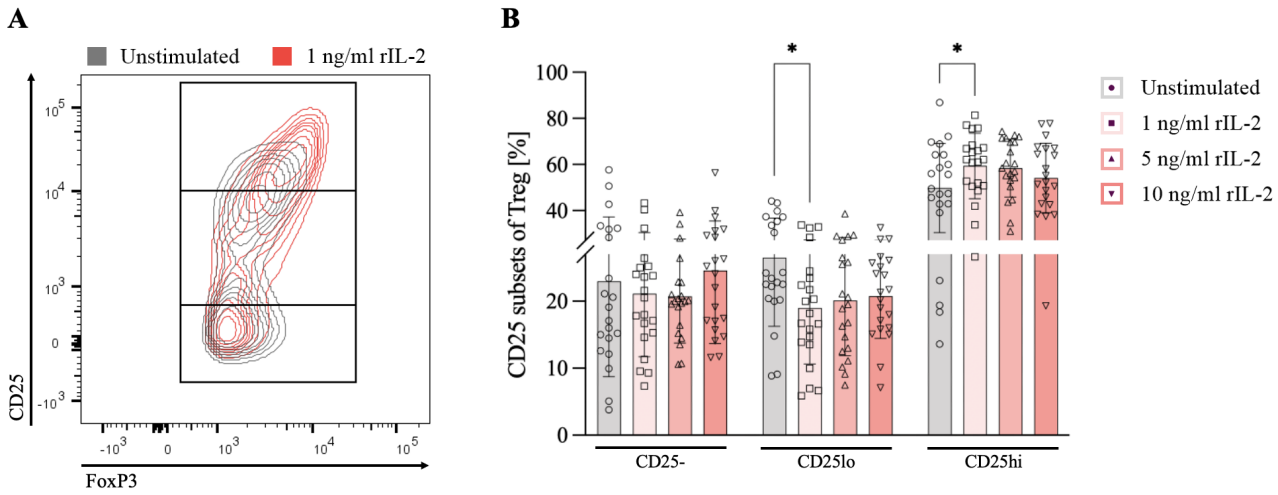

Figure 5.1 : Changes in Treg subsets according to CD25 expression after rIL-2 stimulation. PBMC of SSc patients were stimulated with different concentrations of rIL-2 for 24h and frequencies of CD25 subsets among FoxP3+CD127lo Treg were determined via flow cytometry. **A**) Representative merged contour plot of one SSc patient showing expression pattern of CD25 subsets among FoxP3+CD127lo Treg after stimulation with 1 ng/ml rIL-2 (red) or left untreated (gray). **B**) Frequencies of the CD25-, CD25lo and CD25hi subsets among FoxP3+CD127lo Treg after stimulation with 0 ng/ml (unstimulated), 1 ng/ml, 5 ng/ml and 10 ng/ml. CD25+ among FoxP3+CD127lo Treg threshold was determined by a CD25 FMO sample. Statistical comparison was performed using the Friedman test with Dunn's correction within each CD25 subset. Median values with error bars, indicating the IQR, are shown (n = 21).

The merged contour plot (fig. 5.1A) presents the distribution of the CD25 subsets (CD25-, CD25lo and CD25hi) among FoxP3+CD127lo Treg of one representative SSc patient after 1 ng/ml rIL-2 stimulation or left untreated. The stimulated PBMC showed a shift towards increased frequencies of CD25hi Treg (red contour) after low-dose rIL-2 stimulation in comparison to the unstimulated control (gray contour). Quantitative analysis (fig. 5.1B) confirmed this shifting trend by revealing a statistically significant increase in frequencies of CD25hi Treg after stimulation with 1 ng/ml rIL-2 in comparison to the unstimulated control ($p < 0.05$). The frequencies of the CD25hi Treg subset could not be further increased with an increasing rIL-2 concentration. Correspondingly, the frequencies of CD25lo Treg were significantly decreased after applying the same concentration of rIL-2 compared to the unstimulated control ($p < 0.05$). Within the CD25- Treg subset, no statistical difference was apparent between the control and the different rIL-2 concentrations.

Having established that stimulation with low-dose rIL-2 (1 ng/ml) promoted the recovery of CD25hi Treg, the next step was to investigate whether this stimulation similarly causes increased expression of CD25 molecules at single cell level. To this end, a detailed analysis of CD25 molecules per cell was performed within the CD25hi Treg subset following rIL-2 stimulation in 22 SSc patients. *QuantiBRITE™ PE** beads were used for quantifying PE-coupled molecules per cell after the initial acquisition of CD25hi Treg. This approach aimed to provide deeper insights into the distribution of CD25 proteins among CD25hi Treg.

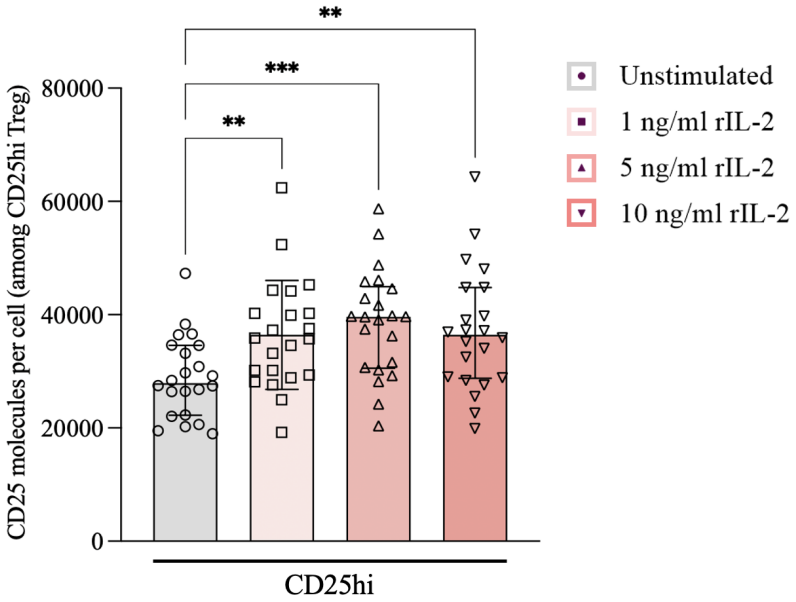

Figure 5.2 : Changes in CD25 molecules per cell after rIL-2 stimulation. PBMC of SSc patients were stimulated with different concentrations of rIL-2 for 24h and CD25 molecules per cell were determined via flow cytometry using *QuantiBRITE™ PE** beads. Quantitative analysis of the CD25 molecules per cell among CD3+CD4+FoxP3+CD127loCD25hi Treg after stimulation with 0 ng/ml (unstimulated), 1 ng/ml, 5 ng/ml and 10 ng/ml. CD25+ among FoxP3+CD127lo Treg threshold was determined by a CD25 FMO sample. Statistical comparison was performed using the RM one-way ANOVA with Holm-Šídák correction. Mean values with error bars, indicating the SD, are shown. Test for normally distributed data was successful and tested with the Kolmogorov-Smirnow and Shapiro-Wilk test (n = 22).

After stimulation with 1 ng/ml rIL-2, the mean value of CD25 molecules within the CD25hi subset among FoxP3+CD127lo Treg increased significantly by 30.5% in comparison to the unstimulated control ($p < 0.01$). This statistically significant increase

in CD25 molecules among CD25hi Treg compared to the control was also achieved after stimulation with 5 ng/ml (41.9% increase; $p < 0.001$) and 10 ng/ml rIL-2 (30.4% increase; $p < 0.01$). When comparing the mid- and high-dose with the low-dose rIL-2, no further significant increase was observed (fig. 5.2).
The results demonstrate that low-dose rIL-2 stimulation (1 ng/ml) effectively recovered the expression of CD25 molecules on Treg, specifically among the CD25hi subset in SSc patients. This effect was confirmed both at the population level (increased frequencies of CD25hi Treg) and at the single-cell level (increased CD25 molecule expression per CD25hi Treg). Higher concentrations of rIL-2 did not yield additional benefits, indicating that even minimal dosing is sufficient to restore CD25hi Treg.

5.1.2 Changes in Treg phenotpye and suppressive state after rIL-2 stimulation

Building on the previous findings, the next step aimed to determine whether rIL-2 stimulation influences the frequencies of functionally relevant Treg subsets, including Helios+ among total Treg and CD39+ among CD25+ Treg, in the SSc patient cohort. These subsets are associated with origin and suppressive functionality, respectively [236, 237] and their evaluation after rIL-2 stimulation in comparison to the medium control could provide further insights into the immunomodulatory effects of this cytokine.

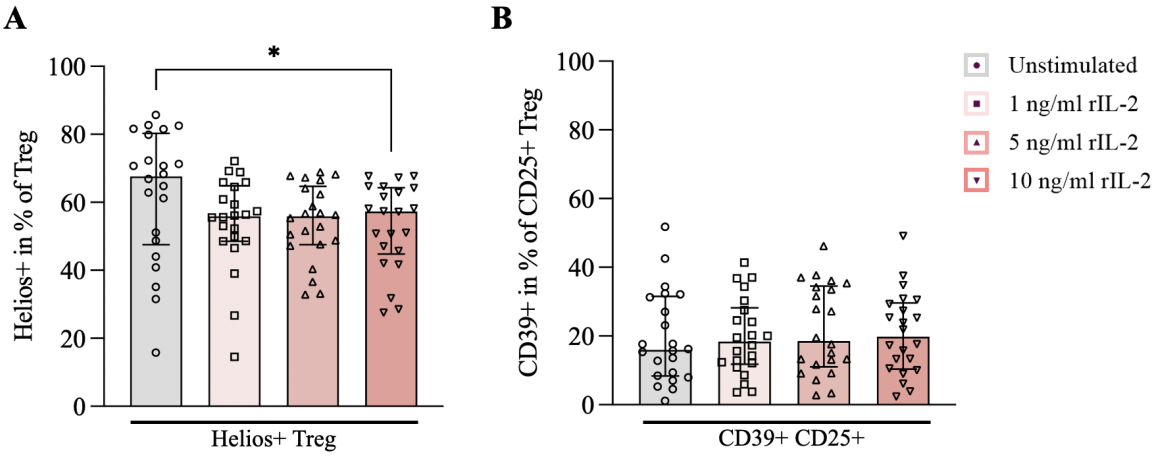

Figure 5.3 : Changes in origin and suppressive state of Treg after rIL-2 stimulation. PBMC of SSc patients were stimulated with 0 ng/ml (unstimulated), 1 ng/ml, 5 ng/ml and 10 ng/ml of rIL-2 for 24h and used to identify frequencies of (**A**) Helios+ cells among CD3+CD4+FoxP3+CD127lo Treg and (**B**) CD39+ cells among CD3+CD4+FoxP3+CD127loCD25+ Treg via flow cytometry. Statistical comparisons were done using a Friedman test with Dunn's correction for multiple comparisons. Median values with error bars, indicating the IQR, are shown (n = 22).

The frequencies of Helios+ among total FoxP3+CD127lo Treg (fig. 5.3A) showed a trend towards a decrease after stimulation with rIL-2, but only after application of 10 ng/ml rIL-2 it decreased significantly by 15.2% in comparison to the unstimulated control ($p < 0.05$). In contrast, no significant changes nor trends were observed comparing the frequencies of CD39+ among CD25+ Treg after rIL-2 stimulation (fig. 5.3B).
These findings suggest that only high-dose rIL-2 stimulation (10 ng/ml) may reduce the frequencies of Helios+ cells among total Treg, a subset associated with thymic-derived Treg, potentially indicating a shift in Treg composition. In contrast, frequencies of CD39+ cells among Treg remained unaffected across all rIL-2 concentrations, suggesting that this immunosuppressive subset is stable and not modulated by rIL-2 in the same way.

To further elucidate the functional impact of rIL-2 stimulation on the Treg compartment, it was essential to assess whether the observed shifts in subset distribution and surface marker expression reflected quantitative changes or an actual improvement of Treg fitness. Rather than simply expanding the Treg population, effective low-dose rIL-2 therapy is thought to recover existing Treg. Therefore, following the analysis of

the origin and suppressive state of Treg, attention turned to evaluating proliferation-associated marker expression by quantifying frequencies of Ki67+ cells among CD25 Treg subsets in the same SSc patient cohort after rIL-2 stimulation compared to the unstimulated medium control.

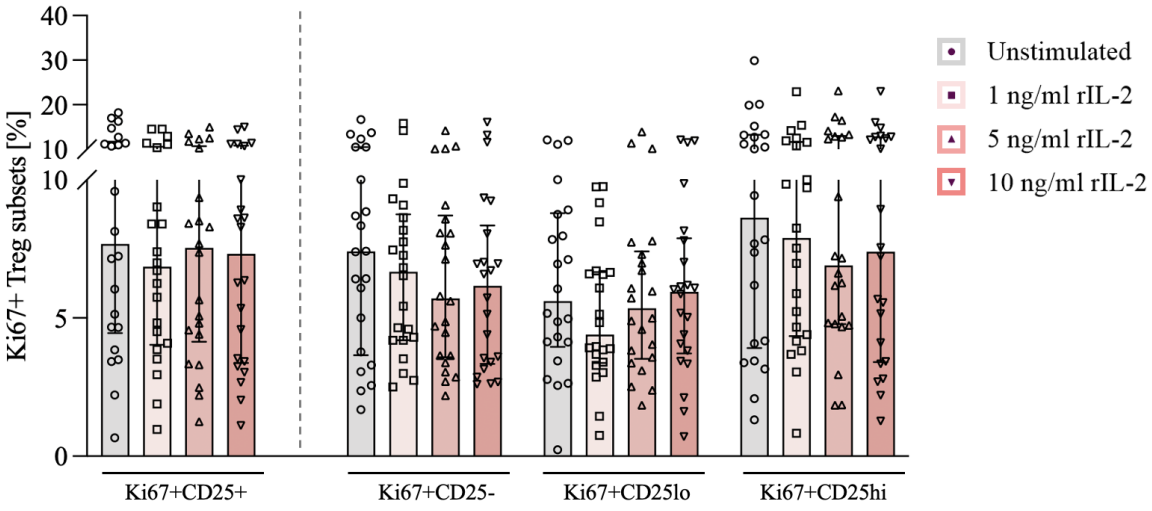

Figure 5.4 : Changes in proliferative state of CD25 Treg subsets after rIL-2 stimulation. PBMC of SSc patients were stimulated with 0 ng/ml (unstimulated), 1 ng/ml, 5 ng/ml and 10 ng/ml of rIL-2 for 24h and used to identify frequencies of Ki67+ cells among CD25 subsets in CD3+CD4+FoxP3+CD127lo Treg via flow cytometry. Statistical comparisons were done using a Friedman test with Dunn's correction for multiple comparisons within each CD25 subset. Median values with error bars, indicating the IQR, are shown (n = 22).

Comparing the frequencies of Ki67+ cells among CD25 Treg subsets after rIL-2 stimulation, no statistically significant difference was observed at all. The visual trend showed a slight decrease in frequencies in all Ki67+ cells among CD25 subsets, but this was associated with a high IQR and therefore could not be statistically proven. These findings suggest that, despite the recovery of CD25hi Treg upon rIL-2 stimulation, the proliferative activity of these cells, as indicated by the Ki67 expression, remained unchanged. This may imply that the functional recovery of Treg following low-dose rIL-2 does not primarily rely on proliferative expansion, but rather on qualitative modulation of pre-existing Treg.

5.1.3 Gene expression analyses of Treg-associated genes upon rIL-2 stimulation

Following the assessment of Treg subsets upon stimulation with rIL-2 via flow cytometry, the molecular effects of rIL-2 stimulation were further investigated on mRNA expression levels to complement the flow cytometry results. To this end, 2 x 10^6 PBMC/well of 10 SSc patients were sown and stimulated in triplicates for 24h (1, 5, or 10 ng/ml rIL-2 or left untreated) according to the protocol of subsection 3.1.4. Afterwards, RNA was isolated and a subsequent cDNA synthesis using 100 ng purified RNA was performed (see subsections 3.2.1 and 3.2.4). To quantify the expression of key genes involved in IL-2 signaling and Treg function, a qPCR was carried out. Specifically, expression of IL-2 receptor chains (*IL2RA, IL2RB* and *IL2RG*), as well as other Treg-associated genes were determined, to evaluate whether rIL-2 stimulation influences the transcriptional profile.

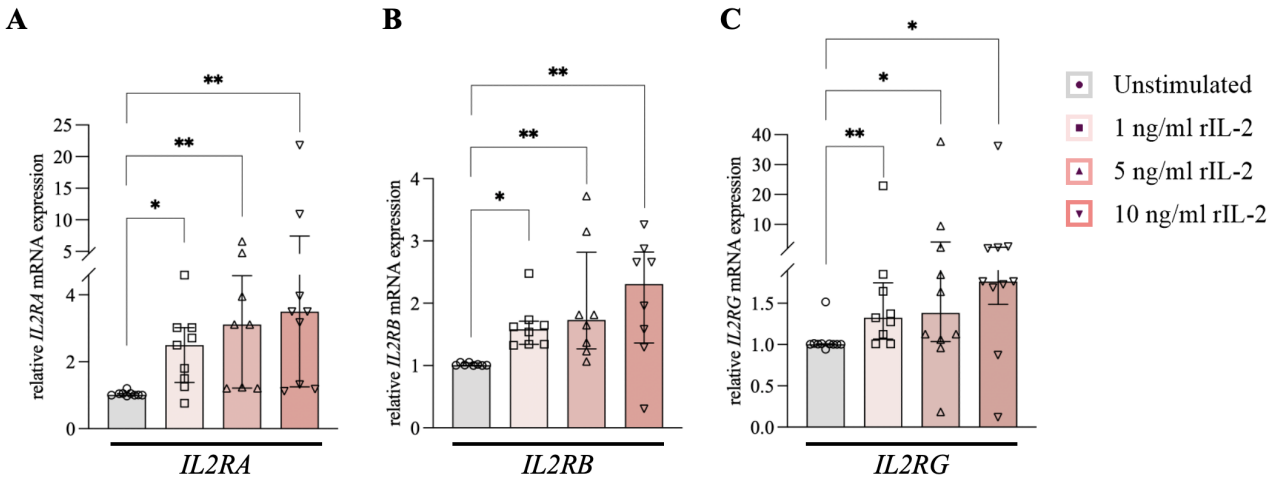

Figure 5.5 : Changes in relative mRNA expression levels of IL-2 receptor chains upon 24h rIL-2 stimulation. PBMC of SSc patients were isolated and stimulated for 24h with 0 ng/ml (unstimulated), 1 ng/ml, 5 ng/ml and 10 ng/ml rIL-2. Subsequent cDNA synthesis with 100 ng purified RNA was performed and relative mRNA expression levels of (**A**) *IL2RA*, (**B**) *IL2RB* and (**C**) *IL2RG* were analyzed by qPCR using the ΔΔCT method. Statistical comparisons were done using a Friedman test with Dunn's correction for multiple comparisons. Shown are median values with error bars indicating the IQR for three biological and two technical replicates per donor PBMC. *18sRNA* was used as housekeeping gene (n = 10). In groups with <10 data points, either a damage to RNA integrity or poor RNA concentration was present.

The mRNA expression of all three IL2 receptor chain genes showed a similar trend towards an increase in gene expression after rIL-2 stimulation compared to the unstimulated control (fig 5.5). Regarding the effect of low-dose rIL-2 (1 ng/ml), the mRNA expression of *IL2RA*, *IL2RB* and *IL2RG* was significantly higher in comparison to the unstimulated control ($p < 0.05$; $p < 0.05$ and $p < 0.01$, respectively). This effect was strongest for *IL2RA*, with a 2.5-fold increase in relative gene expression compared to the control (fig. 5.5A). Although the apparent trend suggested a dose-dependent increase in gene expression of all genes, this could not be proven statistically. Accordingly, there was no further statistically significant increase in relative gene expression starting from the 1 ng/ml rIL-2 concentration. These results suggest that low-dose rIL-2 is sufficient to transcriptionally upregulate IL-2 receptor components, particularly IL2RA, supporting the observed phenotypic enhancement of CD25 expression on Treg.

After evaluating the relative gene expression of the three IL-2 receptor chains, the mRNA expression of the Treg-associated genes *CTLA4, IL-10* and *ENTPD1* was determined after rIL-2 stimulation.

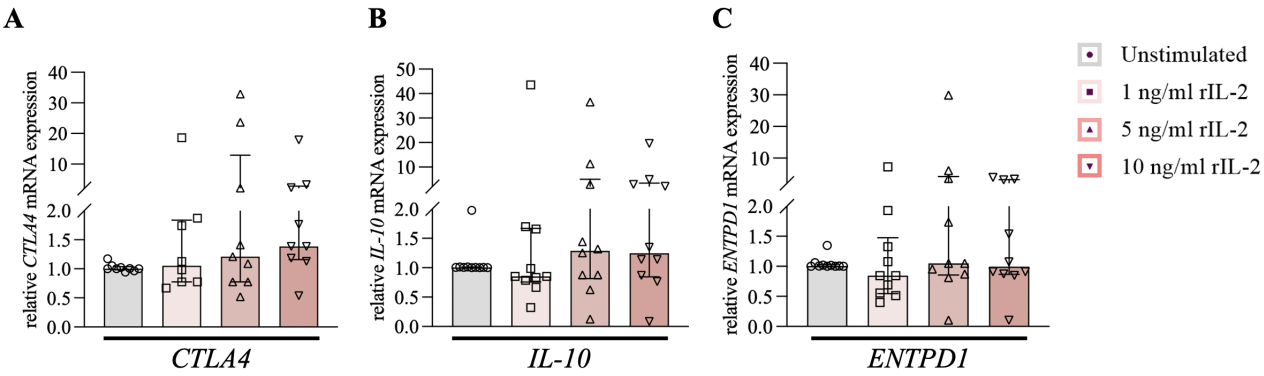

Figure 5.6 : Changes in relative mRNA expression levels of Treg-associated genes after rIL-2 stimulation. PBMC of 10 SSc patients were isolated and stimulated for 24h with 0 ng/ml (unstimulated), 1 ng/ml, 5 ng/ml and 10 ng/ml rIL-2. Subsequent cDNA synthesis with 100 ng purified RNA was performed and relative mRNA expression levels of (**A**) *CTLA4*, (**B**) *IL-10* and (**C**) *ENTPD1* were analyzed by qPCR using the ΔΔCT method. Statistical comparisons were done using a Friedman test with Dunn's correction for multiple comparisons. Shown are median values with error bars indicating the IQR for three biological and two technical replicates per donor PBMC. *18sRNA* was used as housekeeping gene (n = 10). In groups with <10 data points, either a damage to RNA integrity or poor RNA concentration was present.

The relative gene expression of the Treg-associated genes *CTLA4, IL-10* and *ENTPD1* remained unchanged after stimulation with rIL-2 regardless of the concentration compared to the unstimulated control (fig. 5.6). This suggests that short-term rIL-2 stimulation does not markedly alter the transcriptional levels of these functional Treg markers, indicating that the observed effects of rIL-2 may primarily involve receptor expression and surface phenotype rather than immediate transcriptional modulation of immunosuppressive effector genes.

5.1.4 TGFβ1 and IL-10 secretion of PBMC upon rIL-2 stimulation

Since activated Treg secrete TGFβ1 and IL-10 to a larger extend [238, 239], the impact of the rIL-2 stimulation on the secretion of these proteins was determined using cell culture supernatants. After PBMC from 5 SSc patients were stimulated with 0 ng/ml (unstimulated), 1 ng/ml, 5 ng/ml and 10 ng/ml rIL-2 for 24h, the cell suspension was harvested and centrifuged to obtain the cell culture supernatant. The concentration of TGFβ1 and IL-10 in the supernatants of differently stimulated PBMC was measured in duplicates using an ELISA (see 3.3.1).

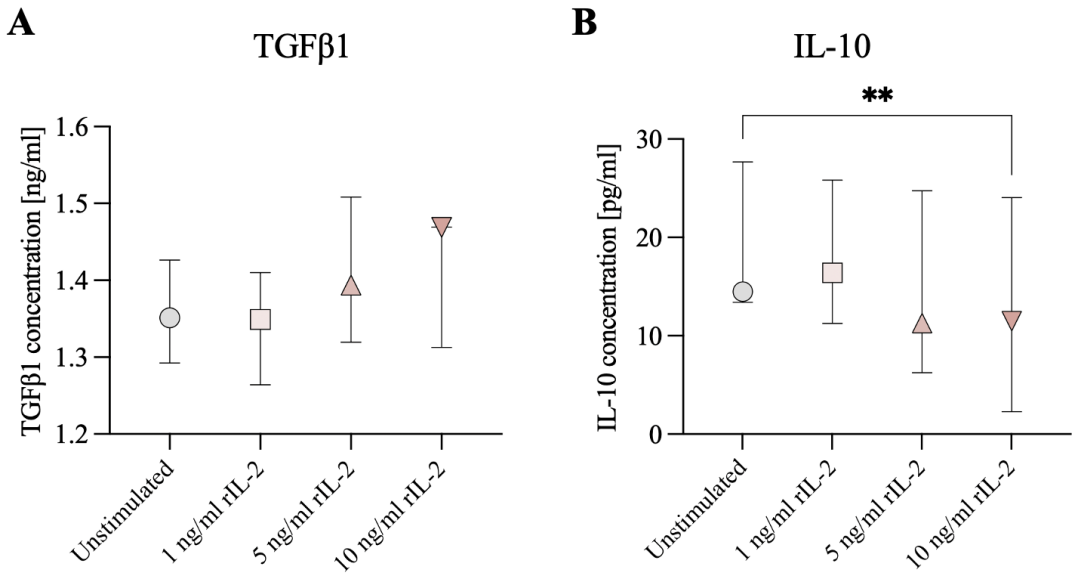

Figure 5.7 : Changes in TGFβ1 and IL-10 concentration after rIL-2 stimulation. PBMC of SSc patients were isolated and stimulated for 24h with 0 ng/ml (unstimulated), 1 ng/ml, 5 ng/ml and 10 ng/ml rIL-2. Cell suspension was centrifuged, cell culture supernatant was obtained and concentrations of (**A**) TGFβ1 and (**B**) IL-10 were determined using an ELISA. Statistical comparisons were done using a Friedman test with Dunn's correction for multiple comparisons. Shown are median values with error bars indicating the IQR for two technical replicates per donor PBMC (n = 5).

The stimulation with low-dose rIL-2 (1 ng/ml) showed no statistically significant changes on the concentration of TGFβ1 compared to the control (fig. 5.7A). A trend towards an increase could only be recognized from 5 ng/ml rIL-2, which became stronger again with an increase of 9% after 10 ng/ml rIL-2 compared to the unstimulated control (from 1.35 ng/ml to 1.49 ng/ml median levels). Nevertheless, none of the concentrations reached statistical significance. For IL-10 (fig. 5.7B), an opposite result was found, reflecting a decrease in concentration of IL-10 after increasing rIL-2 concentration in the cell culture. However, this decrease only reached statistical significance when comparing the unstimulated control with the 10 ng/ml rIL-2 sample, even if the IQR appears relatively large (20.7% decrease; $p < 0.01$). These findings suggest differential sensitivity of Treg-associated cytokines to rIL-2, with IL-10 being more susceptible to modulation under these conditions.

CHAPTER 6

Discussion

In the following chapter, the generated data will be interpreted within biological and clinical contexts, drawing on current literature findings. Additionally, novel conceptual models of pathogenesis will be developed, along with a discussion of the study's limitations and future perspectives.

6.1 Global immune dysregulations in VEDOSS and SSc

In the present study, a broad exploratory approach at numerous levels was conducted to identify dysbalances and dysregulations of the immunesystem and inflammatory proteome of pre-clinical and established SSc. First of all, suitable patients had to be recruited for the study, whereby care was always taken to ensure that all inclusion criteria were met. With regard to SSc patients, particular attention was paid to the heterogeneity of the disease in order to cover the entire spectrum of manifestations and symptoms. Furthermore, as the state of research and thus also the treatment options are constantly evolving, as Lescoat et al. recently summarized, not all patients included in the study met the recommendations for diagnosis according to the 2013 ACR/EULAR criteria [240]. Comprehensive immunophenotyping was performed with isolated PBMC of the recruited patients by flow cytometry to determine the frequencies of 55 different immune cell subsets. After implementing these data in a multivariate dimensionality-reduction analysis (PLS-DA), it was first shown that the immunophenotype of the VEDOSS cohort is localized between that of a healthy individual and a patient with established SSc. This confirms the assumption that VEDOSS patients represent both clinically and immunologically the pre-disease stage of established SSc and thus provides the rationale for the importance of the following results and their implications for disease pathogenesis.

6.2 Evidence for an IL-2 deprived state across immune cells in early and established SSc

Building on the previously described overview analysis, the data acquired from univariate group comparisons based on the measured cell frequencies collectively point toward a systemic IL-2 deprived immune state in both early and established SSc. Most striking was the progressive shift in Treg subset composition, with a decline in functionally potent CD25hi Treg and a concomitant rise in CD25lo and CD25- subsets, despite stable overall Treg frequencies, indicating a qualitative impairment in IL-2 responsiveness. This phenotype is further supported by the downregulation of CD56hi NK cells, which are known to be IL-2 dependent, the upregulation of pro-inflammatory Th17 cells, a population counter-regulated by Treg-mediated suppression and reduced non-switched memory B cell frequencies. Together, these findings suggest that insufficient IL-2 signaling contributes to the loss of immune regulation

and promotes inflammation early in disease development.

6.2.1 Dysregulation of the Treg-IL-2 axis

Comparisons of individual Treg subset frequencies between the cohorts initially revealed a clear picture of significantly lower frequencies of FoxP3+CD127loCD25+ Treg in the SSc cohort compared to both VEDOSS patients and HC. Given that the CD25 subsets - CD25-, CD25lo and CD25hi - differ in their functional capacity to maintain immune homeostasis, the division of Treg into these subsets revealed a clear shift depending on the disease stage. In SSc patients, the frequencies of the CD25hi Treg subset was significantly lower compared to HC, with a similar trend already observable in VEDOSS patients. These findings are supported by a study by Antiga et al., which also reported a reduction in circulating CD4+FoxP3+CD25hi Treg in established SSc. Although their study included only 15 SSc patients and did not characterize Treg based on the crucial marker for naturally occuring Treg, low levels of CD127, their results align with the present findings by demonstrating a decrease in the functionally most active Treg subset [241, 242]. Particularly noteworthy and of great importance in the present study are the the step-like changes in the CD25- and CD25lo Treg subsets. The frequencies of CD25lo Treg were significantly higher in VEDOSS patients compared to both SSc patients and the HC cohort, while SSc patients exhibited increased frequencies of CD25- Treg. This pattern suggests a progressive decline in Treg functionality as the disease advances. Notably, the frequencies of total Treg remained unchanged across cohorts, indicating that the overall Treg population is not necessarily diminished but rather undergoes a shift in phenotype. This shift likely reflects an impairment in suppressive capacity, reinforcing the notion that Treg dysfunction in SSc is driven by qualitative rather than quantitative changes.
It is plausible that during SSc pathogenesis, the essential Treg growth factor IL-2, as outlined in the introduction, is insufficiently available to support functionally active Treg survival, proliferation and expansion. Moreover, this deficiency likely arises during the early stages of SSc, manifesting as a progressive, measurable decline over time. Since IL-2 levels can hardly be measured directly on protein-expression levels due to its short half-life of 6-20 minutes, the expression of CD25 is determined instead [243, 244]. The expression of CD25 is regulated by interaction with IL-2, creating a positive feedback loop in which IL-2 signaling activates the signal transducer and activator of transcription 5 (STAT5), which subsequently binds to the *Cd25* gene locus, further enhancing CD25 expression and reinforcing Treg sensitivity to IL-2 [245, 246]. The phenomenon of an IL-2-deprived Treg phenotype emerging early in SSc is also supported by key findings in SLE patients. Spee-Mayer et al. demonstrated that

IL-2 protein levels were significantly lower in the cell culture supernatants of PBMC from SLE patients after 44 hours of culturing compared to those from healthy individuals. Additionally, a decrease of CD25hi Treg frequencies accompanied by drastically increased CD25- Treg frequencies in SLE PBMC highlight and confirm the pattern of an IL-2 insufficiency [102].

Another indication of the continuous development of the IL-2-deprived Treg phenotype arises from the observation that VEDOSS patients exhibited significantly higher frequencies of Ki67+ cells among CD25- Treg compared to SSc patients. Rather than indicating active proliferation of stable CD25- Treg, which is unlikely given their impaired capacity for IL-2-driven expansion, this may reflect a population of recently activated or transitioning Treg that are losing CD25 expression due to insufficient IL-2 availability, despite recent proliferative activity. This interpretation aligns with the notion of early Treg destabilization and supports the hypothesis of a progressive shift from CD25lo to dysfunctional CD25- Treg during disease progression. In line with this phenotypic shift and the associated loss of suppressive capacity, a significant reduction in frequencies of CD39+ cells among CD25+ Treg was observed not only in established SSc but already in VEDOSS patients. Given that CD39 catalyzes the hydrolysis of ATP into immunosuppressive adenosine (see fig. 1.2), its decreased expression may result in a loss of inhibitory signaling. This could, in turn, promote Tcon hyperactivity and contribute to an imbalance between Treg and Tcon, further exacerbating immune dysregulation already early during disease development. Nonetheless, the remaining functionally active Treg appear to utilize their full suppressive repertoire in an attempt to counteract this imbalance. This is shown by the increased frequencies of immunosuppressive CTLA4+ cells among CD25+ Treg in SSc patients and CTLA4+ cells among CD25lo Treg in VEDOSS patients, both compared to the HC cohort. The upregulation of CTLA4, a key regulator of Treg-mediated suppression, suggests a compensatory mechanism aimed at maintaining a certain suppression level despite the progressive Treg-Tcon imbalance and decline in IL-2 levels in other suppressive pathways. This is particularly evident in SSc patients, where a significant negative correlation was found between the EUSTAR AI and frequencies of CTLA4+ cells among CD25+ and of CTLA4+ cells among CD25hi Treg, further supporting the compensatory role of CTLA4+ Treg and its clinical relevance. Indeed, a study by Hwang et al. postulated that overexpression of CTLA4 can compensate for IL-2 deficiency, which was demonstrated by transgenic overexpression of CTLA4 that partially rescued a lymphoproliferative disorder in IL-$2^{-/-}$ mice [247].

Additionally, disturbances in IL-2 signaling may also impact CD4+ memory T cell homeostasis, further contributing to immune dysregulation in SSc. Notably, while

frequencies of EM T cells correlated negatively with six out of eleven measured anti-GPCR and anti-GF aAbs only in SSc, but not in VEDOSS, CM T cells were more frequent in SSc than in VEDOSS. Given that frequencies of EM T cells remained unchanged between SSc and VEDOSS, this pattern suggests an impaired differentiation from the central to the effector state. It is known that IL-2 plays a crucial role in memory CD4+ T cell survival and transition, influencing the balance between central and effector memory subsets [246, 248]. IL-2 deficiency in SSc may contribute to the retention of antigen-experienced T cells in a central memory state rather than progressing toward an effector phenotype. Mechanistically, IL-2 production is regulated by several factors, including the transcription factor B lymphocyte-induced maturation protein 1 (BLIMP1), which acts as a negative regulator of IL-2 expression. BLIMP1 is activated by IL-2 itself, establishing a negative feedback loop that represses further IL-2 production. Notably, CM T cells, especially those capable of homing to lymph nodes, express low levels of BLIMP1 under physiological conditions and thus retain the ability to produce IL-2 [245]. However, in the context of chronic immune activation, such as in SSc, prolonged antigen exposure might lead to the upregulation of BLIMP1 in these cells, progressively reducing their capacity to secrete IL-2. This suggests that while an increased frequencies of CM T cells is observed in SSc, these cells may already be transitioning toward a dysfunctional or exhausted phenotype, ultimately contributing to IL-2 deprivation and immune dysregulation. Supporting this assumption, an *in vivo* study by Aqel et al. demonstrated that in a mouse model of encephalomyelitis, CD4+ memory T cells exhibited high BLIMP1 expression. Notably, immunizing the mice with BLIMP1 resulted in a delayed disease onset, highlighting its critical role in regulating memory T cells within an inflammatory environment [249].

6.2.2 Treg/Tcon imbalance with a Th17 predominance

Building upon the physiological balance between Treg and Tcon, both VEDOSS and SSc patients exhibit pronounced imbalances potentially driven by IL-2 deprivation, promoting Tcon hyperactivity. These imbalances were particularly evident in the relationship between CD25hi Treg and various Th subsets. Across all four Th subsets - Th1, Th2, Th9 and Th17 - a significant shift in the ratio was observed, with a marked reduction of CD25hi Treg per Th subset in both VEDOSS and SSc patients compared to HC. Remarkably, this decline followed a gradual pattern across the two disease stages, similar to what has already been observed for CD25hi Treg abundance, supporting the fact that the Treg/Tcon imbalance progressively worsens with disease progression. In general, a Treg/Tcon imbalance is already well known in autoimmune

diseases. In SLE, Humrich et al. discovered *in vivo* in the lupus-prone mouse model NZBxNZW F1 already at disease onset an imbalance between Treg and effector Tcon, which is related to the systemic reduction of IL-2 levels in the pre-disease phase of the disease [100]. In particular, the pronounced shift in the balance between CD25hi Treg and Th17 cells, favoring the Th17 subset, in both VEDOSS and SSc patients compared to the HC cohort provides further insight into the overall dysbalance between protective Treg and pro-inflammatory T cells. Additionally, it is known that Treg exhibit plasticity under pro-inflammatory conditions and can undergo transdifferentiation into Th17 cells. This concept of Treg plasticity is further supported by previous studies demonstrating the conversion of CD25+ Treg into Th17 cells under inflammatory conditions. Research by Komatsu et al. illustrated in a mouse model of rheumatoid arthritis that CD25lo Treg transition into Th17 cells, driven by IL-6 from synovial fibroblasts, which facilitates the proliferation of pathogenic Th17 cells under autoimmune conditions [250]. In alignment with these findings, Ushigome et al. showed that during a drug-induced hypersensitivity syndrome, IL-6-producing CD16+ non-classical monocytes are more prominently recruited, promoting the transition from a Treg to a Th17 response [251]. These assumption align with the current study's observations, which showed that non-classical monocytes seemed to be elevated in SSc patients compared to VEDOSS patients and healthy individuals, despite lacking statistical confirmation due to a high IQR (Kruskal-Wallis-based comparison across all three cohorts: $p = 0.1$; Mann-Whitney U-comparison between VEDOSS and SSc: $^*p = 0.039$). In relation to SSc and to highlight the importance, the main secreted cytokine of Th17 cells, IL-17A, has been implicated in the pathogenesis by promoting myofibroblast transformation as well as skin and lung fibrosis [107, 252]. Under physiological conditions, IL-2 plays a critical role in repressing Th17 differentiation by promoting STAT5 activation, which antagonizes the Th17-driving STAT3 pathway [253]. Consequently, an IL-2-deprived state favors Th17 cell differentiation and proliferation. Considering the increased Th17 cell frequencies in VEDOSS and SSc patients, alongside the IL-2 deprived Treg phenotype, it can be hypothesized that IL-2 deficiency develops in two different ways. Firstly, Kim et al. showed that the phosphatase and tensin homologue (PTEN) is a key factor that regulates Th17 differentiation by suppressing IL-2 production. Functionally, they proved that PTEN deficiency increases IL-2 and phosphorylation of STAT5, but reduces STAT3 phosphorylation, thereby inhibiting Th17 cell differentiation [254]. Secondly, Luo and colleagues showed in the autoimmune disease primary Sjögren's syndrome (pSS), whose characteristic sicca symptoms are also very common in SSc patients, that Th17 cells are elevated and associated with diminished IL-2 levels and decreased phospho-

rylation of STAT5 compared to healthy subjects. Correspondingly, *in vitro* treatment with IL-2 led to an activation of STAT5, which competed with STAT3 for binding to the *Il17a* locus and directly suppressed Th17 differentiation without affecting Treg cells. These findings suggest that reduced IL-2 levels may promote Th17 expansion [255].

6.2.3 Disturbed homeostasis of NK cell subsets

The interplay between IL-2 and immune cell regulation extends beyond Treg and Th17 cells, influencing a variety of other immune components including NK cells. Similar to the CD25hi Treg subset, both the immunoregulatory CD3-CD56hi NK and the cytotoxic CD3-CD56lo NK cell subsets showed a stepwise decrease in frequencies in VEDOSS and SSc compared to the HC cohort. At least for established SSc, Guo et al. confirmed these findings by adding that the absolute counts of CD3-CD56+ NK cells were also significantly reduced compared to HC and correlated with a higher incidence of complicated PAH [152]. In this context, IL-2 is known to play a role in NK cell activation, homeostasis and cytotoxicity, making its deprivation in VEDOSS and SSc a likely contributing factor to the observed decline in frequencies of NK cells. Kim and colleagues have shown that IL-2 deprivation severely impairs NK cell cytotoxicity by selectively downregulating NKp30, a key activating receptor, while leaving NKp46 unaffected. This impairment significantly reduced NK cell-mediated cytotoxicity, underscoring the importance of IL-2 in maintaining NK cell effector functions. The selective impact on NKp30-dependent cytotoxicity suggests that IL-2 availability directly regulates NK cell-mediated immune responses, potentially compromising immune surveillance in VEDOSS and SSc [256]. Beyond direct activation, IL-2 is also essential for NK cell expansion, particularly within the CD56hi NK subset. Spee-Mayer et al. demonstrated in PBMC of SLE patients that low-dose IL-2 expands CD56hi NK cells which may lead to a contact-dependent cell cycle arrest of effector Tcon via the retention of the cycle inhibitor p21 [102]. This highlights a potential feedback loop in which IL-2 not only supports the activation of NK cells, but also enables them to regulate excessive Tcon responses. Moreover, the same research group added that the expansion of CD56hi NK cells is accompanied by an increase in CD25hi Treg, indicating an intricate interplay between NK cells and Treg in IL-2-dependent immune homeostasis [102]. Given these findings, therapeutic strategies aimed at restoring IL-2 levels, either through cytokine supplementation or modulation of Treg-NK interactions, may help rebalance immune responses even in early disease stages. In addition to the role of CD3-CD56+ NK cells in VEDOSS and SSc, another subset of NK cells, the CD3+CD56+ NK T cells, also exhibits dynamic

changes across disease stages. Unlike the steady decline observed in classical CD3- NK cells, the CD3+ NK T subset showed a slight increase in VEDOSS compared to HC, followed by a significant drop in established SSc. This suggests that NK T cells may participate in early immune regulation, potentially counteracting excessive immune activation. Interestingly, their negative correlation with the EUSTAR AI in VEDOSS patients further supports their role in modulating disease activity at early stages. Indeed, similar results could be found in a different immune-mediated disease. Koreck et al. found in patients with established psoriasis, an autoimmune disease characterized by patches of abnormal skin, that CD3+CD56+ NK T cells were significantly reduced compared to controls and the frequencies increased after conducting antipsoriatic therapies [257]. The slight increase in NK T cell frequencies observed in VEDOSS patients may once again be explained by a compensatory mechanism. It is well established that NK T cells can exhibit NK cell-like cytotoxic activity in an inflammatory environment. This cytotoxic potential is primarily attributed to the killer cell Ig-like receptor (KIR)+ subset within the NK T cell fraction, which may transiently expand in response to immune dysregulation in early disease stages. [258, 259]. To better understand these phenomena, especially in the pre-diseased phase, it is important to investigate the potential mechanisms underlying these variations and their impact on disease progression.

6.2.4 Involvement of B cell subsets

In addition to its well-established role in Treg homeostasis and NK cell function, IL-2 also influences B cell development and differentiation. In the present study, total B cell frequencies were significantly reduced in SSc patients, while non-switched memory B cells, defined by their CD27+IgD+IgM+ phenotype, were already significantly decreased in VEDOSS patients and remained low in established SSc. Indeed, Simon et al. found that non-switched B cells were significantly reduced in blood of SSc patients and several studies reported a similar reduction in frequencies of non-switched memory B cells in patients with SLE, suggesting a link between B cell subset alterations and autoimmune pathogenesis and an early and persistent disruption of B cell homeostasis throughout disease progression [260 –262]. In context with an IL-2 deprived state, recent evidence indicates that absence of IL-2 can impair the development and maintenance of certain B cell subsets. Studies have shown that IL-2 influences B cell fate decisions, including the differentiation into plasma cells and the regulation of memory B cell subsets [263, 264]. IL-2 signaling promotes plasma cell differentiation by repressing the BTB Domain And CNC Homolog 2 (BACH2), a transcription factor that inhibits this process. In the absence of IL-2, BACH2 remains

active, hindering the transition of B cells into plasma cells [263]. This mechanism may contribute to the reduced levels of non-switched memory B cells observed in VEDOSS and SSc patients. A reduced availability of IL-2 may therefore impair the generation or persistence of non-switched memory B cells, either by limiting their transition from naive precursors or by failing to support their survival in the periphery. Additionally, Inaba and colleagues show that low-dose IL-2 therapy enhances IL-10 production in activated B cells, indicating that IL-2 also supports the induction of regulatory B cells (Bregs), a subset critical for immunomodulation in autoimmune conditions. These effects were linked to BACH2 downregulation, as BACH2 was found to bind the IL-10 gene promoter and restrict its expression. Loss or suppression of BACH2 increased IL-10 secretion, suggesting that IL-2 facilitates a Breg phenotype by relieving BACH2-mediated repression [265]. This adds another layer to how IL-2 deprivation may contribute to immune dysregulation and align with the broader immune signature of IL-2 deficiency observed in SSc and VEDOSS.

6.2.5 Targeted Treg recovery

Based on the new findings and the preceding discussion about the disturbances in the Treg/IL-2 axis observed in VEDOSS and SSc, a mechanistic proof-of-principle approach has been rationalized to specifically restore Treg activity in established SSc. This included an *in vitro* low-dose IL-2 stimulation to enhance Treg function with a selected dose range from 0 ng/ml - 10 ng/ml. The designation of 1 ng/ml as a low-dose has been demonstrated by several studies, by proving that Treg are highly sensitive to IL-2 leading to elevated expression of CD25 and selective induction of STAT5 phosphorylation, allowing them to respond to lower IL-2 concentrations compared to other Tcon or NK cell subsets [102, 266, 267]. In the present study, the stimulation of PBMC from SSc patients with 1 ng/ml rIL-2 induced a significant increase in frequencies of CD25hi Treg compared to the unstimulated control. This shift was accompanied by a corresponding reduction in CD25lo Treg, while the CD25- Treg subset remained unchanged, indicating a selective effect on distinguished Treg subsets. Notably, increasing rIL-2 concentrations did not further enhance the proportion of CD25hi Treg, suggesting that a low-dose application is sufficient to optimize Treg recovery. To assess the impact of IL-2 stimulation at the single-cell level, a quantification of CD25 molecules per cell within the CD25hi Treg subset was conducted. Similarly, the stimulation with 1 ng/ml rIL-2 resulted in a significant increase in the amount of CD25 per cell among CD25hi Treg compared to the unstimulated control. Higher rIL-2 concentrations (5 ng/ml and 10 ng/ml) led to further increases, though these did not significantly exceed the effects observed at 1 ng/ml. These results

indicate that low-dose IL-2 effectively enhances both the frequency and activation status of CD25hi Treg in SSc without additional benefit at higher doses. Furthermore, no differences were observed in the frequencies of Ki67+ cells among CD25+ Treg subsets following rIL-2 stimulation, supporting the evidence that rIL-2 does not simply increase the overall Treg population but rather reactivates pre-existing Treg and enhances their suppressive capacity. This approach has already been used in the past with PBMC from SLE patients with the same results. Here, Spee-Mayer et al. was also able to selectively restore CD25hi Treg frequencies after low-dose rIL-2 stimulation [102]. A randomized, double-blind, placebo-controlled trial by He et al. in patients with SLE demonstrated that low-dose IL-2 treatment led to an early expansion of Treg frequencies, followed subsequently by an increase in CD56hi NK cell frequencies. These immunological changes were accompanied by a rapid clinical improvement in the IL-2-treated group compared to the placebo group [268].
To obtain a more comprehensive view, also at the transcriptional level, the mRNA expression of the three IL-2 receptor chains and Treg-associated genes was also determined *in vitro* after rIL-2 application using qPCR. All three IL-2 receptor chains exhibited a significant increase in relative gene expression after stimulation with 1 ng/ml rIL-2 compared to the unstimulated control. However, a stepwise trend towards an increase in gene expression was observed with higher rIL-2 concentrations. It is important to note that this experiment was conducted using mRNA extracted from stimulated bulk PBMC. Consequently, the analysis was not limited to Treg but included all cell types expressing IL-2 receptor chains, such as Tcon, which may have contributed to the observed expression pattern. In addition, there were no changes in *CTLA4*, *IL-10* and *ENTPD1* gene expression after rIL-2 stimulation, which is probably related to the short stimulation duration of only 24h. For instance, the expression of CTLA4 is subject to post-transcriptional controls, including intracellular trafficking and surface expression dynamics. An *in vivo* study demonstrated that CTLA4 proteins in Treg are localized in submembrane vesicles that rapidly recycle to and from the cell surface, a process that may not be immediately evident at the mRNA level within a 24-hour timeframe [269]. However, extending the stimulation period beyond 24 hours and incorporating additional activating signals could potentially reveal more pronounced transcriptional responses for these genes. Given that Treg characteristically maintaining immune tolerance by secreting inhibitory cytokines such as TGFβ1 and IL-10 and considering that TGFβ1 is known to be highly upregulated and serve as a marker for vascular and fibrotic involvement in SSc patients, it was essential to assess whether rIL-2 stimulation enhances the secretion of these cytokines [202, 270, 271]. To this end, ELISAs were performed to quantify protein concentrations in

the cell culture supernatant after 24h of rIL-2 stimulation. The analysis revealed no significant differences in TGFβ1 and IL-10 levels following low-dose rIL-2 stimulation compared to the control. However, a trend toward increased TGFβ1 concentration was observed after stimulation with 10 ng/ml rIL-2, accompanied by a significant decrease in IL-10 concentration. These findings suggest that low-dose IL-2 application, at least *in vitro*, does not exert pro-fibrotic effects.
Together, these findings provide a mechanistic proof-of-principle for targeted Treg recovery through low-dose IL-2 administration in SSc. Given the critical role of CD25hi Treg in immune homeostasis, the data support the rationale for therapeutic IL-2 modulation as a potential strategy to restore immune balance and counteract disease progression in SSc. Moreover, this strategy could potentially serve as a preventive intervention in VEDOSS patients by counteracting the development of the IL-2-deprived Treg phenotype and restoring balance between Treg and Tcon populations.

6.2.6 Perspectives and limitations

The fact that disturbances in the Treg-IL-2 axis, specifically an IL-2-deprived Treg phenotype, manifest early in the course of disease, long before the diagnosis of established SSc, underscores the urgent need for novel interventional strategies aimed at preventing disease progression and organ damage. The *in vitro* rIL-2 stimulation experiment further validated this concept, reinforcing previous findings from other autoimmune diseases, such as SLE and providing the rationale for conducting a clinical trial to evaluate low-dose IL-2 as a therapeutic strategy for restoring Treg activity in SSc patients. In fact, a recent interventional open-label phase 1–phase 2a study conducted by Barde et al. showed that the blood cell count of the CD25hi Treg subset increased significantly upon low-dose IL-2 application and met the primary efficacy endpoint already at day 8. Unfortunately, neither CD25- and CD25lo Treg subsets nor crucial Tcon subsets, such as Th17 cells, were recorded in this clinical trial [53]. Building on these findings, future research should conduct a similar proof-of-principle approach in VEDOSS patients while incorporating functional experiments to investigate the mechanisms underlying reduced IL-2 synthesis. In addition, longitudinal studies in VEDOSS patients would be valuable to determine the exact time point of the onset of the IL-2-deprived Treg phenotype in relation to clinical outcomes. Unfortunately, this was not feasible within the timeframe of the present study due to the challenges associated with recruiting VEDOSS patients and, regarding the longitudinal study, the time interval between the diagnosis of VEDOSS and established SSc. Nevertheless, the complex interplay of various immune cell subsets and signaling molecules has once again demonstrated that a limited focus on isolated

cell types is inadequate for accurately defining the early stages of disease. Indeed, as previously described, there are always multiple interacting factors, particularly within the adaptive immune system, that influence one another and trigger distinct symptoms under pathological conditions. A prime example of this complexity is the crucial involvement of Th subsets, particularly Th17 cells, as well as NK cells, which are critical contributors to the dysregulation of the Treg/IL-2 axis. This hypothesis was further affirmed by the Random Forest prediction analysis, which showed that the immunophenotype-based separation, generated by a machine-learning algorithm, between healthy individuals and VEDOSS patients was primarily driven by the frequencies of, Th17 cells, CD25lo Treg and CD39+ cells among CD25+ Treg. A similar complexity emerged in the differentiation between VEDOSS and established SSc patients, where the key determinants were proliferating Ki67+ cells among CD25- Treg, as well as the reduction in CD25hi Treg and CD56hi NK cells. The fact that the classification accuracy exceeded 80% in both the separation between HC and VEDOSS and between VEDOSS and SSc raises the question of whether such predictive analyses should be integrated into clinical practice. The more immunophenotypic data are collected from VEDOSS and SSc patients, the better the algorithm can be trained, ultimately leading to increased precision in the prediction process. However, this also highlights a key limitation of the present study. Given the substantial heterogeneity of disease stages, continuous recruitment of new patients is essential to increase the overall dataset volume and enhance the statistical power of median values in the analyses.

6.3 Dysregulation of the Th17-IL-17 axis

The quantitative increase of Th17 cells within the progression of established SSc has already been well established in the literature and with the help of the research results of this study it is now possible to classify the influence of this immune cell type, especially in the pre-clinical stage. The observed increase in frequencies of Th17 cells in VEDOSS compared to HC has already been linked to the IL-2-deprived Treg phenotype. However, this finding can now be considered from an additional perspective, given that the Olink® proteomic analysis revealed significantly higher serum levels of IL-17A in SSc patients compared to VEDOSS patients, despite comparable Th17 cell frequencies. Since the differentiation of Th17 cells from naive CD4+ T cells depends on signals from IL-6 and TGFβ and the serum levels of these two molecules did not significantly differ between VEDOSS and SSc patients, it is plausible that Th17 frequencies remain unchanged between these groups [272]. Supporting this

assumption, intermediate monocytes, a subset specialized in producing large amounts of pro-inflammatory cytokines including IL-6, were found to be significantly elevated in both VEDOSS and SSc patients compared to HC, yet their frequencies were almost equal between each other [273]. This suggests that despite the increased availability of IL-6-producing monocytes, other regulatory mechanisms may influence IL-17A secretion and Th17 activity, particularly during the transition from VEDOSS to SSc. This highlights the relevance of the significantly elevated IL-17A levels observed in SSc serum. Moreover, IL-17A is known to enhance monocyte adhesion to endothelial cells, thereby promoting their recruitment to sites of inflammation. The reduced frequencies of total monocytes observed in VEDOSS and SSc patients in this study may thus reflect their migration from the peripheral blood into affected tissues, suggesting an IL-17A-driven mechanism contributing to local immune activation in established SSc. [274]. This interplay between IL-17A and monocytes could be particularly relevant in vascular pathology, given that monocytes contribute to endothelial homeostasis and repair [275, 276]. Their reduction might exacerbate vascular damage, a hallmark of SSc, which in turn could further promote Th17 activation, as stressed endothelial cells can release cytokines that sustain Th17 function and survival. This mechanism may contribute to the observed IL-17A elevation in SSc, in contrast to VEDOSS, where the inflammatory network may not yet be fully dysregulated. Nevertheless, either together with IL-17F as a heterodimer or as a homodimer, these cytokines form the starting point of a specific IL-17 signaling pathway that regulates the innate and adaptive immune response as well as a broad spectrum of chronic inflammatory and tissue remodeling processes [277 –279]. Notably, KEGG enrichment analysis revealed that a substantial proportion of differentially expressed inflammatory proteins between VEDOSS and SSc patients could be directly linked to this pathway. To further delineate the specific proteins involved in the IL-17 pathway and their localization within it, KEGG pathway mapping was performed. This analysis identified a total of 14 measured proteins associated with the pathway, 10 of which were significantly upregulated in SSc patients compared to the VEDOSS cohort. Although healthy individuals were not included in the Olink® analysis, a recently published study by Seki et al. demonstrated that this IL-17A-dependent signaling pathway is highly active in SSc patients compared to healthy controls. Moreover, they observed a strong association between elevated IL-17A serum levels and an increased prevalence of PAH in SSc patients [280]. This correlation provides a potential explanation for the lower IL-17A levels observed in VEDOSS patients, as they typically exhibit only minimal subclinical manifestations. Notably, none of the VEDOSS patients recruited for this study showed a PAH. Correspondingly, this finding raises the possibility that

increasing IL-17A levels could serve as a predictive biomarker for early detection of lung involvement in SSc. Since IL-6 is induced and secreted in response to IL-17A signaling, the fact that distinct positive correlations between IL-6 and inflammatory markers such as CRP and NT-proBNP, as well as with the overall EUSTAR AI were exclusively observed in the SSc cohort, supports the hypothesis for organ manifestation in dependency of an activated IL-17A pathway. In line with that, the same study by Seki et al. showed that IL-6 levels were also significantly elevated in SSc patients compared to HC and additionally correlated with reduced lung function [280, 281]. The fact that IL-6 serum levels did not differ significantly between VEDOSS and SSc patients in the present study suggests that VEDOSS patients may already be at risk for developing lung inflammation, despite the absence of the previously mentioned correlations with clinical inflammatory markers and disease activity in the VEDOSS cohort.

6.3.1 IL-17 signaling pathway-mediated immune dysregulation

Building on the findings of Seki et al. regarding pathological alterations in the IL-17 signaling pathway in SSc patients, the present study identified additional IL-17A-dependent factors, such as MMP-1 or CXCL10, that may contribute not only to lung inflammation but also to tissue remodeling processes in SSc. Notably, a study by Ross et al. was the first to demonstrate increased CXCL10 expression in skin biopsies of VEDOSS patients, which was accompanied by enhanced collagen deposition. Furthermore, elevated serological CXCL10 levels were detected in VEDOSS patients compared to healthy individuals [192]. The findings of the present study, which showed significantly higher levels of serum CXCL10 in SSc compared to VEDOSS patients, align with and further support these observations. Given the role of CXCL10 as a key driver of the polarization and enhancement of the function of various effector Tcon subsets, its progressive increase from HC to VEDOSS (Ross et al.) and VEDOSS to SSc (present study) may reflect a shift towards a more pronounced pro-inflammatory and fibrotic environment. This gradual process is also supported by the significant positive correlation of CXCL10 and the EUSTAR AI exclusively in VEDOSS patients, suggesting that CXCL10 may contribute not only to early immune dysregulation in VEDOSS, but also to the persistence and amplification of inflammation and tissue remodeling in established SSc [282]. Supporting this hypothesis, CXCL10 levels in SSc patients exhibited significant positive correlations with six anti-GPCR aAbs, including the well-characterized AT1R and ETAR. As described in the introduction, these aAbs are implicated in vascular dysfunction and fibrosis, key pathological features of SSc. Notably, VEDOSS patients did not show any of these correlations, which

may indicate that the pathological interplay between CXCL10 and anti-GPCR aAbs becomes more relevant as the disease progresses and could potentially be prevented in VEDOSS patients. Interestingly, despite measuring aAb levels against CXCR3, the primary receptor of CXCL10, no significant correlation was observed, suggesting that CXCL10 elevation in SSc is not directly driven by the CXCR3-Th1 axis. This interpretation is further supported by the lack of differences in frequencies of Th1 cells between SSc patients and HC, indicating that other immune mechanisms, such as aAb-mediated signaling or IFN-driven pathways, may predominate in regulating CXCL10 expression [283, 284]. In line with that and regarding the AT1R, Stegbauer et al. showed in an *in vivo* mouse model of established multiple sclerosis that specifically blocking AT1R impairs the release of several chemokines, including CXCL10 and may therefore have a beneficial effect on the progression of autoimmune diseases [285]. Taken together, this finding highlights the potential role of CXCL10 as a mediator linking immune dysregulation with aAb-driven vascular and fibrotic changes in SSc, reinforcing its relevance as a biomarker downstream of the IL-17 signaling cascade and potential therapeutic target.

6.3.2 Perspectives and limitations

This study was the first to show that in addition to the suspected involvement of Th17 cells in Treg/Tcon dysregulation in VEDOSS patients, the IL-17 signaling pathway might also play an essential role in disease progression. The findings of this study provide new insights into the role of this certain pathway in the transition from VEDOSS to established SSc, emphasizing its contribution to immune dysregulation, inflammation and tissue remodeling. The identification of significantly increased IL-17A serum levels in SSc compared to VEDOSS, despite comparable Th17 frequencies, highlights the complexity of IL-17A regulation and suggests additional factors influencing its secretion. Notably, the involvement of monocytes in IL-17A-driven immune responses, including their adhesion to endothelial cells and contribution to vascular pathology, presents a promising option for further research. Additionally, the progressive increase of CXCL10 from VEDOSS to SSc, along with its correlation with disease activity, suggests a potential role in early immune dysregulation and fibrotic changes, reinforcing its relevance as a biomarker and possible therapeutic target. Despite these advancements, the study has several limitations. First, while IL-17A-mediated immune activation appears to be a key driver of disease progression, the precise mechanisms by which IL-17A influences cellular dynamics and endothelial function remain incompletely understood. The observed reduction in frequencies of total monocytes raises questions regarding their differentiation, tissue recruitment

and functional plasticity in VEDOSS and SSc, which were not fully addressed in this study. Furthermore, the lack of healthy subjects in the Olink® proteomic analysis limits direct comparisons and the ability to establish a definitive baseline for IL-17A-related immune alterations. Additionally, while the Seki et al. showed a potential link between IL-17A and PAH development, longitudinal studies with VEDOSS patients would be beneficial to determine whether IL-17A levels can serve as a predictive biomarker for lung involvement in early disease stages. Interestingly, the human monoclonal antibodies blocking either only IL-17A (Secukinumab) or IL-17A and IL-17F together (Bimekizumab) have already demonstrated their efficacy in psoriatic arthritis (PsA) [286 –288]. Given the critical role of IL-17A in disease progression highlighted in both the literature and the present study, targeting IL-17A and IL-17F simultaneously may help mitigate immune dysregulation and vascular pathology in SSc or may even prevent its occurence completely in VEDOSS patients. Future clinical trials investigating IL-17 blockers in this context could provide valuable insights into its potential for early intervention and disease modification. Unfortunately, the expression of IL-17F could not be determined in this study, as this cytokine is not present in the predefined Olink® inflammation panel. Lastly, the correlation between CXCL10 and anti-GPCR aAbs provides intriguing evidence for their interplay in vascular dysfunction and fibrosis but further mechanistic studies are necessary to establish a causal relationship and evaluate potential therapeutic interventions targeting this pathway. Overall, this study underscores the significance of IL-17A signaling in early and established pathogenesis, offering new perspectives on disease progression and potential biomarkers. However, further investigations, including functional studies and longitudinal patient cohorts, are needed to validate these findings and explore their clinical implications.

To conclude the discussion of the Treg-IL-2 and Th17-IL-17 axes and their role in SSc pathogenesis, the following illustration (fig. 6.1) summarizes the key immunological findings of this study in connection with the current literature. It provides a comprehensive visual summary of the proposed mechanisms driving disease progression from VEDOSS to established SSc.

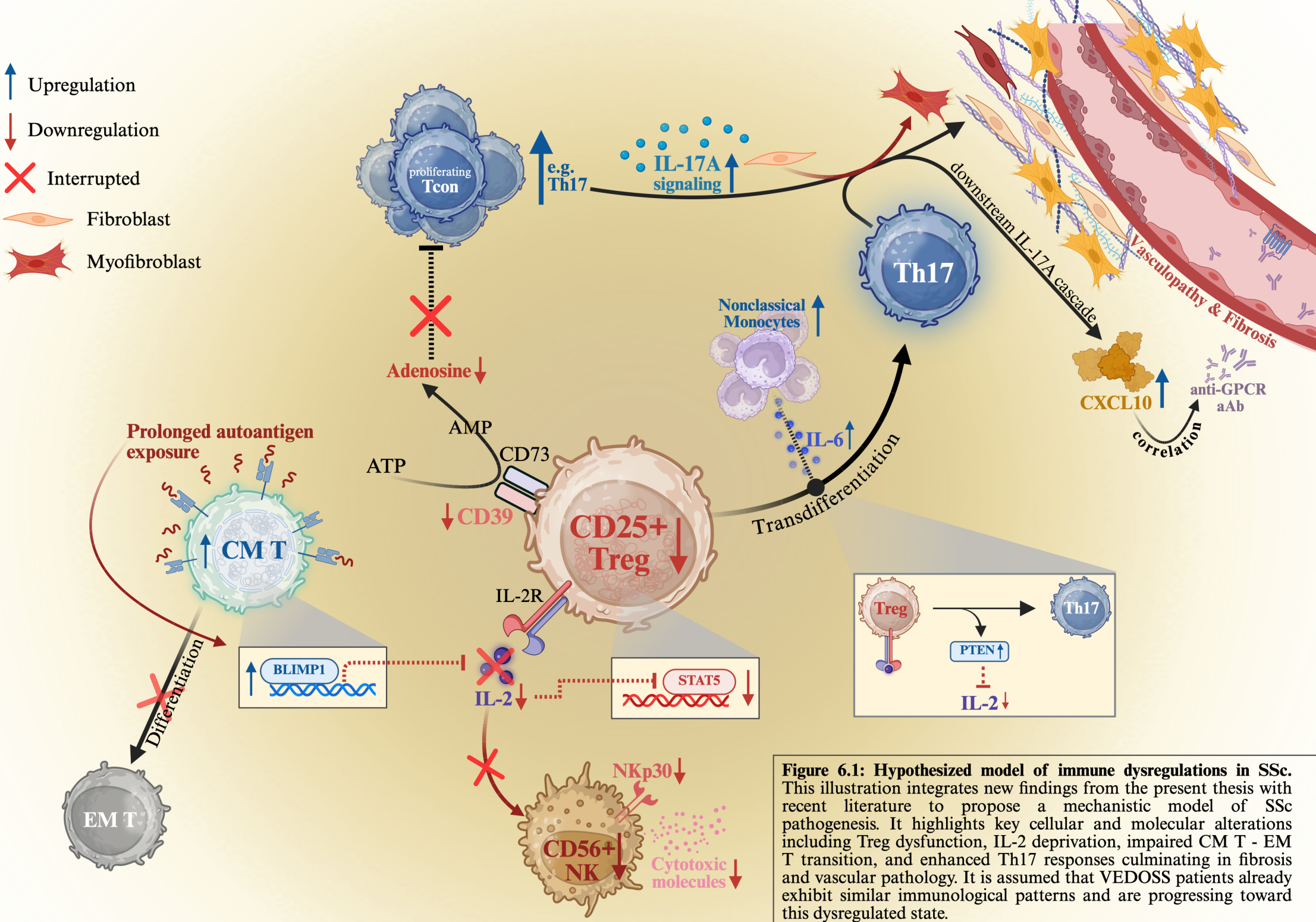

Figure 6.1: Hypothesized model of immune dysregulations in SSc. This illustration integrates new findings from the present thesis with recent literature to propose a mechanistic model of SSc pathogenesis. It highlights key cellular and molecular alterations including Treg dysfunction, IL-2 deprivation, impaired CM T - EM T transition, and enhanced Th17 responses culminating in fibrosis and vascular pathology. It is assumed that VEDOSS patients already exhibit similar immunological patterns and are progressing toward this dysregulated state.

6.4 Alterations in B cells and quantities of autoantibodies

B cells and plasma cells play a pivotal role in the immunopathogenesis and transition from VEDOSS to the established SSc, by contributing to immune interactions and being the source of pathogenic aAb production and therefore by promoting autoimmune conditions. The present study highlighted key alterations in B cell subsets together with aAbs levels, suggesting a dynamic shift in immune processes as the disease progresses. The first notable finding was the reduction in frequencies of total CD19+ B cells in SSc compared to VEDOSS and HC, which was accompanied by a decrease in frequencies of non-switched memory B cells in both patient cohorts compared to HC. However, caution is warranted when interpreting the biological significance of these reduced total B cell frequencies in SSc. Although patients undergoing rituximab therapy were excluded from the analyses, many other SSc patients were receiving different immunosuppressive treatments, some of which have also B cell-depleting effects, like mycophenolate or methotrexat [289, 290]. Therefore, the observed reductions in frequencies of B cells exclusively in SSc patients may, at least in part, be influenced by immunosuppressive medication rather than reflecting intrinsic disease mechanisms alone. In addition, studies by Taylor et al. and Böhm et al. have shown that mycophenolate and methotrexate also have aAb-reducing properties, suggesting that anti-GPCR aAb titers may also be affected by these treatments, potentially explaining why PAR2, β2 and ETAR aAb levels were higher in VEDOSS patients compared to those with SSc [291, 292]. In contrast, the assumption of very early expansion of anti-GPCR aAbs should still be considered, as only in the VEDOSS cohort the frequencies of total B cells showed a significant positive correlation with six anti-GPCR aAb levels, including those that showed higher levels compared to the SSc group. This finding suggests that early in the disease process, B cell activity is strongly linked to the production of anti-GPCR aAbs, which may contribute to the initiation and amplification of inflammatory pathways. As the disease progresses to established SSc, this correlation weakens, possibly due to a shift in the immune landscape driven by chronic inflammation, immunosuppressive treatments and potential interference with B cell functionality. Regarding the observed reduction of frequencies in non-switched memory B cells in both VEDOSS and SSc patients compared to healthy individuals, a study by Simon et al. confirmed this finding at least in established SSc, stating that this could be due to an imbalance between activated memory and tolerogenic B cell types [260].

This study highlights the evolving role of B cells and anti-GPCR aAbs in the transition

from VEDOSS to established SSc and their drug-related complications for conducting appropriate research. Future investigations should focus on treatment-naive patients and longitudinal studies to distinguish disease-driven changes from medication effects. Functional analyses of B cell subsets could further clarify their role in early SSc pathogenesis and progression. An additional limitation is that baseline aAb titers in healthy serum were not measured in this study. Future research should include these measurements, particularly to facilitate comparisons between HC and VEDOSS, as aAbs targeting various GPCRs, whether agonistic or antagonistic, are commonly present under physiological conditions in human serum and contribute to the regulation of physiological processes, including immune function [66, 293].

6.5 Conclusion and outlook

This study adds a crucial piece to the existing knowledge on the immune pathogenesis and transition from the early preclinical stage to established SSc. The findings presented here strongly indicate that disease progression is a gradual and dynamic process, characterized by emerging imbalances between effector and regulatory components of both the innate and adaptive immune systems. Furthermore, this study helped unravel parts of the complex network of immune interactions, identifying key components and immune signatures that may act as disease drivers. Based on these findings, two principal models of disease progression, as outlined in this discussion, were highlighted and aligned with current research from the literature. It can be concluded that both the Treg-IL-2 and Th17-IL-17 axes play a central role in disease progression, with their interplay further amplifying immune dysregulation. These pathways represent promising targets for therapeutic intervention. In particular, clinical trials should be conducted to assess the applicability and efficacy of low-dose IL-2 therapy in restoring functional Treg subsets. On the other hand, considering the dysregulation within the Th17-IL-17 axis, further research should focus on elucidating the precise functional consequences of these disturbances. Instead of solely targeting secreted cytokines downstream of the IL-17 signaling pathway, a more upstream intervention directly at the level of Th17 cells should be considered. In this context, low-dose IL-2 therapy may offer an additional benefit by suppressing Th17 differentiation through STAT5 activation, making it a promising dual-acting immunomodulatory strategy. Additionally, the formation of subcohorts within the established SSc patient group, based on specific organ manifestations, could provide deeper insights into cytokine expression patterns and help identify molecular factors contributing to distinct organ involvement.

Given the rapid advancements in technology and the increasing integration of artificial intelligence in healthcare, machine-learning-based early detection of autoimmune diseases represents one of the most promising approaches. In this study, the Random Forest algorithm demonstrated high accuracy in classifying a patient's disease stage only based on immunophenotyping data. This was further enhanced for the first time by incorporating a multi-omics approach, integrating in-depth immunophenotyping, aAb levels and cytokine profiles. The PCA and variable importance analysis revealed a clear separation between VEDOSS and SSc patients, providing initial evidence that machine-learning-based diagnostics could be significantly more effective and efficient than conventional methods. If immunophenotyping and proteomic analyses can be further optimized for ease of use and automated evaluation, their clinical implementation could enable the early identification of autoimmune diseases and pave the way for individualized treatment strategies aiming to prevent the progression to established disease. Since early diagnosis remains key to improving patient outcomes and preventing irreversible organ damage, integrating AI-driven diagnostics into routine clinical practice could mark a major step forward in autoimmune disease management.

"Patients can struggle for years before they get a diagnosis and even then, the names we give these diseases are like umbrella terms that overlook the biological diversity behind complex diseases."

(Quote from an interview in ScienceDaily® from february 24, 2025. Maxim Zaslavsky and his colleagues on their development of a highly accurate artificial intelligence that demonstrates great progress in the early diagnosis of autoimmune diseases [294].)

Bibliography

[1] A. Bergamasco, N. Hartmann, L. Wallace, and P. Verpillat, "Epidemiology of systemic sclerosis and systemic sclerosis-associated interstitial lung disease," *Clinical Epidemiology*, vol. 11, Apr. 2019.

[2] E. R. Volkmann, K. Andréasson, and V. Smith, "Systemic sclerosis," *The Lancet*, vol. 401, no. 10373, Jan. 2023, ISSN: 0140-6736.

[3] J. J. Solomon, A. L. Olson, A. Fischer, T. Bull, K. K. Brown, and G. Raghu, "Scleroderma lung disease," *European Respiratory Review*, vol. 22, no. 127, Feb. 2013, ISSN: 0905-9180, 1600-0617.

[4] X. Ma, R. Tang, M. Luo, Z. Zeng, Y. Shi, B. Tang, and R. Xiao, "Efficacy of mycophenolate mofetil versus cyclophosphamide in systemic sclerosis-related interstitial lung disease: A systematic review and meta-analysis," *Clinical Rheumatology*, vol. 40, no. 8, Aug. 2021, ISSN: 1434-9949.

[5] R. T. Domsic, S. I. Nihtyanova, S. R. Wisniewski, M. J. Fine, M. Lucas, C. K. Kwoh, C. P. Denton, and T. A. Medsger Jr., "Derivation and External Validation of a Prediction Rule for Five-Year Mortality in Patients With Early Diffuse Cutaneous Systemic Sclerosis," *Arthritis & Rheumatology*, vol. 68, no. 4, 2016, ISSN: 2326-5205.

[6] M. Bairkdar, M. Rossides, H. Westerlind, R. Hesselstrand, E. V. Arkema, and M. Holmqvist, "Incidence and prevalence of systemic sclerosis globally: A comprehensive systematic review and meta-analysis," *Rheumatology*, vol. 60, no. 7, Jul. 2021, ISSN: 1462-0324.

[7] P. Mani, D. Gonzalez, S. Chatterjee, and M. D. Faulx, "Cardiovascular complications of systemic sclerosis: What to look for," *Cleveland Clinic Journal of Medicine*, vol. 86, no. 10, Oct. 2019, ISSN: 0891-1150, 1939-2869.

[8] A. Gabrielli, E. V. Avvedimento, and T. Krieg, "Scleroderma," *The New England Journal of Medicine*, vol. 360, no. 19, May 2009, ISSN: 1533-4406.

[9] J. Barnes and M. D. Mayes, "Epidemiology of systemic sclerosis: Incidence, prevalence, survival, risk factors, malignancy, and environmental triggers," *Current Opinion in Rheumatology*, vol. 24, no. 2, Mar. 2012, ISSN: 1531-6963.

[10] M. Hughes, J. D. Pauling, L. Armstrong-James, C. P. Denton, P. Galdas, and C. Flurey, "Gender-related differences in systemic sclerosis," *Autoimmunity Reviews*, vol. 19, no. 4, Apr. 2020, ISSN: 1568-9972.

[11] U. A. Walker, A. Tyndall, L. Czirják, C. Denton, D. Farge-Bancel, O. Kowal-Bielecka, U. Müller-Ladner, C. Bocelli-Tyndall, and M. Matucci-Cerinic, "Clinical risk assessment of organ manifestations in systemic sclerosis: A report from the EULAR Scleroderma Trials And Research group database," *Annals of the Rheumatic Diseases*, vol. 66, no. 6, Jun. 2007, ISSN: 0003-4967.

[12] E. C. LeRoy, C. Black, R. Fleischmajer, S. Jablonska, T. Krieg, T. A. Medsger, N. Rowell, and F. Wollheim, "Scleroderma (systemic sclerosis): Classification, subsets and pathogenesis," *The Journal of Rheumatology*, vol. 15, no. 2, Feb. 1988, ISSN: 0315-162X.

[13] E. C. LeRoy and T. A. Medsger, "Criteria for the classification of early systemic sclerosis.," *The Journal of Rheumatology*, vol. 28, no. 7, Jul. 2001, ISSN: 0315-162X, 1499-2752.

[14] F. van den Hoogen *et al.*, "2013 classification criteria for systemic sclerosis: An American college of rheumatology/European league against rheumatism collaborative initiative," *Annals of the Rheumatic Diseases*, vol. 72, no. 11, Nov. 2013, ISSN: 0003-4967, 1468-2060.

[15] C. Yang, S. Tang, D. Zhu, Y. Ding, and J. Qiao, "Classical Disease-Specific Autoantibodies in Systemic Sclerosis: Clinical Features, Gene Susceptibility, and Disease Stratification," *Frontiers in Medicine*, vol. 7, Nov. 2020, ISSN: 2296-858X.

[16] A. Stochmal, J. Czuwara, M. Trojanowska, and L. Rudnicka, "Antinuclear Antibodies in Systemic Sclerosis: An Update," *Clinical Reviews in Allergy & Immunology*, vol. 58, no. 1, Feb. 2020, ISSN: 1559-0267.

[17] C. Ferri *et al.*, "Systemic sclerosis Progression INvestiGation (SPRING) Italian registry: Demographic and clinico-serological features of the scleroderma spectrum," *Clinical and Experimental Rheumatology*, vol. 38 Suppl 125, no. 3, 2020, ISSN: 0392-856X.

[18] S. Jaafar, A. Lescoat, S. Huang, J. Gordon, M. Hinchcliff, A. A. Shah, S. Assassi, R. Domsic, E. J. Bernstein, V. Steen, S. Elliott, F. Hant, F. V. Castelino, V. K. Shanmugam, C. Correia, J. Varga, V. Nagaraja, D. Roofeh, T. Frech, and D. Khanna, "Clinical characteristics, visceral involvement, and mortality in at-risk or early diffuse systemic sclerosis: A longitudinal analysis of an observational prospective multicenter US cohort," *Arthritis Research & Therapy*, vol. 23, 2021, ISSN: 1478-6354.

[19] D. Khanna, D. E. Furst, P. J. Clements, Y. Allanore, M. Baron, L. Czirjak, O. Distler, I. Foeldvari, M. Kuwana, M. Matucci-Cerinic, M. Mayes, T. Medsger, P. A. Merkel, J. E. Pope, J. R. Seibold, V. Steen, W. Stevens, and C. P. Denton, "Standardization of the modified Rodnan skin score for use in clinical trials of systemic sclerosis," *Journal of scleroderma and related disorders*, vol. 2, no. 1, 2017, ISSN: 2397-1983.

[20] S. Amjadi, P. Maranian, D. E. Furst, P. J. Clements, W. K. Wong, A. E. Postlethwaite, P. P. Khanna, and D. Khanna, "Course of Modified Rodnan Skin Score in Systemic Sclerosis Clinical Trials: Analysis of 3 Large Multicenter, Randomized Clinical Trials," *Arthritis and rheumatism*, vol. 60, no. 8, Aug. 2009, ISSN: 0004-3591.

[21] G. Valentini *et al.*, "The European Scleroderma Trials and Research group (EUSTAR) task force for the development of revised activity criteria for systemic sclerosis: Derivation and validation of a preliminarily revised EUSTAR activity index," *Annals of the Rheumatic Diseases*, vol. 76, no. 1, Jan. 2017, ISSN: 0003-4967, 1468-2060.

[22] A. J. Tyndall *et al.*, "Causes and risk factors for death in systemic sclerosis: A study from the EULAR Scleroderma Trials and Research (EUSTAR) database," *Annals of the Rheumatic Diseases*, vol. 69, no. 10, Oct. 2010, ISSN: 0003-4967.

[23] T. A. Mcnearney, J. D. Reveille, M. Fischbach, A. W. Friedman, J. R. Lisse, N. Goel, F. K. Tan, X. Zhou, C. Ahn, C. A. Feghali-Bostwick, M. Fritzler, F. C. Arnett, and M. D. Mayes, "Pulmonary involvement in systemic sclerosis: Associations with genetic, serologic, sociodemographic, and behavioral factors," *Arthritis Care & Research*, vol. 57, no. 2, 2007, ISSN: 1529-0131.

[24] *Deepa*, R. P. Rachel, P. Ramchandran, U. Devaraj, S. A. Arnold, V. Shobha, and G. D'souza, "Pulmonary involvement in systemic sclerosis: A clinical profile," *Lung India : Official Organ of Indian Chest Society*, vol. 33, no. 2, 2016, ISSN: 0970-2113.

[25] P. Faverio, F. De Giacomi, L. Sardella, G. Fiorentino, M. Carone, F. Salerno, J. Ora, P. Rogliani, G. Pellegrino, G. F. Sferrazza Papa, F. Bini, B. D. Bodini, G. Messinesi, A. Pesci, and A. Esquinas, "Management of acute respiratory failure in interstitial lung diseases: Overview and clinical insights," *BMC Pulmonary Medicine*, vol. 18, no. 1, May 2018, ISSN: 1471-2466.

[26] L. Gao, J. Skinner, T. Nath, Q. Lin, M. Griffiths, R. L. Damico, M. W. Pauciulo, W. C. Nichols, P. M. Hassoun, A. D. Everett, and R. A. Johns, "Resistin predicts disease severity and survival in patients with pulmonary arterial hypertension," *Respiratory Research*, vol. 25, no. 1, Jun. 2024, ISSN: 1465-993X.

[27] G. E. Tzelepis, N. L. Kelekis, S. C. Plastiras, P. Mitseas, N. Economopoulos, C. Kampolis, E. J. Gialafos, I. Moyssakis, and H. M. Moutsopoulos, "Pattern and distribution of myocardial fibrosis in systemic sclerosis: A delayed enhanced magnetic resonance imaging study," *Arthritis & Rheumatism*, vol. 56, no. 11, 2007, ISSN: 1529-0131.

[28] S. Bosello, G. De Luca, G. Berardi, G. Canestrari, C. de Waure, F. A. Gabrielli, C. Di Mario, F. Forni, E. Gremese, and G. Ferraccioli, "Cardiac troponin T and NT-proBNP as diagnostic and prognostic biomarkers of primary cardiac involvement and disease severity in systemic sclerosis: A prospective study," *European Journal of Internal Medicine*, vol. 60, Feb. 2019, ISSN: 1879-0828.

[29] K. A. L. Mueller, I. I. Mueller, D. Eppler, C. S. Zuern, P. Seizer, U. Kramer, I. Koetter, M. Roecken, R. Kandolf, M. Gawaz, T. Geisler, J. C. Henes, and K. Klingel, "Clinical and histopathological features of patients with systemic sclerosis undergoing endomyocardial biopsy," *PloS One*, vol. 10, no. 5, 2015, ISSN: 1932-6203.

[30] L. Mouthon, G. Bussone, A. Berezné, L.-H. Noël, and L. Guillevin, "Scleroderma Renal Crisis," *The Journal of Rheumatology*, vol. 41, no. 6, Jun. 2014, ISSN: 0315-162X, 1499-2752.

[31] C. Foocharoen, P. Tonsawan, P. Pongkulkiat, S. Anutrakulchai, A. Mahakkanukrauh, and S. Suwannaroj, "Management review of scleroderma renal crisis: An update with practical pointers," *Modern Rheumatology*, vol. 33, no. 1, Jan. 2023, ISSN: 1439-7595.

[32] L. Bütikofer, P. A. Varisco, O. Distler, O. Kowal-Bielecka, Y. Allanore, G. Riemekasten, P. M. Villiger, and S. Adler, "ACE inhibitors in SSc patients display a risk factor for scleroderma renal crisis—a EUSTAR analysis," *Arthritis Research & Therapy*, vol. 22, 2020, ISSN: 1478-6354.

[33] J. L. Tandaipan and I. Castellví, "Systemic sclerosis and gastrointestinal involvement," *Revista Colombiana de Reumatología (English Edition)*, vol. 27, Apr. 2020, ISSN: 2444-4405.

[34] M. Abu-Shakra, F. Guillemin, and P. Lee, "Gastrointestinal manifestations of systemic sclerosis," *Seminars in Arthritis and Rheumatism*, vol. 24, no. 1, Aug. 1994, ISSN: 0049-0172.

[35] Z. H. McMahan, S. Kulkarni, J. Chen, J. Z. Chen, R. J. Xavier, P. J. Pasricha, and D. Khanna, "Systemic sclerosis gastrointestinal dysmotility: Risk factors, pathophysiology, diagnosis and management," *Nature Reviews Rheumatology*, vol. 19, no. 3, Mar. 2023, ISSN: 1759-4804.

[36] Z. H. McMahan and L. K. Hummers, "Gastrointestinal involvement in systemic sclerosis: Diagnosis and management," *Current Opinion in Rheumatology*, vol. 30, no. 6, Nov. 2018, ISSN: 1531-6963.

[37] J. Avouac *et al.*, "Characteristics of joint involvement and relationships with systemic inflammation in systemic sclerosis: Results from the EULAR Scleroderma Trial and Research Group (EUSTAR) database," *The Journal of Rheumatology*, vol. 37, no. 7, Jul. 2010, ISSN: 1499-2752.

[38] P. J. Clements, Y. Allanore, D. Khanna, M. Singh, and D. E. Furst, "Arthritis in systemic sclerosis: Systematic review of the literature and suggestions for the performance of future clinical trials in systemic sclerosis arthritis," *Seminars in Arthritis and Rheumatism*, vol. 41, no. 6, Jun. 2012, ISSN: 1532-866X.

[39] K. B. Morrisroe, M. Nikpour, and S. M. Proudman, "Musculoskeletal Manifestations of Systemic Sclerosis," *Rheumatic Disease Clinics*, vol. 41, no. 3, Aug. 2015, ISSN: 0889-857X, 1558-3163.

[40] M. Cutolo, S. Soldano, and V. Smith, "Pathophysiology of systemic sclerosis: Current understanding and new insights," *Expert Review of Clinical Immunology*, vol. 15, no. 7, Jul. 2019, ISSN: 1744-8409.

[41] G. Riemekasten and J. H. Distler, "A broad look into the future of systemic sclerosis," *Therapeutic Advances in Musculoskeletal Disease*, vol. 14, Aug. 2022, ISSN: 1759-720X.

[42] L. A. Aguila, H. C. da Silva, A. C. Medeiros-Ribeiro, B. G. Bunjes, A. P. Luppino-Assad, and P. D. Sampaio-Barros, "Is exposure to environmental factors associated with a characteristic clinical and laboratory profile in systemic sclerosis? A retrospective analysis," *Rheumatology International*, vol. 41, no. 6, Jun. 2021, ISSN: 1437-160X.

[43] J. Ko, M. Noviani, V. R. Chellamuthu, S. Albani, and A. H. L. Low, "The Pathogenesis of Systemic Sclerosis: The Origin of Fibrosis and Interlink with Vasculopathy and Autoimmunity," *International Journal of Molecular Sciences*, vol. 24, no. 18, Sep. 2023, ISSN: 1422-0067.

[44] A. J. Freemont, J. Hoyland, P. Fielding, N. Hodson, and M. I. V. Jayson, "Studies of the microvascular endothelium in uninvolved skin of patients with systemic sclerosis: Direct evidence for a generalized microangiopathy," *British Journal of Dermatology*, vol. 126, no. 6, Jun. 1992, ISSN: 0007-0963.

[45] D. J. Abraham, T. Krieg, J. Distler, and O. Distler, "Overview of pathogenesis of systemic sclerosis," *Rheumatology*, vol. 48, no. suppl_3, Jun. 2009, ISSN: 1462-0324.

[46] D. C. Zanin-Silva, M. Santana-Gonçalves, M. Y. Kawashima-Vasconcelos, and M. C. Oliveira, "Management of Endothelial Dysfunction in Systemic Sclerosis: Current and Developing Strategies," *Frontiers in Medicine*, vol. 8, Dec. 2021, ISSN: 2296-858X.

[47] S. Wedgwood, D. M. McMullan, J. M. Bekker, J. R. Fineman, and S. M. Black, "Role for endothelin-1-induced superoxide and peroxynitrite production in rebound pulmonary hypertension associated with inhaled nitric oxide therapy," *Circulation Research*, vol. 89, no. 4, Aug. 2001, ISSN: 1524-4571.

[48] O. Cabral-Marques *et al.*, "GPCR-specific autoantibody signatures are associated with physiological and pathological immune homeostasis," *Nature Communications*, vol. 9, no. 1, Dec. 2018, ISSN: 2041-1723.

[49] A. E. Abdulle, G. F. H. Diercks, M. Feelisch, D. J. Mulder, and H. van Goor, "The Role of Oxidative Stress in the Development of Systemic Sclerosis Related Vasculopathy," *Frontiers in Physiology*, vol. 9, Aug. 2018, ISSN: 1664-042X.

[50] A. Yoshizaki, K. Yanaba, Y. Iwata, K. Komura, A. Ogawa, Y. Akiyama, E. Muroi, T. Hara, F. Ogawa, M. Takenaka, K. Shimizu, M. Hasegawa, M. Fujimoto, T. F. Tedder, and S. Sato, "Cell adhesion molecules regulate fibrotic process via Th1/Th2/Th17 cell balance in a bleomycin-induced scleroderma model," *Journal of Immunology (Baltimore, Md.: 1950)*, vol. 185, no. 4, Aug. 2010, ISSN: 1550-6606.

[51] T. Taniguchi, Y. Asano, K. Akamata, S. Noda, T. Takahashi, Y. Ichimura, T. Toyama, M. Trojanowska, and S. Sato, "Fibrosis, vascular activation, and immune abnormalities resembling systemic sclerosis in bleomycin-treated Fli-1-haploinsufficient mice," *Arthritis & Rheumatology (Hoboken, N.J.)*, vol. 67, no. 2, Feb. 2015, ISSN: 2326-5205.

[52] Y. Asano, "The Pathogenesis of Systemic Sclerosis: An Understanding Based on a Common Pathologic Cascade across Multiple Organs and Additional Organ-Specific Pathologies," *Journal of Clinical Medicine*, vol. 9, no. 9, Sep. 2020, ISSN: 2077-0383.

[53] F. Barde, R. Lorenzon, E. Vicaut, S. Rivière, P. Cacoub, C. Cacciatore, M. Rosenzwajg, A. Daguenel-Nguyen, O. Fain, D. Klatzmann, and A. Mekinian, "Induction of regulatory T cells and efficacy of low-dose interleukin-2 in systemic sclerosis: Interventional open-label phase 1–phase 2a study," *RMD Open*, vol. 10, no. 2, Apr. 2024, ISSN: 2056-5933.

[54] C. Kayser and M. J. Fritzler, "Autoantibodies in Systemic Sclerosis: Unanswered Questions," *Frontiers in Immunology*, vol. 6, Apr. 2015, ISSN: 1664-3224.

[55] H. Graßhoff, K. Fourlakis, S. Comdühr, and G. Riemekasten, "Autoantibodies as Biomarker and Therapeutic Target in Systemic Sclerosis," *Biomedicines*, vol. 10, no. 9, Sep. 2022, ISSN: 2227-9059.

[56] A. Kill, C. Tabeling, R. Undeutsch, A. A. Kühl, J. Günther, M. Radic, M. O. Becker, H. Heidecke, M. Worm, M. Witzenrath, G.-R. Burmester, D. Dragun, and G. Riemekasten, "Autoantibodies to angiotensin and endothelin receptors in systemic sclerosis induce cellular and systemic events associated with disease pathogenesis," *Arthritis Research & Therapy*, vol. 16, no. 1, 2014, ISSN: 1478-6354.

[57] E. C. LeRoy, "Increased collagen synthesis by scleroderma skin fibroblasts in vitro: A possible defect in the regulation or activation of the scleroderma fibroblast," *Journal of Clinical Investigation*, vol. 54, no. 4, Oct. 1974, ISSN: 0021-9738.

[58] Y. Shima, "Cytokines Involved in the Pathogenesis of SSc and Problems in the Development of Anti-Cytokine Therapy," *Cells*, vol. 10, no. 5, May 2021, ISSN: 2073-4409.

[59] S. Piera-Velazquez and S. A. Jimenez, "Endothelial to Mesenchymal Transition: Role in Physiology and in the Pathogenesis of Human Diseases," *Physiological Reviews*, vol. 99, no. 2, Apr. 2019, ISSN: 0031-9333.

[60] Z. Yin, L. D. Carbone, M. Gotoh, A. Postlethwaite, A. L. Bolen, G. J. Tigyi, K. Murakami-Murofushi, and M. A. Watsky, "Lysophosphatidic acid-activated Cl- current activity in human systemic sclerosis skin fibroblasts," *Rheumatology (Oxford, England)*, vol. 49, no. 12, Dec. 2010, ISSN: 1462-0324.

[61] D. Fang, B. Chen, A. Lescoat, D. Khanna, and R. Mu, "Immune cell dysregulation as a mediator of fibrosis in systemic sclerosis," *Nature Reviews Rheumatology*, vol. 18, no. 12, Dec. 2022, ISSN: 1759-4804.

[62] W. Jin, Y. Zheng, and P. Zhu, "T cell abnormalities in systemic sclerosis," *Autoimmunity Reviews*, vol. 21, no. 11, Nov. 2022, ISSN: 1873-0183.

[63] C. Mo, Z. Zeng, Q. Deng, Y. Ding, and R. Xiao, "Imbalance between T helper 17 and regulatory T cell subsets plays a significant role in the pathogenesis of systemic sclerosis," *Biomedicine & Pharmacotherapy*, vol. 108, Dec. 2018, ISSN: 0753-3322.

[64] N. Dumoitier, B. Chaigne, A. Régent, S. Lofek, M. Mhibik, P. Dorfmüller, B. Terrier, J. London, A. Bérezné, N. Tamas, N. Varin-Blank, and L. Mouthon, "Scleroderma Peripheral B Lymphocytes Secrete Interleukin-6 and Transforming Growth Factor β and Activate Fibroblasts," *Arthritis & Rheumatology (Hoboken, N.J.)*, vol. 69, no. 5, May 2017, ISSN: 2326-5205.

[65] M. Trojanowska, J. Varga, and D. Lagares, "Cellular and Molecular Mechanisms of Fibrosis in Systemic Sclerosis," in *Scleroderma: From Pathogenesis to Comprehensive Management*, Y. Allanore, J. Varga, C. P. Denton, M. Kuwana, L. Chung, and A. A. Shah, Eds., Cham: Springer International Publishing, 2024, ISBN: 978-3-031-40658-4.

[66] R. Akbarzadeh, A. Müller, J. Y. Humrich, and G. Riemekasten, "When natural antibodies become pathogenic: Autoantibodies targeted against G protein-coupled receptors in the pathogenesis of systemic sclerosis," *Frontiers in Immunology*, vol. 14, Jun. 2023.

[67] M. A. Skiba and A. C. Kruse, "Autoantibodies as Endogenous Modulators of GPCR Signaling," *Trends in pharmacological sciences*, vol. 42, no. 3, Mar. 2021, ISSN: 0165-6147.

[68] O. Cabral-Marques and G. Riemekasten, "Functional autoantibodies targeting G protein-coupled receptors in rheumatic diseases," *Nature Reviews Rheumatology*, vol. 13, no. 11, Nov. 2017, ISSN: 1759-4804.

[69] M. O. Becker *et al.*, "Vascular Receptor Autoantibodies in Pulmonary Arterial Hypertension Associated with Systemic Sclerosis," *American Journal of Respiratory and Critical Care Medicine*, vol. 190, no. 7, Oct. 2014, ISSN: 1073-449X.

[70] F. S. Müller *et al.*, "Autoantibodies against the chemokine receptor 3 predict cardiovascular risk," *European Heart Journal*, vol. 44, no. 47, Nov. 2023, ISSN: 0195-668X.

[71] A. Killl, C. Tabeling, A. A. Kühl, J. Günther, M. O. Becker, K. Mattat, H. Heidecke, D. Dragun, G.-R. Burmester, and G. Riemekasten, "Anti-At1r and Anti-Etar Autoantibodies from Patients with SSC and their Agonistic Effects," *Annals of the Rheumatic Diseases*, vol. 73, no. Suppl 2, Jun. 2014, ISSN: 0003-4967, 1468-2060.

[72] J. Avouac, G. Riemekasten, C. Meune, B. Ruiz, A. Kahan, and Y. Allanore, "Autoantibodies against Endothelin 1 Type A Receptor Are Strong Predictors of Digital Ulcers in Systemic Sclerosis," *The Journal of Rheumatology*, vol. 42, no. 10, Oct. 2015, ISSN: 0315-162X, 1499-2752.

[73] D. Nemazee, "Mechanisms of central tolerance for B cells," *Nature reviews. Immunology*, vol. 17, no. 5, May 2017, ISSN: 1474-1733.

[74] K. Elkon and P. Casali, "Nature and functions of autoantibodies," *Nature clinical practice. Rheumatology*, vol. 4, no. 9, Sep. 2008, ISSN: 1745-8382.

[75] G. Bussone, H. Dib, M. C. Tamby, C. Broussard, C. Federici, G. Woimant, L. Camoin, L. Guillevin, and L. Mouthon, "Identification of new autoantibody specificities directed at proteins involved in the transforming growth factor β pathway in patients with systemic sclerosis," *Arthritis Research & Therapy*, vol. 13, no. 3, May 2011, ISSN: 1478-6354.

[76] J. Höppner, C. Tabeling, V. Casteleyn, C. Kedor, W. Windisch, G. R. Burmester, D. Huscher, and E. Siegert, "Comprehensive autoantibody profiles in systemic sclerosis: Clinical cluster analysis," *Frontiers in Immunology*, vol. 13, Jan. 2023, ISSN: 1664-3224.

[77] D. Pattanaik, M. Brown, and A. Postlethwaite, "Vascular involvement in systemic sclerosis (scleroderma)," *Journal of Inflammation Research*, Jul. 2011, ISSN: 1178-7031.

[78] D. Pattanaik, M. Brown, B. C. Postlethwaite, and A. E. Postlethwaite, "Pathogenesis of Systemic Sclerosis," *Frontiers in Immunology*, vol. 6, Jun. 2015, ISSN: 1664-3224.

[79] X. Yue *et al.*, "Induced antibodies directed to the angiotensin receptor type 1 provoke skin and lung inflammation, dermal fibrosis and act species overarching," *Annals of the Rheumatic Diseases*, vol. 81, no. 9, Sep. 2022, ISSN: 0003-4967, 1468-2060.

[80] J. Günther, A. Kill, M. O. Becker, H. Heidecke, J. Rademacher, E. Siegert, M. Radić, G.-R. Burmester, D. Dragun, and G. Riemekasten, "Angiotensin receptor type 1 and endothelin receptor type A on immune cells mediate migration and the expression of IL-8 and CCL18 when stimulated by autoantibodies from systemic sclerosis patients," *Arthritis Research & Therapy*, vol. 16, no. 2, 2014, ISSN: 1478-6354.

[81] D. Ernst, J. Westerbergh, G. Sogkas, A. Jablonka, G. Ahrenstorf, R. E. Schmidt, H. Heidecke, L. Wallentin, G. Riemekasten, and T. Witte, "Lowered anti-beta1 adrenergic receptor antibody concentrations may have prognostic significance in acute coronary syndrome," *Scientific Reports*, vol. 9, no. 1, Oct. 2019, ISSN: 2045-2322.

[82] J. C. Venter, C. M. Fraser, and L. C. Harrison, "Autoantibodies to beta 2-adrenergic receptors: A possible cause of adrenergic hyporesponsiveness in allergic rhinitis and asthma," *Science (New York, N.Y.)*, vol. 207, no. 4437, Mar. 1980, ISSN: 0036-8075.

[83] W. T. Gunning, S. M. Stepkowski, P. M. Kramer, B. L. Karabin, and B. P. Grubb, "Inflammatory Biomarkers in Postural Orthostatic Tachycardia Syndrome with Elevated G-Protein-Coupled Receptor Autoantibodies," *Journal of Clinical Medicine*, vol. 10, no. 4, Feb. 2021, ISSN: 2077-0383.

[84] S. Kumar, J. Singh, R. Kedika, F. Mendoza, S. A. Jimenez, E. S. Blomain, A. J. DiMarino, S. Cohen, and S. Rattan, "Role of muscarinic-3 receptor antibody in systemic sclerosis: Correlation with disease duration and effects of IVIG," *American Journal of Physiology-Gastrointestinal and Liver Physiology*, vol. 310, no. 11, Jun. 2016, ISSN: 0193-1857.

[85] P. Wang, D. Wu, Z. Gong, M. Adu-Gyamfi, J. Kamhieh-Milz, D. L. M. da Fonseca, G. Sürücü, M. I. Ashraf, H. Heidecke, D. Sikorska, O. Cabral-Marques, G. Moll, G. Riemekasten, J. Witowski, and R. Catar, "Stimulation of endothelin-1 production by autoantibodies present in patients with scleroderma renal crisis," *Clinical Immunology*, Feb. 2025, ISSN: 1521-6616.

[86] F. Cevikbas, S. Seeliger, M. Fastrich, H. Hinte, D. Metze, C. Kempkes, B. Homey, and M. Steinhoff, "Role of protease-activated receptors in human skin fibrosis and scleroderma," *Experimental Dermatology*, vol. 20, no. 1, 2011, ISSN: 1600-0625.

[87] Y. Hamaguchi, M. Hasegawa, C. Tanaka, S. Kumada, S. Sato, K. Takehara, and M. Fujimoto, "Elevated serum placenta growth factor (PlGF) levels in patients with systemic sclerosis: A possible role in the development of skin but

not lung fibrosis," *Journal of Dermatological Science*, vol. 58, no. 3, Jun. 2010, ISSN: 0923-1811, 1873-569X.

[88] A. Ocon, S. Lokineni, and B. Korman, "Understanding and Therapeutically Targeting the Scleroderma Myofibroblast," *Current Treatment Options in Rheumatology*, vol. 8, no. 1, Mar. 2022, ISSN: 2198-6002.

[89] J. D. Fontenot, J. P. Rasmussen, L. M. Williams, J. L. Dooley, A. G. Farr, and A. Y. Rudensky, "Regulatory T Cell Lineage Specification by the Forkhead Transcription Factor Foxp3," *Immunity*, vol. 22, no. 3, Mar. 2005, ISSN: 1074-7613.

[90] J. Ohmes, S. Comdühr, R. Akbarzadeh, G. Riemekasten, and J. Y. Humrich, "Dysregulation and chronicity of pathogenic T cell responses in the pre-diseased stage of lupus," *Frontiers in Immunology*, vol. 13, Oct. 2022.

[91] S. Sakaguchi, "Naturally arising Foxp3-expressing CD25+CD4+ regulatory T cells in immunological tolerance to self and non-self," *Nature Immunology*, vol. 6, no. 4, Apr. 2005, ISSN: 1529-2916.

[92] J. M. Kim, J. P. Rasmussen, and A. Y. Rudensky, "Regulatory T cells prevent catastrophic autoimmunity throughout the lifespan of mice," *Nature Immunology*, vol. 8, no. 2, Feb. 2007, ISSN: 1529-2916.

[93] S. Sakaguchi, N. Sakaguchi, M. Asano, M. Itoh, and M. Toda, "Immunologic self-tolerance maintained by activated T cells expressing IL-2 receptor alpha-chains (CD25). Breakdown of a single mechanism of self-tolerance causes various autoimmune diseases.," *The Journal of Immunology*, vol. 155, no. 3, Aug. 1995, ISSN: 0022-1767.

[94] B.-I. Moon, T. H. Kim, and J.-Y. Seoh, "Functional Modulation of Regulatory T Cells by IL-2," *PLOS ONE*, vol. 10, no. 11, Nov. 2015, ISSN: 1932-6203.

[95] C. A. Piccirillo and E. M. Shevach, "Naturally-occurring CD4+CD25+ immunoregulatory T cells: Central players in the arena of peripheral tolerance," *Seminars in Immunology*, Regulatory T Cells, vol. 16, no. 2, Apr. 2004, ISSN: 1044-5323.

[96] A. Schmidt, N. Oberle, and P. H. Krammer, "Molecular Mechanisms of Treg-Mediated T Cell Suppression," *Frontiers in Immunology*, vol. 3, Mar. 2012, ISSN: 1664-3224.

[97] O. Goldmann, O. V. Nwofor, Q. Chen, and E. Medina, "Mechanisms underlying immunosuppression by regulatory cells," *Frontiers in Immunology*, vol. 15, Feb. 2024, ISSN: 1664-3224.

[98] D. M. Sansom and L. S. K. Walker, "The role of CD28 and cytotoxic T-lymphocyte antigen-4 (CTLA-4) in regulatory T-cell biology," *Immunological Reviews*, vol. 212, Aug. 2006, ISSN: 0105-2896.

[99] S. Deaglio, K. M. Dwyer, W. Gao, D. Friedman, A. Usheva, A. Erat, J.-F. Chen, K. Enjyoji, J. Linden, M. Oukka, V. K. Kuchroo, T. B. Strom, and S. C. Robson, "Adenosine generation catalyzed by CD39 and CD73 expressed on regulatory T cells mediates immune suppression," *Journal of Experimental Medicine*, vol. 204, no. 6, May 2007, ISSN: 0022-1007.

[100] J. Y. Humrich, H. Morbach, R. Undeutsch, P. Enghard, S. Rosenberger, O. Weigert, L. Kloke, J. Heimann, T. Gaber, S. Brandenburg, A. Scheffold, J. Huehn, A. Radbruch, G.-R. Burmester, and G. Riemekasten, "Homeostatic imbalance of regulatory and effector T cells due to IL-2 deprivation amplifies murine lupus," *Proceedings of the National Academy of Sciences*, vol. 107, no. 1, Jan. 2010.

[101] A. Farooq, S. Trehan, G. Singh, N. Arora, T. Mehta, P. Jain, G. Bector, A. Jain, R. S. Arora, and P. Puri, "A Comprehensive Review of Low-Dose Interleukin-2 (IL-2) Therapy for Systemic Lupus Erythematosus: Mechanisms, Efficacy, and Clinical Applications," *Cureus*, vol. 16, no. 9, ISSN: 2168-8184.

[102] C. von Spee-Mayer, E. Siegert, D. Abdirama, A. Rose, A. Klaus, T. Alexander, P. Enghard, B. Sawitzki, F. Hiepe, A. Radbruch, G.-R. Burmester, G. Riemekasten, and J. Y. Humrich, "Low-dose interleukin-2 selectively corrects regulatory T cell defects in patients with systemic lupus erythematosus," *Annals of the Rheumatic Diseases*, vol. 75, no. 7, Jul. 2016, ISSN: 0003-4967.

[103] J. Y. Humrich, P. Cacoub, M. Rosenzwajg, F. Pitoiset, H. P. Pham, J. Guidoux, D. Leroux, T. Vazquez, G. Riemekasten, J. S. Smolen, G. Tsokos, and D. Klatzmann, "Low-dose interleukin-2 therapy in active systemic lupus erythematosus (LUPIL-2): A multicentre, double-blind, randomised and placebo-controlled phase II trial," *Annals of the Rheumatic Diseases*, vol. 81, no. 12, Dec. 2022, ISSN: 1468-2060.

[104] J. Y. Humrich, C. Von Spee-Mayer, E. Siegert, M. Bertolo, A. Rose, D. Abdirama, P. Enghard, B. Stuhlmüller, B. Sawitzki, D. Huscher, F. Hiepe, T. Alexander, E. Feist, A. Radbruch, G.-R. Burmester, and G. Riemekasten, "Low-dose interleukin-2 therapy in refractory systemic lupus erythematosus: An investigator-initiated, single-centre phase 1 and 2a clinical trial," *The Lancet Rheumatology*, vol. 1, no. 1, Sep. 2019, ISSN: 26659913.

[105] C. Frantz, C. Auffray, J. Avouac, and Y. Allanore, "Regulatory T Cells in Systemic Sclerosis," *Frontiers in Immunology*, vol. 9, Oct. 2018, ISSN: 1664-3224.

[106] L. Banica, A. Besliu, G. Pistol, C. Stavaru, R. Ionescu, A.-M. Forsea, C. Tanaseanu, S. Dumitrache, D. Otelea, I. Tamsulea, S. Tanaseanu, C. Chitonu, S. Paraschiv, M. Balteanu, M. Stefanescu, and C. Matache, "Quantification and molecular characterization of regulatory T cells in connective tissue diseases," *Autoimmunity*, vol. 42, no. 1, Jan. 2009, ISSN: 1607-842X.

[107] S. Kobayashi, Y. Nagafuchi, H. Shoda, and K. Fujio, "The Pathophysiological Roles of Regulatory T Cells in the Early Phase of Systemic Sclerosis," *Frontiers in Immunology*, vol. 13, May 2022, ISSN: 1664-3224.

[108] X. Zhu and J. Zhu, "CD4 T Helper Cell Subsets and Related Human Immunological Disorders," *International Journal of Molecular Sciences*, vol. 21, no. 21, Oct. 2020, ISSN: 1422-0067.

[109] R. V. Luckheeram, R. Zhou, A. D. Verma, and B. Xia, "CD4+T Cells: Differentiation and Functions," *Clinical and Developmental Immunology*, vol. 2012, 2012, ISSN: 1740-2522.

[110] J. Zhu, H. Yamane, and W. E. Paul, "Differentiation of Effector CD4 T Cell Populations," *Annual review of immunology*, vol. 28, 2010, ISSN: 0732-0582.

[111] N. Gagliani and S. Huber, "Basic Aspects of T Helper Cell Differentiation," *Methods in Molecular Biology (Clifton, N.J.)*, vol. 1514, 2017, ISSN: 1940-6029.

[112] S. J. Szabo, S. T. Kim, G. L. Costa, X. Zhang, C. G. Fathman, and L. H. Glimcher, "A Novel Transcription Factor, T-bet, Directs Th1 Lineage Commitment," *Cell*, vol. 100, no. 6, Mar. 2000, ISSN: 0092-8674, 1097-4172.

[113] P. Bălănescu, A. Lădaru, E. Bălănescu, A. Nicolau, C. Băicuş, and G. A. Dan, "IL-17, IL-6 and IFN-γ in systemic sclerosis patients," *Romanian Journal of Internal Medicine*, vol. 53, no. 1, Oct. 2015.

[114] T. Matsushita, M. Hasegawa, Y. Hamaguchi, K. Takehara, and S. Sato, "Longitudinal analysis of serum cytokine concentrations in systemic sclerosis: Association of interleukin 12 elevation with spontaneous regression of skin sclerosis," *The Journal of Rheumatology*, vol. 33, no. 2, Feb. 2006, ISSN: 0315-162X.

[115] M. Larché, D. S. Robinson, and A. B. Kay, "The role of T lymphocytes in the pathogenesis of asthma," *Journal of Allergy and Clinical Immunology*, vol. 111, no. 3, Mar. 2003, ISSN: 0091-6749.

[116] B. Bosnjak, B. Stelzmueller, K. J. Erb, and M. M. Epstein, "Treatment of allergic asthma: Modulation of Th2 cells and their responses," *Respiratory Research*, vol. 12, no. 1, Dec. 2011, ISSN: 1465-993X.

[117] J. A. Walker and A. N. J. McKenzie, "TH2 cell development and function," *Nature Reviews Immunology*, vol. 18, no. 2, Feb. 2018, ISSN: 1474-1733, 1474-1741.

[118] J. Zhu, H. Yamane, J. Cote-Sierra, L. Guo, and W. E. Paul, "GATA-3 promotes Th2 responses through three different mechanisms: Induction of Th2 cytokine production, selective growth of Th2 cells and inhibition of Th1 cell-specific factors," *Cell Research*, vol. 16, no. 1, Jan. 2006, ISSN: 1748-7838.

[119] L. I. Sakkas and D. P. Bogdanos, "The Role of T Cells in Systemic Sclerosis: An Update," *Immuno*, vol. 2, no. 3, Sep. 2022, ISSN: 2673-5601.

[120] T. A. Wynn, "Fibrotic disease and the Th1/Th2 paradigm," *Nature reviews. Immunology*, vol. 4, no. 8, Aug. 2004, ISSN: 1474-1733.

[121] J. Varga and D. Abraham, "Systemic sclerosis: A prototypic multisystem fibrotic disorder," *The Journal of Clinical Investigation*, vol. 117, no. 3, Mar. 2007, ISSN: 0021-9738.

[122] A. Wangoo, T. Sparer, I. N. Brown, V. A. Snewin, R. Janssen, J. Thole, H. T. Cook, R. J. Shaw, and D. B. Young, "Contribution of Th1 and Th2 cells to protection and pathology in experimental models of granulomatous lung disease," *Journal of Immunology (Baltimore, Md.: 1950)*, vol. 166, no. 5, Mar. 2001, ISSN: 0022-1767.

[123] R. J. Noelle and E. C. Nowak, "Cellular sources and immune functions of interleukin-9," *Nature Reviews Immunology*, vol. 10, no. 10, Oct. 2010, ISSN: 1474-1741.

[124] M. H. Kaplan, M. M. Hufford, and M. R. Olson, "The Development and in vivo function of TH9 cells," *Nature reviews. Immunology*, vol. 15, no. 5, May 2015, ISSN: 1474-1733.

[125] G. Guggino, M. L. Pizzo, D. D. Liberto, A. Rizzo, P. Cipriani, P. Ruscitti, G. Candore, C. M. Gambino, G. Sireci, F. Dieli, R. Giacomelli, G. Triolo, and F. Ciccia, "Interleukin-9 over-expression and T helper 9 polarization in systemic sclerosis patients," *Clinical and Experimental Immunology*, vol. 190, no. 2, Aug. 2017.

[126] X. Chi, W. Jin, X. Zhao, T. Xie, J. Shao, X. Bai, Y. Jiang, X. Wang, and C. Dong, "RORγt expression in mature TH17 cells safeguards their lineage specification by inhibiting conversion to TH2 cells," *Science Advances*, vol. 8, no. 34, Aug. 2022, ISSN: 2375-2548.

[127] G. Castro, X. Liu, K. Ngo, A. D. Leon-Tabaldo, S. Zhao, R. Luna-Roman, J. Yu, T. Cao, R. Kuhn, P. Wilkinson, K. Herman, M. I. Nelen, J. Blevitt, X. Xue, A. Fourie, and W.-P. Fung-Leung, "RORγt and RORα signature genes in human Th17 cells," *PLOS ONE*, vol. 12, no. 8, Aug. 2017, ISSN: 1932-6203.

[128] S. N. Harbour, D. F. DiToro, S. J. Witte, C. L. Zindl, M. Gao, T. R. Schoeb, G. W. Jones, S. A. Jones, R. D. Hatton, and C. T. Weaver, "Th17 Cells Require Ongoing Classic IL-6 Receptor Signaling to Retain Transcriptional and Functional Identity," *Science immunology*, vol. 5, no. 49, Jul. 2020, ISSN: 2470-9468.

[129] A. Gabsi, X. Heim, A. Dlala, A. Gati, H. Sakhri, A. Abidi, S. Amri, B. Neili, A. S. Leroyer, A. Bertaud, M. Smiti Khanfir, F. Said, M. H. Houman, B. Granel, M. Blot-Chabaud, N. Bardin, and R. Marrakchi, "TH17 cells expressing CD146 are significantly increased in patients with Systemic sclerosis," *Scientific Reports*, vol. 9, Nov. 2019, ISSN: 2045-2322.

[130] X. Yang, J. Yang, X. Xing, L. Wan, and M. Li, "Increased frequency of Th17 cells in systemic sclerosis is related to disease activity and collagen overproduction," *Arthritis Research & Therapy*, vol. 16, no. 1, Jan. 2014, ISSN: 1478-6362.

[131] X. Xing, A. Li, H. Tan, and Y. Zhou, "IFN-γ+IL-17+Th17 cells regulate fibrosis through secreting IL-21 in systemic scleroderma," *Journal of Cellular and Molecular Medicine*, vol. 24, no. 23, Dec. 2020, ISSN: 1582-1838.

[132] L. Lei, C. Zhao, F. Qin, Z.-Y. He, X. Wang, and X.-N. Zhong, "Th17 cells and IL-17 promote the skin and lung inflammation and fibrosis process in a bleomycin-induced murine model of systemic sclerosis," *Clinical and Experimental Rheumatology*, vol. 34 Suppl 100, no. 5, 2016, ISSN: 0392-856X.

[133] J. Choi and S. Crotty, "Bcl6-Mediated Transcriptional Regulation of Follicular Helper T cells (TFH)," *Trends in immunology*, vol. 42, no. 4, Apr. 2021, ISSN: 1471-4906.

[134] S. G. Tangye, C. S. Ma, R. Brink, and E. K. Deenick, "The good, the bad and the ugly - TFH cells in human health and disease," *Nature Reviews. Immunology*, vol. 13, no. 6, Jun. 2013, ISSN: 1474-1741.

[135] J. Qi, C. Liu, Z. Bai, X. Li, and G. Yao, "T follicular helper cells and T follicular regulatory cells in autoimmune diseases," *Frontiers in Immunology*, vol. 14, Apr. 2023, ISSN: 1664-3224.

[136] J. Choi, H. Diao, C. E. Faliti, J. Truong, M. Rossi, S. Bélanger, B. Yu, A. W. Goldrath, M. E. Pipkin, and S. Crotty, "Bcl-6 is the nexus transcription factor of T follicular helper cells (TFH) via repressor-of-repressor circuits," *Nature immunology*, vol. 21, no. 7, Jul. 2020, ISSN: 1529-2908.

[137] M. Sahinoglu, G. Sargin, I. Yavasoglu, and T. Senturk, "The relationship between peripheral T follicular helper cells and disease severity in systemic sclerosis," *Clinical and Experimental Medicine*, vol. 24, no. 1, 2024, ISSN: 1591-8890.

[138] V. S. Wacleche, R. Wang, and D. A. Rao, "Identification of T Peripheral Helper (Tph) Cells," *Methods in Molecular Biology (Clifton, N.J.)*, vol. 2380, 2022, ISSN: 1940-6029.

[139] Y. Huang, X. Ba, L. Han, H. Wang, W. Lin, Z. Chen, and S. Tu, "T peripheral helper cells in autoimmune diseases: What do we know?" *Frontiers in Immunology*, vol. 14, Apr. 2023, ISSN: 1664-3224.

[140] T. I. Papadimitriou, J. M. J. Lemmers, A. P. M. van Caam, J. L. Vos, E. L. Vitters, L. Stinissen, S. I. van Leuven, M. I. Koenders, P. M. van der Kraan, H. J. P. M. Koenen, R. L. Smeets, R. Nijveldt, M. C. Vonk, and R. M. Thurlings, "Systemic sclerosis-associated pulmonary arterial hypertension is characterized by a distinct peripheral T helper cell profile," *Rheumatology (Oxford, England)*, vol. 63, no. 9, Mar. 2024, ISSN: 1462-0324.

[141] A. Lanzavecchia and F. Sallusto, "Dynamics of T lymphocyte responses: Intermediates, effectors, and memory cells," *Science (New York, N.Y.)*, vol. 290, no. 5489, Oct. 2000, ISSN: 0036-8075.

[142] F. Sallusto, J. Geginat, and A. Lanzavecchia, "Central Memory and Effector Memory T Cell Subsets: Function, Generation, and Maintenance," *Annual Review of Immunology*, vol. 22, no. 1, Apr. 2004, ISSN: 0732-0582, 1545-3278.

[143] J. I. Gray, L. M. Westerhof, and M. K. L. MacLeod, "The roles of resident, central and effector memory CD4 T-cells in protective immunity following infection or vaccination," *Immunology*, vol. 154, no. 4, 2018, ISSN: 1365-2567.

[144] G. Almanzar, M. Schmalzing, M. Klein, D. Hilligardt, P. Morris, K. Höfner, N. El Hajj, H. Kneitz, V. Wild, A. Rosenwald, S. Benoit, H. Hamm, H.-P. Tony, T. Haaf, M. Goebeler, and M. Prelog, "Memory CD4+ T cells lacking expression of CCR7 promote pro-inflammatory cytokine production in patients

with diffuse cutaneous systemic sclerosis," *European Journal of Dermatology*, vol. 29, no. 5, Sep. 2019, ISSN: 1952-4013.

[145] M. Hasegawa and S. Sato, "The roles of chemokines in leukocyte recruitment and fibrosis in systemic sclerosis," *Frontiers in Bioscience-Landmark*, vol. 13, no. 10, May 2008, ISSN: 2768-6701.

[146] J. D. Brandstadter and Y. Yang, "Natural killer cell responses to viral infection," *Journal of Innate Immunity*, vol. 3, no. 3, 2011, ISSN: 1662-8128.

[147] T. Michel, A. Poli, A. Cuapio, B. Briquemont, G. Iserentant, M. Ollert, and J. Zimmer, "Human CD56bright NK Cells: An Update," *Journal of Immunology (Baltimore, Md.: 1950)*, vol. 196, no. 7, Apr. 2016, ISSN: 1550-6606.

[148] R. Jacobs, G. Hintzen, A. Kemper, K. Beul, S. Kempf, G. Behrens, K. W. Sykora, and R. E. Schmidt, "CD56bright cells differ in their KIR repertoire and cytotoxic features from CD56dim NK cells," *European Journal of Immunology*, vol. 31, no. 10, Oct. 2001, ISSN: 0014-2980.

[149] M. A. Cooper, T. A. Fehniger, and M. A. Caligiuri, "The biology of human natural killer-cell subsets," *Trends in Immunology*, vol. 22, no. 11, Nov. 2001, ISSN: 1471-4906.

[150] A. Poli, T. Michel, M. Thérésine, E. Andrès, F. Hentges, and J. Zimmer, "CD56bright natural killer (NK) cells: An important NK cell subset," *Immunology*, vol. 126, no. 4, Apr. 2009, ISSN: 1365-2567.

[151] S. L. McQuaid, S. T. Loughran, P. A. Power, P. Maguire, A. Szczygiel, and P. A. Johnson, "Low-dose IL-2 induces CD56bright NK regulation of T cells via NKp44 and NKp46," *Clinical and Experimental Immunology*, vol. 200, no. 3, Jun. 2020, ISSN: 1365-2249.

[152] R. Guo, L. Mi, J. Gao, Y. Yang, M. Zhao, X. He, Y. Ji, Y. Hu, Y. Gao, and K. Xu, "Natural killer cells are decreased in systemic sclerosis and have diagnostic value for pulmonary arterial hypertension incorporation," *Scientific Reports*, vol. 15, no. 1, Feb. 2025, ISSN: 2045-2322.

[153] M. Horikawa, M. Hasegawa, K. Komura, I. Hayakawa, K. Yanaba, T. Matsushita, K. Takehara, and S. Sato, "Abnormal natural killer cell function in systemic sclerosis: Altered cytokine production and defective killing activity," *The Journal of Investigative Dermatology*, vol. 125, no. 4, Oct. 2005, ISSN: 0022-202X.

[154] V. Riccieri, G. Parisi, A. Spadaro, R. Scrivo, F. Barone, T. Moretti, G. Bernardini, R. Strom, E. Taccari, and G. Valesini, "Reduced circulating natural killer T cells and gamma/delta T cells in patients with systemic sclerosis," *The Journal of Rheumatology*, vol. 32, no. 2, Feb. 2005, ISSN: 0315-162X.

[155] C. F. Beesley, N. R. Goldman, T. E. Taher, C. P. Denton, D. J. Abraham, R. A. Mageed, and V. H. Ong, "Dysregulated B cell function and disease pathogenesis in systemic sclerosis," *Frontiers in Immunology*, vol. 13, Jan. 2023, ISSN: 1664-3224.

[156] T. Fetter, D. Niebel, C. Braegelmann, and J. Wenzel, "Skin-Associated B Cells in the Pathogenesis of Cutaneous Autoimmune Diseases—Implications for Therapeutic Approaches," *Cells*, vol. 9, no. 12, Dec. 2020, ISSN: 2073-4409.

[157] C. Scaletti, S. Pratesi, S. Bellando Randone, L. Di Pietro, C. Campochiaro, F. Annunziato, and M. Matucci Cerinic, "The B-cells paradigm in systemic sclerosis: An update on pathophysiology and B-cell-targeted therapies," *Clinical and Experimental Immunology*, vol. 219, no. 1, Jan. 2025, ISSN: 1365-2249.

[158] Y. Zhou, Y. Zhang, J. Han, M. Yang, J. Zhu, and T. Jin, "Transitional B cells involved in autoimmunity and their impact on neuroimmunological diseases," *Journal of Translational Medicine*, vol. 18, Mar. 2020, ISSN: 1479-5876.

[159] S. Yurasov, H. Wardemann, J. Hammersen, M. Tsuiji, E. Meffre, V. Pascual, and M. C. Nussenzweig, "Defective B cell tolerance checkpoints in systemic lupus erythematosus," *The Journal of Experimental Medicine*, vol. 201, no. 5, Mar. 2005, ISSN: 0022-1007.

[160] H. Wardemann, S. Yurasov, A. Schaefer, J. W. Young, E. Meffre, and M. C. Nussenzweig, "Predominant Autoantibody Production by Early Human B Cell Precursors," *Science*, vol. 301, no. 5638, Sep. 2003.

[161] M. Z. Syeda, T. Hong, C. Huang, W. Huang, and Q. Mu, "B cell memory: From generation to reactivation: A multipronged defense wall against pathogens," *Cell Death Discovery*, vol. 10, no. 1, Mar. 2024, ISSN: 2058-7716.

[162] P. D. Pioli, "Plasma Cells, the Next Generation: Beyond Antibody Secretion," *Frontiers in Immunology*, vol. 10, Nov. 2019, ISSN: 1664-3224.

[163] L. Khodadadi, Q. Cheng, A. Radbruch, and F. Hiepe, "The Maintenance of Memory Plasma Cells," *Frontiers in Immunology*, vol. 10, Apr. 2019, ISSN: 1664-3224.

[164] N. Robillard, S. Wuillème, P. Moreau, and M. C. Bene, "Immunophenotype of Normal and Myelomatous Plasma-Cell Subsets," *Frontiers in Immunology*, vol. 5, Mar. 2014, ISSN: 1664-3224.

[165] L. Soto, A. Ferrier, O. Aravena, E. Fonseca, J. Berendsen, A. Biere, D. Bueno, V. Ramos, J. C. Aguillón, and D. Catalán, "Systemic Sclerosis Patients Present Alterations in the Expression of Molecules Involved in B-Cell Regulation," *Frontiers in Immunology*, vol. 6, Sep. 2015, ISSN: 1664-3224.

[166] M. De Santis, S. L. Bosello, G. Peluso, M. Pinnelli, S. Alivernini, G. Zizzo, M. Bocci, A. Capacci, G. La Torre, A. Mannocci, G. Pagliari, F. Varone, R. Pistelli, F. M. Danza, and G. Ferraccioli, "Bronchoalveolar lavage fluid and progression of scleroderma interstitial lung disease," *The Clinical Respiratory Journal*, vol. 6, no. 1, Jan. 2012, ISSN: 1752-699X.

[167] L. Guillevin, A. Bérezné, R. Seror, L. Teixeira, J. Pourrat, A. Mahr, E. Hachulla, C. Agard, J. Cabane, P. Vanhille, J.-R. Harle, I. Deleveaux, and L. Mouthon, "Scleroderma renal crisis: A retrospective multicentre study on 91 patients and 427 controls," *Rheumatology (Oxford, England)*, vol. 51, no. 3, Mar. 2012, ISSN: 1462-0332.

[168] C. V. Jakubzick, G. J. Randolph, and P. M. Henson, "Monocyte differentiation and antigen-presenting functions," *Nature Reviews. Immunology*, vol. 17, no. 6, Jun. 2017, ISSN: 1474-1741.

[169] A. M. Zawada, K. S. Rogacev, B. Rotter, P. Winter, R.-R. Marell, D. Fliser, and G. H. Heine, "SuperSAGE evidence for CD14++CD16+ monocytes as a third monocyte subset," *Blood*, vol. 118, no. 12, Sep. 2011, ISSN: 1528-0020.

[170] C. Shi and E. G. Pamer, "Monocyte recruitment during infection and inflammation," *Nature reviews. Immunology*, vol. 11, no. 11, Oct. 2011, ISSN: 1474-1733.

[171] G. Thomas, R. Tacke, C. C. Hedrick, and R. N. Hanna, "Nonclassical patrolling monocyte function in the vasculature," *Arteriosclerosis, Thrombosis, and Vascular Biology*, vol. 35, no. 6, Jun. 2015, ISSN: 1524-4636.

[172] C. Auffray, D. Fogg, M. Garfa, G. Elain, O. Join-Lambert, S. Kayal, S. Sarnacki, A. Cumano, G. Lauvau, and F. Geissmann, "Monitoring of blood vessels and tissues by a population of monocytes with patrolling behavior," *Science (New York, N.Y.)*, vol. 317, no. 5838, Aug. 2007, ISSN: 1095-9203.

[173] J. Cros, N. Cagnard, K. Woollard, N. Patey, S.-Y. Zhang, B. Senechal, A. Puel, S. K. Biswas, D. Moshous, C. Picard, J.-P. Jais, D. D'Cruz, J.-L. Casanova, C. Trouillet, and F. Geissmann, "Human CD14dim monocytes patrol and sense nucleic acids and viruses via TLR7 and TLR8 receptors," *Immunity*, vol. 33, no. 3, Sep. 2010, ISSN: 1097-4180.

[174] M. P. Hayes, J. Wang, and M. A. Norcross, "Regulation of interleukin-12 expression in human monocytes: Selective priming by interferon-gamma of lipopolysaccharide-inducible p35 and p40 genes," *Blood*, vol. 86, no. 2, Jul. 1995, ISSN: 0006-4971.

[175] T. A. Wynn and K. M. Vannella, "Macrophages in Tissue Repair, Regeneration, and Fibrosis," *Immunity*, vol. 44, no. 3, Mar. 2016, ISSN: 1097-4180.

[176] S. K. Mathai, M. Gulati, X. Peng, T. R. Russell, A. C. Shaw, A. N. Rubinowitz, L. A. Murray, J. M. Siner, D. E. Antin-Ozerkis, R. R. Montgomery, R. A. S. Reilkoff, R. J. Bucala, and E. L. Herzog, "Circulating monocytes from systemic sclerosis patients with interstitial lung disease show an enhanced profibrotic phenotype," *Laboratory Investigation; a Journal of Technical Methods and Pathology*, vol. 90, no. 6, Jun. 2010, ISSN: 1530-0307.

[177] N. Binai, S. O'Reilly, B. Griffiths, J. M. van Laar, and T. Hügle, "Differentiation potential of CD14+ monocytes into myofibroblasts in patients with systemic sclerosis," *PloS One*, vol. 7, no. 3, 2012, ISSN: 1932-6203.

[178] J. S. Berkowitz, T. Tabib, H. Xiao, G. M. Sadej, D. Khanna, P. Fuschiotti, R. A. Lafyatis, and J. Das, "Cell Type-Specific Biomarkers of Systemic Sclerosis Disease Severity Capture Cell-Intrinsic and Cell-Extrinsic Circuits," *Arthritis & Rheumatology (Hoboken, N.J.)*, vol. 75, no. 10, Oct. 2023, ISSN: 2326-5205.

[179] G. Villanueva-Martin, M. Acosta-Herrera, E. G. Carmona, M. Kerick, N. Ortego-Centeno, J. L. Callejas-Rubio, N. Mages, S. Klages, S. Börno, B. Timmermann, L. Bossini-Castillo, and J. Martin, "Non-classical circulating monocytes expressing high levels of microsomal prostaglandin E2 synthase-1 tag an aberrant IFN-response in systemic sclerosis," *Journal of Autoimmunity*, vol. 140, Nov. 2023, ISSN: 1095-9157.

[180] A. van Caam, M. Vonk, F. van den Hoogen, P. van Lent, and P. van der Kraan, "Unraveling SSc Pathophysiology; The Myofibroblast," *Frontiers in Immunology*, vol. 9, 2018, ISSN: 1664-3224.

[181] J. E. Pope, C. P. Denton, S. R. Johnson, A. Fernandez-Codina, M. Hudson, and T. Nevskaya, "State-of-the-art evidence in the treatment of systemic sclerosis," *Nature Reviews. Rheumatology*, vol. 19, no. 4, 2023, ISSN: 1759-4790.

[182] K. Komura, K. Yanaba, J.-D. Bouaziz, A. Yoshizaki, M. Hasegawa, J. Varga, K. Takehara, and T. Matsushita, "Perspective to precision medicine in scleroderma," *Frontiers in Immunology*, vol. 14, Jan. 2024, ISSN: 1664-3224.

[183] D. Khanna, A. Lescoat, D. Roofeh, E. J. Bernstein, E. A. Kazerooni, M. D. Roth, F. Martinez, K. R. Flaherty, and C. P. Denton, "Systemic Sclerosis-associated interstitial lung disease," *Arthritis & rheumatology (Hoboken, N.J.)*, vol. 74, no. 1, Jan. 2022, ISSN: 2326-5191.

[184] S. Bellando-Randone and M. Matucci-Cerinic, "Very early systemic sclerosis," *Best Practice & Research Clinical Rheumatology*, How to Investigate: Very Early Inflammatory Rheumatic Diseases, vol. 33, no. 4, Aug. 2019, ISSN: 1521-6942.

[185] M. Vasile, J. Avouac, I. Sciarra, K. Stefanantoni, N. Iannace, E. Cravotto, G. Valesini, Y. Allanore, and V. Riccieri, "From VEDOSS to established systemic sclerosis diagnosis according to ACR/EULAR 2013 classification criteria: A French-Italian capillaroscopic survey," *Clinical and Experimental Rheumatology*, vol. 36 Suppl 113, no. 4, 2018, ISSN: 0392-856X.

[186] E. Blaja, S. Jordan, C.-M. Mihai, R. Dobrota, M. O. Becker, B. Maurer, M. Matucci-Cerinic, and O. Distler, "The Challenge of Very Early Systemic Sclerosis: A Combination of Mild and Early Disease?" *The Journal of Rheumatology*, vol. 48, no. 1, Jan. 2021, ISSN: 1499-2752.

[187] M. Matucci-Cerinic, Y. Allanore, L. Czirják, A. Tyndall, U. Müller-Ladner, C. Denton, G. Valentini, O. Distler, K. Fligelstone, A. Tyrrel-Kennedy, D. Farge, O. Kowal-Bielecka, F. van den Hoogen, M. Cutolo, P. D. Sampaio-Barros, P. Nash, K. Takehara, and D. E. Furst, "The challenge of early systemic sclerosis for the EULAR Scleroderma Trial and Research group (EUSTAR) community. It is time to cut the Gordian knot and develop a prevention or rescue strategy," *Annals of the Rheumatic Diseases*, vol. 68, no. 9, Sep. 2009, ISSN: 0003-4967.

[188] F. van den Hoogen *et al.*, "Classification Criteria for Systemic Sclerosis: An ACR-EULAR Collaborative Initiative," *Arthritis and rheumatism*, vol. 65, no. 11, Nov. 2013, ISSN: 0004-3591.

[189] V. S. Siqueira, M. F. S. Helbingen, A. C. Medeiros-Ribeiro, H. Carriço da Silva, R. Miossi, A. P. Luppino-Assad, and P. D. Sampaio-Barros, "Predictors of progression to systemic sclerosis: Analysis of very early diagnosis of systemic sclerosis in a large single-centre cohort," *Rheumatology (Oxford, England)*, vol. 61, no. 9, Aug. 2022, ISSN: 1462-0332.

[190] C. Bellocchi, A. Chung, and E. R. Volkmann, "Predicting the Progression of Very Early Systemic Sclerosis: Current Insights," *Open Access Rheumatology : Research and Reviews*, vol. 14, Sep. 2022, ISSN: 1179-156X.

[191] S. Bellando-Randone and M. Matucci-Cerinic, "Very Early Systemic Sclerosis and Pre-systemic Sclerosis: Definition, Recognition, Clinical Relevance and Future Directions," *Current Rheumatology Reports*, vol. 19, no. 10, Sep. 2017, ISSN: 1534-6307.

[192] R. L. Ross, B. Caballero-Ruiz, E. L. Clarke, V. Kakkar, C. W. Wasson, P. Mulipa, E. De Lorenzis, W. Merchant, S. Di Donato, A. Rindone, A. L. Herrick, C. P. Denton, N. A. Riobo-Del Galdo, and F. Del Galdo, "Biological hallmarks of systemic sclerosis are present in the skin and serum of patients with Very Early Diagnosis of SSc (VEDOSS)," *Rheumatology (Oxford, England)*, Dec. 2024, ISSN: 1462-0332.

[193] G. De Luca, C. Campochiaro, G. Peretto, E. Busnardo, M. Matucci-Cerinic, and L. Dagna, "Cardiac involvement, a threatening very early manifestation of systemic sclerosis: Evidence from VEDOSS patients," *Clinical and Experimental Rheumatology*, Aug. 2023, ISSN: 1593-098X.

[194] S. Bellando-Randone *et al.*, "Gut microbiota in very early systemic sclerosis: The first case-control taxonomic and functional characterisation highlighting an altered butyric acid profile," *RMD Open*, vol. 10, no. 4, Nov. 2024, ISSN: 2056-5933.

[195] J. Pourahmad and A. Salimi, "Isolated Human Peripheral Blood Mononuclear Cell (PBMC), a Cost Effective Tool for Predicting Immunosuppressive Effects of Drugs and Xenobiotics," *Iranian Journal of Pharmaceutical Research : IJPR*, vol. 14, no. 4, 2015, ISSN: 1735-0328.

[196] K. M. McKinnon, "Flow Cytometry: An Overview," *Current protocols in immunology*, vol. 120, Feb. 2018.

[197] H. Drescher, S. Weiskirchen, and R. Weiskirchen, "Flow Cytometry: A Blessing and a Curse," *Biomedicines*, vol. 9, no. 11, Nov. 2021, ISSN: 2227-9059.

[198] K. R. Patel, J. T. Roberts, and A. W. Barb, "Multiple Variables at the Leukocyte Cell Surface Impact Fc γ Receptor-Dependent Mechanisms," *Frontiers in Immunology*, vol. 10, Feb. 2019, ISSN: 1664-3224.

[199] P. S. Aranda, D. M. LaJoie, and C. L. Jorcyk, "Bleach Gel: A Simple Agarose Gel for Analyzing RNA Quality," *Electrophoresis*, vol. 33, no. 2, Jan. 2012, ISSN: 0173-0835.

[200] A. I. Dragan, R. Pavlovic, J. B. McGivney, J. R. Casas-Finet, E. S. Bishop, R. J. Strouse, M. A. Schenerman, and C. D. Geddes, "SYBR Green I: Fluorescence Properties and Interaction with DNA," *Journal of Fluorescence*, vol. 22, no. 4, Jul. 2012, ISSN: 1573-4994.

[201] B. E. Hoffman, A. T. Martino, B. K. Sack, O. Cao, G. Liao, C. Terhorst, and R. W. Herzog, "Nonredundant Roles of IL-10 and TGF-β in Suppression of Immune Responses to Hepatic AAV-Factor IX Gene Transfer," *Molecular Therapy*, vol. 19, no. 7, Mar. 2011.

[202] Y. P. Rubtsov, J. P. Rasmussen, E. Y. Chi, J. Fontenot, L. Castelli, X. Ye, P. Treuting, L. Siewe, A. Roers, W. R. Henderson, W. Muller, and A. Y. Rudensky, "Regulatory T Cell-Derived Interleukin-10 Limits Inflammation at Environmental Interfaces," *Immunity*, vol. 28, no. 4, Apr. 2008, ISSN: 1074-7613.

[203] R. A. Peterson and J. E. Cavanaugh, "Ordered quantile normalization: A semiparametric transformation built for the cross-validation era," *Journal of Applied Statistics*, vol. 47, no. 13-15, ISSN: 0266-4763.

[204] H. Wickham, "Data Analysis," in *Ggplot2: Elegant Graphics for Data Analysis*, H. Wickham, Ed., Cham: Springer International Publishing, 2016, ISBN: 978-3-319-24277-4.

[205] J. Ooms, *Writexl: Export Data Frames to Excel 'xlsx' Format*, Oct. 2024.

[206] Francois Husson, Julie Josse, *missMDA: Handling Missing Values with Multivariate Data Analysis*, May 2010.

[207] H. Wickham, R. François, L. Henry, and D. Vaughan, *Dplyr: A Grammar of Data Manipulation*, 2023.

[208] F. Rohart, B. Gautier, A. Singh, and K.-A. Lê Cao, "mixOmics: An R package for 'omics feature selection and multiple data integration," *PLoS Computational Biology*, vol. 13, no. 11, Nov. 2017, ISSN: 1553-734X.

[209] K. Slowikowski, *Ggrepel: Automatically Position Non-Overlapping Text Labels with 'ggplot2'*, 2024.

[210] W. Revelle, *Psych: Procedures for Psychological, Psychometric, and Personality Research*, 2024.

[211] T. Wei, *Corrplot: Visualization of a Correlation Matrix*, 2024.

[212] F. Harrell, *Hmisc: Harrell Miscellaneous*, Dec. 2024.

[213] G. Csárdi, T. Nepusz, V. Traag, S. Horvát, F. Zanini, D. Noom, K. Müller, M. Salmon, M. Antonov, and C. Z. I. igraph author details, *Igraph: Network Analysis and Visualization*, Dec. 2024.

[214] T. L. Pedersen and RStudio, *Ggraph: An Implementation of Grammar of Graphics for Graphs and Networks*, Mar. 2024.

[215] A. Kowarik and M. Templ, "Imputation with the R package VIM," *Journal of Statistical Software*, vol. 74, Oct. 2016.

[216] M. Hao, Y. Wang, and S. H. Bryant, "An efficient algorithm coupled with synthetic minority over-sampling technique to classify imbalanced PubChem BioAssay data," *Analytica chimica acta*, vol. 806, Jan. 2014, ISSN: 0003-2670.

[217] T. Nukui and A. Onogi, "An R package for ensemble learning stacking," *Bioinformatics Advances*, vol. 3, no. 1, Sep. 2023, ISSN: 2635-0041.

[218] F. Daniel, M. Corporation, S. Weston, and D. Tenenbaum, *doParallel: Foreach Parallel Adaptor for the 'parallel' Package*, Feb. 2022.

[219] L. Breiman, A. Cutler, A. Liaw, and M. Wiener, *randomForest: Breiman and Cutlers Random Forests for Classification and Regression*, Sep. 2024.

[220] X. Robin, N. Turck, A. Hainard, N. Tiberti, F. Lisacek, J.-C. Sanchez, and M. Müller, "pROC: An open-source package for R and S+ to analyze and compare ROC curves," *BMC bioinformatics*, vol. 12, Mar. 2011, ISSN: 1471-2105.

[221] H.-G. Drost and H. Tjeldnes, *Biomartr: Genomic Data Retrieval*, Dec. 2023.

[222] G. Yu, L.-G. Wang, Y. Han, and Q.-Y. He, "clusterProfiler: An R Package for Comparing Biological Themes Among Gene Clusters," *OMICS : a Journal of Integrative Biology*, vol. 16, no. 5, May 2012, ISSN: 1536-2310.

[223] M. Carlson, *Genome wide annotation for Human.*

[224] H. Wickham, D. Vaughan, M. Girlich, K. Ushey, P. Software, and PBC, *Tidyr: Tidy Messy Data*, Jan. 2024.

[225] Z. Gu, L. Gu, R. Eils, M. Schlesner, and B. Brors, "Circlize Implements and enhances circular visualization in R," *Bioinformatics (Oxford, England)*, vol. 30, no. 19, Oct. 2014, ISSN: 1367-4811.

[226] E. Neuwirth, *RColorBrewer: ColorBrewer Palettes*, Apr. 2022.

[227] W. Luo and C. Brouwer, "Pathview: An R/Bioconductor package for pathway-based data integration and visualization," *Bioinformatics (Oxford, England)*, vol. 29, no. 14, Jul. 2013, ISSN: 1367-4811.

[228] L. Petelytska, F. Bonomi, C. Cannistrà, E. Fiorentini, S. Peretti, S. Torracchi, P. Bernardini, C. Coccia, R. D. Luca, A. Economou, J. Levani, M. Matucci-Cerinic, O. Distler, and C. Bruni, "Heterogeneity of determining disease severity, clinical course and outcomes in systemic sclerosis-associated interstitial lung disease: A systematic literature review," *RMD Open*, vol. 9, no. 4, Nov. 2023, ISSN: 2056-5933.

[229] A. Lescoat, "Very Early Diagnosis of Systemic Sclerosis: Deciphering the heterogeneity of systemic sclerosis in the very early stages of the disease," *Journal of Scleroderma and Related Disorders*, vol. 8, no. 1, Oct. 2022.

[230] P. S. Gromski, H. Muhamadali, D. I. Ellis, Y. Xu, E. Correa, M. L. Turner, and R. Goodacre, "A tutorial review: Metabolomics and partial least squares-discriminant analysis–a marriage of convenience or a shotgun wedding," *Analytica Chimica Acta*, vol. 879, Jun. 2015, ISSN: 1873-4324.

[231] E. Vivier, D. H. Raulet, A. Moretta, M. A. Caligiuri, L. Zitvogel, L. L. Lanier, W. M. Yokoyama, and S. Ugolini, "Innate or Adaptive Immunity? The Example of Natural Killer Cells," *Science (New York, N.Y.)*, vol. 331, no. 6013, Jan. 2011, ISSN: 0036-8075.

[232] H. Jiang and J. Jiang, "Balancing act: The complex role of NK cells in immune regulation," *Frontiers in Immunology*, vol. 14, Nov. 2023, ISSN: 1664-3224.

[233] Y. Su, S. Liu, C. Long, Z. Zhou, Y. Zhou, and J. Tang, "The cross-talk between B cells and macrophages," *International Immunopharmacology*, vol. 143, Dec. 2024, ISSN: 1567-5769.

[234] M. Binda, B. Moccaldi, G. Civieri, A. Cuberli, A. Doria, F. Tona, and E. Zanatta, "Autoantibodies Targeting G-Protein-Coupled Receptors: Pathogenetic, Clinical and Therapeutic Implications in Systemic Sclerosis," *International Journal of Molecular Sciences*, vol. 25, no. 4, Feb. 2024, ISSN: 1422-0067.

[235] F. Harris, Y. A. Berdugo, and T. Tree, "IL-2-based approaches to Treg enhancement," *Clinical and Experimental Immunology*, vol. 211, no. 2, Nov. 2022, ISSN: 0009-9104.

[236] J. Gu, X. Ni, X. Pan, H. Lu, Y. Lu, J. Zhao, S. Guo Zheng, K. L. Hippen, X. Wang, and L. Lu, "Human CD39hi regulatory T cells present stronger stability and function under inflammatory conditions," *Cellular and Molecular Immunology*, vol. 14, no. 6, Apr. 2016, ISSN: 1672-7681.

[237] H. Nakagawa, J. M. Sido, E. E. Reyes, V. Kiers, H. Cantor, and H.-J. Kim, "Instability of Helios-deficient Tregs is associated with conversion to a T-effector phenotype and enhanced antitumor immunity," *Proceedings of the National Academy of Sciences*, vol. 113, no. 22, May 2016.

[238] T. Komai, M. Inoue, T. Okamura, K. Morita, Y. Iwasaki, S. Sumitomo, H. Shoda, K. Yamamoto, and K. Fujio, "Transforming Growth Factor-β and Interleukin-10 Synergistically Regulate Humoral Immunity via Modulating Metabolic Signals," *Frontiers in Immunology*, vol. 9, Jun. 2018, ISSN: 1664-3224.

[239] K. Presser, D. Schwinge, M. Wegmann, S. Huber, S. Schmitt, A. Quaas, J. H. Maxeiner, S. Finotto, A. W. Lohse, M. Blessing, and C. Schramm, "Coexpression of TGF-β1 and IL-10 Enables Regulatory T Cells to Completely Suppress Airway Hyperreactivity1," *The Journal of Immunology*, vol. 181, no. 11, Dec. 2008, ISSN: 0022-1767.

[240] A. Lescoat, E. Bertoldo, J. Čolić, T. Santiago, Y. A. Suliman, J. Emmel, P. G. Conaghan, Y. Allanore, and F. del Galdo, "Results from the international collaborative systematic literature review informing the 2023 EULAR recommendations for the treatment of systemic sclerosis," *Annals of the Rheumatic Diseases*, vol. 84, no. 1, Jan. 2025, ISSN: 0003-4967.

[241] E. Antiga, P. Quaglino, S. Bellandi, W. Volpi, E. Del Bianco, A. Comessatti, S. Osella-Abate, C. De Simone, A. Marzano, M. Bernengo, P. Fabbri, and M. Caproni, "Regulatory T cells in the skin lesions and blood of patients with systemic sclerosis and morphoea," *British Journal of Dermatology*, vol. 162, no. 5, May 2010, ISSN: 0007-0963.

[242] N. Yu, X. Li, W. Song, D. Li, D. Yu, X. Zeng, M. Li, X. Leng, and X. Li, "CD4(+)CD25 (+)CD127 (low/-) T cells: A more specific Treg population in human peripheral blood," *Inflammation*, vol. 35, no. 6, Dec. 2012, ISSN: 1573-2576.

[243] W. Jeal and K. L. Goa, "Aldesleukin (recombinant interleukin-2): A review of its pharmacological properties, clinical efficacy and tolerability in patients with renal cell carcinoma," *BioDrugs: Clinical Immunotherapeutics, Biopharmaceuticals and Gene Therapy*, vol. 7, no. 4, Apr. 1997, ISSN: 1173-8804.

[244] H. A. Martinez *et al.*, "Regulatory T cells use heparanase to access IL-2 bound to extracellular matrix in inflamed tissue," *Nature Communications*, vol. 15, Feb. 2024, ISSN: 2041-1723.

[245] O. Boyman and J. Sprent, "The role of interleukin-2 during homeostasis and activation of the immune system," *Nature Reviews. Immunology*, vol. 12, no. 3, Feb. 2012, ISSN: 1474-1741.

[246] T. R. Malek, "The biology of interleukin-2," *Annual Review of Immunology*, vol. 26, 2008, ISSN: 0732-0582.

[247] K. W. Hwang, W. B. Sweatt, M. Mashayekhi, D. A. Palucki, H. Sattar, E. Chuang, and M.-L. Alegre, "Transgenic expression of CTLA-4 controls lymphoproliferation in IL-2-deficient mice," *Journal of Immunology (Baltimore, Md.: 1950)*, vol. 173, no. 9, Nov. 2004, ISSN: 0022-1767.

[248] K. R. Charley, A. G. Ramstead, J. G. Matous, Y. Kumaki, L. M. Sircy, J. S. Hale, and M. A. Williams, "Effector-Phase IL-2 Signals Drive Th1 Effector and Memory Responses Dependently and Independently of TCF-1," *The Journal of Immunology*, vol. 212, no. 4, Dec. 2023, ISSN: 0022-1767.

[249] S. I. Aqel, M. C. Granitto, P. K. Nuro-Gyina, W. Pei, Y. Liu, A. E. Lovett-Racke, M. K. Racke, and Y. Yang, "Distinct roles for Blimp-1 in autoreactive CD4 T cells during priming and effector phase of autoimmune encephalomyelitis," *Journal of Neuroimmunology*, vol. 325, Dec. 2018, ISSN: 0165-5728.

[250] N. Komatsu, K. Okamoto, S. Sawa, T. Nakashima, M. Oh-hora, T. Kodama, S. Tanaka, J. A. Bluestone, and H. Takayanagi, "Pathogenic conversion of Foxp3+ T cells into TH17 cells in autoimmune arthritis," *Nature Medicine*, vol. 20, no. 1, Jan. 2014, ISSN: 1546-170X.

[251] Y. Ushigome, Y. Mizukawa, M. Kimishima, Y. Yamazaki, R. Takahashi, Y. Kano, and T. Shiohara, "Monocytes are involved in the balance between regulatory T cells and Th17 cells in severe drug eruptions," *Clinical and Experimental Allergy: Journal of the British Society for Allergy and Clinical Immunology*, vol. 48, no. 11, Nov. 2018, ISSN: 1365-2222.

[252] L. Lei, X.-n. Zhong, C. Zhao, C.-d. Mi, J.-q. Li, and J.-j. Zeng, "Expression and significance of Th17 cells and related cytokines in a murine model of systemic sclerosis," *Beijing Da Xue Xue Bao. Yi Xue Ban = Journal of Peking University. Health Sciences*, vol. 44, no. 2, Apr. 2012, ISSN: 1671-167X.

[253] A. Laurence, C. M. Tato, T. S. Davidson, Y. Kanno, Z. Chen, Z. Yao, R. B. Blank, F. Meylan, R. Siegel, L. Hennighausen, E. M. Shevach, and J. J. O'shea, "Interleukin-2 signaling via STAT5 constrains T helper 17 cell generation," *Immunity*, vol. 26, no. 3, Mar. 2007, ISSN: 1074-7613.

[254] H. S. Kim, S. W. Jang, W. Lee, K. Kim, H. Sohn, S. S. Hwang, and G. R. Lee, "PTEN drives Th17 cell differentiation by preventing IL-2 production," *Journal of Experimental Medicine*, vol. 214, no. 11, Oct. 2017, ISSN: 0022-1007.

[255] J. Luo, B. Ming, C. Zhang, X. Deng, P. Li, Z. Wei, Y. Xia, K. Jiang, H. Ye, W. Ma, Z. Liu, H. Li, X.-P. Yang, and L. Dong, "IL-2 Inhibition of Th17 Generation Rather Than Induction of Treg Cells Is Impaired in Primary Sjögren's Syndrome Patients," *Frontiers in Immunology*, vol. 9, Aug. 2018, ISSN: 1664-3224.

[256] N. Kim, E. Yi, E. Lee, H. J. Park, and H. S. Kim, "Interleukin-2 is required for NKp30-dependent NK cell cytotoxicity by preferentially regulating NKp30 expression," *Frontiers in Immunology*, vol. 15, Apr. 2024, ISSN: 1664-3224.

[257] A. Koreck, A. Surányi, B. J. Szöny, Á. Farkas, Z. Bata-Csörgö, L. Kemény, and A. Dobozy, "CD3+CD56+ NK T cells are significantly decreased in the peripheral blood of patients with psoriasis," *Clinical and Experimental Immunology*, vol. 127, no. 1, Jan. 2002, ISSN: 0009-9104.

[258] H. H. Van Acker, A. Capsomidis, E. L. Smits, and V. F. Van Tendeloo, "CD56 in the Immune System: More Than a Marker for Cytotoxicity?" *Frontiers in Immunology*, vol. 8, Jul. 2017, ISSN: 1664-3224.

[259] W. K. Chan, P. Rujkijyanont, G. Neale, J. Yang, R. Bari, N. Das Gupta, M. Holladay, B. Rooney, and W. Leung, "Multiplex and genome-wide analyses reveal distinctive properties of KIR+ and CD56+ T cells in human blood," *Journal of Immunology (Baltimore, Md.: 1950)*, vol. 191, no. 4, Aug. 2013, ISSN: 1550-6606.

[260] D. Simon, P. Balogh, A. Bognár, Z. Kellermayer, P. Engelmann, P. Németh, N. Farkas, T. Minier, V. Lóránd, L. Czirják, and T. Berki, "Reduced non-switched memory B cell subsets cause imbalance in B cell repertoire in systemic sclerosis," *Clinical and Experimental Rheumatology*, vol. 34 Suppl 100, no. 5, 2016, ISSN: 0392-856X.

[261] W. Zhang, Y.-F. Wang, F.-L. Hu, F.-A. Lu, T. Wu, Y.-L. Feng, and K. Li, "Dysfunction of CD27+IgD+ B cells correlates with aggravated systemic lupus erythematosus," *Clinical Rheumatology*, vol. 41, no. 5, May 2022, ISSN: 1434-9949.

[262] B. Rodríguez-Bayona, A. Ramos-Amaya, J. J. Pérez-Venegas, C. Rodríguez, and J. A. Brieva, "Decreased frequency and activated phenotype of blood CD27 IgD IgM B lymphocytes is a permanent abnormality in systemic lupus erythe-

matosus patients," *Arthritis Research & Therapy*, vol. 12, no. 3, 2010, ISSN: 1478-6362.

[263] N. Hipp, H. Symington, C. Pastoret, G. Caron, C. Monvoisin, K. Tarte, T. Fest, and C. Delaloy, "IL-2 imprints human naive B cell fate towards plasma cell through ERK/ELK1-mediated BACH2 repression," *Nature Communications*, vol. 8, Nov. 2017, ISSN: 2041-1723.

[264] K. Kometani, R. Nakagawa, R. Shinnakasu, T. Kaji, A. Rybouchkin, S. Moriyama, K. Furukawa, H. Koseki, T. Takemori, and T. Kurosaki, "Repression of the transcription factor Bach2 contributes to predisposition of IgG1 memory B cells toward plasma cell differentiation," *Immunity*, vol. 39, no. 1, Jul. 2013, ISSN: 1097-4180.

[265] A. Inaba, Z. K. Tuong, T. X. Zhao, A. P. Stewart, R. Mathews, L. Truman, R. Sriranjan, J. Kennet, K. Saeb-Parsy, L. Wicker, F. Waldron-Lynch, J. Cheriyan, J. A. Todd, Z. Mallat, and M. R. Clatworthy, "Low-dose IL-2 enhances the generation of IL-10-producing immunoregulatory B cells," *Nature Communications*, vol. 14, no. 1, Apr. 2023, ISSN: 2041-1723.

[266] M. Hirakawa, T. R. Matos, H. Liu, J. Koreth, H. T. Kim, N. E. Paul, K. Murase, J. Whangbo, A. C. Alho, S. Nikiforow, C. Cutler, V. T. Ho, P. Armand, E. P. Alyea, J. H. Antin, B. R. Blazar, J. F. Lacerda, R. J. Soiffer, and J. Ritz, "Low-dose IL-2 selectively activates subsets of CD4+ Tregs and NK cells," *JCI insight*, vol. 1, no. 18, Nov. 2016, ISSN: 2379-3708.

[267] A. Ghelani, D. Bates, K. Conner, M.-Z. Wu, J. Lu, Y.-L. Hu, C.-M. Li, A. Chaudhry, and S. J. Sohn, "Defining the Threshold IL-2 Signal Required for Induction of Selective Treg Cell Responses Using Engineered IL-2 Muteins," *Frontiers in Immunology*, vol. 11, 2020, ISSN: 1664-3224.

[268] J. He *et al.*, "Efficacy and safety of low-dose IL-2 in the treatment of systemic lupus erythematosus: A randomised, double-blind, placebo-controlled trial," *Annals of the Rheumatic Diseases*, vol. 79, no. 1, Jan. 2020, ISSN: 0003-4967, 1468-2060.

[269] X. Tai, F. Van Laethem, L. Pobezinsky, T. Guinter, S. O. Sharrow, A. Adams, L. Granger, M. Kruhlak, T. Lindsten, C. B. Thompson, L. Feigenbaum, and A. Singer, "Basis of CTLA-4 function in regulatory and conventional CD4+ T cells," *Blood*, vol. 119, no. 22, May 2012, ISSN: 0006-4971.

[270] S. Ayub, T. Shafi, R. Rasool, M. A. Dangroo, M. A. Bindroo, A. Gull, L. A. Al-Keridis, N. Alshammari, M. Saeed, and Z. A. Shah, "Evaluating the role of active TGF-β1 as inflammatory biomarker in Kashmiri (North-Indian) patients with systemic sclerosis: A case-control study," *Advances in Rheumatology*, vol. 64, no. 1, Dec. 2024, ISSN: 2523-3106.

[271] N. Askenasy, A. Kaminitz, and S. Yarkoni, "Mechanisms of T regulatory cell function," *Autoimmunity Reviews*, vol. 7, no. 5, May 2008, ISSN: 1568-9972.

[272] R. Pappu, V. Ramirez-Carrozzi, and A. Sambandam, "The interleukin-17 cytokine family: Critical players in host defence and inflammatory diseases," *Immunology*, vol. 134, no. 1, Sep. 2011, ISSN: 0019-2805.

[273] M. F. de Aguiar, H. Torquato, B. R. Salu, A. C. D. Oliveira, M. L. V. Oliva, E. J. Paredes-Gamero, W. H. Abdulahad, E. Brouwer, and A. W. S. de Souza, "Monocyte subsets and monocyte-related chemokines in Takayasu arteritis," *Scientific Reports*, vol. 13, no. 1, Feb. 2023, ISSN: 2045-2322.

[274] I.-C. Lin, J.-L. Suen, S.-K. Huang, M.-H. Chou, H.-C. Kuo, M.-H. Lo, K.-C. Kuo, and L. Wang, "Involvement of IL-17 A/IL-17 Receptor A with Neutrophil Recruitment and the Severity of Coronary Arteritis in Kawasaki Disease," *Journal of Clinical Immunology*, vol. 44, no. 3, Mar. 2024, ISSN: 1573-2592.

[275] C. Erbel, M. Akhavanpoor, D. Okuyucu, S. Wangler, A. Dietz, L. Zhao, K. Stellos, K. M. Little, F. Lasitschka, A. Doesch, M. Hakimi, T. J. Dengler, T. Giese, E. Blessing, H. A. Katus, and C. A. Gleissner, "IL-17A Influences Essential Functions of the Monocyte/Macrophage Lineage and Is Involved in Advanced Murine and Human Atherosclerosis," *The Journal of Immunology Author Choice*, vol. 193, no. 9, Nov. 2014, ISSN: 0022-1767.

[276] M. Medrano-Bosch, B. Simón-Codina, W. Jiménez, E. R. Edelman, and P. Melgar-Lesmes, "Monocyte-endothelial cell interactions in vascular and tissue remodeling," *Frontiers in Immunology*, vol. 14, Jul. 2023, ISSN: 1664-3224.

[277] A. Goepfert, S. Lehmann, J. Blank, F. Kolbinger, and J.-M. Rondeau, "Structural Analysis Reveals that the Cytokine IL-17F Forms a Homodimeric Complex with Receptor IL-17RC to Drive IL-17RA-Independent Signaling," *Immunity*, vol. 52, no. 3, Mar. 2020, ISSN: 1074-7613.

[278] A. Beringer, M. Noack, and P. Miossec, "IL-17 in Chronic Inflammation: From Discovery to Targeting," *Trends in Molecular Medicine*, vol. 22, no. 3, Mar. 2016, ISSN: 1471-4914, 1471-499X.

[279] D. D. Patel and V. K. Kuchroo, "Th17 Cell Pathway in Human Immunity: Lessons from Genetics and Therapeutic Interventions," *Immunity*, vol. 43, no. 6, Dec. 2015, ISSN: 1074-7613.

[280] N. Seki, H. Tsujimoto, S. Tanemura, S. Ishigaki, H. Takei, K. Sugahara, K. Yoshimoto, M. Akiyama, Y. Kaneko, K. Chiba, and T. Takeuchi, "Th17/IL-17A axis is critical for pulmonary arterial hypertension (PAH) in systemic sclerosis (SSc): SSc patients with high levels of serum IL-17A exhibit reduced lung functions and increased prevalence of PAH," *Cytokine*, vol. 176, Apr. 2024, ISSN: 1043-4666.

[281] L. Wang, T. Yi, M. Kortylewski, D. M. Pardoll, D. Zeng, and H. Yu, "IL-17 can promote tumor growth through an IL-6–Stat3 signaling pathway," *The Journal of Experimental Medicine*, vol. 206, no. 7, Jul. 2009, ISSN: 0022-1007.

[282] N. Karin and H. Razon, "Chemokines beyond chemo-attraction: CXCL10 and its significant role in cancer and autoimmunity," *Cytokine*, Special Issue: Chemokines - beyond Chemotaxis, vol. 109, Sep. 2018, ISSN: 1043-4666.

[283] M. Buttmann, F. Berberich-Siebelt, E. Serfling, and P. Rieckmann, "Interferon-beta is a potent inducer of interferon regulatory factor-1/2-dependent IP-10/CXCL10 expression in primary human endothelial cells," *Journal of Vascular Research*, vol. 44, no. 1, 2007, ISSN: 1018-1172.

[284] S. Yeruva, G. Ramadori, and D. Raddatz, "NF-κB-dependent synergistic regulation of CXCL10 gene expression by IL-1β and IFN-γ in human intestinal epithelial cell lines," *International Journal of Colorectal Disease*, vol. 23, no. 3, Mar. 2008, ISSN: 0179-1958.

[285] J. Stegbauer, D.-H. Lee, S. Seubert, G. Ellrichmann, A. Manzel, H. Kvakan, D. N. Muller, S. Gaupp, L. C. Rump, R. Gold, and R. A. Linker, "Role of the renin-angiotensin system in autoimmune inflammation of the central nervous system," *Proceedings of the National Academy of Sciences*, vol. 106, no. 35, Sep. 2009.

[286] P. Mease and I. B. McInnes, "Secukinumab: A New Treatment Option for Psoriatic Arthritis," *Rheumatology and Therapy*, vol. 3, no. 1, Apr. 2016, ISSN: 2198-6576.

[287] R. Adams, A. Maroof, T. Baker, A. D. G. Lawson, R. Oliver, R. Paveley, S. Rapecki, S. Shaw, P. Vajjah, S. West, and M. Griffiths, "Bimekizumab, a Novel Humanized IgG1 Antibody That Neutralizes Both IL-17A and IL-17F," *Frontiers in Immunology*, vol. 11, Aug. 2020, ISSN: 1664-3224.

[288] Z. Ali, R. Matthews, A. Al-Janabi, and R. B. Warren, "Bimekizumab: A dual IL-17A and IL-17F inhibitor for the treatment of psoriasis and psoriatic arthritis," *Expert Review of Clinical Immunology*, vol. 17, no. 10, Oct. 2021, ISSN: 1744-8409.

[289] R. Ganschow, M. Lyons, M. J. Kemper, and M. Burdelski, "B-cell dysfunction and depletion using mycophenolate mofetil in a pediatric combined liver and kidney graft recipient," *Pediatric Transplantation*, vol. 5, no. 1, 2001, ISSN: 1399-3046.

[290] S. Glaesener, T. D. Quách, N. Onken, F. Weller-Heinemann, F. Dressler, H.-I. Huppertz, A. Thon, and A. Meyer-Bahlburg, "Distinct Effects of Methotrexate and Etanercept on the B Cell Compartment in Patients With Juvenile Idiopathic Arthritis," *Arthritis & Rheumatology (Hoboken, N.j.)*, vol. 66, no. 9, Sep. 2014, ISSN: 2326-5191.

[291] E. B. Taylor and M. J. Ryan, "Immunosuppression With Mycophenolate Mofetil Attenuates Hypertension in an Experimental Model of Autoimmune Disease," *Journal of the American Heart Association: Cardiovascular and Cerebrovascular Disease*, vol. 6, no. 3, Feb. 2017, ISSN: 2047-9980.

[292] I. Böhm, "Decrease of B-cells and autoantibodies after low-dose methotrexate," *Biomedicine & Pharmacotherapy*, vol. 57, no. 7, Sep. 2003, ISSN: 0753-3322.

[293] G. Riemekasten, F. Petersen, and H. Heidecke, "What Makes Antibodies Against G Protein-Coupled Receptors so Special? A Novel Concept to Understand Chronic Diseases," *Frontiers in Immunology*, vol. 11, Dec. 2020, ISSN: 1664-3224.

[294] M. E. Zaslavsky *et al.*, "Disease diagnostics using machine learning of B cell and T cell receptor sequences," *Science*, vol. 387, no. 6736, Feb. 2025.

Acronyms

ACE	Angiotensin-converting enzyme	**ACR**	American College of Rheumatology
AI	Activity index	**AI**	Artificial intelligence
ANA	Anti-nuclear antibodies	**ANCOVA**	Analysis of covariance
ANOVA	Analysis of variance	**aAb**	Autoantibody
APC	Antigen-presenting cell	**ATP**	Adenosine triphosphate
AT1R	Angiotensin II receptor type 1	**BACH2**	BTB Domain And CNC Homolog 2
BAL	Bronchoalveolar lavage fluid	**Bcl-6**	B-cell lymphoma 6
BLIMP1	B lymphocyte-induced maturation protein 1	**Breg**	Regulatory B cell
BSA	Bovine serum albumin	**CCL**	CC chemokine ligand
CD	Cluster of differentiation	**CK**	Creatine kinase
CM	Central memory	**CRP**	C reactive protein
CT	Cycle threshold	**CTLA4**	T-lymphocyte-associated protein 4
CXCL	C-X-C motif chemokine	**CXCR**	C-X-C motif chemokine receptor
dc	Diffuse cutaneous	**DNA**	Deoxyribonucleic acid
ECM	Extracellular matrix	**EIA**	Enzyme immunoassay
ELISA	Enzyme-linked immunosorbent assay	**EM**	Effector memory
ET-1	Endothelin-1	**ETAR**	Endothelin-1 type A receptor
EUSTAR	European Alliance of Associations for Rheumatology	**FMO**	Fluorescence minus one
FoxP3	Forkhead box P3	**FcR**	Fc receptor
FGF	Fibroblast growth factor	**FSC**	Forward scatter
GATA3	GATA binding protein 3	**GERD**	Gastroesophageal reflux disease
GIT	Gastrointestinal tract	**GO**	Gene Ontology
GPCR	G protein-coupled receptor	**HC**	Healthy control
IFN	Interferon	**IgG**	Immunoglobulin G
ILD	Interstitial lung disease	**IL**	Interleukin
IQR	Interquartile range	**KEGG**	Kyoto Encyclopedia of Genes and Genomes
KIR	Killer cell Ig-like receptor	**lc**	Limited cutaneous

M3	Muscarinic acetylcholine receptor M3	**M4**	Muscarinic acetylcholine receptor M4
MDB	Membrane desalting buffer	**MCP**	Monocyte chemotactic protein
mRSS	Modified Rodnan Skin Score	**NK**	Natural killer
NO	Nitric oxide	**NPX**	Normalized protein expression
NTpro BNP	N-terminal prohormone of brain natriuretic peptide	**PAH**	Pulmonary arterial hypertension
PAR1	Protease-activated receptor 1	**PAR2**	Protease-activated receptor 2
PBMC	Peripheral blood mononuclear cells	**PCA**	Principal component analysis
PBS	Phosphate-buffered saline	**PCR**	Polymerase chain reaction
PDGF	Platelet-derived growth factor	**PEA**	Proximity extension assay
PF	Puffy fingers	**PH**	Pulmonary hypertension
PlGF	Placenta growth factor	**PLS-DA**	Partial least squares-discriminant analysis
pSS	Primary Sjögren's syndrome	**PsA**	Psoriatic arthritis
PTEN	Phosphatase and tensin homologue	**rIL**	Recombinant interleukin
RNA	Ribonucleic acid	**ROC**	Receiver operating characteristic
ROR	RAR-related orphan receptor	**RP**	Raynaud's phenomenon
RT	Room temperature	**SCS**	Single-cell suspension
SLE	Systemic lupus erythematosus	**SMOTE**	Synthetic minority over-sampling technique
SRC	Scleroderma renal crisis	**SSC**	Side scatter
SSc	Systemic sclerosis	**STAT**	Signal transducer and activator of transcription
T-bet	T-box expressed in T cells	**Tc**	Cytotoxic T
Tcon	Conventional T	**Tfh**	T follicular helper
TFR	Tendon friction rubs	**TGFβ**	Transforming growth factor beta
Th	T helper	**TNF**	Tumor necrosis factor
Tph	T peripheral helper	**Treg**	Regulatory T
VEDOSS	Very Early Diagnosis Of Systemic Sclerosis	**VEGF**	Vascular endothelial growth factor
vWF	von Willebrand factor	**α-SMA**	Alpha-smooth muscle actin
β1	Beta-1 adrenergic receptor	**β2**	Beta-2 adrenergic receptor

List of Figures

List of Tables

APPENDIX A

Appendix

The appendix provides supplementary data and detailed information that supports the main content of the study. It includes additional analyses, figures and tables that offer further insights into the study's findings and methodologies.

A.1 Immunophenotyping p-values and log2FC

Table A.1 : Referring to the volcano plots (fig. 4.2A), distinct p-values based on a Mann-Whitney U test and the calculated log2FC comparing cell frequencies from isolated PBMC of HC and VEDOSS patients are shown. Sorted by ascending p-values, with significance marked with asterisks.

Cell type	**p-value**	**log2FC**
Monocytes	0.001197602**	-0.733677755
Th17	0.001727343**	0.743873451
CD25lo Treg	0.001810231**	0.237125912
Non-switched memory B	0.003221054**	-0.852155804
CTLA4+CD25lo Treg	0.007632032**	1.026116636
CD39+CD25+ Treg	0.010637086*	-0.349750423
Intermediate Monocytes	0.013712318*	0.488515405
Ki67+ Naive Th	0.018696862*	0.610205627
CD56+ NK	0.02206934*	-0.734942752
CD56lo NK	0.028629607*	-0.772184274
Transitional B	0.040067509*	0.249809584
CD56hi NK	0.0440857*	-0.274666873
Ki67+ Th1	0.044474174*	0.944558442
IgM memory only B	0.048604118*	-0.419753294
Th9	0.055022095	0.394075021
Helios+ Treg	0.055030098	-0.097143258
CD25hi Treg	0.055963636	-0.216393612
Plasma cells	0.084287466	-0.495410916
Ki67+CD25- Treg	0.086476125	0.599401014
CTLA4+CD25+ Treg	0.092902237	0.840160974
Switched memory B	0.11854035	-0.125485147
Ki67+ Tfh	0.149286966	0.641657489
Ki67+ Treg	0.149353976	0.42236405
CD4+ Th	0.159715943	-0.195792182

Ki67+CD25+ Treg	0.16953491	0.42455774
Tph	0.17669736	0.264117902
Ki67+ EM	0.233209472	0.785576469
Tc	0.24002335	-0.130713692
CTLA4+CD25- Treg	0.275703841	0.408985283
Ki67+CD25hi Treg	0.291050995	0.296895135
Ki67+ CM	0.296238051	0.626241808
B cells	0.30722637	-0.117478334
Ki67+CD25lo Treg	0.328875816	0.321596364
Classical Monocytes	0.42481396	-0.034946129
Ki67+ Th17	0.433361331	0.407964346
Treg	0.44844688	-0.0842831
HLA-DR+ Monocytes	0.573187806	-0.088321576
CM	0.641595979	0.094837635
CTLA4+CD25hi Treg	0.657937361	0.308911767
Ki67+ Th2	0.69106991	0.063178229
NK T	0.69745495	-0.435978605
Ki67+ Th9	0.705204225	0.612401711
Nonclassical Monocytes	0.742436618	-0.008003695
Th1	0.811562567	0.018086239
Th2	0.811562567	-0.017251984
Naive B	0.841858093	-0.030477846
CD28lo Th1	0.864761786	0.540241533
Ki67+ Tph	0.882660585	0.497501509
Memory B	0.897278961	0.273373287
CD25- Treg	0.912531586	-0.190219548
Lymphocytes	0.947451436	-0.014164938
EM	0.954729852	0.032782122
Naive T	0.954732831	-0.005241866
Tfh	0.990941898	-0.030449321
CD25+ Treg	1	0.041782773

Table A.2 : Referring to the volcano plots (fig. 4.2B), distinct p-values based on a Mann-Whitney *U* test and the calculated log2FC comparing cell frequencies from isolated PBMC of VEDOSS and SSc patients are shown. Sorted by ascending p-values, with significance marked with asterisks.

Cell type	**p-value**	**log2FC**
CD25+ Treg	0.000147498***	0.228878283
CD25- Treg	0.000210387***	-0.790798202
NK T	0.002955805**	0.937717713
CD56hi NK	0.003483419**	0.804931456
B cells	0.005756386**	0.608597999
CD25hi Treg	0.008345795**	0.319989376
Ki67+CD25- Treg	0.008425067**	0.791472922
Ki67+ Naive T	0.010953842*	0.516474505
Lymphocytes	0.017757482*	0.204740109
CD25lo Treg	0.018025824*	0.172921493
Ki67+ CM	0.036940426*	0.917022152
Nonclassical Monocytes	0.041122569*	-0.448284422
CM	0.04223817*	-0.285233472
CTLA4+CD25hi Treg	0.047580581*	-0.889899492
Naive T	0.063869308	0.168989963
CTLA4+CD25- Treg	0.090355403	0.346610824
Naive B	0.092977474	-0.237457484
Ki67+ Treg	0.104685486	0.319950252
Ki67+ Th17	0.143274205	0.593217954
Tph	0.17451499	0.192853011
Ki67+ Th1	0.176276496	0.721814466
Ki67+ Tfh	0.190956718	0.47476394
Treg	0.253909759	0.166604068
CD8+ Tc	0.253950334	0.433422224
Tfh	0.258612365	0.098995121

Ki67+ Th9	0.264722852	0.70489542
Monocytes	0.338878132	-0.109452978
CD56+ NK	0.339175089	0.228737706
Ki67+ Th2	0.391403332	0.150029381
Ki67+ CD25lo Treg	0.394535965	0.243218663
CD56lo NK	0.402134751	0.183962929
CTLA4+ CD25+ Treg	0.413336308	-0.513183593
Ki67+ Tph	0.472814895	0.670077203
IgM memory only B	0.479806559	-0.220364284
Ki67+CD25+ Treg	0.504700954	0.147097774
Th1	0.514988179	0.077121574
Th2	0.514988179	-0.070751624
Ki67+CD25hi Treg	0.534021241	0.105700639
Plasma cells	0.544623517	0.08220345
CTLA4+CD25lo Treg	0.547830424	-0.046568068
Transitional B	0.554048549	0.047091071
CD4+ Th	0.562757359	-0.051168536
Non-switched memory B	0.564130811	0.026603828
Intermediate Monocytes	0.638644088	0.07783676
Memory B	0.647293229	0.248203502
Ki67+ EM	0.664234354	0.596832829
CD28lo Th1	0.676402991	0.172175558
Helios+ Treg	0.676413022	0.057696928
EM	0.688660447	-0.022275427
CD39+CD25+ Treg	0.742665608	-0.034015393
Switched memory B	0.79522969	0.177664362
HLA-DR+ Monocytes	0.80992368	0.012200268
Th9	0.929051716	-0.116344242
Th17	0.942329029	-0.044106854
Classical Monocytes	0.949770534	0.005252337

A.2 Influence of age and sex on CD25 subsets of Tregs

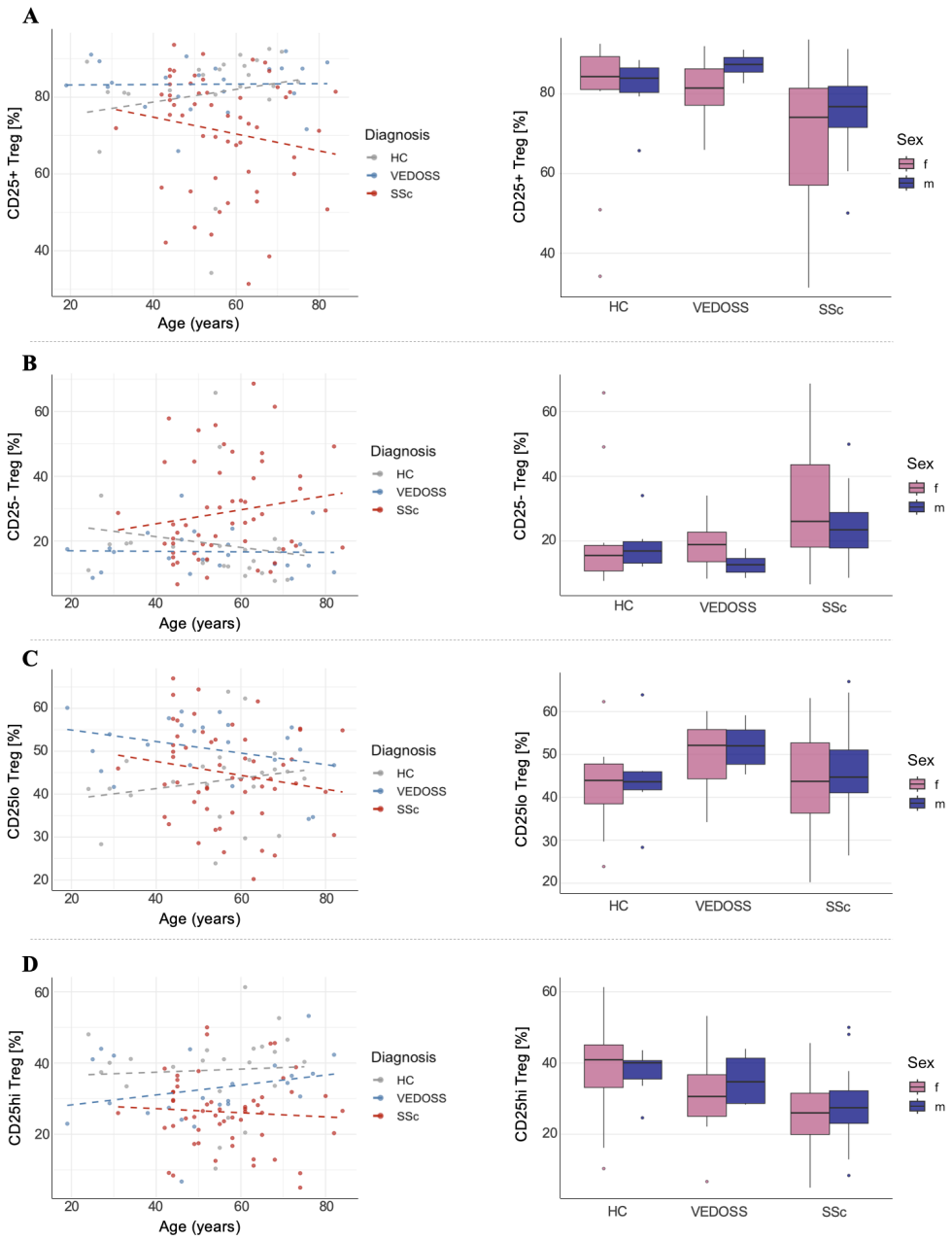

Figure A.1 : Confounder analysis for CD25 subsets among Treg. For the PBMCs of 23 HC, 23 VEDOSS and 54 SSc patients, CD25 subset frequencies among CD3+CD4+Foxp3+CD127lo Treg were identified via flow cytometry. Confounder analysis was carried out via an ANCOVA and visualized for the variable age as a scatter plot with regression lines and for sex as a boxplot with outliers. Results of the ANCOVA using (**A**) CD25+ Treg, (**B**) CD25- Treg, (**C**) CD25lo Treg and (**D**) CD25hi Treg dataset showed no significant results. That means age and sex did not influence the CD25 subset frequencies.

A.3 Correlation between cell frequencies and aAb values in VEDOSS and SSc patients: specified p- and r-values

Table A.3 : p- and r-values based on a Spearman's r test identifying correlations between cell frequencies and aAb levels VEDOSS patients. Only significant correlations are displayed ($p < 0.05$) and marked with asterisks.

Correlation	**p-value**	**r-value**
CD8+ Tc vs. AT1R	0.048*	0.448
CD8+ Tc vs. ETAR	0.023*	0.505
CD8+ Tc vs. M4	0.026*	0.493
Treg vs. PAR2	0.024*	-0.503
Th1 vs. ETAR	0.016*	0.532
Th1 vs. M4	0.020*	0.514
Th1 vs. PAR1	0.048*	0.448
Th2 vs. ETAR	0.016*	-0.532
Th2 vs. M4	0.020*	-0.514
Th2 vs. PAR1	0.048*	-0.448
Th9 vs. CXCR3	0.008**	0.571
Th9 vs. PAR1	0.005*	0.598
Th9 vs. PlGF	0.033*	0.478
Ki67+ Th2 vs. PAR2	0.010*	-0.560
Ki67+ Th9 vs. β1	0.007**	-0.586
Ki67+ Th17 vs. CXCR3	0.015*	-0.535
Ki67+ Tph vs. PAR2	0.015*	-0.536
Ki67+ naive T vs. β1	0.022*	-0.509
Ki67+ EM vs. CXCR3	0.041*	-0.460
Ki67+ EM vs. PAR2	0.011*	-0.553
Ki67+ EM vs. PlGF	0.023*	-0.507
Ki67+ CM vs. PAR2	0.005**	-0.605

B cells vs. AT1R	0.006**	0.607
B cells vs. ETAR	0.004**	0.626
B cells vs. β1	0.013*	0.558
B cells vs. β2	0.009**	0.579
B cells vs. M4	0.018*	0.535
B cells vs. M3	0.015*	0.549
Naive B vs. β1	0.018*	0.535
IgM memory only B vs. PAR2	0.016*	-0.546
Monocytes vs. PAR1	0.030*	-0.498

Table A.4 : p- and r-values based on a Spearman's r test identifying correlations between cell frequencies and aAb levels SSc patients. Only significant correlations are displayed ($p < 0.05$) and marked with asterisks.

Correlation	**p-value**	**r-value**
Treg vs. PlGF	0.018*	-0.332
CTLA4+CD25- Treg vs. FGF2	0.026*	-0.315
CTLA4+CD25lo Treg vs. FGF2	0.046*	-0.284
Ki67+CD25+ Treg vs. PAR1	0.030*	-0.304
Tfh vs. ETAR	0.017*	0.333
Tfh vs. β1	0.019*	0.327
Tfh vs. M4	0.048*	0.278
Tfh vs. M3	0.028*	0.308
EM vs. AT1R	0.010*	-0.357
EM vs. ETAR	0.025*	-0.314
EM vs. β1	0.025*	-0.314
EM vs. β2	0.030*	-0.304
EM vs. CXCR3	0.049*	-0.278
EM vs. FGF2	0.007**	-0.379
CM vs. PlGF	0.041*	0.290
Ki67+ Th1 vs. PlGF	0.0055**	-0.387

Ki67+ Th9 vs. CXCR3	0.028*	-0.308
Ki67+ Th9 vs. PlGF	0.035*	-0.299
Ki67+ Tph vs. PlGF	0.021*	-0.325
Ki67+ Tfh vs. PlGF	0.019*	-0.332
Ki67+ naive T vs. PlGF	0.024*	-0.319
Ki67+ naive T vs. FGF2	0.047*	-0.283
Ki67+ EM vs. PlGF	0.015*	-0.342
Transitional B vs. ETAR	0.028*	-0.339
Transitional B vs. β1	0.026*	-0.343
Transitional B vs. β2	0.027*	-0.342

A.4 Random Forest error rate analysis: HC vs VEDOSS classification

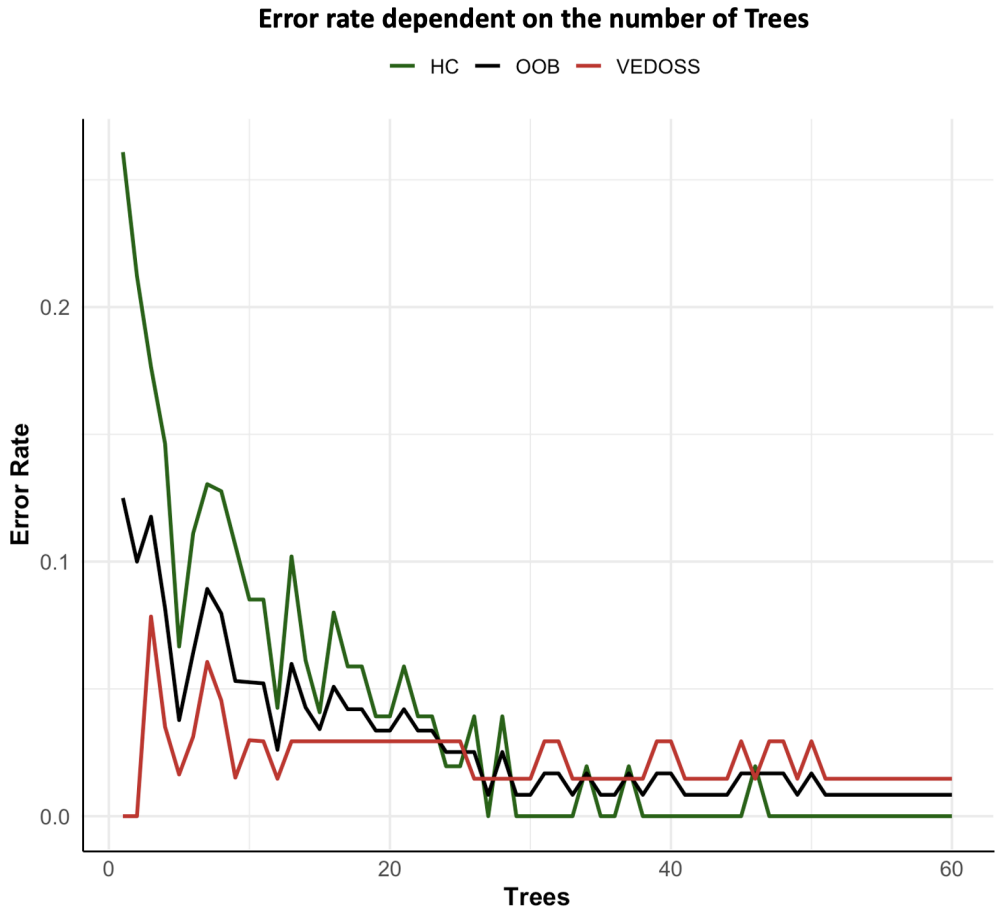

Figure A.2 : Error rate trends of the Random Forest algorithm for classifying HC vs VEDOSS patients and depicted as a function of the number of decision trees. Immunophenotyping data (cell frequencies) from the PBMC of 23 HC, 22 VEDOSS patients, acquired by flow cytometry, was used. Error rates for HC (green), VEDOSS (red), and the Out-of-Bag (OOB; black) error are indicated. Error rates stabilize as the number of trees increases, indicating improved model performance with more trees.

A.5 Random Forest error rate analysis: VEDOSS vs SSc classification

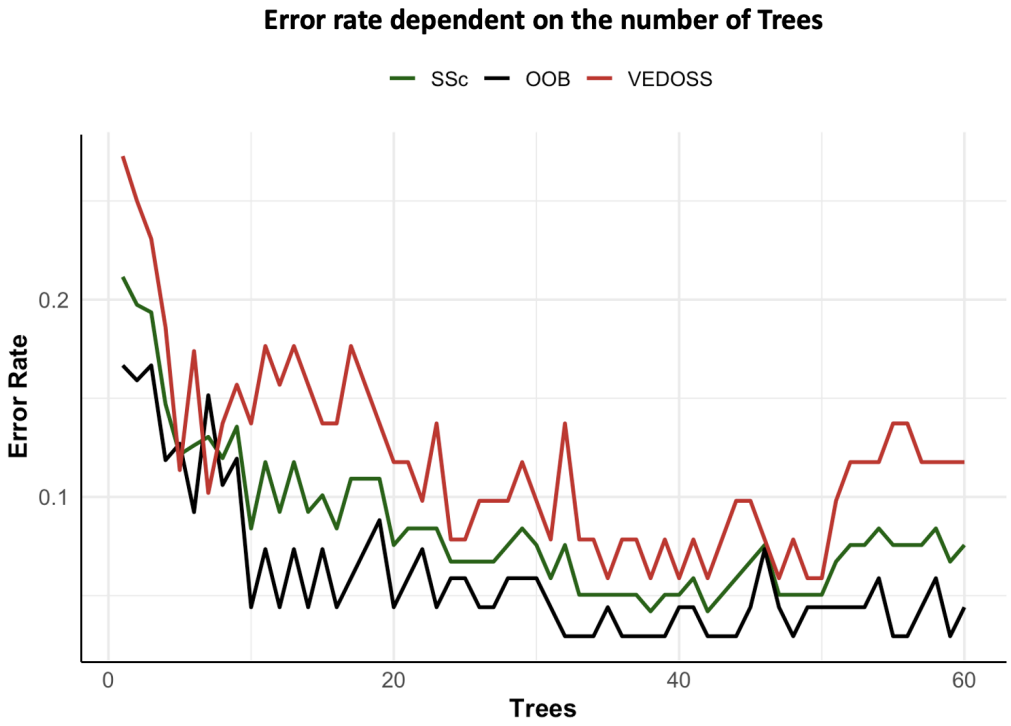

Figure A.3 : Error rate trends of the Random Forest algorithm for classifying VEDOSS vs SSc patients and depicted as a function of the number of decision trees. Immunophenotyping data (cell frequencies) from the PBMC of 22 VEDOSS and 54 SSc patients, acquired by flow cytometry, was used. Error rates for SSc (green), VEDOSS (red), and the Out-of-Bag (OOB; black) error are indicated. Error rates stabilize as the number of trees increases, indicating improved model performance with more trees.

A.6 Olink p-values and log2FC

Table A.5 : Olink® PEA p-values based on a Welch's t test and the calculated log2FC comparing protein expression in serum of VEDOSS and SSc patients. Sorted by ascending p-values, with significance marked with asterisks.

Protein	p-value	log2FC
IL17A	0.000101829***	0.684428786
MCP1	0.00193086**	0.055505146
CCL20	0.002415644**	0.164784261
CST5	0.003177954**	0.08300608
CCL11	0.005105237**	0.054858306
CXCL11	0.007291252**	0.079567145
CXCL9	0.008973545**	0.11233342
MCP3	0.014477185*	0.216520711
CX3CL1	0.017266001*	0.089382635
MMP1	0.017738318*	0.036172032
CDCP1	0.023100028*	0.163393316
IL4	0.023359534*	0.75878464
CXCL10	0.033306724*	0.069510903
IL17C	0.0333871*	0.17387436
HGF	0.035455507*	0.038507254
IL8	0.036599435*	0.080738358
CCL3	0.042595915*	0.081046832
MCP4	0.058810465	0.026289128
IL10RB	0.06161167	0.039307244
IL22RA1	0.06560144	0.149369732
OSM	0.076403167	0.077233028
TNFRSF9	0.079389222	0.065151634
VEGFA	0.081383153	0.034753979
CCL28	0.086431703	0.146125777
ADA	0.090657116	0.057444832

CSF1	0.108262455	0.013032451
TGFalpha	0.111058163	0.082872878
IL12B	0.125608693	0.065221421
CCL25	0.126217182	0.052741869
IL6	0.143645605	0.170757322
IL13	0.172251805	0.505248021
NT3	0.17526284	-0.083068289
uPA	0.187682084	0.018953279
CCL19	0.189188725	0.037082004
CASP8	0.191393909	0.093939744
Flt3L	0.193088876	0.027062416
SIRT2	0.225757054	0.08438665
IFNgamma	0.229045614	0.072077197
CD5	0.246417288	0.033819765
SLAMF1	0.24758382	0.074775181
CD40	0.248744273	0.015603254
TNFSF14	0.298376687	0.043628831
STAMBP	0.301300849	0.037619499
FGF21	0.310658611	0.111563118
BetaNGF	0.316691843	0.091495041
MMP10	0.32310941	0.025666454
OPG	0.324868544	0.013438055
CCL4	0.360301868	0.029108127
AXIN1	0.376235902	0.084212652
IL33	0.387224587	0.133929398
CD8A	0.389618253	-0.03288231
SCF	0.404837356	-0.009893905
PDL1	0.431595206	0.016031297
ENRAGE	0.442900076	0.041509186
CXCL1	0.443028136	0.0140907
DNER	0.478928198	0.008640137

IL5	0.481488738	0.144959837
IL2RB	0.483210114	-0.13659574
TNFB	0.484668061	0.0325609
X4EBP1	0.486174042	0.042576045
GDNF	0.488268028	0.031685574
ST1A1	0.501647982	0.033316035
CXCL6	0.513771412	0.013764573
IL10	0.516952635	0.042681756
FGF19	0.523010027	-0.027454634
LIFR	0.537936078	0.016401318
IL10RA	0.55081974	0.300917507
FGF5	0.572598149	0.076037103
ARTN	0.573840436	0.098182162
IL24	0.600389757	-0.489489755
CCL23	0.603942928	-0.007949269
FGF23	0.604306557	0.074722424
LAPTGFbeta1	0.683109991	0.009914455
CD6	0.687620528	-0.014693398
IL2	0.695398765	-0.062461681
TNF	0.73093526	0.020693423
CD244	0.736762181	-0.007374341
MCP2	0.769641917	0.005913483
IL18R1	0.80554526	-0.004252345
IL15RA	0.808018204	0.027735693
TWEAK	0.811754113	-0.004198691
IL20	0.811930742	-0.10700132
TRANCE	0.83710348	0.01137312
CXCL5	0.855944105	-0.003395627
TSLP	0.862769995	0.046453555
IL7	0.898706145	0.012966281
LIF	0.905560006	-0.061536631

TRAIL	0.916776693	-0.001560294
IL18	0.940249629	-0.002294324
IL20RA	0.941946082	0.010618238
NRTN	0.973734594	0.016617055